

The thermal history of the western Lower Saxony Basin, Germany

Von der Fakultät für Georessourcen und Materialtechnik der
Rheinisch-Westfälischen Technischen Hochschule Aachen

zur Erlangung des akademischen Grades eines
Doktors der Naturwissenschaften

genehmigte Dissertation

vorgelegt von

Diplom-Geologin Yvonne Adriasola Muñoz

aus Räckelwitz

**Berichter: Univ.-Prof. Dr.rer.nat. Ralf Littke
PD Dr.rer.nat. Ulrich Glasmacher**

Tag der mündlichen Prüfung: 22.12.2006

Adriasola Yvonne Munoz
The themal history of the western Lower Saxony Basin. Germany

ISBN: 3-86130-884-3
1. Auflage 2007

Bibliografische Information der Deutschen Bibliothek

Die Deutsche Bibliothek verzeichnet diese Publikation in der Deutschen Nationalbibliografie; detaillierte bibliografische Daten sind im Internet über <http://dnb.ddb.de> abrufbar.

Das Werk einschließlich seiner Teile ist urheberrechtlich geschützt. Jede Verwendung ist ohne die Zustimmung des Herausgebers außerhalb der engen Grenzen des Urhebergesetzes unzulässig und strafbar. Das gilt insbesondere für Vervielfältigungen, Übersetzungen, Mikroverfilmungen und die Einspeicherung und Verarbeitung in elektronischen Systemen.

Vertrieb:

1. Auflage 2007
© Verlagshaus Mainz GmbH Aachen
Süsterfeldstr. 83, 52072 Aachen
Tel. 0241/87 34 34
Fax 0241/87 55 77
www.Verlag-Mainz.de

Herstellung:

Druck und Verlagshaus Mainz GmbH Aachen
Süsterfeldstraße 83
52072 Aachen
Tel. 0241/87 34 34
Fax 0241/87 55 77
www.DruckereiMainz.de
www.Druckservice-Aachen.de

Satz: nach Druckvorlage des Autors
Umschlaggestaltung: Druckerei Mainz

printed in Germany

Acknowledgements

First of all I wish to thank Prof. Dr. Ralf Littke and Dr. Manfred Brix for their supervision and the useful and extensive discussions about theoretical aspects of the geochemical investigations, basin modelling and fission track dating in general, and for the possibility to use the experimental devices used for taking detailed measurements. I am grateful to Prof. Littke and Priv.-Doz. Dr. Ulrich Glasmacher for acting as examiners of this thesis.

The implementation was supported by many persons. Lots of knowledge about the geology of the study area came from the very excited Dr. Horst Klassen, who organized a field trip to show Dr. Manfred Brix and me all the outcrops in the study area. Thus, we were able to obtain a really good collection of samples for fission track dating and maturity measurements.

During my visits to the Geologischer Dienst NRW, Dr. Günther Drozdowski, Dr. Dirk Juch and Dr. Volker Wrede always supported me with lots of tectonic information about the Ibbenbüren area and the Osning lineament.

From industry I received lots of assistance with very interesting ideas and had informative discussions with Dr. Heinz-Jürgen Brink and Dr. Martin Jentsch (both former BEB), Dr. Georg Bresser (former Preussag/Gaz de France) and Dr. Ingrid Winter (DGMK).

Furthermore, I was provided with lots of useful details about the Lower Saxony Basin by Dr. Franz Kockel, Dr. Peter Gerling and Dr. Peer Hoth from the BGR Hannover as well as Dr. Volker Lüders of the GFZ Potsdam.

Proof reading by Dr. Rolando di Primio, and PD Dr. Ulrich Glasmacher helped to improve chapters 2 and 3 respectively.

I express my gratitude to all the people who helped with sample preparation and experimental problems: Rolf Mildenerger, Frank Hansen, Dr. Bernd Krooss, Ina Blumenstein and Jens Köster.

I gratefully acknowledge the financial support received from the Deutsche Forschungsgemeinschaft (DFG; Li 618/12). The study was performed under the SPP 1135 Project “Dynamics of synsedimentary systems under varying stress regimes: The example of the Central European Basin” under the aegis of the DFG and DGMK in conjunction with the RWTH Aachen. Sample material was provided by various German oil companies (BEB, Mobil, Preussag, RWE-Dea and Wintershall) and quarries (DSK Anthrazit Ibbenbüren, Piesberger Steinindustrie GmbH & Co. KG).

I saved lots of time because I received administrative support from Dorit Kanellis and Renate Wuropulos. Of course, I will always remember the fruitful and scientific atmosphere which I got to know at the institute. I will especially always keep in mind the nice lunch breaks with my work colleagues Danny, Sabine, Susanne, Marta, Andreas Beha, Andreas Busch, Yves, Dirk and Sandra.

Thanks to all my friends who indulged me, when I was unbalanced and unintimate. Beyond doubt some of the persons were my housemates in the Monheimsallee (Silke, Michael, Jochen, Elmar, Jérôme, and Anika), and my new housemates in the UK (Matt, Neil, AJ and Olaia).

Finally, I want to thank my husband, my family and my sister for all the support they gave me throughout the time of this work.

Abstract

For the last 30 years the maturity and geophysical anomalies within the Lower Saxony Basin (LSB) have been interpreted as the result of a deep lying igneous intrusion called “Bramsche Massif”. Based on the lignite/subbituminous coal stage of Upper Campanian rocks overlying the Lower Cretaceous units, a late Early Cretaceous or early Late Cretaceous age was concluded for the time of intrusion.

To improve the understanding of the structural evolution of the basin the aim of this work was to provide a better coverage with maturity and palaeotemperature data in order to discriminate structural domains and to constrain time-temperature paths by the application of fission track thermochronology.

The combined analysis of different thermal indicators (e.g. vitrinite reflectance and fission track data) should help to reconstruct the temperature history of the basin.

Chapter 2 presents the results of vitrinite reflectance measurements for different wells and pseudo-wells in the basin performed to obtain calibration data for 1D basin modelling. In this context the influence of temperature on organic matter was evaluated. Based on the rank gradient first assumptions could be obtained about the temperature and burial history sediments must have experienced.

The ascertained maturity data for the central and southern part of the LSB confirm a low reflectance increase with depth which is more likely caused by deep burial than by an igneous intrusion.

Maturity data also allowed calculating palaeo-temperatures for the time of maximum burial or maximum temperatures. Thus, a first guess about the amount of erosion could be achieved.

The implementation of the maturity values as calibration data in the 1D modelling led to a cumulative thickness of eroded sedimentary rocks between 1300m (northern margin) and 7300m (Piesberg area). Slightly, elevated heat flows were assumed for the inversion time.

To obtain a more detailed temperature and cooling history of the basin, zircon and apatite fission tracks covering stratigraphic levels from Upper Carboniferous to Lower Cretaceous were analyzed.

Investigations on zircon and apatite fission tracks indicate a complex thermal history of the basin. The data imply that the Lower Saxony Basin has experienced three thermal heating events after the deposition of the Carboniferous. The regional pattern of the fission track ages is dominated by a decrease in zircon FT ages towards the basin centre. Mixed zircon FT ages of

the basin margins are at about 300Ma. A young age of 130Ma in the basin centre indicates that highest temperatures were already reached in or before the Lower Cretaceous. These findings would ask for much higher sedimentation rates during Upper Jurassic and earliest Cretaceous times than previously assumed. Moreover, fission track ages imply that the high thermal maturity of the organic matter in the centre of the Lower Saxony Basin was already obtained in the Upper Jurassic/Early Cretaceous.

An explanation for the differences of eroded thicknesses as well as for the regional pattern of zircon fission track ages might be variable synsedimentary subsidence within the LSB during late Jurassic and early Cretaceous times based on rift and wrench tectonics. Due to the extension graben and secondary half-graben systems were formed. In the course of the compressional phase during the inversion period these areas became those with strongest uplift.

Apatite fission track ages show a south to north decrease within the basin. Oldest ages of Late Cretaceous age indicate a cooling after the inversion and occur in the southern part of the basin. In contrast, apatite fission track ages of the northern margin indicate a renewed temperature increase during the last 10Ma.

Based on these findings a new heat flow history has to be assumed with high heat flows occurring during Upper Jurassic/Lower Cretaceous times in conjunction with the rifting taking place at this time.

These results have a major influence on the hydrocarbon generation of the Mesozoic source rocks within this basin. The expulsion of hydrocarbons started during Jurassic and Lower Cretaceous times and not as previously assumed in Upper Cretaceous times.

This outcome has an impact on the filling of hydrocarbon traps and also the hydrocarbon preservation on margins of the LSB. It could be therefore of interest for further exploration targets.

Zusammenfassung

Seit etwa 30 Jahren werden die hohe Inkohlung und die geophysikalischen Anomalien des südwestlichen Niedersächsischen Beckens als Resultat einer tief liegenden Intrusion, des so genannten “Bramscher Massivs”, interpretiert. Das Intrusions-Ereignis wurde in der Unter- bzw. frühen Oberkreide vermutet, da niedriginkohlte oberkretazische Sedimente hochinkohlte unterkretazische Schichten überlagern.

Um die strukturelle Geschichte des Beckens besser zu verstehen, war das Ziel der Arbeit, durch eine größere Abdeckung mit Reifedaten maximale Paläotemperaturen zu ermitteln und diesbezüglich strukturelle Bereiche des Beckens zu unterscheiden. Darüber hinaus sollten mit der Anwendung von Spaltspuren-Thermo-Chronologie Zeit-Temperatur-Pfade bestimmt und Inversions-/Erosionsbeträge ermittelt werden.

Die Einbeziehung verschiedener thermischer Indikatoren (z.B. Vitrinit-Reflexionen und Spaltspurendaten) sollte helfen, die Temperaturgeschichte des Beckens zu rekonstruieren.

Kapitel 2 zeigt Ergebnisse der Reifebestimmungen für das Becken, die durchgeführt wurden, um Kalibrationsdaten für die 1D Modellierung zu erhalten. In diesem Zusammenhang wurde der Einfluss der Temperatur auf das organische Material diskutiert. Anhand des Inkohlungsgradienten konnten erste Aussagen über die Temperatur- und Absenkungsgeschichte der Sedimente getroffen werden. Die erhobenen Reifedaten für den zentralen und südlichen Teil des Niedersächsischen Beckens bestätigen einen geringeren Reflexionsanstieg mit der Tiefe, was eher auf eine tiefe Versenkung als auf eine magmatische Intrusion hindeutet.

Außerdem erlauben Reifedaten die Berechnung von Paläotemperaturen für die Zeit der maximalen Versenkung oder maximal erfahrener Temperaturen. So konnten auch erste Abschätzungen für den Erosionsbetrag ermittelt werden.

Die Einbindung der Vitrinit-Reflexionen als Kalibrationsparameter in die 1D Modellierungen führte zu kumulativen Erosionsmächtigkeiten zwischen 1300m (nördlicher Beckenrand) und 7300m (Piesberg). Basierend auf einer Ausdünnung der Lithosphäre aufgrund von Hebung und Erosion wurden für die Zeit der Inversion erhöhte Wärme Flüsse angenommen.

Um eine ausführlichere Temperatur- und Abkühlungsgeschichte für das Becken zu erhalten, wurden Zirkon- und Apatit-Spaltspuren analysiert, die ein stratigraphisches Intervall vom Oberkarbon bis zur Unterkreide abdecken.

Die Untersuchungen der Zirkon- und Apatit-Spaltspuren deuten auf eine komplexe Temperaturgeschichte des Beckens hin. Die Daten implizieren, dass

das Niedersächsische Becken nach der Ablagerung des Oberkarbons drei thermische Ereignisse durchlebt hat. Dabei wird das regionale Muster der Spaltspurenalter von einer Abnahme der Zirkonalter in Richtung Beckenzentrum dominiert. Gemischte Zirkonalter am Beckenrand zeigen ein durchschnittliches Alter von ungefähr 300Ma an. Ein junges Alter von 130Ma im Beckenzentrum deutet darauf hin, dass die höchsten Temperaturen bereits während oder vor der Unterkreide erreicht wurden. Außerdem zeigen die Spaltspurenalter, dass die hohe Maturität des organischen Materials dort bereits während der Zeit Oberjura/Unterkreide erreicht wurde. Basierend auf diesen Ergebnissen sind höhere Sedimentationsraten für den Oberen Jura und die Unterkreide notwendig als vorher angenommen.

Eine Erklärung für die abweichenden Erosionsmächtigkeiten und das regionale Muster der Zirkonalter innerhalb des Niedersächsischen Beckens könnte eine unterschiedliche synsedimentäre Subsidenz –hervorgerufen durch Rift- und Zerrungstektonik während des späten Jura und der frühen Kreide– sein. Aufgrund von Dehnung wurden dabei Graben- und Halbgraben-Systeme geformt. Vorherrschende Kompression während der Inversionsperiode führte dazu, dass diese Gebiete am stärksten herausgehoben wurden.

Apatit-Spaltspurenalter zeigen ein Süd–Nordgefälle innerhalb des Beckens. Die ältesten (Oberkreide-) Alter weisen auf eine Abkühlung nach der Inversion hin und treten im südlichen Teil des Beckens auf. Apatit-Spaltspurenalter vom Nordrand des Beckens hingegen offenbaren einen erneuten Temperaturanstieg während der letzten 10Ma.

Aufgrund dieser Resultate musste eine neue Wärmeflussgeschichte für das Becken mit hohen Wärmeflüssen zur Zeit des Rifting während Oberjura/Unterkreide angenommen werden.

Diese Ergebnisse haben einen großen Einfluss auf die Kohlenwasserstoffgeneration der mesozoischen Muttergesteine im Niedersächsischen Becken. Die Expulsion der Kohlenwasserstoffe startete somit bereits während des Jura und der Unterkreide und nicht, wie vorher angenommen erst in der Oberkreide. Dieses Ergebnis hat eine große Auswirkung auf die Füllung der Fallenstrukturen mit Kohlenwasserstoffen und deren Erhaltung im Bereich der Beckenränder und könnte somit von Interesse für kommende Explorationen sein.

Contents

Acknowledgements

Abstract

Zusammenfassung

Contents

1. Introduction	1
1.1. Study area	1
1.2. Geological frame	1
1.3. The evolution of the legend “Bramsche Massif”	2
1.4. The doubts	3
1.5. Thesis overview	4
1.5.1. Chapter 2	4
1.5.2. Chapter 3	4
1.5.3. Chapter 4	5
1.5.3. Chapter 5	5
2. Numerical modelling of burial and temperature history as an approach for an alternative interpretation of the Bramsche anomaly, Lower Saxony Basin	7
2.1. Abstract	7
2.2. Introduction	7
2.3. Geological background	9
2.4. Samples and methods	13
2.4.1. Samples	13
2.4.2. Vitrinite reflectance	13
2.5. Thermal modelling	15
2.5.1. Discretisation of geologic history, heat flow, and erosion	15
2.5.2. Conceptual model and input data	17
2.5.3. Calibration Data	18
2.6. Results and discussion	18
2.6.1. Coalification pattern	18
2.6.2. Thermal modelling: the Ibbenbüren area (southern LSB margin)	21
2.6.3. Thermal modelling: the Bramsche area (central LSB)	30
2.6.4. Thermal modelling: the northern LSB margin	32
2.6.5. Thermal modelling: synthesis of results, and general discussion	32
2.6.6. Uncertainties in modelling results	38
2.7. Conclusions	40

3. New information on the thermal history of the southwestern Lower Saxony Basin, northern Germany, based on fission track analysis	43
3.1. Abstract	43
3.2. Introduction	43
3.3. Geological Setting	46
3.4. Sampling and Laboratory Procedures	47
3.5. Results and Discussion	50
3.5.1. Vitrinite reflectance measurements	50
3.5.2. Fission track analysis	50
3.5.2.1. Zircon fission track results	50
3.5.2.2. Apatite fission track results	66
3.5.3. Regional Cooling and Denudation Pattern	73
3.6. Summary	73
4. Fluid systems and basin evolution of the western Lower Saxony Basin, Germany	77
4.1. Abstract	77
4.2. Introduction	77
4.3. Methods	81
4.3.1. Geochemical investigations (TOC and Rock-Eval data)	81
4.3.2. Fluid inclusions	82
4.3.3. 2D move (Structural investigations)	82
4.3.4. Numerical Basin Modelling	83
4.4. Results	85
4.4.1. Geochemical investigations	85
4.4.2. Fluid Inclusions	85
4.4.3. Structural overview and geological setting	93
4.4.4. Basin Modelling	101
4.4.5. Hydrocarbon generation	101
4.5. Interpretation and Discussion	104
4.6. Conclusions	117
5. Final conclusions	119
5.1. Sedimentary basin evolution	119
5.2. High maturity based on deep burial or an igneous intrusion?	122
5.3. Heat flow	124
5.4. Petroleum systems	126
5.5. Conclusion	129
6. References	
CV	

1. Introduction

1.1. Study area

The study area is located in NW-Germany within the Lower Saxony Basin (LSB). The LSB extends from the Dutch border throughout northern Germany in an almost west-east direction and covers a surface of approximately 250 by 120km.

The LSB separates the Pompeckj High in the north from the Rhenish Massif in the south. The study area is situated in the southwestern part of the LSB and comprises the easting between 25 60 000 and 34 89 000 as well as the northing between 58 40 000 and 57 75 000 (Gauss-Krüger-System).

1.2. Geological frame

The Lower Saxony Basin (LSB) belongs to the Central European Basin System. The Central European Basin System was initiated by rifting and/or thermal subsidence of the lithosphere during the Permian (Plein 1978, Ziegler 1982, Bachmann and Grosse 1989, van Wees et al. 2000). The Permian Basin is underlain by Palaeozoic rocks of mainly Upper Carboniferous age, including coal-bearing sequences which are the principal source of many gas fields, including the very large Groningen field in the Netherlands (Glennie 2001).

A general re-configuration of the Central European Basin system took place during Late Mesozoic times with the initiation of the Alpine orogeny. Based on this evolution numerous basins became inverted (Ziegler 1982, 1987, Betz et al. 1987).

The LSB is one of several Late Jurassic-Early Cretaceous rift and wrench induced basins. Basement and basin fill of the LSB are composed of Carboniferous, Permian, Mesozoic, and Cenozoic sedimentary rocks. After initial extension during the Permian, the main subsidence occurred in Late Jurassic and Early Cretaceous times (Kockel et al. 1994). It led to the deposition of several thousand metres of sediments. Inversion of the LSB during the Late Cretaceous brought in many places Jurassic and Triassic rocks and in rare cases even the Carboniferous basement back to the surface.

Today the LSB represents an E-W striking, highly differentiated Mesozoic basin, which contains numerous commercial oil and gas fields.

1.3. The evolution of the legend “Bramsche Massif”

The LSB has been intensively investigated mainly because of its economic importance (Betz et al. 1987, Kockel et al. 1994).

Thus, for instance, Teichmüller et al. (1979, 1984) presented the maturation distribution for the Carboniferous surface in northwestern Germany in combination with gas fields known at that time.

An obvious anomalously high maturity of organic matter on the southern rim of the LSB ensured further investigations (Bartenstein et al. 1971, Koch and Arnemann 1975, Deutloff et al. 1980, Braukmann 1984, Buntebarth 1985, Teichmüller and Teichmüller 1985, Büchner 1986, Littke and Rullkötter 1987, Rullkötter et al. 1988, Schmitz and Wentzlow 1990). Coalification measurements (vitrinite reflectance) in the LSB provided evidence for extremely high thermal maturity of coaly organic matter in the area of Bramsche (NW of Osnabrück; Teichmüller and Teichmüller 1951, 1985, Bartenstein et al. 1971, Koch and Arnemann 1975) reaching 4.5%VRr in Upper Jurassic sedimentary rocks. Some areas of this high maturity coincide more or less with hydrothermal mineralization in Carboniferous and Permian rocks (Stadler and Teichmüller 1971).

The area of anomalous high coalification within this part of the LSB also matches well with a magnetic and a positive gravimetric anomaly. First hints on magnetic anomalies within the LSB were already reported in the early 20th century in the area of Bramsche (Schmidt 1914, cited in Breyer 1971). Kaiser (1930, cited in Hahn and Kind 1971) found that this anomaly could be due to the presence of a geometric body lying horizontally at great depth. This body was also deduced from positive gravity anomalies (Flotow et al. 1931) leading to the conclusion that it should have a higher density than the surrounding rocks (Reich 1948, 1949).

Based on these findings it was assumed that an igneous intrusion at more than 5 kilometres depth heated the overlying sedimentary rocks leading to high maturity. The coalification data also provided first evidence for the timing of this heating event: Because Upper Campanian rocks overlying the Lower Cretaceous units are in the lignite/subbituminous coal stage the timing of the intrusion should have been of either late Early Cretaceous or early Late Cretaceous age (Stadler and Teichmüller 1971).

This fact led to the conclusion that large intrusive bodies, which ascended at the beginning of the inversion of the LSB, are the cause of the observed maturity and gravity pattern (Hahn and Kind 1971, Stadler 1971, Giebler-Degro 1986, Bachmann and Grosse 1989). These intrusives are known as Bramsche Massif, Massif of Vlotho etc. (Uchte, Loccum) and are situated within the southern part of the LSB.

Additional studies on the palaeogeothermics of the area supported the igneous intrusion theory (e.g. Mundry 1971, Thyssen et al. 1971, Buntebarth and Teichmüller 1979, Giebeler-Degro 1986) and the Bramsche intrusion became an often cited although never drilled example for the geophysical and geochemical effects of magmatic intrusions in sedimentary basins.

Later, similar findings in the southern parts of the LSB were interpreted in the same way and the Vlotho Massif and Uchte Massif were established further to the east (Nodop 1971, Hahn et al. 1976, Deutloff et al. 1980). Further interpretations on petrographic and geochemical parameters used this explanation scheme to clarify observations on illite crystallinity (Brauckmann 1984), conodont alteration indices (Noeth 1991), fluid inclusion trapping temperatures (Jochum et al. 1995a), trace element redistribution in black shales (Jochum et al. 1995b) and petroleum generation under the influence of rapid heating by an igneous intrusion (Leythaeuser et al. 1980, 1988, Altebäumer 1982, Altebäumer et al. 1983, Littke et al. 1988, Rullkötter et al. 1988).

1.4. The doubts

In recent years, the existence of the Bramsche Massif and the associated Cretaceous intrusions (Vlotho, Uchte, Loccum) became doubtful. Schmitz and Wentzlow (1990) suggested that the occurrence of anomalously high maturities can in some cases be attributed to substantial subsidence, followed by intense inversion without magmatic heating (see also Mackenzie et al. 1988).

For instance, in the westernmost parts of the LSB close to the Dutch border, geophysical anomalies indicated another igneous intrusion (Bachmann and Grosse 1989). Numerical modelling by Leischner et al. (1993) suggested enhanced heat flows for this area, but the absolute values were still very similar to those at the southern margin of the LSB observed at present (about 80mW/m^2).

A further east located thermal anomaly was investigated by Petmecky et al. (1999). Based on fluid inclusion studies, fission track data, and numerical modelling, they falsified the theory of an igneous intrusion for this area. Instead deep burial during Early Cretaceous times followed by Late Cretaceous/Tertiary uplift exceeding 4 kilometres was responsible for high maturation.

Baldschuhn and Kockel (1999) assumed up to 8 kilometres of uplift and erosion for parts of the Ibbenbüren area west of the Bramsche Massif. Büker (1996) also suggested deep burial rather than an igneous intrusion as the cause for the anthracite stage coalification in this area, but the total amount of uplift and erosion was calculated to be significantly lower than 8 kilometres.

1.5. Thesis overview

The objective of this thesis was to test the two different hypothesis of either an igneous intrusion or deep burial followed by uplift and erosion, because these two alternative interpretations imply two contrasting concepts for hydrocarbon exploration. In the case of an intrusion, the whole area would have experienced too high temperatures to be of any economic interest. With the alternative scenario of an inverted and partly overthrust basin, the southern margin of the basin might at least be a possible gas play. It is the objective of this study to support a decision between the two models.

The procedure to achieve the target was carried out as follows: at first samples were taken to obtain maturity information and consequently gain some calibration data for the modelling. Additionally, because of sparse information regarding the temperature history, apatite and zircon fission track data were ascertained to clarify the cooling history of the basin.

Furthermore structural balancing was performed on three geological interpreted profiles. All of this information was later included in the numerical modelling to achieve a realistic temperature history for the basin.

The experimental programme consisted of:

standard geochemical characterisation techniques (TOC, Rockeval, vitrinite reflectance),

microscopic measurements of apatite and zircon fission tracks,

fluid inclusion investigations.

1.5.1. Chapter 2

This chapter describes the 1D modelling technique which was used a) to gain improved insight into the occurred heat flow in this area over the time, and b) to estimate the amount of erosion during the inversion.

Prior to modelling vitrinite reflectances were measured to provide calibration data for the modelling. The data were implemented afterwards in the 1D modelling of 6 wells and 2 pseudo wells.

The conceptual model for the 1D simulation is outlined in detail, describing the burial history of the basin after Carboniferous times.

1.5.2. Chapter 3

Chapter 3 represents the results of fission track dating in combination with the earlier gained results from 1D modelling.

Extractions of minerals for the fission track analysis as well as the measurement technique are explained in detail. Furthermore, the influence of temperature on the maturity indicators is described.

Vitrinite reflectance data were converted into palaeo-temperatures and gave evidence about the highest experienced temperatures of the samples. Compared with the different time-temperature windows resulting from fission track analysis, a cooling history for each sample could be extracted.

Based on these cooling paths the temperature history gained from 1D modelling had to be revised.

1.5.3. Chapter 4

This chapter represents the outcome of structural balancing of three profiles and new fluid inclusion data. All of these data were implemented into the 2D modelling.

Based on the obtained complex burial history of the study area the product of the 2D modelling was an elaborated temperature history. Derivations of maturation and hydrocarbon expulsion for three source rocks over the time were obtained from palaeo-temperatures that occurred within the basin.

1.5.3. Chapter 5

The last chapter summarizes all previous observation. Thereby the findings are finally described and discussed.

Increasing attention is paid to maturation of the source rocks and their hydrocarbon generation and timing in combination with trap formation and the accumulation of seals. In this context the influence of the uplift and erosion on trap formation as well as the impact of the thrusting during the inversion is explained.

The chapter ends with an outlook on further exploration potential within the Lower Saxony Basin.

2. Numerical modelling of burial and temperature history as an approach for an alternative interpretation of the Bramsche anomaly, Lower Saxony Basin

Keywords *Lower Saxony Basin, Bramsche Massif, vitrinite reflectance, basin modelling, temperature history*

2.1. Abstract

The Lower Saxony Basin, Germany, is one of several sedimentary basins within the Central European Basin system. In its southwestern part, anomalously high maturity of organic matter has been observed reaching 4.5% VRr in Upper Jurassic sedimentary rocks in an area which coincides with a magnetic and a positive gravimetric anomaly. This anomaly has often been interpreted as the consequence of a deep seated igneous intrusion, the so-called Bramsche Massif. However, results obtained from calibrated numerical modelling are not in accordance with this scenario. Instead, a burial by approximately four kilometres of now eroded Cretaceous rocks was revealed to be the probable cause for the anomaly. Data and modelling results from 6 boreholes and 2 pseudo-wells support this view.

2.2. Introduction

The Lower Saxony Basin (LSB) is one of several sedimentary basins within the European Basin System (van Wees et al. 2000, Ziegler 1982, 1990). In its southwestern part, i.e. in the area of Bramsche, evidence for extremely high thermal maturity of coaly organic matter has been found during past decades (Teichmüller and Teichmüller 1951, Teichmüller et al. 1984, Bartenstein et al. 1971, Koch and Arnemann 1975). The central part of the anomaly is characterised by anthracitisation of coal in lowermost Cretaceous sedimentary rocks (Wealden), whereas in the peripheral areas coalification in the same stratigraphic level does not exceed the lignite stage (Teichmüller and Teichmüller 1958). In the center of the anomaly, vitrinite reflectance measured on organic material from Upper Jurassic sedimentary rocks reaches values between 2.99 to 4.56% VRr, i.e. the meta-anthracite rank (Bartenstein et al. 1971). Furthermore, rank gradients in the coal-bearing Carboniferous sequence are up to 0.16% in this area (Teichmüller 1963, Buntebarth 1985), whereas they are lower than 0.10% in the buried Rhenish Massif in the south (Münsterland Block, Teichmüller et al. 1983).

Based on the above mentioned findings and due to the presence of a magnetic (Schmidt 1914, cited in Breyer 1971) and positive gravimetric anomaly (Kaiser 1930, cited in Hahn and Kind 1971, Flotow et al. 1931) it was assumed that a

deep lying igneous intrusion, the Bramsche Massif, at more than 5 kilometres depth heated the overlying sedimentary rocks leading to high coalification values (Mundry 1971, Thyssen et al. 1971, Buntebarth and Teichmüller 1979, Giebeler-Degro 1986). In accordance with the lignite/subbituminous coal stage of Upper Campanian rocks overlying the Lower Cretaceous units, it was concluded that the intrusion was emplaced either in late Early Cretaceous or in early Late Cretaceous times (Stadler and Teichmüller 1971). Calculations for the Ibbenbüren area by Buntebarth (1985) based on an empirical method suggested high "geothermal gradients" for the upper crust ranging between 65° and 92°C/km which would correspond to extremely high heat flows between 140 and 175 mW/m² at the time of maximum burial, i.e. the late Early Cretaceous or early Late Cretaceous.

Contradicting opinions however, were published with respect to maximum burial depths and thicknesses of now-eroded sedimentary rocks. Füchtbauer and Müller (1970) argued that the thermo-metamorphic alteration of Carboniferous sandstones in the area of Bramsche could reflect a maximum burial depth of 8000m. Based on seismic velocity measurements on Carboniferous sedimentary rocks in the vicinity of the Bramsche anomaly, a possible uplift by 6000m for the centre of the LSB was assumed by Brink (2002). More recent evaluations in the Ibbenbüren area led to the estimation of 4500m of subsidence (Thiermann 1980; Drozdowski 1988), whereas Baldschuhn and Kockel (1999) concluded an uplift of 8000m according to thickness extrapolations for this area. Based on reconstructions of missing layer-thicknesses, Nodop (1971) in contrast proposed a maximum burial depth of the LSB of only up to 3500m followed by inversion exhumation.

Detailed numerical modelling studies using data from several wells were published for areas east and west of the Bramsche Massif. For an area situated between the Bramsche Massif and the Netherlands (Figures 2.1, 2.2), Leischner et al. (1993) suggested enhanced heat flows during maximum burial, but the absolute values were still very similar to those observed at present (about 80mW/m²) along the southern margin of the LSB. The study was based on fluid inclusion studies, fission track data, maturity-versus-depth profiles, and numerical modelling. Using a similar approach, Petmecky et al. (1999) falsified the theory of an igneous intrusion in the area of Uchte, east of the Bramsche Massif (Figure 2.2). Instead, he postulated that deep burial during Early Cretaceous times followed by Late Cretaceous/Tertiary uplift was responsible for high maturation. A possible mechanistic explanation for this evolution would be the development of a half-graben followed by inversion (McClay 1995).

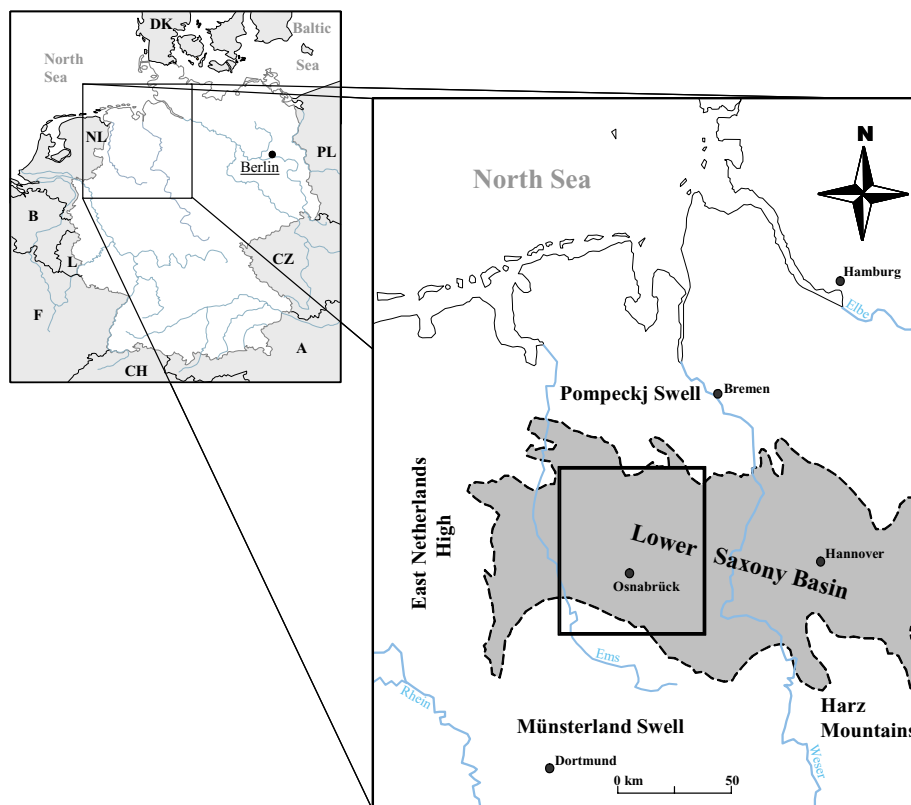


Figure 2.1: Location of the study area in Europe.

This study has the overall objective to reconstruct the thermal and burial history of the southern part of the LSB by testing different scenarios of basin subsidence and uplift including emplacement of igneous intrusions. Data from 6 wells and 2 pseudo-wells were used to establish numerical 1D models which were calibrated by vitrinite reflectance data. The major focus is on the period of deepest burial when maximum temperatures prevailed and on the following uplift period, i.e. on the Cretaceous. The study is part of the scientific priority programme "Dynamics of Sedimentary Systems under varying stress regimes: the Central European Basin System" of the DFG.

2.3. Geological background

The Lower Saxony Basin (LSB) is situated at the southern margin of the Central European Basin System and flanks to the north the London-Brabant, Rhenish, and Bohemian Massifs. The LSB represents an E-W-striking, highly differentiated Meso-Cenozoic basin (Betz et al. 1987, Baldschuhn et al. 1991, Kockel et al. 1994) and was initiated by rifting and/or thermal subsidence of the lithosphere during the Permian. The rifting centre was situated north of the LSB (Plein 1978, Ziegler 1982, Bachmann and Grosse 1989, Neunzert et al. 1996,

van Wees et al. 2000). Economically important is the basement consisting of marine Devonian and Lower Carboniferous and coal-bearing Upper Carboniferous rocks which act as important source rocks for natural gas (Littke

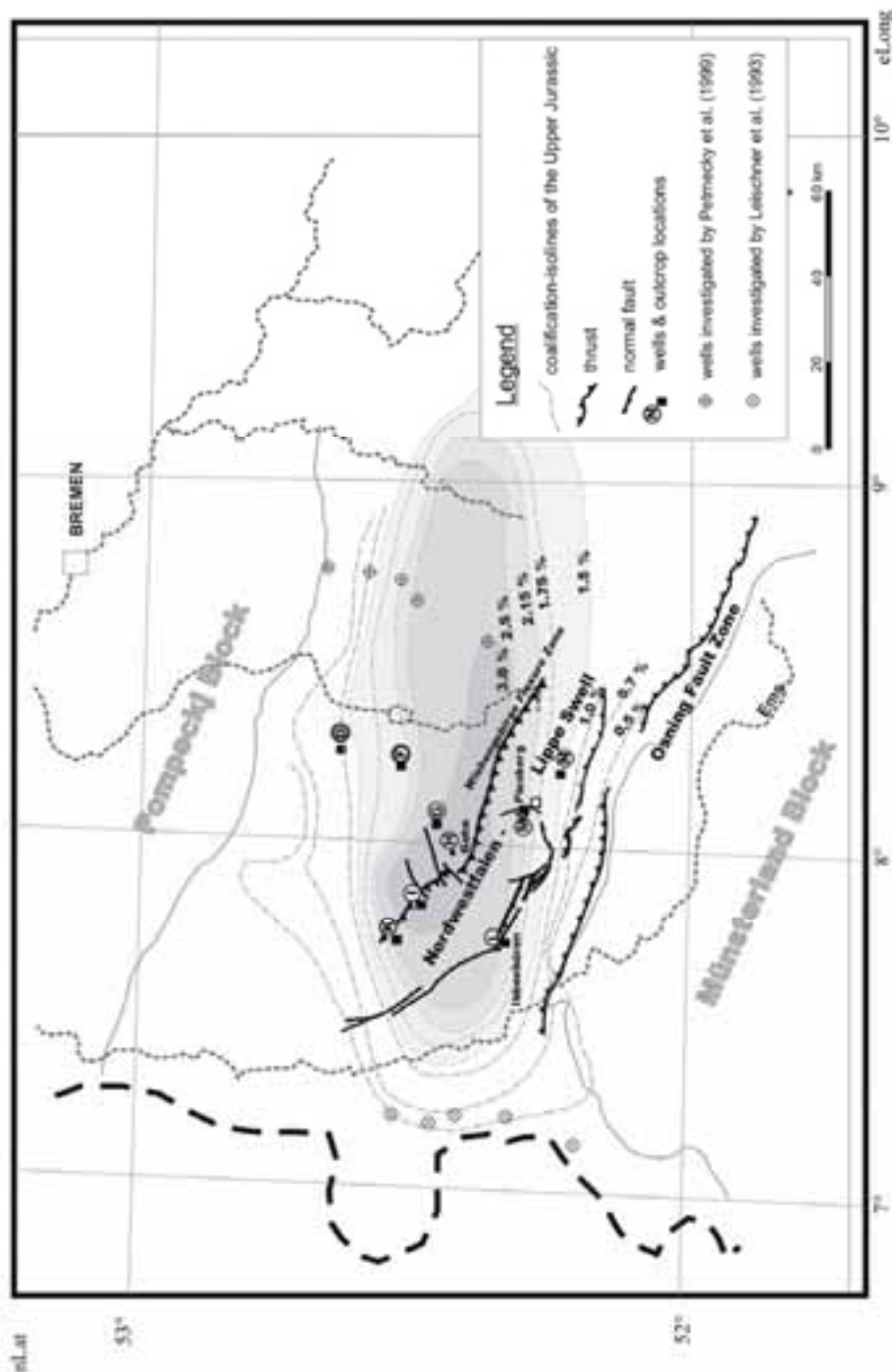


Figure 2.2: Coalification map of the Late Jurassic based on Bartenstein et al. (1971).

et al. 1995). Based on rift and wrench tectonics in the Late Jurassic, the LSB began to subside rapidly, bordered in the south by the Rhenish Massif, in the west by the Central Netherlands High, in the north by the Pompeckj Block, and in the east by the N-S-trending Gifhorn Trough (Figure 2.1, Kockel et al. 1994). During Coniacian and Santonian times, the LSB was inverted and existing normal faults became reactivated and transformed into steep thrusts and reverse faults (Baldschuhn and Kockel 1999). A general overview on the stratigraphy is given in Figure 2.3.

During the Late Carboniferous, the study area was situated in a foredeep of the rising Variscan mountain belt that was forming towards the south. A thick coal-bearing sedimentary sequence was deposited and partly eroded during the Variscan (Hercynian) orogeny, i.e. during the latest Carboniferous and/or earliest Permian (Süss 1996). The Upper Carboniferous deposits correspond to a deltaic system and are characterized by fluvial and marine sedimentary rocks (mainly silt- and sandstones) with intercalations of coal. Geologically, the folded Upper Carboniferous rocks are regarded as the basement of the Central European Basin System including the LSB, but they are not the economic basement since they provide major gas source rocks and even reservoir rocks to the petroleum system. Rotliegend deposits marking the opening of the Central European Basin System are rare in the LSB and restricted to its northern part; they exist in great thickness and with abundant volcanoclastic material in the area of the Pompeckj Block further north (Figure 2.1).

In the LSB, the transgression of the hypersaline Zechstein Sea led to the deposition of the basal sediments covering the mildly folded Upper Carboniferous units. The related sedimentary rocks consist mainly of salt, anhydrite, dolomite, and limestone with decreasing thickness towards the south. During Triassic times the LSB received thick post-rift sediments with clastic material predominating during the Lower and Upper Triassic (Bunter and Keuper) and carbonates representing the Mid Triassic (Muschelkalk). The thickness of Triassic deposits was governed by the existence of several NNE-striking depressions and swells. In the study area, thickness of Bunter clastics increases from SE (Hunte Swell, Trusheim 1961) to NW (Emsland area). Minor uplift events followed by terrestrial and fluvial intercalations affected deposition during Keuper time.

During the Jurassic, the depositional environment shifted to shallow marine. This evolution led to the deposition of a sedimentary succession consisting of shales, marls, carbonates, and sands, the latter being more abundant in the Upper Jurassic (Gramann et al. 1997). Regression of the sea during latest Jurassic and earliest Cretaceous times led to terrestrial intercalations ("Wiehengebirgsquarzit", Wealden facies). Based on strong vertical and horizontal movements along the southern fault-bounded border of the LSB,

thick shallow marine to terrestrial sequences developed in the Tithonian ("Münder Marl" and "Serpulit") as well as in the lowermost Cretaceous ("Wealden", Skupin 2003).

Up to the Barrêman and earliest Aptian, dark-coloured clastic sediments with commonly high concentrations of organic matter were deposited. A change of the depositional environment towards more "open-marine" conditions and warmer (Tethyan) water occurred during the Early Aptian. Later, light-coloured marls predominate the sedimentary sequence (Mutterlose 1992, Jendrzewski 1995).

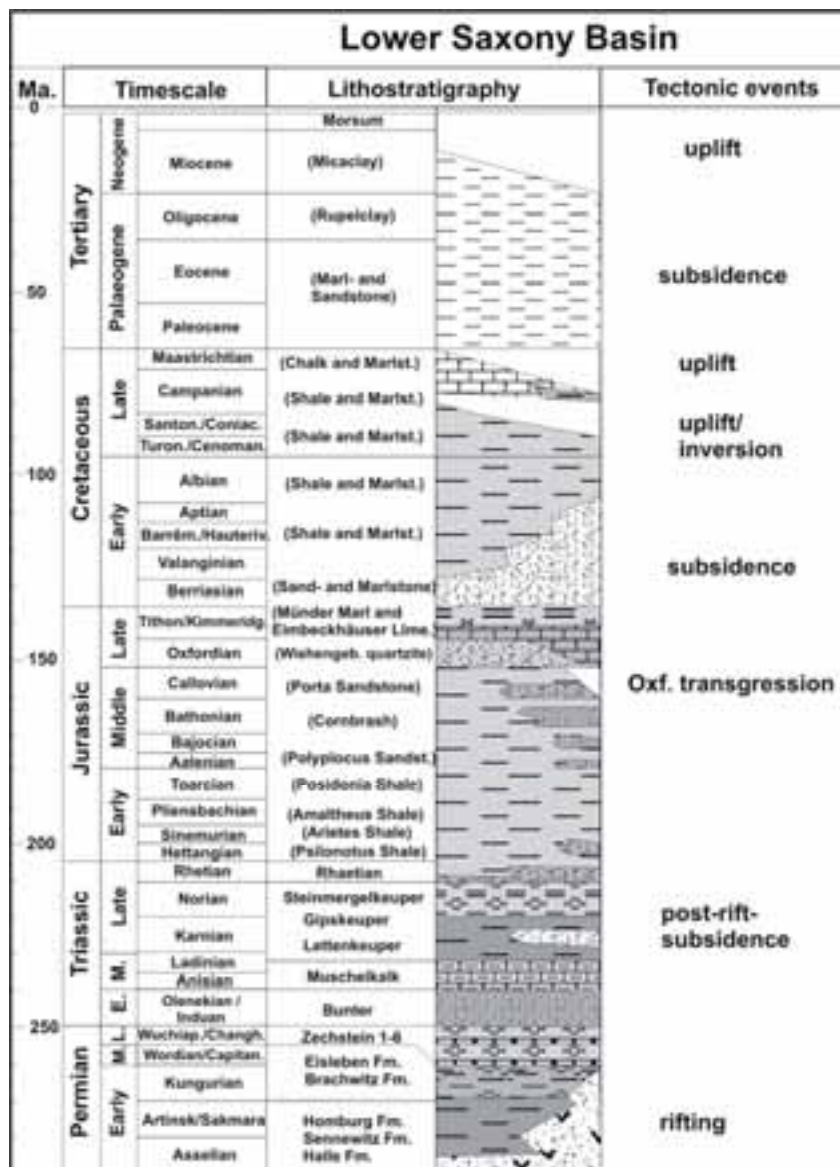


Figure 2.3: Generalized stratigraphy of the Lower Saxony Basin from Permian until recent times based on the German Stratigraphic Commission (2002).

Due to inversion tectonics in the Coniacian/Santonian, the LSB developed to the Lower Saxony Tectogene. During this inversion, the basin fill was uplifted and overthrust on the Münsterland Block to the south as well as on the Pompeckj Block to the north (Drozdowski 2003). Due to subsequent erosion, the sedimentary record of the Upper Cretaceous is almost lost. Sedimentation resumed again in the Paleocene-Oligocene. From the Miocene onwards, minor erosion occurred in the LSB.

2.4. Samples and methods

2.4.1. Samples

Organic matter-rich sedimentary rocks from different stratigraphic units were sampled for petrological investigations to obtain information on the regional maturity pattern. With respect to cores and cuttings from boreholes, an attempt was made to sample as many stratigraphic intervals as possible. This goal could not always be achieved, since for some wells sample material was not continuously available over the entire depth range. Collected samples consist mainly of coals and organic matter bearing dark shales. About 30 samples yielded valid new vitrinite reflectance data (Table 2.1).

2.4.2. Vitrinite reflectance

Reflectance of coal macerals has long been used to evaluate coal rank (Taylor et al. 1998). Vitrinite is the maceral most often used for this purpose because its optical properties alter more uniformly during rank advance than do those of other maceral groups. Moreover, vitrinite reflectance has been the major calibration parameter for modelling the thermal history of sedimentary rocks (Radke et al. 1997) since the results of Lopatin were published (Lopatin 1971, Waples 1980).

Vitrinite reflectance measurements were obtained from randomly oriented vitrinite grains using a Zeiss universal microspectrometer and followed established procedures as described in Taylor et al. (1998), with two isotropic glass standards of 0.89 and 1.70% reflectance. Random vitrinite reflectance values measured on dispersed organic material often differ from those measured on coals and show more scatter (Scheidt and Littke 1989). Causes for these deviations include measurements of allochthonous vitrinites of higher maturity, measurements from inertinite or solid bitumen which are difficult to distinguish from vitrinite at high coalification levels, as well as artefacts due to small particle size and a lower quality of the polished surface. The standard deviation of vitrinite reflectance values should be less than 0.1-0.2% for mean reflectance values below 2.0% and increase with maturity; however, measurements on dispersed organic material can show standard deviations exceeding these values.

Standard deviations obtained in the framework of this study are summarized in Table 2.1.

Table 2.1: Results of vitrinite reflectance measurements.

Location	Depth [m]	Northing	Easting	Lithology	Stratigraphy	VRr [%]	Std. Dev. [%]	Meas. Points
E-Gehn	Surface	58 12 975	34 25 750	coal	Oxfordian	3.56	0.256	60
E-Gehn	Surface	58 12 975	34 25 750	coal	Oxfordian	3.76	0.235	59
W-Gehn	Surface	58 11 075	34 23 700	coal	Oxfordian	4.09	0.147	50
Ibbenbüren	Surface	57 97 917	34 10 482	coal	Westphalian C	1.50	0.075	60
Piesberg	Surface	57 98 775	34 32 675	coal	Westphalian C	4.69	0.16	50
Piesberg	Surface	57 98 800	34 33 075	coal	Westphalian C	4.73	0.163	51
Piesberg	Surface	57 98 725	34 33 775	coal	Westphalian C	4.31	0.151	51
Piesberg	Surface	57 98 725	34 33 775	coal	Westphalian C	4.55	0.252	60
Piesberg	Surface	57 98 725	34 33 775	coal	Westphalian C	4.74	0.144	80
Vehrte	Surface	58 02 075	34 42 975	shale	Toarcian	1.94	0.28	50
Well G	80	-	-	shale	Up. Malm	2.65	0.318	48
Well G	205	-	-	shale	Up. Malm	3.03	0.313	14
Well G	295	-	-	shale	Kimmeridgian	3.07	0.298	22
Well G	490	-	-	shale	Kimmeridgian	3.13	0.209	10
Well G	620	-	-	shale	Oxfordian	3.06	0.262	13
Well G	770	-	-	shale	Dogger	3.39	0.204	12
Well G	930	-	-	shale	Dogger	3.27	0.298	25
Well G	1755	-	-	shale	Hettangian	3.99	0.36	35
Well G	1872	-	-	shale	Up. Keuper	4.26	0.297	50
Well G	1930	-	-	marlstone	Mid Keuper	4.47	0.272	35
Well G	2222	-	-	marlstone	Up. Muschelk.	4.51	0.21	50
Well G	2587	-	-	siltstone	Mid Bunter	4.65	0.171	41
Well G	3467	-	-	shale	Westphalian D	4.50	0.242	30
Well G	3486	-	-	sandstone	Westphalian D	4.64	0.142	50
north of Well E	1807	-	-	shale	Bajocian	0.79	0.128	63
Well E	1976	-	-	shale	Toarcian	0.93	0.152	67
Well E	2318	-	-	shale	Mid Bunter	1.37	0.374	29
Well E	3538	-	-	shale/siltstone	Carbonif.	1.99	0.199	16

The complete vitrinite reflectance data set consists of outcrop and core samples and is a compilation of personal measurements (Table 2.1), industrial data, data from the VIDABA (vitrinite data base of BGR, Hannover), and numerous published data (Bartenstein et al. 1971, Teichmüller et al. 1979, Teichmüller and Teichmüller 1985, Lommerzheim 1988, Günther et al. 1998). Stratigraphically, the data set covers Westphalian B to Tertiary sedimentary rocks.

2.5. Thermal modelling

Since the early publications of Lopatin (1971), Waples (1980), and Welte and Yücker (1981), the numerical simulation of burial, erosion, and thermal histories of sedimentary basins became a widely used method in geology, particularly in petroleum exploration. Here, 1D thermal modelling was applied using PetroMod software of IES, Jülich, Germany. Thermal and burial histories were calibrated by comparing measured and calculated vitrinite reflectance data (Figure 2.4). For the calculation of vitrinite reflectance, the kinetic EASY%Ro algorithm (Sweeney and Burnham 1990) was used. For a detailed discussion of the basin modelling concept and limitations see Poelchau et al. (1997) and Yalcin et al. (1997).

2.5.1. Discretisation of geologic history, heat flow, and erosion

Each numerical simulation has to be based on a conceptual model which describes basic geological processes, i.e. deposition, non-deposition, and erosion during the geologic evolution of the study area. This results in a basic set of input data for the simulation (Welte and Yalcin 1988). A major problem of the conceptual model is the reconstruction of time spans which are not represented by a physical record of sedimentary rocks, either due to sedimentation followed by erosion or to periods of non-deposition.

The following description of the geological history of the LSB is mainly based on the work of Thiermann (1970), Klassen (1984), Baldschuhn et al. (1999, 2001), Mutterlose and Bornemann (2000), and the Geologischer Dienst NRW (2003) and serves as a base for the conceptual model (see Table 2.2).

As basement of the sedimentary sequence the Westphalian B which had been cored in the Ibbenbüren area was selected. About 1500m of coal-bearing siliciclastic sedimentary rocks (Westphalian C and D) cover the basement, as also documented in the Ibbenbüren area wells. Between the latest Carboniferous and the earliest Permian, a period of non-deposition was assumed for a large part of the basin. Sedimentation followed by erosion is a more likely scenario for this time span as recorded for the Münsterland Block further south (Littke et al. 2000). The thermal effect of this possible depositional period was however,

clearly overwhelmed by Mesozoic events, especially those of Cretaceous times. Furthermore, the effect of this Late Carboniferous depositional event on gas generation from the coal-bearing Westphalian is beyond the scope of this study. Therefore, to keep the conceptual model as simple as possible, non-deposition was used as input data for this period.

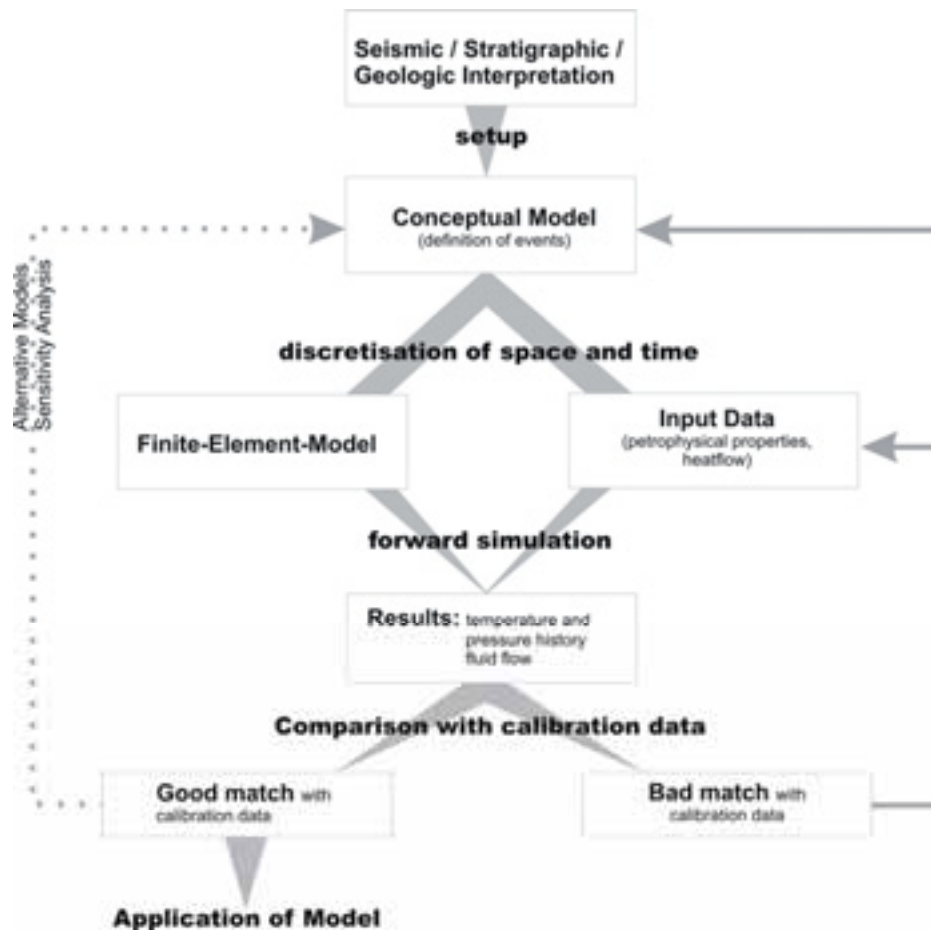


Figure 2.4: Scheme of the numerical modelling procedure (see text for further explanation).

Eruptive rocks were documented in the lithological log of well D and well A5 (Petmecky et al. 1999), and point to a volcanic event during Rotliegend times in the northern part of the study area. This coincided with the syn-rift stage of the Central European Basin System and certainly affected the then deposited sequence through elevated heat flow. Zechstein thickness increases from 200m in the southern part up to 930m in the northern part of the basin. The Triassic is characterised by short tectonic events reflected by discontinuities (e.g. Hardegsen- and Solling-Diskordanz; Steinmergelkeuper-Diskordanz). These

events were short and insignificant with respect to burial and thermal history and, therefore, not included in the conceptual model (Table 2.2). During Bunter times, the presence of the NNE-striking Hunte Swell resulted in a shift of the depositional center westwards into the Niederrhein-Ems Depression. The cumulative thickness increases from 440m to 890m in this direction. Overlying Muschelkalk strata are dominated by playa lake sediments with increasing contributions of halite north of the line Veltheim-Lübecke-Hunteburg. Keuper (Upper Triassic) thickness changes from the northern margin (164m) towards the center of the basin (363m), reflecting a different tectonic setting. During the Early Jurassic, a WNW-ESE striking graben evolved. Subsidence was significant in the centre of the basin, where up to 700m of Liassic and 600m of Dogger sediments accumulated. During the Late Jurassic and earliest Cretaceous, subsidence increased. For example, sedimentary rocks of Berriasian age (Upper Munder Marl/Serpulit) are more than 1000m thick in the central part of the LSB. Gramann et al. (1997) supposed rift events for the western part of the LSB based on thickness differences of up to 1000m in the Munder Marl Formation.

The Berriasian-Barrêmian sequence contains numerous sandstones along the basin margin (Osning Sandstone in the south, Bentheim and Gildehaus Sandstone in the west). The subsequent early Cretaceous succession is dominated by a clay-rich basin facies indicating high subsidence and high sedimentation rates. A decreasing cumulative thickness of Post-Berriasian/Lower Cretaceous deposits from the western part of the LSB (1950m) towards the eastern part (1200m) is remarkable. In the south, Cretaceous strata are partly or completely eroded. The sequence of Upper Cretaceous sedimentary rocks is incomplete in the LSB with greatest thicknesses of Cenomanian to Santonian sedimentary rocks in the north (up to 525m). Due to major uplift of the LSB during the Coniacian/Santonian inversion period, erosion of Cretaceous to Carboniferous deposits occurred along and to the south of the Nordwestfalen-Lippe Swell. At the beginning of the Campanian, tectonic movements had almost ceased. Deposits are rare, but recorded for the so-called Dammer Oberkreidemulde (230m). After a short inversion and erosion phase in Maastrichtian times, sedimentation resumed during the Paleocene-Miocene with approximately 150-200m of sediments deposited. This depositional phase was followed by moderate erosion until recent times.

2.5.2. Conceptual model and input data

Based on the geological history, about 40 events of deposition, erosion, or non-deposition were defined (Table 2.2). For each event, absolute ages, thicknesses, lithologies and related petrophysical properties, sediment-water interface temperatures, and heat flow values were defined. The heat flow history was kept as simple as possible and the heat flow values for the period of maximum

temperatures (early Late Cretaceous) were calibrated using vitrinite reflectance data; they are thus a result of the modelling approach. Surface temperatures were calculated based on the palaeolatitude of central Europe, water depth during deposition, and general climatic information (Wygrala 1989). Present-day formation temperatures were used to calibrate present-day heat flow together with the information on subsurface temperatures (Haenel 1980). Absolute ages were extracted from the geological time scale of the German Stratigraphic Commission (2002). Thicknesses were derived from well data, seismic profiles, and geological maps. Average thermal conductivities were calculated using lithological information and default thermal conductivities for major lithologies taking into account the interlayering of coals, shales, siltstones, sandstones, and conglomerates. Table 2.3 summarizes lithologic composition and important physical properties of the formations as defined for this study. The temperatures at the sediment-water interface were estimated using information on the palaeolatitude, palaeoclimate, and palaeo water depths of the study area during basin evolution (see Wygrala 1989 for details). These data allow the calculation of compaction and temperature fields.

2.5.3. Calibration Data

For the calibration of the models, vitrinite reflectance data and other maturity parameters, including water and volatile matter content of coals (on an ash-free basis) were used. The latter had to be converted into vitrinite reflectance according to Teichmüller et al. (1983). The possible pitfalls of maturity conversions are described in Radke et al. (1997). Vitrinite reflectance data from 8 wells are the basis for the calibration of 1D simulations of burial and thermal history.

2.6. Results and discussion

2.6.1. Coalification pattern

The coalification pattern in the Lower Saxony Basin has already been described by Koch and Arnemann (1975) and Teichmüller et al. (1984) who published a coalification map of the Upper Jurassic (Figure 2.2). In the framework of the study presented here, additional vitrinite reflectance measurements were performed; results are shown in Table 2.1. Furthermore, numerical simulation allowed the assessment of coalification for different stratigraphic levels, e.g. for the top of the Carboniferous or the base Cretaceous, even for wells which did not penetrate these units. The new coalification data confirm the previous results, clearly showing an increasing maturity from the margins towards the centre of the LSB. An example of which is shown in Figure 2.5 for the Kimmeridgian surface. This map is a combination of vitrinite reflectance

Table 2.2: Input data for modelling of burial, erosion, and temperature of well G (Figure 2.2). For physical rock properties see Table 2.3. Input data for other wells followed basically the same conceptual model.

Event	Name	Thickness [m]	Erosion [m]	Deposition Age from [Ma] to [Ma]	Erosion Age from [Ma] to [Ma]	Lithology	Water depth [m]	SWI [°C]	Heatflow [mW/m ²]
46	Quaternary	55.00		1.8	3.00	Sandstone	0	5.00	60.00
45	Oligocene		-70.00	0.00	5.3		0	16.00	60.00
44	Miocene		-84.00				0	16.00	60.00
43	Miocene	84.00		5.3		mixing	30	16.00	60.00
42	Oligocene	70.00		23.80		mixing	30	17.00	60.00
41	Campanian		-230.00	71.30			0	17.00	60.00
40	Campanian	230.00		71.30		SHALEcarb	30	18.00	60.00
39	Malm		-160.00		74.40		0	18.00	63.00
38	Münder Mergel		-900.00		75.80		0	18.00	63.00
37	Serpulit Fm.		-50.00		77.20		0	18.00	63.00
36	Wealden		-700.00		78.60		0	19.00	63.00
35	Valanginian		-300.00		80.00		0	19.00	63.00
34	Hauterivian		-400.00		81.40		0	19.00	63.00
33	Barremian		-300.00		82.80		0	19.00	63.00
32	Aptian		-275.00		84.20		0	19.00	63.00
31	Albian		-375.00		85.60		0	19.00	63.00
30	Upper Cretaceous		-525.00		87.00		0	19.00	63.00
29	Upper Cretaceous	525.00		87.00		SHALEcalc	80	20.00	60.00
28	Albian	375.00		98.50		SHALEcalc	100	19.00	60.00
27	Aptian	275.00		112.20		SHALEcalc	100	18.00	60.00
26	Barremian	300.00		120.00		SHALEcalc	100	18.00	60.00
25	Hauterivian	400.00		127.00		SHALEcalc	75	18.00	60.00
24	Valanginian	300.00		132.00		SHALEcalc	50	18.00	60.00

Table 2.2 (cont.).

Event	Name	Thickness [m]	Erosion [m]	Deposition Age from [Ma] to [Ma]	Erosion Age from [Ma] to [Ma]	Lithology	Water depth [m]	SWI [°C]	Heatflow [mW/m ²]
23	Wealden	700.00		140.00 to 137.00		mixing	5	19.00	60.00
22	Serpulit Fm.	50.00		141.00 to 140.00		mixing	10	19.00	60.00
21	Münder Marl	900.00		144.00 to 141.00		mixing	10	19.00	60.00
20	Malm	341.00		146.00 to 144.00		mixing	20	19.00	60.00
19	Kimmeridgian	314.00		152.50 to 146.00		mixing	10	18.00	60.00
18	Oxfordian	95.00		156.50 to 152.50		mixing	10	17.00	60.00
17	Dogger		-50.00		161.50 to 156.50		0	17.00	60.00
16	Dogger	525.00		178.00 to 161.50		mixing	75	14.00	60.00
15	Liassic	725.00		200.00 to 178.00		mixing	100	13.00	60.00
14	Rhät	84.00		209.00 to 200.00		mixing	5	15.00	60.00
13	Mid Keuper	243.00		232.50 to 209.00		mixing	5	15.00	60.00
12	Lower Keuper	36.00		235.00 to 232.50		mixing	5	15.00	60.00
11	Upper Muschelkalk	36.00		238.50 to 235.00		mixing	30	9.00	60.00
10	Mid Muschelkalk	101.00		240.00 to 238.50		mixing	15	9.00	60.00
9	Lower Muschelkalk	102.00		243.00 to 240.00		Marl	30	9.00	60.00
8	Upper Bunter	133.00		244.50 to 243.00		mixing	20	6.00	60.00
7	Mid Bunter	79.00		246.00 to 244.50		Shale	15	6.00	60.00
6	Lower Bunter	234.00		251.00 to 246.00		mixing	15	4.00	60.00
5	Zechstein	573.00		258.00 to 251.00		mixing	15	4.00	60.00
4	Westphalian D		-490.00		305.00 to 258.00		0	1.00	75.00
3	Westphalian D	650.00		308.00 to 305.00		mixing	5	3.00	75.00
2	Westphalian C	850.00		311.00 to 308.00		mixing	5	3.00	60.00
1	Westphalian B	850.00		313.50 to 311.00		mixing	5	4.00	60.00

calculated in the course of the numerical modelling and measurements as published by Bartenstein et al. (1971). The map shows a strong maturity increase towards the centre of the basin.

The high maturity of organic matter in the LSB might result from deep burial as suggested by Petmecky et al. (1999) for the area further east. In this case, the coalification isolines of the Upper Jurassic should indicate the palaeo-contours of the Lower Saxony Basin at the time of maximum burial before inversion. The different configurations of the coalification isolines at the centre of the basin should suggest fluctuations in thickness of the sequences deposited between the Late Jurassic and Late Cretaceous rather than differences in heat flows during the time of maximum temperatures (see below). For example, strong subsidence and high sedimentation rates have to be assumed for the Wiehengebirge Flexure Zone, which has been interpreted as a swell during Late Jurassic times (Klassen 1991, Baldschuhn et al. 2001).

2.6.2. Thermal modelling: the Ibbenbüren area (southern LSB margin)

A series of simulation runs were carried out for individual wells. Calibration was based on a comparison of measured vitrinite reflectance data and calculated vitrinite reflectance applying the EASY%Ro algorithm (Sweeney and Burnham 1990). This method has been successfully used for calibration purposes and is applicable for maturation values as high as 4.6%VRr. In the study area, some vitrinite reflectance values are, however, higher than 4.6%VRr. These values were integrated into the calculated vitrinite reflectance trend by extrapolating the calculated curve.

In the Ibbenbüren area at the southern border of the LSB, Carboniferous rocks which are in the low volatile bituminous coal/antracite rank (about 2% vitrinite reflectance VRr) are mined close to the surface. Reasons for this high coalification level have been a matter of debate. Based on numerical basin modelling techniques described above, the contrasting theories about deep burial by 8000m of overburden (Baldschuhn and Kockel 1999) and high geothermal gradients corresponding high heat flows of 155mW/m² (Buntebarth 1985) were tested. Firstly, a best fit model was developed, and calibrated by the vitrinite reflectance depth trend which is of high quality for the coal-bearing sequence drilled in Ibbenbüren. The greatest problem for thermal modelling of the Ibbenbüren area is the time gap from the Westphalian until recent times, which is not documented by any sedimentary rocks (Figure 2.6a). This time gap permits many different models explaining the high thermal maturity, i.e. maximum temperatures could have been reached at any time between the Late Carboniferous and the Late Cretaceous. However, the close proximity to the Bramsche area in the north and the Münsterland Block in the south suggests that maximum temperatures are either due to Permo- Carboniferous events or to Late

Table 2.3: Lithological composition and physical rock properties assigned to layers used in simulation.

well	Sand/S.congl. [%]	Silt/sandy [%]	Shale [%]	Marlstone [%]	Limestone [%]	Dolomite [%]	Anhyd./Gyps. [%]	Salt [%]	Coal [%]	Compressibility		Matrix Thermal Conductivity		Matrix Heat Capacity	
										[1/10 GPa]	Max	[W/mK]	20°C	100°C	[cal/gK]
well D										Min	Max	20°C	100°C	20°C	100°C
Quaternary	100	-	-	-	-	-	-	-	-	10.0	500.0	3.12	2.64	0.178	0.209
Eocene	8	7*	52	33	-	-	-	-	-	10.0	36249.0	1.86	1.78	0.210	0.255
Hauterivian	-	-	50	50	-	-	-	-	-	10.0	51961.5	1.72	1.65	0.213	0.258
Vaianginian	-	-	50	50	-	-	-	-	-	10.0	51961.5	1.72	1.65	0.213	0.258
Wealden	-	-	50	43	6	-	-	-	-	10.0	37296.0	1.77	1.69	0.211	0.256
Upper Malm	-	-	45	44	-	6	5/	-	-	8.9	23526.7	1.91	1.80	0.210	0.253
Kimmeridgian	-	-	-	-	60	40	-	-	-	10.0	184.0	3.19	2.80	0.198	0.225
Dogger	6	-	50	39	5	-	-	-	-	10.0	32311.6	1.84	1.75	0.210	0.255
Lias	5	-	57	33	5	-	-	-	-	10.0	34323.9	1.88	1.79	0.211	0.255
Upper-Mid Keuper	50	-	25	25	-	-	-	-	-	10.0	9936.1	2.11	1.95	0.202	0.243
Lower Keuper	8	-	58	34	-	-	-	-	-	10.0	41278.2	1.84	1.76	0.211	0.256
Upper Muschelk.	-	-	-	46	54	-	-	-	-	10.0	348.9	2.54	2.34	0.201	0.235
Mid Muschelk.	-	-	-	15	13	2	2/	68	-	2.0	15.8	4.46	3.84	0.204	0.219
Lower Muschelk.	-	-	-	47	43	-	-	-	-	10.0	335.9	2.56	2.36	0.201	0.235
Upper Bunter	-	-	-	-	-	-	2/	98	-	1.0	4.3	5.65	4.73	0.206	0.212
Mid Bunter	27	26	24	23	-	-	-	-	-	10.0	9010.2	2.14	1.98	0.202	0.243
Lower Bunter	-	22	36	33	9	-	-	-	-	10.0	14889.1	1.98	1.86	0.206	0.248
Zechstein	-	-	8	-	2	-	44/	46	-	1.3	9.3	4.79	4.03	0.192	0.206
New Red	-	50*	50*	-	-	-	-	-	-	10.0	11619.0	2.24	2.11	0.203	0.245
Westphalian D/C	/11	52	37	-	-	-	-	-	-	10.0	3192.6	2.43	2.21	0.197	0.236

Table 2.3 (cont.).

well	Sand/S.congl. [%]	Silt/sandy [%]	Shale [%]	Marlstone [%]	Limestone [%]	Dolomite [%]	Anhyd./Gyps. [%]	Salt [%]	Coal [%]	Matrix Density [kg/m ³]	Compressibility [1/10 GPa]		Matrix Thermal Conductivity [W/mK]		Matrix Heat Capacity [cal/gK]	
											Min	Max	20°C	100°C	20°C	100°C
well E																
Tertiary	-	14 *	86	-	-	-	-	-	-	2678.0	10.0	46004.9	2.02	1.94	0.211	0.256
Aptian	-	-	54	46	-	-	-	-	-	2667.5	10.0	51961.5	1.72	1.65	0.213	0.258
Barrémian	-	-	39	61	-	-	-	-	-	2674.2	10.0	4417.3	1.90	1.81	0.210	0.252
Hauteriv./Niagan.	-	-	23	77	-	-	-	-	-	2660.0	10.0	47665.1	1.59	1.52	0.212	0.258
Wealden	-	-	92	-	-	-	-	-	8 (sh.)	2663.5	10.0	54112.5	1.96	1.88	0.212	0.257
Upper Malm	-	-	86	-	5	9	-	-	-	2704.8	7.9	17439.4	2.24	2.11	0.209	0.250
Upper Kimmeridgian	-	-	93	-	1	6	-	-	-	2690.5	8.7	31736.9	2.10	2.00	0.210	0.254
Mid-Lower Kimmdg.	1	-	94	-	5	-	-	-	-	2681.3	10.0	42389.3	2.02	1.94	0.212	0.256
Bathonian	3	-	-	97	-	-	-	-	-	2655.1	10.0	39317.4	1.53	1.46	0.211	0.257
Bajocian	-	3	97	-	-	-	-	-	-	2679.6	10.0	54096.5	2.00	1.92	0.212	0.257
Upper Bunter	-	-	48	-	-	-	10	42	-	2478.6	3.0	404.2	3.37	3.02	0.206	0.232
Mid - Lower Bunter	-	39	61	-	-	-	-	-	-	2673.8	10.0	13048.3	2.32	2.17	0.203	0.244
Zechstein 4-2	-	-	5	-	-	-	22	73	-	2216.8	1.1	5.6	4.03	3.48	0.237	0.247
Zechstein 1	-	-	-	-	13	87	-	-	-	2847.9	1.4	7.4	4.64	3.85	0.178	0.195
New Red-Carbonif.	93	7	-	-	-	-	-	-	-	2660.0	10.0	500.0	3.12	2.64	0.178	0.209
well F																
Quaternary	68	-	29	3	-	-	-	-	-	2666.0	10.0	2102.4	2.72	2.40	0.189	0.224
Tertiary	91	-	-	9	-	-	-	-	-	2662.5	10.0	615.1	3.03	2.59	0.181	0.213
Münder Marl	-	-	17	-	-	-	10/13	60	-	2331.4	1.5	17.8	3.75	3.25	0.222	0.237

Table 2.3 (cont.).

well	Sand/S.congl. [%]	Silt/sandy [%]	Shale [%]	Marstone [%]	Limestone [%]	Dolomite [%]	Anhyd/Gyps. [%]	Salt [%]	Coal [%]	Matrix Density		Compressibility		Matrix Thermal Conductivity		Matrix Heat Capacity	
										[kg/m ³]	[1/10 GPa]	Min	Max	20°C	100°C	20°C	100°C
Eimb. Limest.	-	-	-	38	-	-	4/58	-	-	2442.0	2.5	110.1	1.51	1.42	0.293	0.320	
Gigas-Fm.	-	-	28	72	-	-	-	-	-	2662.5	10.0	49056.2	1.63	1.56	0.212	0.258	
Upper Kimmeridgian	-	2	6	92	-	-	-	-	-	2656.8	10.0	44228.9	1.54	1.47	0.212	0.258	
Mid Kimmeridgian	16	-	-	84	-	-	-	-	-	2655.8	10.0	21904.5	1.69	1.58	0.207	0.250	
Bathonian	12	-	-	88	-	-	-	-	-	2655.6	10.0	26224.3	1.64	1.54	0.208	0.252	
well G																	
Upper Malm	-	-	23	61	-	-	16	-	-	2690.5	7.1	11933.7	1.91	1.79	0.207	0.248	
Kimmeridgian	7	2	43	48	-	-	-	-	-	2665.5	10.0	32193.2	1.80	1.71	0.209	0.253	
Oxfordian	68	3	-	29	-	-	-	-	-	2658.5	10.0	1928.6	2.50	2.20	0.188	0.224	
Dogger	-	-	49	51	-	-	-	-	-	2667.5	10.0	51961.5	1.72	1.65	0.213	0.258	
Lias	-	-	93	7	-	-	-	-	-	2678.8	10.0	59143.1	1.95	1.86	0.213	0.258	
Upper Keuper	38	4	58	-	-	-	-	-	-	2672.0	10.0	8940.5	2.37	2.17	0.189	0.238	
Mid Keuper	-	-	77	17	-	-	6	-	-	2684.8	8.9	35530.9	1.99	1.90	0.211	0.255	
Lower Keuper	-	16	84	-	-	-	-	-	-	2677.8	10.0	35747.2	2.06	1.97	0.210	0.254	
Upper Muschelk.	-	-	-	63	34	3	-	-	-	2702.5	10.0	462.8	2.49	2.31	0.203	0.238	
Mid Muschelk.	-	-	-	-	-	-	76	24	-	2684.4	1.0	4.0	5.01	4.15	0.182	0.195	
Upper Bunter	-	-	-	78	-	-	-	22	-	2556.0	6.3	6966.0	1.96	1.82	0.211	0.249	
Mid Bunter	-	-	100	-	-	-	-	-	-	2680.0	10.0	60000.0	1.98	1.91	0.213	0.258	
Lower Bunter	39	61	-	-	-	-	-	-	-	2667.3	10.0	2713.2	2.48	2.25	0.192	0.229	
Zechstein	-	-	-	-	-	4	36	60	-	2435.4	1.1	4.7	5.27	4.39	0.194	0.204	
Westphalian D	68/1	17	13	-	-	-	-	-	1	2654.6	10.0	1486.7	2.73	2.39	0.186	0.221	

Table 2.3 (cont.).

well	Sand/s.congl. [%]	Silt/sandy [%]	Shale [%]	Marlstone [%]	Limestone [%]	Dolomite [%]	Anhyd./Gyps. [%]	Salt [%]	Coal [%]	Matrix Density [kg/m ³]	Compressibility [1/10 GPa]		Matrix Thermal Conductivity [W/mK]		Matrix Heat Capacity [cal/gK]	
											Min	Max	20°C	100°C	20°C	100°C
well I																
Mid Muschelk.	-	12	10	-	24	-	54/	-	-	2788.4	2.9	65.9	3.65	3.15	0.187	0.212
Lower Muschelk.	-	-	-	5	95	-	-	-	-	2708.9	10.0	164.4	2.80	2.54	0.196	0.224
Upper Bunter	-	-	54	-	-	-	46/	-	-	2758.2	3.5	719.7	2.98	2.67	0.195	0.226
Mid Bunter	9	47	44	-	-	-	-	-	-	2675.8	10.0	21430.3	2.08	1.97	0.208	0.252
Lower Bunter	-	13	87	-	-	-	-	-	-	2678.1	10.0	38302.7	2.05	1.96	0.210	0.254
Zechstein	-	-	5	-	-	17	45/	33	-	2611.4	1.7	13.1	4.67	3.92	0.191	0.207
Westphalian D	/1	75	24	-	-	-	-	-	-	2668.6	10.0	4275.7	2.43	2.21	0.197	0.236
well K																
Quaternary	/71	-	-	29	-	-	-	-	-	2660.7	10.0	1372.7	2.41	2.20	0.192	0.229
Miocene	-	20	-	80	-	-	-	-	-	2657.0	10.0	23895.8	1.67	1.57	0.208	0.252
Oligocene	-	20	-	80	-	-	-	-	-	2657.0	10.0	23895.8	1.67	1.57	0.208	0.252
Upper Eocene	/1	7	-	92	-	-	-	-	-	2655.8	10.0	34328.4	1.57	1.49	0.210	0.256
Lower Eocene	-	-	-	100	-	-	-	-	-	2655.0	10.0	45000.0	1.50	1.43	0.212	0.258
Hettg./Sinem.	-	-	99	1	-	-	-	-	-	2679.8	10.0	59827.6	1.97	1.90	0.213	0.258
Upper Keuper	-	77	23	-	-	-	-	-	-	2668.4	10.0	4203.5	2.43	2.21	0.197	0.236
Mid Keuper	-	2	-	83	12	-	3/	-	-	2687.9	9.3	1409.3	2.18	2.05	0.207	0.246
Lower Keuper	-	-	71	-	29	-	-	-	-	2685.8	10.0	15388.4	2.12	2.02	0.210	0.252
Upper Muschelk.	-	-	-	34	66	-	-	-	-	2702.2	10.0	280.0	2.61	2.40	0.199	0.231
Mid Muschelk.	-	-	-	18	5	45	32/	-	-	2801.6	4.8	165.2	3.42	2.94	0.194	0.221

Table 2.3 (cont.).

well	Sand/S.congl. [%]	Silt/sandy [%]	Shale [%]	Marlstone [%]	Limestone [%]	Dolomite [%]	Anhyd/Gyps. [%]	Salt [%]	Coal [%]	Matrix Density [kg/m ³]		Compressibility [1/10 GPa]		Matrix Thermal Conductivity [W/mK]		Matrix Heat Capacity [cal/gK]	
										Min	Max	20°C	100°C	20°C	100°C	20°C	100°C
Lower Muschelk.	-	-	-	10	76	14	-	-	-	2722.1	10.0	285.0	2.77	2.49	0.198	0.227	
Upper Bunter	-	-	84	13	3	-	-	-	-	2677.4	10.0	50208.3	1.92	1.85	0.213	0.257	
Mid Bunter	-	34	63	-	2	-	1/	-	-	2677.4	9.8	15533.1	2.19	2.06	0.205	0.247	
Lower Bunter	-	18	82	-	-	-	-	-	-	2674.9	10.0	17481.4	2.12	2.00	0.207	0.250	
Zechstein	-	-	11	-	2	1	58/	28	-	2635.2	1.4	12.9	4.51	3.81	0.168	0.204	
Westphalian D	40/1	15	44	-	-	-	-	-	-	2672.9	10.0	11380.6	2.23	2.08	0.203	0.245	
well L																	
Westphalian D	49/1	47	3	-	-	-	-	-	-	2668.7	10.0	4069.8	2.35	2.16	0.197	0.236	
Westphalian C	59/5	-	34	-	-	-	-	-	2	2650.3	10.0	6126.9	2.30	2.11	0.199	0.239	
Westphalian B	43	30	25	-	-	-	-	-	2	2651.1	10.0	7544.1	2.21	2.05	0.200	0.241	

* mixed with volcanic material

Cretaceous events (Leischner et al. 1993, Petmecky et al. 1999, Littke et al. 2000).

An excellent visual fit between measured and calculated vitrinite reflectance data was achieved by applying a heat flow of 70mW/m² and a thickness of eroded sedimentary rocks of 4400m (Figure 2.6b). In this model, maximum burial took place during the Late Cretaceous. A maximum burial during Late Carboniferous/ Early Permian times would yield a satisfactory fit as well, but would require deposition of more than 4400m of additional Stephanian/ Upper Permian rocks. This thickness is far greater than that derived for the adjacent Münsterland Block (2800m, Büker et al. 1995, Littke et al. 2000), where maximum burial occurred during latest Carboniferous/ Early Permian. Accordingly, such a scenario of maximum temperatures during the Carboniferous/Permian is not probable for the Ibbenbüren area.

Table 2.3 (cont.).

standard lithologies	Matrix Density	Compressibility		Matrix Thermal Conductivity		Matrix Heat Capacity	
	[kg/m ³]	[1/10 GPa]		[W/mK]		[cal/gK]	
		Min	Max	20°C	100°C	20°C	100°C
Sandstone	2660.0	10.0	500.0	3.12	2.64	0.178	0.209
Siltstone	2672.0	10.0	8000.0	2.14	2.03	0.201	0.242
Shale	2680.0	10.0	60000.0	1.98	1.91	0.213	0.258
Marlstone	2687.0	10.0	940.0	2.23	2.11	0.208	0.248
Limestone	2710.0	10.0	150.0	2.83	2.56	0.195	0.223
Dolomite	2836.0	10.0	250.0	3.81	3.21	0.202	0.229
Anhydrite	2850.0	1.0	4.0	5.69	4.76	0.206	0.212
Gypsum	2300.0	1.0	2.0	1.51	1.41	0.347	0.361
Salt	2160.0	1.0	4.0	5.69	4.76	0.206	0.212
Coal	1680.0	10.0	130000.0	0.50	0.46	0.204	0.248

The thickness of the Permian-to-Jurassic pile was deduced from the thickness in adjacent areas, especially from the Teutoburger Wald area (GK 25 Tecklenburg). In addition, 2130m of Cretaceous sedimentary rocks had to be assumed for the Ibbenbüren area in order to obtain a perfect visual fit. Lithologies were also selected based on those from the adjacent areas; as no great thicknesses of coal or salt exist (which have a great effect on thermal conductivity). As no thick claystone sequences are involved (which bear some uncertainty with respect to compaction), the results on heat flow and thickness of eroded sedimentary rocks are regarded as well constrained.

Alternative models were tested by using i) the assumption of very deep burial for the Ibbenbüren area (8000m, Baldschuhn and Kockel 1999) and ii) the assumption of very high Late Cretaceous heat flows (155mW/m², Buntebarth 1985). In the first case, a very low heat flow of 40mW/m² had to be applied to gain any match (Figure 2.6c). However, even with this unrealistic scenario, the shape of the calculated trend line differs very much from that of the trend line for measured vitrinite reflectance data. Furthermore, the influence of a possible thermal (magmatic) event on the maturity pattern during the early Late Cretaceous was investigated by increasing heat flow values up to 155mW/m² (Buntebarth 1985) during that time. If this high heat flow is combined with the assumption of an eroded thickness of 4000m, calculated vitrinite reflectance values of 4% for surface sediments result, increasing extremely with depth. These values are far too high. In order to obtain a fit for the uppermost sedimentary rocks, a much lower rate of erosion of 2220m was applied (Figure

2.6d). In this scenario, a fit between measured and calculated vitrinite reflectance data could be achieved for the uppermost sedimentary rocks only, but the reflectance gradient is completely different from that displayed by the real maturity data. Accordingly, both the high heat flow and the extreme burial hypotheses have to be discarded.

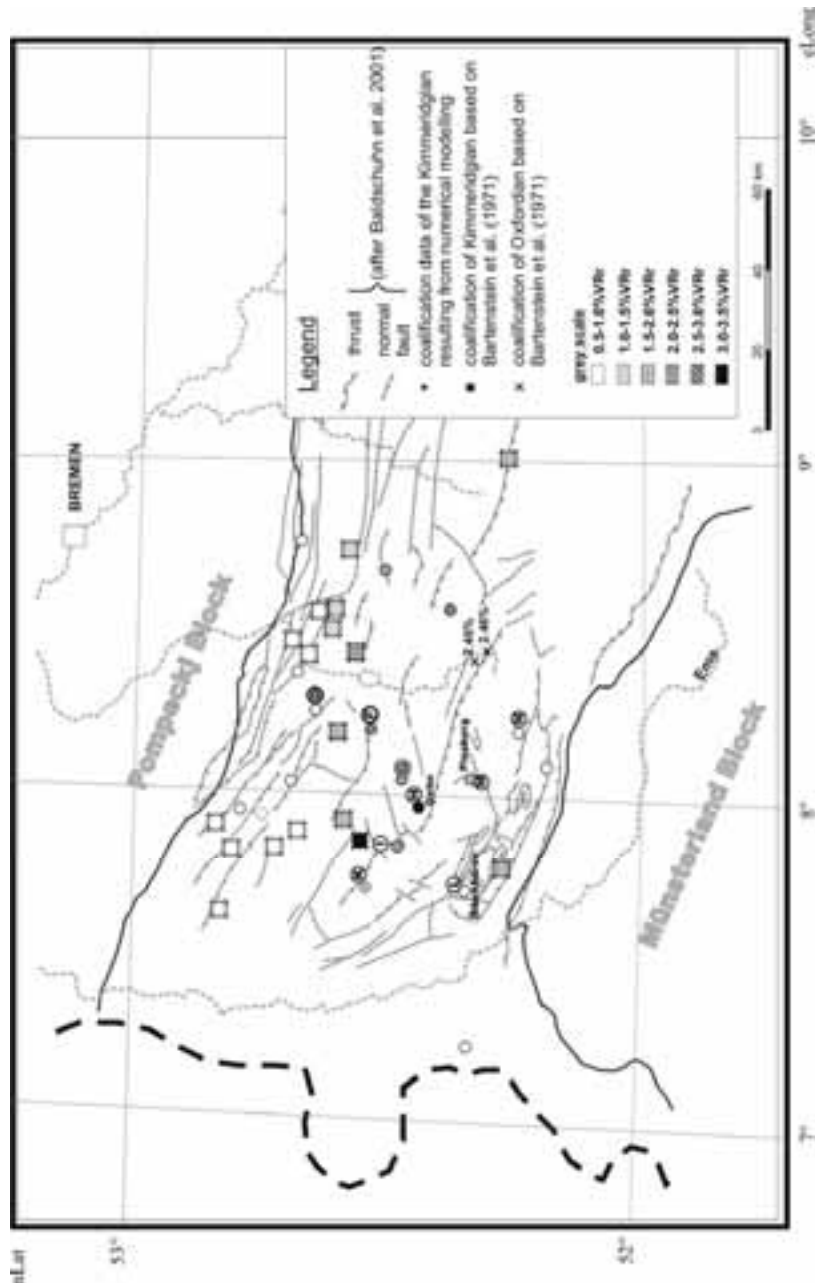


Figure 2.5: New coalification map for the Upper Jurassic with major tectonic structures. Maturity information is based on vitrinite reflectance measurements and subsequent calculations using numerical modelling techniques as described in the text.

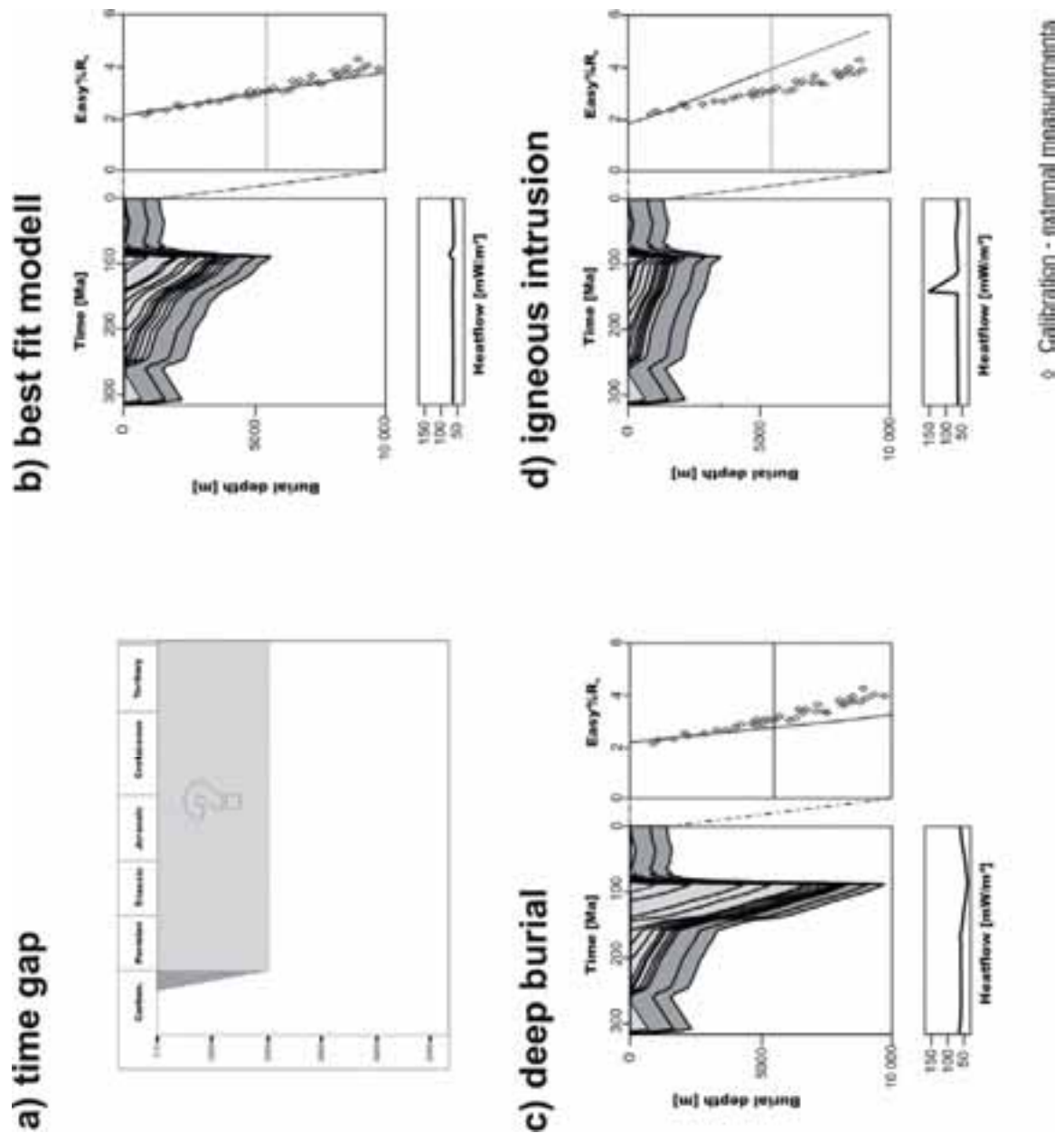


Figure 2.6: Results of numerical modelling for the Ibbenbüren area near the southern border of the LSB. a) shows the time gap in the sedimentary sequence; b) shows the best fit model with a former, now eroded overburden of 4407m and a heat flow of 70mW/m²; in c) the theory of an additional overburden of 8000m after Baldschuhn and Kockel (1999) is tested and d) depicts the assumption of an igneous intrusion (after Buntebarth 1985) with a heat flow of 155mW/m² and additional overburden of 2217m.

2.6.3. Thermal modelling: the Bramsche area (central LSB)

Well G serves as an example for the thermal history in the central part of the maturity anomaly of the LSB (Figure 2.2). This well penetrated a succession of Upper Jurassic to Carboniferous (Westphalian D) sedimentary rocks and reached a final depth of 3644m. Vitrinite reflectance values measured on organic-matter-bearing shales increase with depth from 2.6 to 4.6%VRr (Table 2.1, Figure 2.2). These values imply that the organic material reached the meta-anthracitic stage and experienced temperatures exceeding 250°C. At such high maturity levels, it becomes extremely difficult to distinguish primary and secondary organic particles such as vitrinite, inertinite, and solid bitumen. Moreover, in well G vitrinite reflectance is also influenced by dispersed hydrothermal microveins. In this study, thermally altered vitrinites were found within hydrothermal quartz showing reflectance values of more than 13%. Thus, the hydrothermal alteration took place at temperatures much higher than 480°C and might have also influenced the reflectance pattern in the vicinity of the veins. Such circumstances cause a larger scatter of vitrinite reflectance at great depths; e.g. Teichmüller et al. (1979) measured vitrinite reflectance values of 5.1-5.8%VRr for the Upper Carboniferous which are higher than those determined by other authors. Clearly, the quality of maturity data for well G is not as excellent as in the case of the Ibbenbüren area. However, the effect on the calibrated numerical models, e.g. on calculated eroded thickness and heat flow during times of maximum temperatures is not very large.

Cretaceous sedimentary rocks are missing in the central part of the LSB around well G (Figure 2.7a) but are preserved in more marginal parts of the LSB. Cumulative thickness of preserved Cretaceous sedimentary rocks in the vicinity of the area is about 3300m. This value gives a first indication on eroded sediment thickness, but may be misleading, because the layer thickness can increase significantly towards the basin centre (e.g. Petmecky et al. 1999). A good fit between measured and calculated reflectance was achieved assuming a heat flow of 63mW/m² during maximum burial. Furthermore, the now eroded overburden has a thickness of 3985m (Cretaceous: 3825m) according to the best fit model (Figure 2.7b). This eroded thickness was attributed to Tithonian-Coniacian sedimentary rocks (see Figure 2.7a) and is about 1660m higher than the thickness of the same stratigraphic interval calculated for adjacent areas (2330m in the Ibbenbüren area). Accordingly, a maximum heat flow/minimum erosion scenario and a minimum heat flow/maximum erosion scenario were created. According to these alternative models, a heat flow of at least 60mW/m² and at most 65mW/m² can be assumed to have occurred during the time of maximum temperature and maximum burial, i.e. during the early Late Cretaceous. These values are in any case far lower than heat flows resulting from a large igneous intrusion (100-200mW/m²; Poelchau et al. 1997). Furthermore, the minimum thickness of eroded Cretaceous sedimentary rocks is

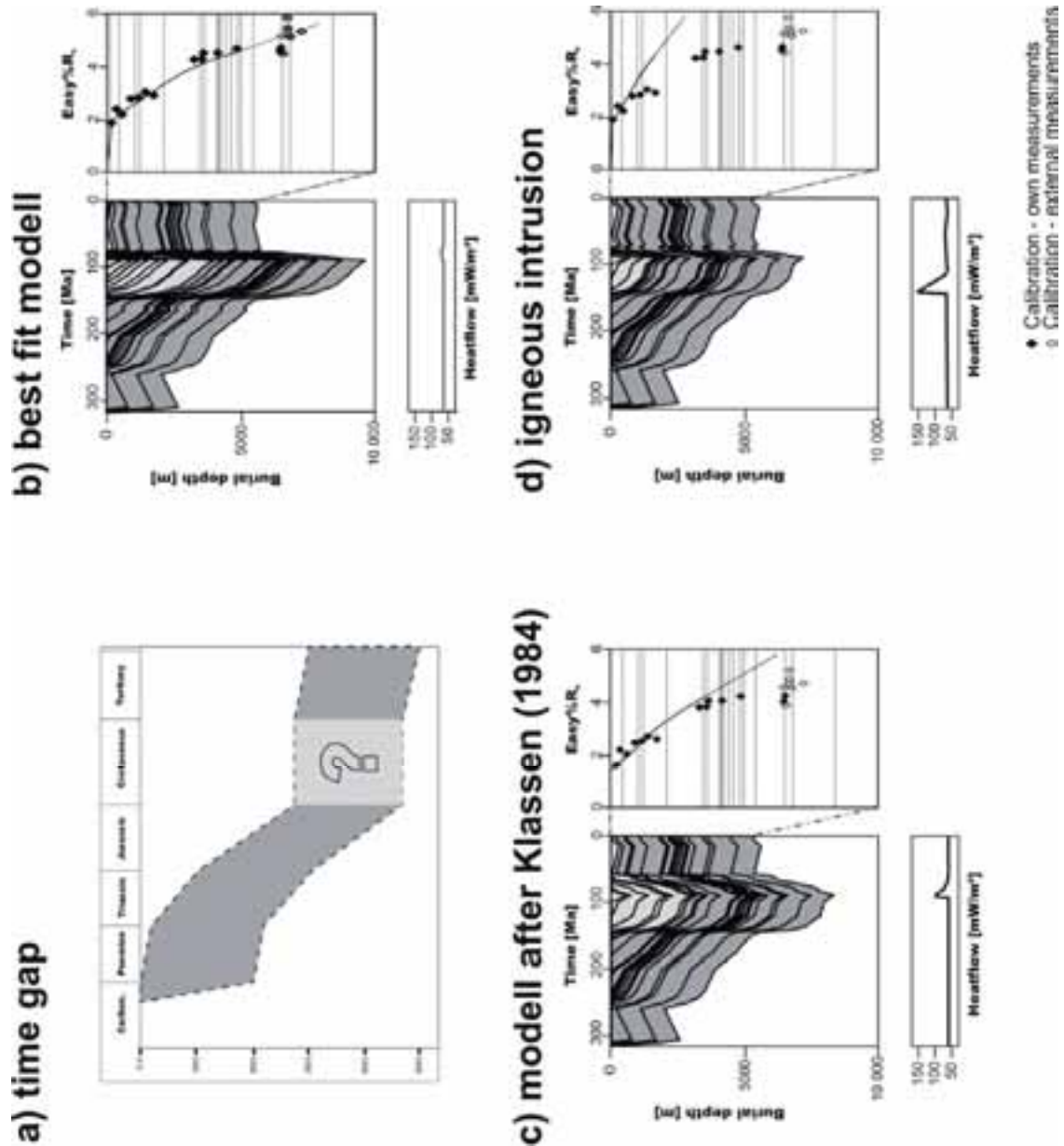


Figure 2.7: Results of numerical modelling for the Bramsche area in the center of the LSB. a) time gap in the sedimentary sequence between Late Jurassic and Tertiary for this area; b) best fit model for Well G with a heat flow of 63mW/m^2 and a former overburden of 3985m ; c) no fit achieved with a cumulative former overburden thickness of only 2960m (after Klassen 1984); d) no fit achieved with assumptions of high heat flow due to an igneous intrusion (heat flow of 155mW/m^2).

3725m and the maximum thickness is 3925m (including the Mnder Marl Formation). These values indicate that, similarly to the southern margin of the LSB further east, huge sedimentation followed by erosion affected the central/southern LSB. Additionally, alternative models with i) a former overburden thickness of only 2960m (according to Klassen 1984, Figure 2.7c) and ii) an intrusive model with heat flows of 155mW/m² (Figure 2.7d) during the early Late Cretaceous were tested. In both cases, a fit between measured and calculated vitrinite reflectance data could be achieved for the uppermost sedimentary rocks only and not for the deeper strata because the calculated vitrinite reflectance-depth gradient differs significantly from the measured gradient.

2.6.4. Thermal modelling: the northern LSB margin

In the northern part of the LSB, the missing stratigraphic section is much smaller than in the central and southern areas; e.g. in well D only the Valanginian to Eocene section is missing (Figure 2.8a). Good calibration data are available for this well from the Hauterivian to the Carboniferous interval allowing a valid maturity trend to be established (Figure 2.8b). This trend can be modelled with a heat flow of 60mW/m² during maximum temperature/maximum burial and a thickness of eroded Cretaceous sedimentary rocks of only 1275m. Results indicate that only the central part of the LSB was a deep depocenter during Early Cretaceous and early Late Cretaceous times, whereas the southern and northern margins were areas of moderate subsidence.

2.6.5. Thermal modelling: synthesis of results, and general discussion

The modelling technique described above was applied to a total of six wells and two pseudowells in the study area. The concept of pseudowells is described in detail in Noeth et al. (2001). Results are summarized in Figures 2.9 and 2.10 as well as Table 2.4.

In the best-fit models calibrated by vitrinite reflectance data, palaeo-heat flows of 60 to 70mW/m² had to be assumed for the time of maximum burial and temperature (early Late Cretaceous). This combination exceeded and overwhelmed the thermal effect of the volcanic event during Rotliegend times. After Bodri and Bodri (1985), the heat flow data for the time of maximum burial imply a crustal thickness of 31 to 35.5km. For some areas such as the Piesberg, only maturity information from surface outcrops was available, and no vitrinite reflectance-depth profile. In this case, heat flow results from the closest well were used as input data in the modelling; in these cases, only the eroded thickness is a modelling result and not the heat flow. It should also be noted that in general only heat flow during time of maximum temperature (Late

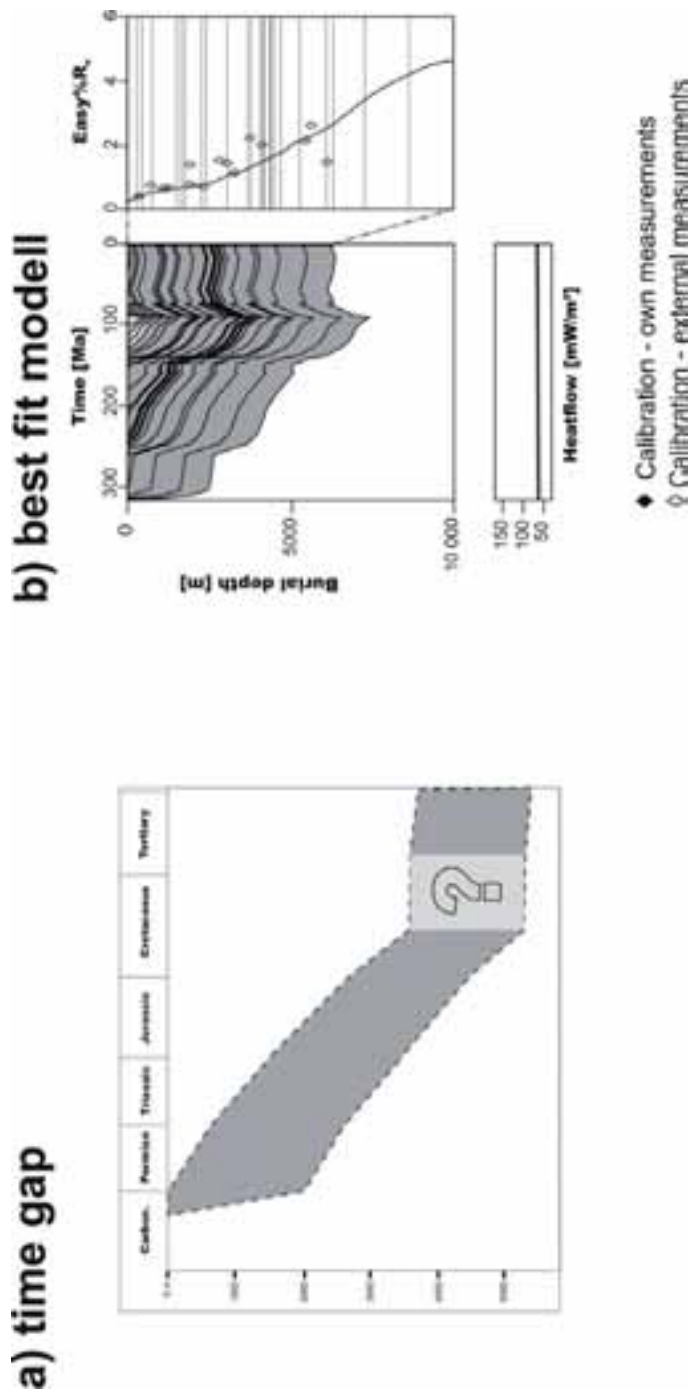


Figure 2.8: Result of numerical modelling for the northern part of the LSB. a) time gap between the Valanginian and Tertiary; b) best fit model with a former overburden of 1275m and a heat flow of 60mW/m².

Cretaceous) may be derived from modelling, because vitrinite reflectance is mainly affected by the maximum temperature reached during burial.

Accordingly, periods during which temperatures were by more than 20-30°C below the maximum temperature hardly affected vitrinite reflectance values (Burnham and Sweeney 1989, Barker and Pawlewicz 1994). Therefore, considering only vitrinite data, there are only few constraints on heat flow evolution during Pre-Cretaceous times, other than the exclusion of exceptionally high vitrinite reflectance modifying “thermal spikes”. For the latest Cretaceous and Tertiary, it seems to be reasonable to assume heat flows of about 60-70mW/m² which are similar both to the modelled Cretaceous heat flows and the present-day heat flows (Haenel 1980).

The resulting heat flows during maximum burial and temperature in the Cretaceous show a slightly increasing trend towards the south and a regional maximum in the area of Ibbenbüren and Osnabrück. Increasing heat flows are associated with periods of lithospheric stretching and thinning as well as asthenospheric rise (Yalcin

et al. 1997). Correlation of heat flow variation and crustal thickness would allow suggesting a crustal-thinning event from the northern margin (35.5km) towards the southern basin (31km). After Allen and Allen (1990), this is in accordance with an active syn-rift event in an extensional basin. The calculated average temperature gradient for the upper 5-8 kilometres of the crust during time of maximum burial varied between 43°C/km on the margins and 47°C/km in the centre of the basin. Thus, the palaeotemperatures at the top of the Carboniferous during maximum burial varied between 207°C (southern margin) and 224°C (northern margin), reaching up to 375°C in the centre of the study area.

All modelled Cretaceous heat flow values are in the range of normal continental heat flows and also in the range of heat flows currently present in the study area. None of the modelling results are in accordance with coalification being due to a magmatic intrusion. This conclusion does, however, not exclude the presence of a deep-seated intrusion. Such an intrusion would not necessarily have had any influence on the maturation pattern. For example, it could be of Permian age, for which large-scale extension in the Central European Basin system is postulated; in this case, it would have affected the deep-lying Pre-Permian rocks only, but the effect on the uppermost Carboniferous units, lying close to the Earth's surface at that time, would have been small. This small additional maturation would have been later overprinted by deep burial during the Cretaceous. In summary, the present-day coalification pattern with anthracitic organic matter outcropping at the surface may well be explained by deep burial of the strata.

Best-fit models also reveal a cumulative thickness of eroded sedimentary rocks between 1275m (northern margin) and 7270m (Piesberg area). The latter value is similar to that favoured by Füchtbauer and Müller (1970), who estimated 8000m of erosion based on compaction of Carboniferous sandstones cropping out at the Piesberg. Reconstructed rates of erosion would have been 0.53mm/a on the top of the broadly anticlinal Nordwestfalen-Lippe Swell and 0.091mm/a on its northern margin [for comparison: Eastern Himalaya: erosion of 2.9mm/a; Western Himalaya: 1mm/a (Galy and France-Lanord 2000)]. These erosion rates are based on the assumption of continuous erosion at constant rates between the onset of uplift (Coniacian; about 89Ma ago) and the end of Santonian times. In reality, erosion rates were certainly variable, reaching much higher values over short times. The numbers above do, however, demonstrate that no exceptionally high erosion rates have to be assumed for this area. Accommodation space for the eroded sediments was available towards the south in the Münsterland Block area and towards the north in the area of the Pompeckj Block which both were subsiding during Late Cretaceous times.

In order to construct burial history curves, information on eroded thickness for individual stratigraphic successions was deduced from data on the thickness of geological formations still preserved in other wells within the LSB or in outcrop

areas at its southern margin. The thickness of eroded Cretaceous units was calculated from the difference between modelled cumulative eroded thickness and the thickness of all eroded Pre-Cretaceous units (see Table 2.4). This calculation resulted in up to 4230m of eroded Cretaceous sedimentary rocks (including the Upper Münders Marl; see Table 2.4) and up to 5150m of eroded Cretaceous plus Upper Jurassic rocks. The highest values were deduced for the Gehn area near Bramsche.

For the Late Jurassic and Cretaceous, a very high thickness results in the central LSB, e.g. at well G or in the Piesberg area. A much lower thickness is calculated for these stratigraphic units at the northern and southern margins (wells D, L, N), whereas the adjacent Münsterland Block and Pompeckj Block were uplifted during this period. The differences of eroded thicknesses represent variable synsedimentary subsidence within the LSB during Late Jurassic and Early Cretaceous times. Two different scenarios can explain the subsidence pattern.

Table 2.4: Modelled, now eroded, former overburden and calculated heat flow values for wells in the LSB.

Well	D	G	H pseudowell	I	K	L	M pseudowell	N
Heat flow [mW/m ²]	60	63	65	60	60	70	70	70

Former overburden thickness in [m] (in parentheses the preserved thickness)

Total:	1275	3985	5150	5905	5525	4407	7266	4417
kro	525	525	525	525	525	600	525	600
kru	750 (298)	1650	1650	1650	1650	1360	1950	1410
Berriasian		1650	2050	1700	1650	170	1850	750
jo		160 (590)	925 (75)	750	750	500	800	500
jm				450	450	260	490	260
ju				750	500 (248)	440	625	440
k				80 (230)		225	300	225
m						152	150	152
s						500	400	80 (377)
z						200	176	

The first simpler possibility is a classical, roughly E-W trending extensional basin, with the Pompeckj Block and the Münsterland Block acting as graben shoulders of the LSB, which were uplifted by at least several hundred metres during Late Jurassic/Earliest Cretaceous times. In this case, secondary half-graben and graben systems should follow the trend of the basin. The same can

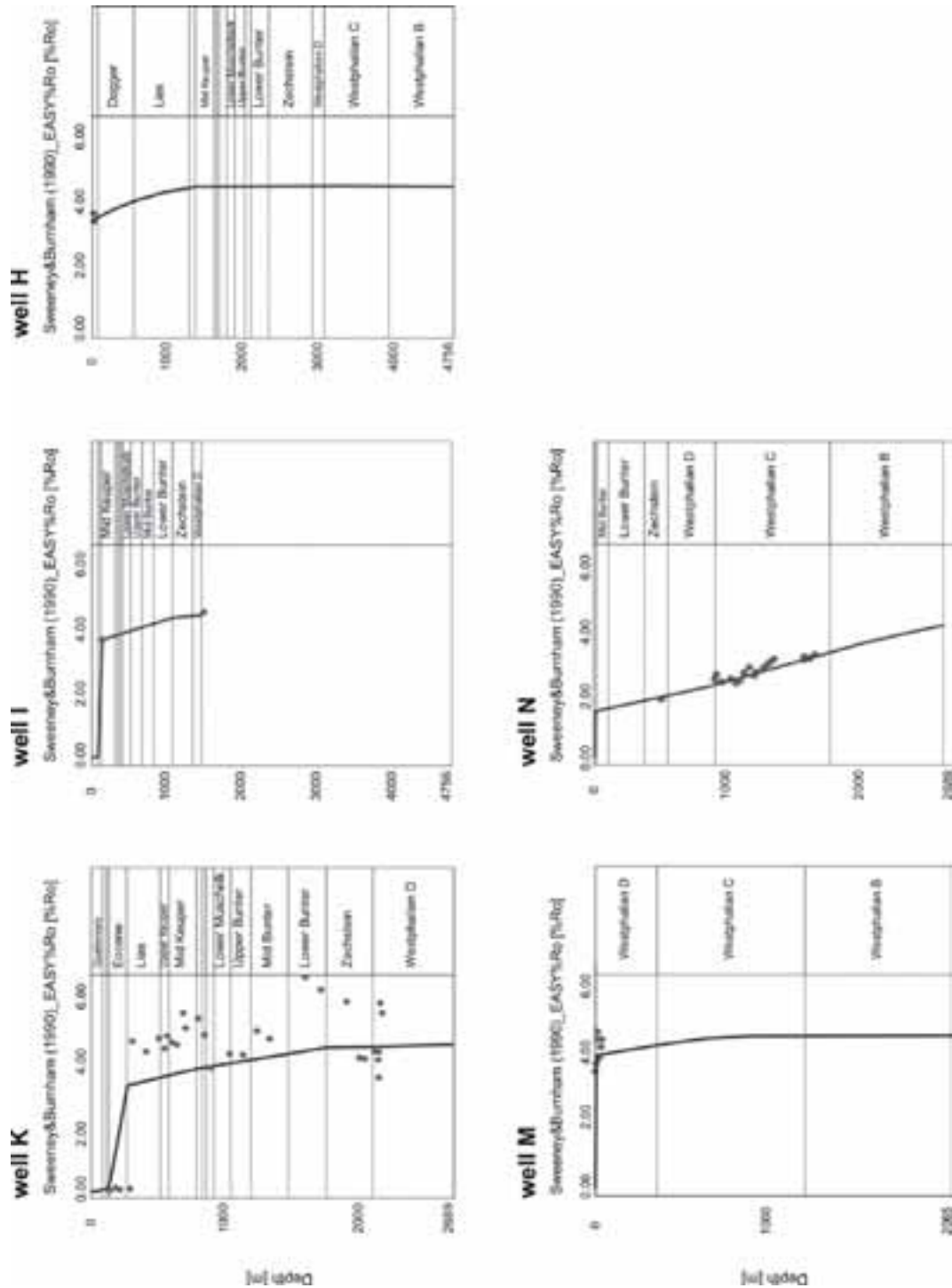


Figure 2.9: Vitrinite reflectance calibration for different wells within the Lower Saxony Basin with the algorithm of Sweeney and Burnham (1990).

be imagined for the general trend of the isolines of coalification, as may be seen in the eastern area of Figure 2.2, if a secondary structure was formed homogeneously within a short time over its whole length. However, this is not necessarily always the case. The main gradient of coalification (within one layer) should generally be oriented perpendicularly to the basin direction and should display sudden changes near the boundary faults of secondary grabens or half-grabens, but only small changes along strike. Resulting differences in maturity can be explained by a normal as by an asymmetric basin fill.

The main boundary faults of the basin in this configuration however, do not trend E–W, but WNW–ESE and display in some places an en-echelon pattern, indicating the involvement of a shear component in the formation of the basin. Therefore, a second, but more complicated model must be considered as well.

The alternative possibility is a pull-apart basin created due to horizontal movements between Pompeckj Block/LSB and LSB/Münsterland Block. In such a context, the fracture pattern may include master faults with associated syn- and antithetic strike-slip faults as well as additional normal faults or thrusts in specific orientations, resulting in a strongly differentiated and asynchronous basin fill (see e.g. the Variscan Saar-Nahe Basin, Hertle and Littke 2000).

Variations in synsedimentary subsidence are observed especially near the tips of strike-slip faults, where small lateral offsets may lead to considerable vertical displacements (Drozdowski and Wrede 1994, Voigt et al. 2002). The resulting thickness and maturation pattern no longer reflects the regional distribution of source areas and the general basin configuration, but instead mirrors the geometry of commonly rhomboid fault-bounded troughs and blocks. Such a pattern seems to be indicated by the isolines of coalification in the western part of Figure 2.2.

More detailed analysis of the basin fill and the fault inventory with respect to the evolution of stress will be carried out in the framework of a current research programme (DFG SPP 1135) and should help to discriminate and explain the patterns described above in detail. At present, the controversial debate is going on with respect to the role of horizontal movements in the CEBS. Furthermore, salt movements may have modified the subsidence pattern dramatically. At present, little Permian salt is present in the LSB, whereas it is known in great thickness in the area of the Pompeckj Block, forming large salt domes and walls. As salt can flow over large horizontal distances (Diegel et al. 1995) the possibility cannot be excluded that much more salt was initially present in the LSB. This escaped northward during Late Jurassic/Cretaceous times, leading to an enforced subsidence in the LSB and a contemporaneous uplift of the Pompeckj Block.

2.6.6. Uncertainties in modelling results

In numerical modelling of complex systems, analysis of uncertainties is necessary in order to evaluate the range of possible models which would still fit the observations. Important uncertainties in basin modelling studies are related to petrophysical properties, mode of heat transfer, calibration data, and/or the algorithm of calculation for calibration data.

With respect to petrophysical properties, the thermal properties heat conductivity and heat capacity are treated here. Others, such as porosity evolution and compaction or permeability distribution as related to fluid flow are beyond the scope of this study. Thermal rock properties were not directly measured for this study, but calculated based on lithology (see above). As there is little salt and coal in the Mesozoic sedimentary sequence, the greatest uncertainty is the heat conductivity of sandstones. The latter differ in heat conductivity due to their quartz content, this mineral having a much higher heat conductivity than feldspars and clay minerals (Yalcin et al. 1997). The default values used for conductivity of sandstones in the PetroMod software are according to experience (e.g. Hertle and Littke 2000), either correct or lower than the real values. The default values are at the lower end of the probable variation. The effect of high sandstone conductivities on modelling results is tested in the following: If sandstone conductivity would be 30% higher than the one used in this simulation and if it is assumed that these sandstones of higher conductivity represent 20% of the sedimentary sequence, a heat conductivity for the entire sequence would result which is 6% higher than the one used in the best-fit models. As $\text{gradT}=\text{Q}/\text{K}$ with Q being the heat flow and K being the heat conductivity, such a misfit would lead to calculated heat flows during maximum burial which are slightly (6%) lower than those given above (Table 2.4). This difference would not influence the conclusions in this paper.

An alternative mode of heat transfer should also not affect the presented conclusions. In principle, water flow (convection) can disturb the temperature field in sedimentary basins significantly. However, to be efficient such convective processes need highly permeable pathways; the generally clay-rich Lower Cretaceous units do not seem to be suitable for this (Table 2.2). Furthermore, there is ample evidence that the entire LSB was strongly heated during the Cretaceous and not only those units were adjacent to permeable fractures. Another option would be the assumption of high radiogenic heat production within the LSB, leading to a rise in temperature. This factor is taken into account by the software; any additional radioactive heating effect would demand more than the average percentages of radioactive elements. No evidence for this is available, but if there had been a greater radiogenic heat production, slightly lower heat flows than those presented in Tables 2.2 and 2.4 would result. This modification would not influence the conclusions presented here.

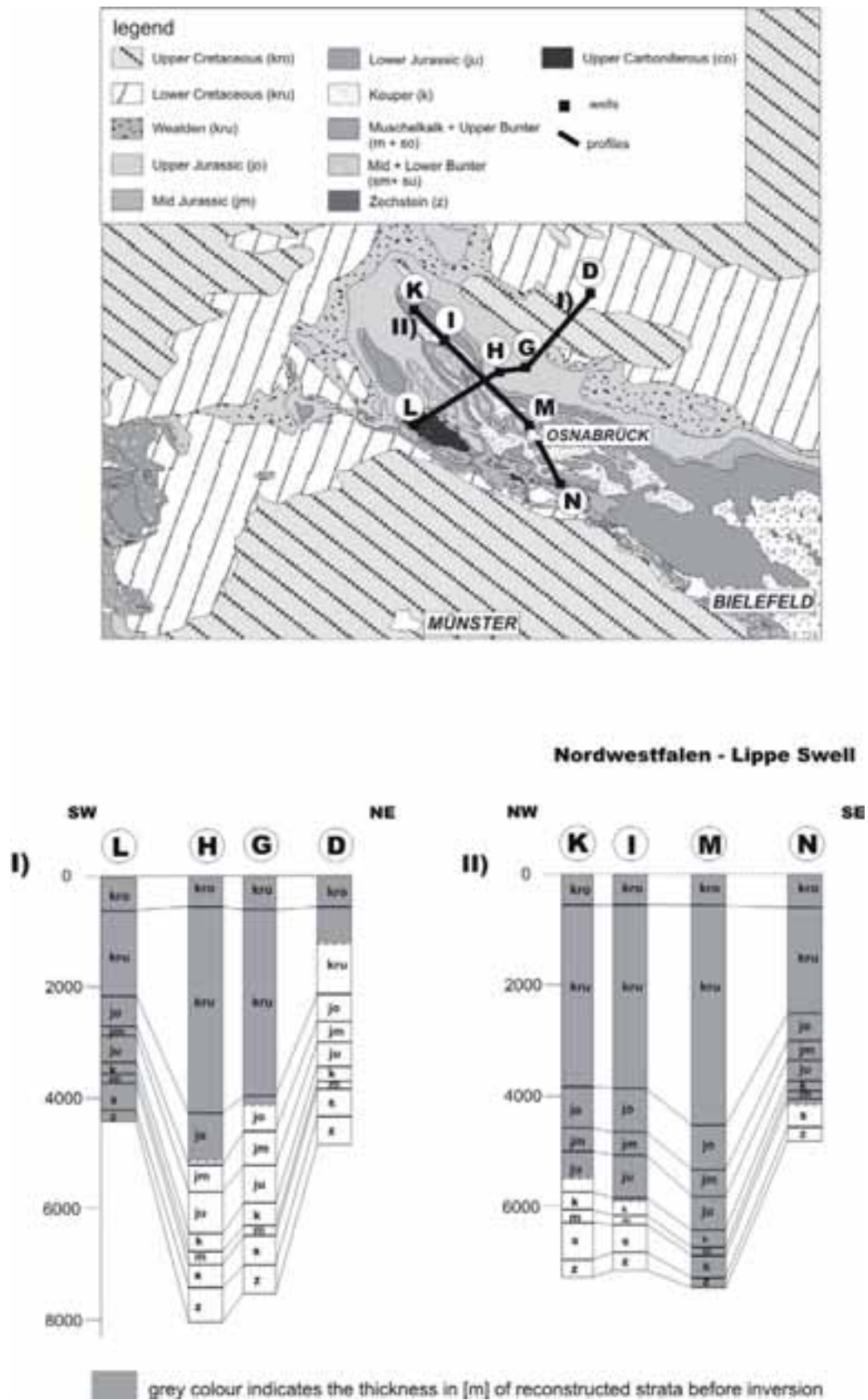


Figure 2.10: Geological map and modelling results on eroded thickness along two profiles through the Lower Saxony Basin.

The third uncertainty is the quality of calibration data used in the modelling. Here, excellent calibration data were available for some areas (e.g. Ibbenbüren, see Figure 2.6) and also for other wells. High-quality data could be obtained from literature and personal measurements. Even if some of the data were false, an excellent data set would remain unchallenged.

The greatest uncertainty appears to be lying in the algorithm used to calculate vitrinite reflectance. Here, the equations of Sweeney and Burnham (1989) were used which are at present regarded as state-of-the-art (Waples et al. 1992, Yalcin et al. 1997). This method is however, not well tested for the very high levels of coalification which are found in the central and southern parts of the LSB. In order to address this concern the algorithms of Lopatin (1971, TTI) and Yamaji (1986) were tested and provided additional evidence for deep burial rather than magmatic intrusion. The lowest overburden (eroded Cretaceous thickness) resulted from the method of Barker and Pawlewicz (1994). Their equation, applied to the data of well G, resulted in only 3685m of overburden rather than 3985m in the best-fit model (Figure 2.11), assuming an average temperature gradient in the uppermost crust at the time of maximum temperature (early Late Cretaceous) of $\sim 41^{\circ}\text{C}/\text{km}$. Although the best-fit model presented here is clearly preferred, even the results reached by applying the latter approach would not affect the general conclusions.

2.7. Conclusions

Numerical simulations of burial history for various deep wells and two outcrop areas at the basin margin as well as detailed coalification studies in the LSB revealed the following:

Basin inversion caused uplift and erosion of Mesozoic sedimentary rocks. Eroded thicknesses ranged from approximately 1280 to 7270m with a southward increasing trend. Erosion occurred during Coniacian or Post-Coniacian times. Reconstructed rates of erosion were 0.53mm/a on the top of the broadly anticlinal Nordwestfalen-Lippe Swell and 0.091mm/a on the northern margin.

Heat flow values during maximum burial range from 60 to 70mW/m². These values imply a concurrent crustal thickness of 31 to 35.5km. The crustal heat flow increases from the northern basin margin towards the Nordwestfalen-Lippe Swell.

Coalification is pre-kinematic with respect to inversion and reflects the former accumulation settings. The generally observed NW-SE striking maturity pattern of the Kimmeridgian strata can be explained by different sedimentation patterns. This is due to the fact that there are still not enough data to characterize the tectonic regime clearly.

Thermal influence of a magmatic intrusion in the study area is not evident from the modelling approach. Thus, the theory of an igneous Cretaceous intrusion as a cause for the coalification pattern appears not to be supported by the results of this modelling study. Fission track analysis on apatites and zircons is currently being performed and will provide detailed information on the maximum temperature and the cooling and uplift history.

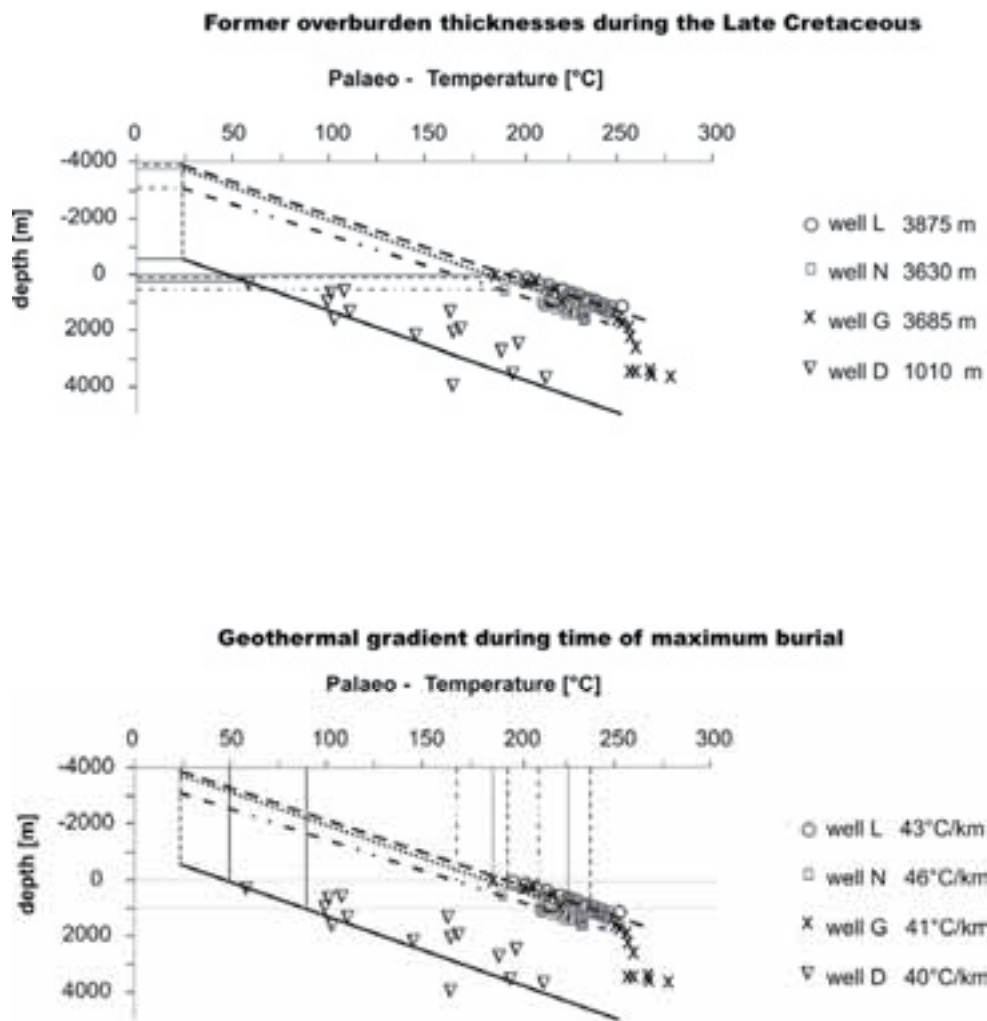


Figure 2.11: Estimation of former overburden thicknesses and average geothermal gradients at the time of maximal burial for different wells according to the algorithm of Barker and Pawlewicz (1994).

3. New information on the thermal history of the southwestern Lower Saxony Basin, northern Germany, based on fission track analysis

Keywords fission track dating, thermal history, northern Germany, Lower Saxony Basin, Bramsche

3.1. Abstract

The southwestern part of the Lower Saxony Basin is characterized by gravity and magnetic anomalies and by an extremely high thermal maturity of organic matter. This was for many years attributed to a Late Cretaceous intrusion, but actually an origin by deep burial is debated. The complex thermal history of the area has been studied by fission track analysis. Zircon data provide evidence for widespread (hydro)thermal activity during the Permian and Upper Jurassic/Lower Cretaceous. Apatite ages indicate a major cooling event in the mid Cretaceous (~89-72Ma) reflecting the time of inversion of the LSB. During the Cretaceous, the cooling of the basin centre was rapid compared to the basin margins. Apatite fission track ages from borehole samples which are recently within the upper part of the APAZ indicate a young heating of the sedimentary sequences until present.

3.2. Introduction

The Lower Saxony Basin (LSB, Figure 3.1), Germany, is one of several sedimentary basins within the Central European Basin system. In the southwestern part, anomalously high maturity of organic matter has been observed reaching 4.5% VRr in Upper Jurassic sedimentary rocks (Teichmüller and Teichmüller 1951, 1984, Bartenstein et al. 1971, Koch and Arnemann 1975). This area coincides with a magnetic and a positive gravimetric anomaly (Schmidt 1914 cited in Breyer 1971, Kaiser 1930 cited in Hahn and Kind 1971, Flotow et al. 1931). This observation has for some decades been interpreted as the effect of an igneous intrusion at a depth of about 5km (Bramsche Massif) which has heated the overlying sedimentary rocks (Mundry 1971, Thyssen et al. 1971, Buntebarth and Teichmüller 1979, Giebeler-Degro 1986). Based on the lignite/subbituminous coal stage of Upper Campanian rocks overlying the Lower Cretaceous units, a late Early Cretaceous or early Late Cretaceous age was concluded for the time of intrusion. In recent years, numerical modelling using stratigraphic, sedimentological, and maturity data from several wells east and west of the Bramsche Massif suggested a different interpretation involving deep burial during Early Cretaceous times followed by Late Cretaceous/Tertiary uplift, probably related to inversion of specific local, fault-limited subbasins

(Leischner et al. 1993, Petmecky et al. 1999). Estimations of maximum burial depths and thicknesses of now eroded sedimentary rocks range from about 3500 to 8000m (Füchtbauer and Müller 1970, Nodop 1971, Thiermann 1980, Drozdowski 1988, Baldschuhn and Kockel 1999, Brink 2002, Senglaub et al. 2006). Calculated geothermal gradients and heat flows also show a wide spread.

The combined analysis of different thermal indicators should help to reconstruct the temperature history of the basin. The regional distribution of their values may contribute to a better understanding of the structural context which is necessary to fully understand the complex basin evolution.

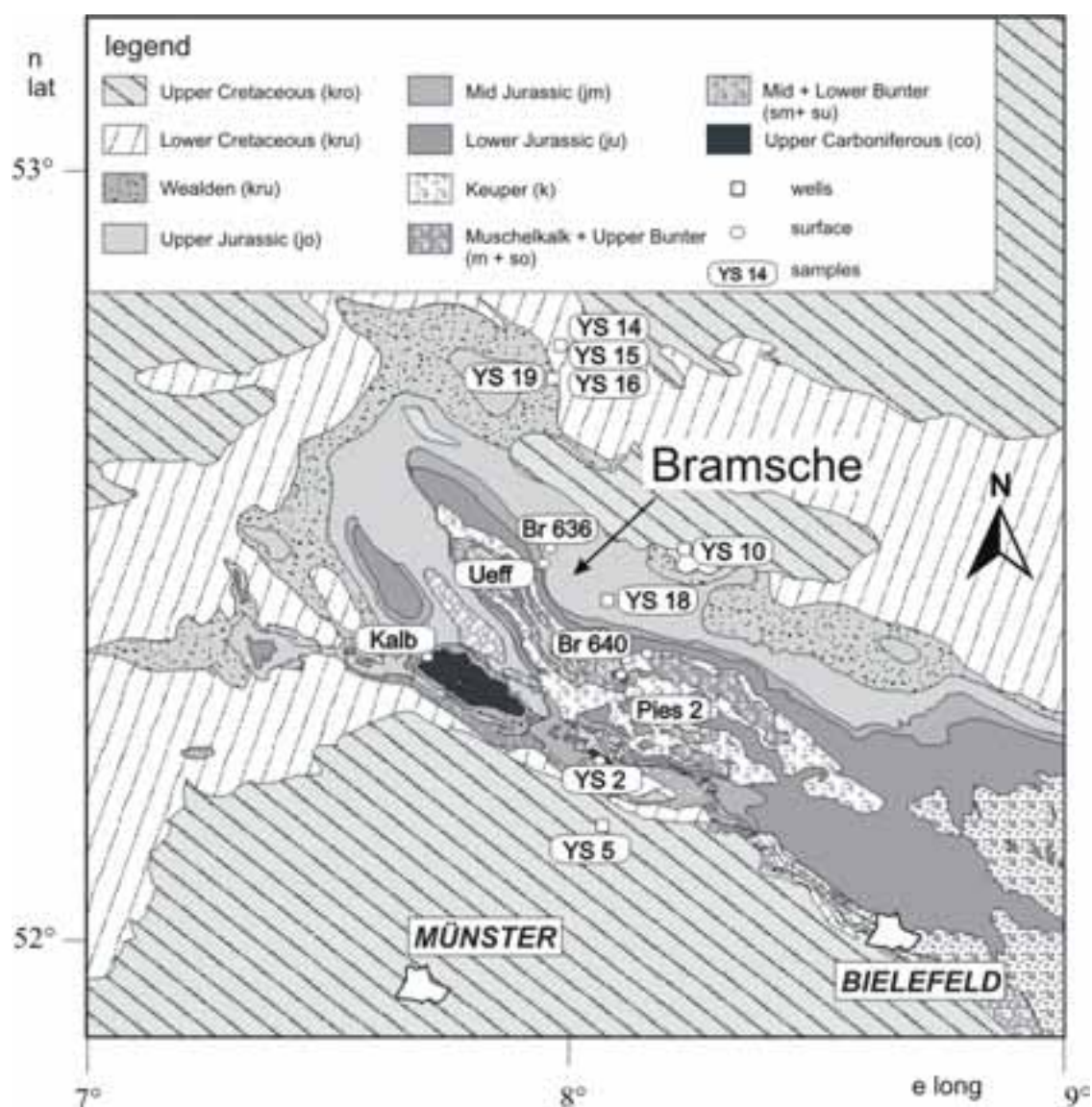


Figure 3.1: Geological map and stratigraphic column of the Lower Saxony Basin (LSB) and sample locations.

The most commonly used thermal indicators in basin studies are coalification and maturation of organic material. They depend greatly on the maximum rock temperature attained and the way in which these temperatures varied over geological time (Taylor et al. 1998). An unusually high degree of coalification is observed in the region of Bramsche. Westphalian D coals have reached the meta-anthracite stage at the Piesberg, and anthracites occur in Early Cretaceous strata near Bohmte. Stadler and Teichmüller (1971) stated that a coalification temperature of about 300°C was necessary for the anthracitization of Cretaceous coals at a depth of only 2000-3000m. They suggested that as the heating source only a magmatic intrusion is possible, the so called Bramsche Massif. The influence of normal geothermal gradients was precluded because with these the temperatures reached would require a subsidence of 10,000-12,000m.

An important factor for the coalification is the duration of heating. Lopatin (1971) and Gretener and Curtis (1982) concluded that the effect of temperature on coalification is exponential whereas the effect of time is linear. However, these authors implied that the effect of time is only noticeable in the range between 70 and 100°C. At high temperatures (> 130°C) the reaction proceeds at such a high rate that time does not play an important role (Gretener and Curtis 1982). Comparing normal burial coalification with coalification caused by extremely high temperatures, Barker (1989) concluded that vitrinite reflectance stabilizes with respect to temperature after about 10^6 - 10^7 years of burial diagenesis; after about 10^4 years in geothermal systems; and about one year or less in contact metamorphism by intrusives.

According to Barker and Goldstein (1990), Mukhopadhyay and Dow (1994) and Barker and Pawlewicz (1994), the increase of vitrinite reflectance with rising temperatures is different for “burial” heating and for “hydrothermal” heating. Barker and Pawlewicz (1994) concluded that peak temperatures (T_{peak}) and vitrinite reflectance data (VRr) can be used to calibrate a geo-thermometer for the burial heating and hydrothermal metamorphism paths.

T_{peak} is calculated using the equations for i) burial heating

$$T_{\text{peak}} = (\ln(\text{VRr}) + 1.68)/0.0124$$

and ii) for hydrothermal metamorphism

$$T_{\text{peak}} = (\ln(\text{VRr}) + 1.19)/0.00782.$$

These equations will be used to interpret the following coalification data. However, because of the time effect and of varying geothermal histories it is impossible to relate a particular degree of coalification to a precise temperature. Typical coalification temperatures are approximately 100-170°C for bituminous coals and 170-250°C for anthracites (Taylor et al. 1998).

An alternative thermal indicator often used in basin studies is fission track analysis. The methodology and its applications are based on the accumulation of lattice damage caused by spontaneous fission of ^{238}U (Wagner and van den Haute 1992; Gallagher et al. 1998). In the classic application of dating volcanic rocks, which underwent a continuous, moderate to fast cooling the stability of fission tracks is described by the concept of a closure temperature (Wagner 1968, Dodson 1973) below which the track accumulation starts. The age then represents the time elapsed since the passage through the respective isotherm. For rocks with other thermal histories, the stability of fission tracks may better be described by the concept of a partial annealing zone (PAZ). This is represented by a temperature range, in which existing linear lattice damages, which at surface temperature are assumed to survive over geological times, are slowly shortened and fade until they finally disappear. This means that in a single sample old shortened tracks occur together with young long tracks, formed during the stay in the PAZ. This process leads to a track length distribution characteristic for the specific thermal history. Applications of this concept concern e.g. sediments being buried and subject to rising temperatures or plutonic rocks experiencing a slow cooling. A combination of the resulting track length distributions and reduced track densities allows modelling the thermal history experienced by the investigated rocks (e.g. Gallagher 1995). Thus, fission track analysis has the advantage that a thermal history may be reconstructed from a single sample. It has been used successfully across a wide range of geological settings to understand sedimentary basin and landscape evolution (Gallagher et al. 1998).

As the PAZ for apatite largely overlaps with the temperature range where the thermal maturation of organic material occurs, apatite fission track analysis has proven to be a valuable tool for the petroleum industry to define the thermal history of a source rock as a proxy of the thermochronological history of oil and gas fields and for the calibration of thermal models. Apatite fission track analysis offers a valuable extension to vitrinite reflectance, especially with respect to analysis of cooling history.

3.3. Geological Setting

The LSB (Figure 3.1) is situated at the southern margin of the Central European Basin System and represents an E-W-striking, highly differentiated Mesozoic basin (Betz et al. 1987, Baldschuhn et al. 1991, Kockel et al. 1994). In the Late Carboniferous (316-300Ma), the later LSB was situated in a foredeep of the rising Variscan mountain belt being formed towards the south. Thus deltaic coal-bearing deposits were accumulated.

In the Early Permian (300-258Ma), a huge denudation occurred causing the erosion of formerly deposited Rotliegend and Upper Carboniferous sediments.

The Permian was also an era of rifting and/or thermal events in the north of the later LSB (Plein 1978, Ziegler 1982, Bachmann and Grosse 1989, Neunzert et al. 1996, van Wees et al. 2000).

From Late Permian to Late Jurassic (258-142Ma) times, a continuous sedimentation took place beginning with the transgressing Zechstein Sea (258-251Ma). During the Triassic (251-200Ma) the LSB received thick post-rift sediments with clastic material predominating the Lower and Upper Triassic (Bunter and Keuper) and carbonates representing the Mid Triassic (Muschelkalk). The thickness of Triassic deposits was governed by the existence of several NNE-striking depressions and swells.

In the Late Jurassic (146-142Ma) the differentiation of the Central European Basin System began with an evolution of the LSB much different from that of adjacent sub-basins. During this time the basin subsided rapidly whereas the neighbouring Rhenish Massif (south), the Central Netherlands High (west), and the Pompeckj Block (north) were uplifted (Kockel et al. 1994). During Coniacian and Santonian times (89-83Ma), the LSB was inverted and existing normal faults became reactivated and transformed into steep thrusts and reverse faults (Baldschuhn and Kockel 1999).

3.4. Sampling and Laboratory Procedures

The investigations are based on detrital apatites and zircons from sandstones. Fission track analyses have up to now been performed on 22 samples covering about 900km² and stratigraphic levels from Upper Carboniferous to Lower Cretaceous. The main objective for the study was to elucidate the thermal history of these sediments in the given geophysical and structural context. Therefore sampling had to cover a large surface area and stratigraphic range. In total 11 wells and 9 surface outcrops were sampled (Figure 3.1).

Apatites and zircons were extracted using conventional techniques by crushing, sieving, separation by Wilfley Table, magnetic and heavy liquid separation as well as final hand picking. Crystals were processed according to the techniques outlined by Hurford et al. (1991). Apatite grains were embedded in epoxy, polished, and etched in 5N HNO₃ for 20s at 20°C to reveal spontaneous tracks. The zircons were mounted in FEP-Teflon, polished, and etched in a KOH-NaOH eutectic melt at 217±4°C, steps varying between 1 and 4 hours, until the majority of the grains was fully etched, using a platinum crucible. Total etch times range from 2 hours to 72 hours. Thermal neutron irradiation was performed in the TRIGA reactor of Oregon State University in Corvallis, Oregon/USA, with a neutron fluence of about 1*10¹⁵ ncm⁻² for zircons and 1.2*10¹⁶ ncm⁻² for apatites.

Table 3.1. CN5 apatite zeta calibration.

Standard	Mineral and number of crystals		Spontaneous		Induced		P(γ^2) (%)	$\rho_i/\rho_s \pm 1\sigma$	Glass	Dosimeter		$\zeta \pm 1\sigma$
	ρ_s	(N _s)	ρ_i	(N _i)	ρ_s	(N _s)				ρ_d	(N _d)	
Durango	0.1544	(252)	1.210	(1,975)	27.63	0.1276 ± 0.0086	CN 5	1.531E+06	10,569	324.60 ± 25.51		
Durango	0.1436	(185)	1.191	(1,534)	23.25	0.1206 ± 0.0095	CN 5	1.531E+06	10,569	324.60 ± 25.52		
Durango	0.1733	(180)	1.524	(1,583)	86.14	0.1137 ± 0.0090	CN 5	1.629E+06	11,683	339.04 ± 27.39		
Durango	0.1424	(234)	1.116	(1,834)	73.68	0.1276 ± 0.0089	CN 5	1.560E+06	10,776	315.51 ± 22.68		
Durango	0.1379	(139)	1.132	(1,141)	88.75	0.1218 ± 0.011	CN 5	1.560E+06	10,776	330.45 ± 30.32		
Durango	0.1520	(209)	1.128	(1,549)	63.54	0.1349 ± 0.0100	CN 5	1.531E+06	10,569	304.01 ± 23.11		
Fish Canyon	0.1841	(135)	1.859	(1,363)	63.15	0.0990 ± 0.0090	CN 5	1.560E+06	10,776	359.84 ± 33.89		
Fish Canyon	0.2388	(186)	1.909	(1,487)	97.01	0.1251 ± 0.0098	CN 5	1.531E+06	10,569	290.33 ± 23.90		
Fish Canyon	0.2470	(177)	2.027	(1,453)	74.20	0.1218 ± 0.0098	CN 5	1.560E+06	10,776	292.58 ± 24.59		
Fish Canyon	0.2170	(273)	1.976	(2,483)	57.70	0.1099 ± 0.0071	CN 5	1.531E+06	10,569	330.25 ± 22.90		
Fish Canyon	0.2130	(265)	2.100	(2,613)	95.01	0.1014 ± 0.0066	CN 5	1.531E+06	10,569	358.09 ± 25.03		
Mt. Dromedary	0.8632	(391)	2.395	(1,085)	63.66	0.3604 ± 0.0215	CN 5	1.547E+06	10,685	353.84 ± 21.50		

326.46 ± 7.24

Track densities (ρ) are as measured and are (10^6 tr cm^{-2}); numbers of tracks counted (N) shown in brackets; $4\pi/2\pi$ geometry correction factor = 0.5. P(γ^2) is probability of obtaining $\gamma^2 =$ value for u degrees whereas u = (number of crystals-1); mean ρ_i/ρ_s ratio used to calculate age and uncertainty where P(γ^2) < 5%.

All samples were analysed using the external detector method (Naeser 1976, Gleadow 1981). The neutron fluence was monitored using uranium-doped Corning glasses CN-5 for apatite and CN-1 for zircon. The muscovite detector micas were etched for 50min in 40% HF at room temperature.

Spontaneous and induced fission track densities were counted on a Zeiss Axioplan optical microscope at 1250 times magnification with a dry 100x objective for the apatites, whereas an oil immersion 100x objective was used for the zircons. The Senglaub CN-5-apatite zeta (Table 3.1), which is used for the first time in this publication and therefore according to the I.U.G.S. recommendations (Hurford 1990) documented here, is based on repeated analyses of Durango, Fish Canyon, and Mount Dromedary samples. The

Brix CN-1–zircon zeta was obtained and monitored by multiple analyses over the last 15 years using Fish Canyon, Tardree, Buluk, and Mount Dromedary standards. Central ages (Galbraith and Laslett 1993) were calculated according to the Zeta-Calibration approach of Hurford and Green (1983) and are reported according to the I.U.G.S. recommendations (Hurford 1990).

Apatite track lengths were measured on horizontal confined tracks following the recommendations of Laslett et al. (1982). The measurements were made applying a 100x dry objective with a total magnification of 1250, using a microcomputer and a digitising Tablet linked to the microscope by a drawing tube. A stage micrometer with μm divisions superimposed on the microscope eye field was used for the calibration with a precision of $\pm 0.2\mu\text{m}$ (Green et al. 1986). All measurements are track-in-track (TINTS), if not otherwise indicated.

Annealing models of the fission tracks in apatite are well defined by experimental and borehole data (e.g. Green et al. 1989, Ketcham et al. 1999). When the models are extrapolated to geologic time, annealing is predicted to occur at a sufficient rate to be measurable above 60°C . Above $110\pm 10^{\circ}\text{C}$ - depending on the chlorine content- the annealing rate is so high that the apatite FT age and mean track length are effectively reduced to zero. This range of temperatures is classified as the apatite partial annealing zone (APAZ). As the source areas of the sandstones did not contain significant amounts of rocks which should provide detrital Cl-rich apatites, the observed crystals were assumed to be prevalingly F- and OH- rich.

The software AFTSolve 1.3.1©2003 by Ketcham and Donelick (2000) allows to obtain the maximum amount of information possible from apatite fission track data through forward and inverse modelling. For this study, the forward modelling with the mono-kinetic annealing model of the Durango apatite by Laslett et al. (1987) was applied. For the age calculation and calibration the approach of pooled ages and for evaluating, how well a calculated fission track length distribution matches the measured data the Kolmogorov-Smirnov Test (or K-S Test) was used. To model the thermal history any available independent constraints of the sample were inserted (e.g. stratigraphic age, down-hole temperature, time of maximum burial and maximum palaeotemperatures). The timing of maximum temperature was estimated based on the total reset zircon age of the sample YS 18 from the basin centre. The K-S and age goodness-of-fit (GOF) test of five models was even higher than 0.50, which is the expected value if the time-temperature path and kinetic model are in fact the most probable ones.

3.5. Results and Discussion

3.5.1. *Vitrinite reflectance measurements*

Vitrinite reflectance data (VRr) illustrating the thermal maturity of the rocks in the study area have been assembled for a large number of samples and numerous new samples were measured in an earlier phase of this project (Table 3.2, Senglaub et al. 2006). The VRr data vary from 0.5% to more than 3.0%VRr for the Jurassic rocks (Figure 3.2) and up to 5.8%VRr for the Carboniferous samples. VRr values were converted to maximum paleotemperatures after Barker and Pawlewicz (1994). The estimated paleotemperatures reach values up to 280°C (normally buried) and up to 381°C (hydrothermally influenced) (see also Table 3.2). The samples used in this study for fission track analysis were collected as close as possible to the location of the VR samples included in Senglaub et al. (2006).

For the central and southern part of the LSB, the reflectance increases only at normal rates with depth which is caused by a deep burial of the Jurassic to Carboniferous sequence at only moderate heat flows. This deep burial was followed by erosion of up to 7000m in the Piesberg area. Modelling results by Senglaub et al. (2006) clearly indicate that a significant pile of several thousand metres (up to 4 kilometres) of Early Cretaceous rocks has been deposited in the central part of the basin. The exact timing of deposition and erosion however, has not been deduced from vitrinite reflectance data and basin modelling so far.

Furthermore, the basin modelling approach calibrated by vitrinite reflectance data allowed the determination of heat flows during times of maximum burial as well as average palaeogeothermal gradients for the upper crust. These gradients are at about $40\pm 2^\circ\text{C}/\text{km}$ during the time of maximum burial in the strongly inverted central and southern part of the LSB and slightly higher in the north (Senglaub et al. 2006). This information can be used to identify the depth of upper and lower boundary of the APAZ.

3.5.2. *Fission track analysis*

3.5.2.1. *Zircon fission track results*

- Upper Carboniferous samples

Nine samples, mainly from the Westphalian C and D sequences of the LSB and the Münsterland Block were successfully dated (Figure 3.3). Some samples yielded ages which are significantly younger than the sedimentation age. This indicates different degrees of annealing which may be differentiated by the following approach starting from a minimum stratigraphic age of 302Ma. If the apparent age subtracted by the 2σ error value exceeds this stratigraphic age,

Table 3.2: Measured vitrinite reflectance and calculated peak temperatures close to the FT samples in comparison to the zircon and apatite fission track ages.

Sample	Stratigr.	Lith.	Depth (m)	VBr (%)	Annotations	Peak (burial) (hydroth.)	Peaktemp. (hydroth.)	Zircon central age (Ma) ± 1σ	Age dispersion (%)	Apatite central age (Ma) ± 1σ	Age dispersion (%)	Mean track length (μm)
YS.14	ewD	SH	3,510	1.70	Senglaub et al. (2006)	178	220	345 ± 19	9.0	12 ± 3	0.0	-
	ewD (?)	SH	3,541	1.78	industrial data	182	226	267 ± 16	1.0	19 ± 7	0.0	-
	ewD (?)	SH	3,906	2.16	industrial data	198	251					
YS.19	?	CARB	3,520	3.7	industrial data	241	314	283 ± 12	3.3	-	-	-
			4,023									
YS.18	jo	SH	1,680	2.58	Senglaub et al. (2006)	212	273					
	jo	SH	1,842	2.64	Senglaub et al. (2006)	214	276					
	jm	SH	2,065	2.98	industrial data	224	292	326 ± 45	30.5	40 ± 4	31.1	11.8 ± 0.5
	jm	SH	2,065	3.08	industrial data	226	296					
YS.18	ewD	SH	3,467	4.50	Senglaub et al. (2006)	257	345					
	ewD	SST	3,486	4.65	Senglaub et al. (2006)	260	349	133 ± 6	3.9	14 ± 3	27.0	-
	ewD	Coal	3,593	5.8	Teichmüller et al. (1984)	277	377					
Ued	ewD	Coal	3,605	5.1	Teichmüller et al. (1984)	267	361					
	jo	Coal	-75	4.56	Bartenstein et al. (1971)	258	346	285 ± 20	20.2	-	-	-
BR.6M	jo	Coal	-75	4.09	Senglaub et al. (2006)	249	332					
	jo	Coal	-70	3.56	Bartenstein et al. (1971)	238	315	296 ± 40	54.1	-	-	-
	jo	Coal	-70	3.76	Senglaub et al. (2006)	243	322					

northern LSB

centre of the LSB

Table 3.2 (cont.).

Sample	Stratigr.	Lith.	Depth (m)	VIR (%)	Annotations	Peaktemp.		Zircon central age (Ma) ± 1σ	Age dispersion (%)	Apatite central age (Ma) ± 1σ	Age dispersion (%)	Mean tracklength (µm)
						Peak (burial)	Peak (hydroth.)					
Flm.2	ewD	Coal	-135	4.8	Teichmüller et al. (1984)	261	353	306 ± 18	4.3	77 ± 6	23.9	13.9 ± 0.2
	ewD	Coal	-135	4.69	Seniglaub et al. (2006)	260	350					
	ewD	Coal	-135	4.73	Seniglaub et al. (2006)	261	351					
	ewD	Coal	-135	4.31	Seniglaub et al. (2006)	253	339					
	ewD	Coal	-135	4.55	Seniglaub et al. (2006)	258	346					
Kath	ewD	Coal	-91	1.8	Teichmüller et al. (1984)	183	227	209 ± 23	0.4	78 ± 6	0.0	13.1 ± 0.2
	ewD	Coal	-91	1.50	Seniglaub et al. (2006)	166	204					
YS.2	z	SfF	-115	0.85	Teichmüller et al. (1984)	122	131	320 ± 23	8.5	-	-	-
	z	SfF	-115	0.93	Seniglaub et al. (2006)	130	143					
YS.5	ju	SfF	188	0.57	Lommerzhelm (1983)	90	80	252 ± 18	23.7	91 ± 31	0.0	13.7 ± 0.5
	ju	SfF	355	0.97	Seniglaub et al. (2006)	133	148					
MS.11	ewA	SfF	1,454	2.2	Teichmüller et al. (1984)	199	253					
	ewA	SfF	1,456	2.21	Lommerzhelm (1983)	199	253					
	cnB	SfF	2,215	6	industrial data	280	381	303 ± 20	1.4	-	-	-
	enA+B	SfF	4,690	5.35	industrial data	271	367					
	enA+B	SfF	4,735	4.76	industrial data	261	352					
YS.13	ewC	Coal	1,136	0.87	Lommerzhelm (1983)	124	134					
	ewC	Coal	1,314	0.9	industrial data	127	139	342 ± 24	9.9	45 ± 4	22.2	12.2 ± 0.2
	ewC	Coal	1,487	1	industrial data	135	152					

southern LSH

Minsterland Block

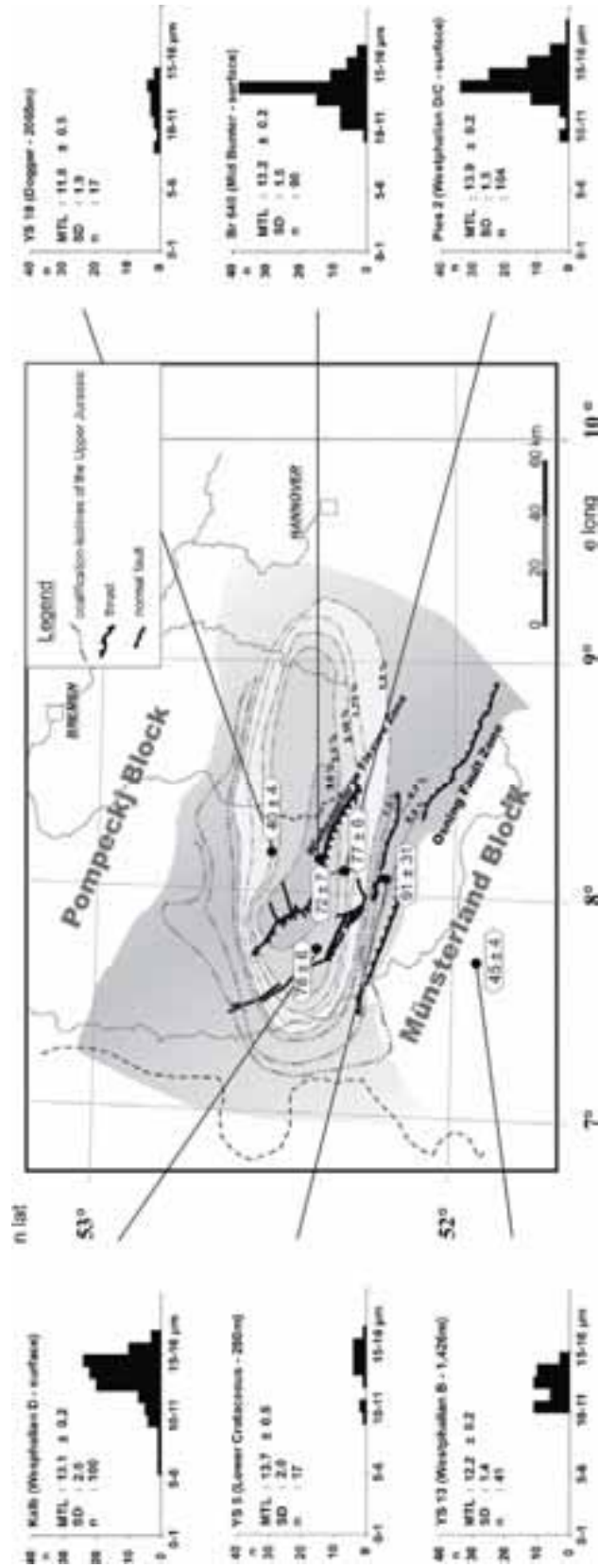


Figure 3.2: Map showing the tectonic setting and the maturity of the Upper Jurassic expressed in VRr (%) in correlation to apatite fission-track lengths distribution. Track lengths histograms illustrate the distribution of confined track lengths, mean track lengths and standard deviations.

annealing of fission tracks inherited from the source area cannot be detected. These samples are classified as not annealed, although a certain degree of annealing cannot be excluded. This problem would especially affect samples for which original grains ages are much older than the stratigraphic age and would require a very strong reduction of apparent grain ages before reaching the reference value. If the apparent age subtracted by the 2σ error value is lower than the stratigraphic age, annealing is at least possible and if the apparent age is

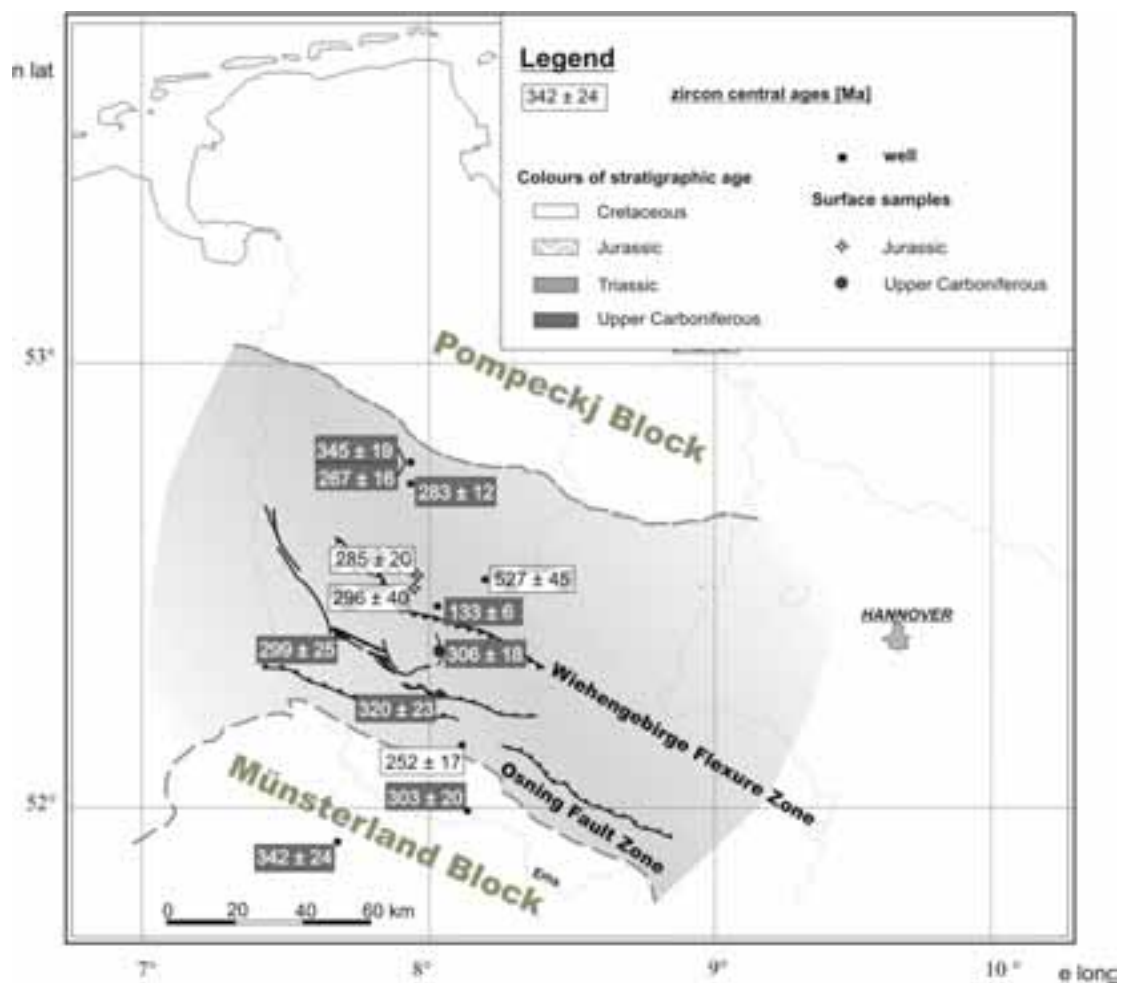


Figure 3.3: Map showing zircon FT ages.

already younger than the stratigraphic age and only the apparent age added by the 2σ error value overlaps with the stratigraphic age, annealing is probable. A sample is significantly annealed, if the apparent age added by the 2σ error value is less than the stratigraphic age. All nine fission track ages passed the χ^2 -test (Table 3.3).

Their single grain age distributions (Figure 3.4) are unimodal and often slightly skewed, with a distinct tail incorporating old ages. This may be taken as another

Table 3.3: Results of apatite and zircon FT dating as well as track length distributions.

Sample	Depth [m]	Coordinates		Stratigr.	D.-age [Ma]	Lith.
		Easting [Gauss-Krüger-System]	Northing			
northern part of the LSB	YS 14	3,541	-	Up. Carbonif.	308-305	Sst.
	YS 15	3,516	-	Up. Carbonif.	308-305	Sst.
	YS 16	3,906	-	Up. Carbonif.	308-305	Sst.
	YS 19	4,023	-	Up. Carbonif.	308-305	Sst.
centre of the LSB	YS 10	2,065	-	Dogger	166-163	Sst.
	YS 18	3,593	-	Up. Carbonif.	308-305	Sst.
	Ueff	-75	34 23 750	Malm	156-152	Sst.
	BR 636	-70	34 25 750	Malm	156-152	Sst.
southern part of the LSB	Br 640	-80	34 37 740	Mid Bunter	249-244	Sst.
	Pies2	-135	34 33 775	Up. Carbonif.	308-305	Sst.
	Kalb	-91	34 08 700	Up. Carbonif.	311-308	Sst.
	YS 2	-115	34 29 050	Up. Carbonif.	308-305	Sst.
Münsterland Block	YS 5	280	-	Low. Cretac.	120-98	Sst.
	YS 11	2,215	-	Up. Carbonif.	326-316	Sst.
	YS 13	1,427	-	Up. Carbonif.	313-311	Sst.

Table 3.3 (cont.).

Sample	n	Spontaneous		Induced		P _T ²	Age dispersion [%]	Central age (± 1σ) [Ma]	Mean track length [μm]	n tracks
		ρ _s	(N _s)	ρ _i	(N _i)					
		[10 ⁵ tracks/cm]	[10 ⁵ tracks/cm]	[10 ⁵ tracks/cm]	[10 ⁵ tracks/cm]	[%]	[%]	[Ma]	[μm]	
YS 14	6	0.62 (13)	7.27 (261)	84.59	0.0	12.1 (3.4)	-	-	-	-
YS 15	5	0.45 (13)	6.62 (192)	97.3	0.0	16.3 (4.7)	-	-	-	-
YS 16	4	0.25 (9)	3.15 (113)	80.14	0.0	19.1 (6.6)	-	-	10.0 ± 0.4	25
YS 19	-	-	-	-	-	-	-	-	-	-
YS 10	19	0.54 (252)	3.78 (1,769)	0.01	31.1	40.2 (4.3)	-	-	11.8 ± 0.5	17
YS 18	15	0.26 (39)	4.81 (731)	2.2	27.0	13.5 (2.5)	-	-	-	-
Ueff	-	-	-	-	-	-	-	-	-	-
BR 636	-	-	-	-	-	-	-	-	-	-
Br 640	12	1.09 (134)	4.08 (501)	87.58	0.8	71.7 (7.0)	-	-	13.2 ± 0.2	90
Pies2	20	0.78 (486)	2.78 (1,732)	0.21	23.9	76.7 (5.8)	-	-	13.9 ± 0.2	104
Kalb	19	0.94 (190)	3.27 (660)	99.99	0.0	77.7 (6.4)	-	-	13.1 ± 0.2	100
YS 2	-	-	-	-	-	-	-	-	-	-
YS 5	2	0.62 (12)	1.60 (31)	62.16	0.0	90.7 (30.9)	-	-	13.7 ± 0.5	17
YS 11	-	-	-	-	-	-	-	-	-	-
YS 13	15	1.30 (262)	7.206 (1,453)	3.5	22.2	44.8 (4.1)	-	-	12.2 ± 0.2	41

Apatite

- (1) Track densities (ρ) are in 10⁵ tracks / cm²; numbers of tracks counted (n) shown in brackets.
- (2) All analyses by external detector method using 0.5 as geometry correction factor.
- (3) Ages calculated as central ages according to Galbraith and Laslett (1993) using dosimeter glass CN-5 and ζ-CN-5 = 334±25 (Bochum, 2003) or ζ-CN-5 = 326±7 (Bochum, 2004) all ζs based on repeated measurements on Fish Canyon Tuff, Durango apatite and Mt. Dromedary Banatite
- (4) P_T² is the probability of obtaining χ² value for v degrees of freedom where v = no. of crystals - 1.

Table 3.3 (cont.).

Sample	n	Spontaneous		Zircons Induced		$P\chi^2$	Age dispersion (%)	Central age (Ma)	Dosimeter		
		ρ_s	(N_s)	ρ_i	(N_i)						
		[10 ⁶ tracks/cm]		[10 ⁶ tracks/cm]		[%]	[%]	[Ma]	P_d		
YS 14	20	43.900	(6,063)	3.367	(465)	26	9.0	13.039 (0.627)	345 (19)	0.4592	(6,342)
YS 15	-	-	-	-	-	-	-	-	-	-	-
YS 16	13	32.980	(3,006)	3.313	(302)	57	1.0	9.954 (0.601)	267 (16)	0.4605	(6,360)
YS 19	20	39.360	(7,120)	3.753	(679)	39	3.3	10.486 (0.421)	283 (12)	0.4631	(6,396)
YS 10	20	48.770	(11,652)	2.532	(605)	< 1	30.5	19.260 (0.803)	527 (45)	0.4554	(6,289)
YS 18	16	22.990	(3,715)	4.697	(759)	58	3.9	4.895 (0.195)	133 (6)	0.4618	(6,378)
Uelf	20	25.257	(4,607)	2.227	(406)	< 1	20.2	11.347 (0.587)	285 (20)	0.4541	(6,271)
BR 636	20	25.570	(4,626)	2.056	(372)	< 1	54.1	12.434 (0.670)	296 (40)	0.4670	(6,449)
Br 640	-	-	-	-	-	-	-	-	-	-	-
Pies2	16	38.510	(4,095)	3.301	(351)	45	4.3	11.667 (0.649)	306 (18)	0.4528	(6,253)
Kalb	9	35.040	(1,742)	3.077	(153)	56	0.4	11.386 (0.960)	299 (25)	0.4515	(6,235)
YS 2	15	31.660	(2,798)	2.659	(235)	33	8.5	11.906 (0.809)	320 (23)	0.4644	(6,413)
YS 5	20	33.480	(7,121)	3.559	(757)	< 1	23.7	9.407 (0.360)	252 (18)	0.4657	(6,431)
YS 11	9	40.390	(2,845)	3.535	(249)	35	1.4	11.426 (0.755)	303 (20)	0.4567	(6,306)
YS 13	8	43.740	(4,108)	3.333	(313)	13	9.9	13.125 (0.770)	342 (24)	0.4580	(6,324)

Zircons

- (1) Track densities (ρ) are in 10⁶ tracks / cm²; numbers of tracks counted (N) shown in brackets.
- (2) All analyses by external detector method using 0.5 as geometry correction factor.
- (3) Ages calculated as central ages according to Galbraith and Laslett (1993) using dosimeter glass CN-1 and ζ -CN-1 = 119±5 (Bochum since 1997), * ζ -CN-1 = 117±5 (London 1990) or ζ -CN-1 = 122±5 (Bochum 1991-1996); all ζ_s s based on repeated measurements on Fish Canyon Tuff, Buluk Member Tuff, Tardree Rhyolite, and Mt. Dromedary Basaltite.
- (4) $P\chi^2$ is the probability of obtaining χ^2 value for v degrees of freedom where v = no. of crystals - 1.

indication that the zircons in the sampled rocks have experienced some degree of annealing. More information on the degree and especially on the timing of the annealing may be obtained by a study of the single grain ages in the specific samples. The characteristics of each sample are described in detail below in order to fix the base for the general interpretation.

The samples YS 14, YS 16, and YS 19 from the northern part of the basin gave fission track central ages of 345 ± 19 , 283 ± 12 , and 267 ± 16 Ma. Whereas a thermal overprint is not obvious from the oldest sample, annealing of fission tracks inherited from the source area is probable in the two younger samples. The oldest single grains from each of the three samples cover the broad range from 585 ± 145 down to 419 ± 116 Ma with overlapping errors on the 1σ level. The youngest ages, however, between 212 ± 43 and 229 ± 45 Ma are identical on the same error level.

The sample YS 18 from the basin centre, yielded an anomalous fission track central age of 133 ± 6 Ma, accompanied by a small age dispersion of only 4%.

The distribution of the single grain ages is very sharp compared to the other samples, and almost symmetrical. All single grain ages, ranging from 176 ± 41 to 103 ± 17 Ma, are clearly younger than the depositional age and indicate a significant annealing of fission tracks inherited from the source area.

The central ages of the samples YS 2, Pies 2, and Kalb representing the southern part of the Wiehengebirge Flexure Zone range from 320 ± 23 to 299 ± 25 Ma and thus are identical on the 1σ error level. The same holds for the youngest single grain ages ranging from 215 ± 51 to 228 ± 55 Ma. The oldest single grain ages from the samples are between 429 ± 94 and 538 ± 184 Ma. Altogether, these data indicate that annealing of fission tracks inherited from the source area is at least possible even for the oldest grains and probable for grains with the youngest ages.

The two samples YS 13 and YS 11 from the Münsterland Block show similar central ages of 342 ± 24 and 303 ± 20 Ma respectively, with errors overlapping on the 1σ level. These ages indicate that annealing of fission tracks inherited from the source area must be considered as possible. The youngest single grain ages from the two samples with 245 ± 58 and 249 ± 50 Ma respectively, are almost identical and make the presence of annealed grains very probable. The population on the other hand, also includes grains with ages of about 500Ma, for which no annealing can be detected using the statistical approach described above. Some annealing, that fails to shift the apparent age far enough to reach the stratigraphic age may not be precluded.

- Mesozoic samples

The four Mesozoic samples from the LSB and the Münsterland Block are less homogeneous than the Carboniferous samples and failed the χ^2 -test at the 5% level (Table 3.3). Most of the frequency distribution curves of single grain ages are bimodal.

The centre of the LSB is represented by 3 samples. The Mid Jurassic sample YS 10 displays a central age of 527 ± 45 Ma. Even the youngest single grain age of 303 ± 25 Ma is clearly older than the depositional age. Therefore any indication of the annealing of fission tracks inherited from the source area is lacking, according to the criteria described above. The frequency distribution of the single grain ages (Figure 3.4) is bimodal and strongly asymmetric with an obvious tail incorporating old ages and a steep slope between 300 and 200 Ma towards younger ages.

The position of this slope corresponds to the youngest single grain ages observed in the Carboniferous samples. On the other hand, the age of 303 ± 25 Ma corresponds to the assumed stratigraphic age of the Carboniferous samples described above. The Upper Jurassic samples Ueff and Br 636 were taken very close to each other and yielded fission track central ages of 285 ± 20 and 296 ± 40 Ma, which are identical on the 1σ error level. Compared to the stratigraphic age of the samples, these ages again do not give any indication that the annealing of fission tracks inherited from the source area may have occurred. The complex single grain age distributions however, clearly provide different information. These distributions show a wide spread and Br 636 is bimodal. Neither of the two submaxima in this sample correspond to the peak in Ueff. Both curves have a clear tail incorporating old ages and a steeper slope towards younger ages.

The younger submaximum in Br 636 is situated at about 140 Ma and corresponds to the single peak in the Carboniferous sample YS 18, located nearby. The youngest grain in Br 636 is with 112 ± 22 Ma clearly younger than in Ueff with 163 ± 40 Ma, but the errors are overlapping on the 1σ level. On the same level, the youngest single grain ages are identical in Br 636 and in the Carboniferous sample YS 18. The oldest single grain ages in these samples are with 685 ± 233 and 477 ± 116 Ma similar to the extremes observed in the Carboniferous samples.

To judge from the fission track central age of 252 ± 18 Ma of the sample YS 5 from the Lower Cretaceous of the Münsterland Block, no annealing of fission tracks inherited from the source area would be expected in this sample. The single grain age distribution is relatively complex. It comprises an isolated old component of 721 ± 222 Ma, a central cluster near 260 Ma, and a younger component causing a change in the steep slope towards younger ages at about

150Ma. Only for the overlap with the Lower Cretaceous and thus indicate a very faint and dubious annealing.

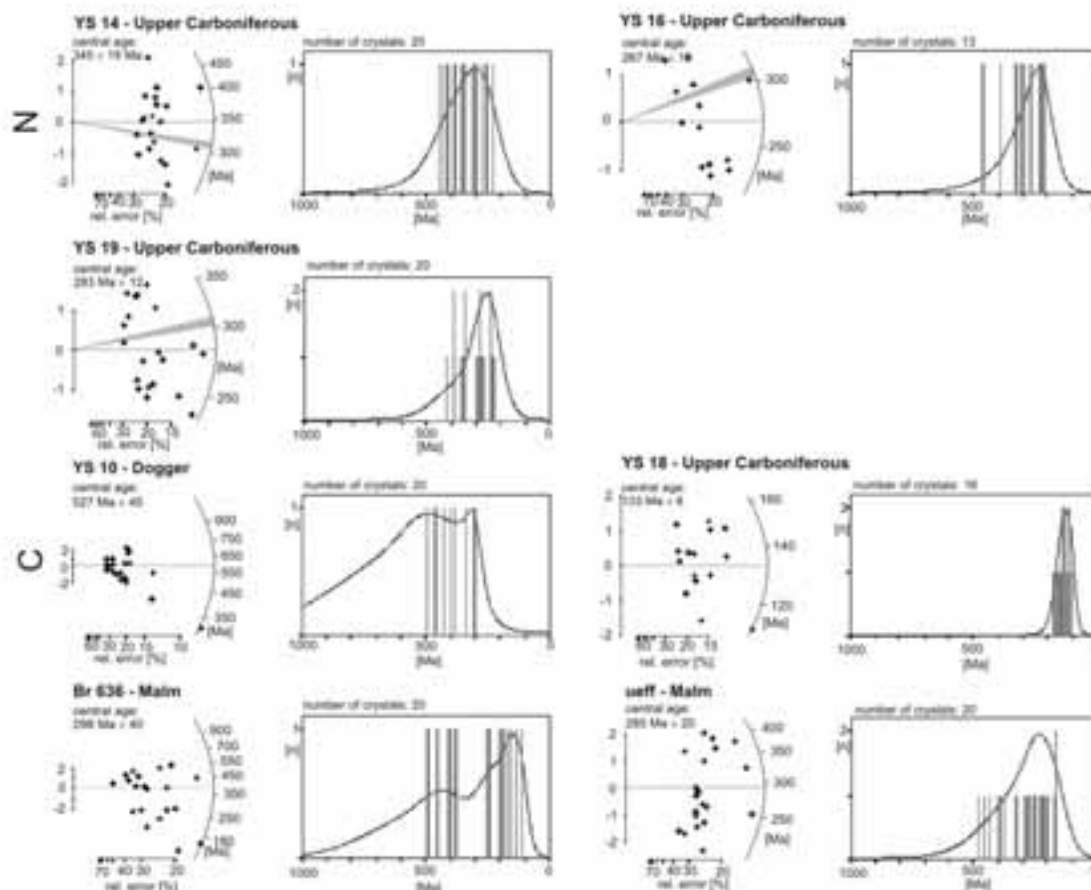


Figure 3.4: Radial plot diagrams and age spectra of zircon fission track ages. The horizontal line represents the central age and the shaded areas the stratigraphic age of each sample. Abbreviations: N= northern part of the basin, C= centre of the basin, S= southern part of the Wiehengebirge Flexure Zone, MB= Münsterland Block. For estimation components in a mixed distribution of zircon fission-track ages Trackkey 4.2 (Dunkl 2002) is used to express the analytical results.

As a summary, possible and probable annealing of fission tracks in zircons from Carboniferous samples has been observed in wide sectors of the studied area, with significant annealing only in one sample. Generally, the single grain age distributions display a broad unimodal shape with a distinct tail incorporating old ages. This corresponds to the pattern resulting from a normal distribution subject to annealing. The youngest single grain age may be used as a proxy for the maximum age of the heating event. The corresponding values for all the Carboniferous samples except YS 18, fall into the narrow range from 212 ± 43 to 249 ± 50 Ma and thus are identical on the 1σ error level. Therefore the observations should indicate that the samples concerned experienced

temperatures corresponding to the ZPAZ during a period of time prior to the Late Triassic or at about 230 ± 20 Ma, respectively. Only sample YS 18, which is characterized by the exceptional young age of 133 ± 6 Ma, shows a sharp and almost symmetrical curve. This age should reflect a cooling age after complete resetting of the zircon fission track system. This resetting may have occurred at the same time as annealing in the other samples, with YS 18 having experienced a deeper burial. The sharp distribution of the single grain ages indicates a fast cooling through the whole ZPAZ, which heating event affecting the zircon fission track system subsequent to that time.

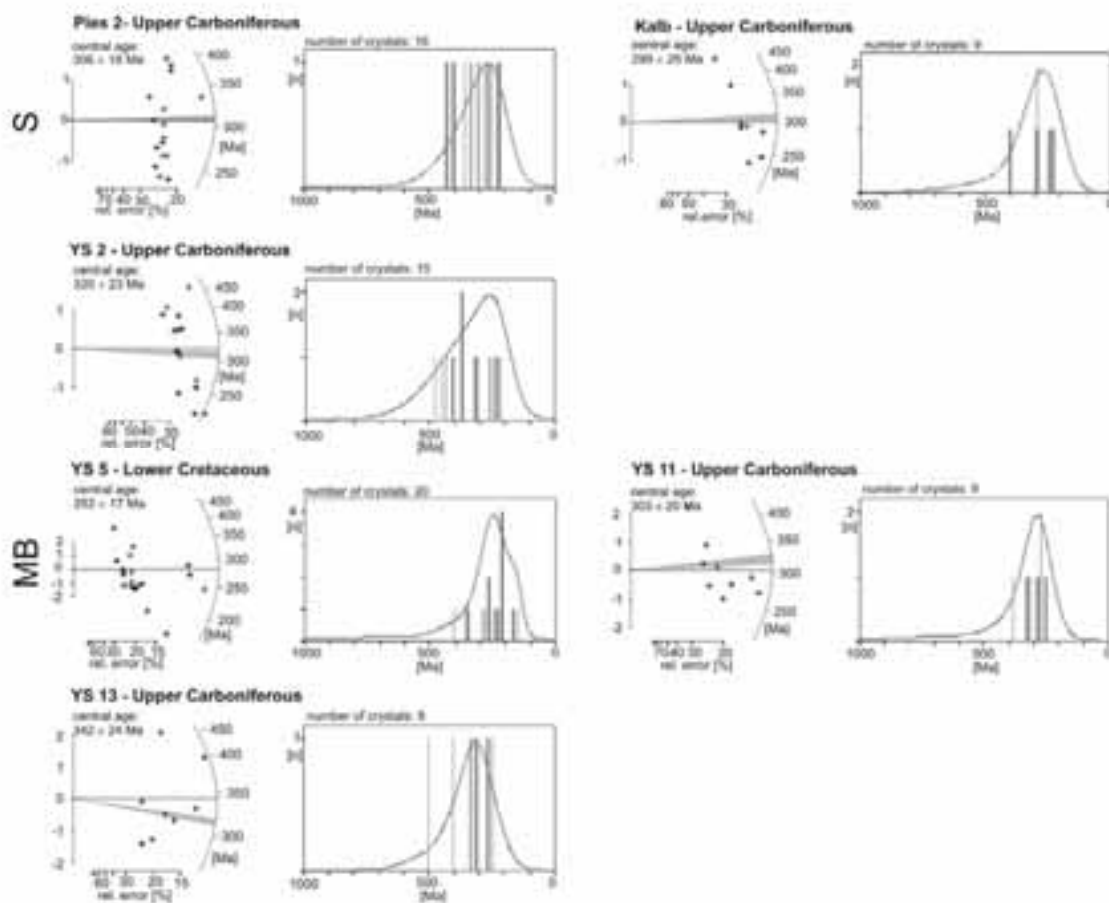


Figure 3.4 (cont.).

The detritus accumulated in the Middle Jurassic was probably derived from Carboniferous rocks outcropping further to the south at that time, which had never experienced any annealing of fission tracks in zircons inherited from the source area. This is indicated by the single grain age distribution in the sample YS 10, which starts at 303 ± 25 Ma, corresponding to the stratigraphic age of the

youngest Carboniferous strata deposited in the area and also including old grains similar to those observed in Carboniferous samples. While the central ages of the Late Jurassic samples Br 636 and Ueff, located further to the west, do not provide any indication of annealing of fission tracks in zircons inherited from the source areas, a few single grain ages point towards some annealing, probably in grains with a high amount of radiation damage. This would lead to the conclusion that the samples were only subject for a short period of time to thermal conditions corresponding to the low temperature part of the ZPAZ. For the only Cretaceous sample, an indication of annealing of fission tracks in zircon is very dubious.

- Interpretation and discussion of the zircon fission track data

Annealing of fission tracks in zircon is a function of temperature, time, and α -radiation damage (Kasuya and Naeser 1988). The amount of α -radiation damage increases with time as well as with uranium and thorium concentrations in zircon. In rocks in which zircons are rapidly cooled from high temperatures, low accumulated radiation damage can be expected (Rahn et al. 2000). Old detrital, especially recycled grains may have accumulated strong radiation damage, which may considerably reduce the boundary temperatures of the zircon partial annealing zone (see e.g. Bernet et al. 2004). Tagami and Shimada (1996) discussed a zircon partial annealing zone (ZPAZ) between ~ 230 and 320°C for a heating duration of about 10^6 years. Fission tracks in zircon grains from Miocene to Pleistocene sandstones and Miocene to Pliocene rhyolites of two drill holes in a sedimentary basin in Japan give indications for a value above 200°C for the low temperature limit of the ZPAZ at a stable temperature for about 1Ma (Hasebe et al. 2003). Furthermore, results of laboratory annealing experiments point towards a similar temperature range of the ZPAZ (Yamada et al. 1995; Tagami et al. 1998). Fission tracks in zircon grains with high α -radiation damage, however, start to anneal at temperatures between 150° and 200°C (Garver and Bartholomew 2001, Riley 2002). Assuming these temperatures over a geological time range ($\sim 10^6$ – 10^7 years), a partial annealing of fission tracks in zircon should occur. Complete annealing of fission tracks in zircon would need temperatures above 320°C for duration of the thermal event in the range of 1–10Ma (Tagami and Shimada 1996, Tagami et al. 1998, Rahn 2001, Brix et al. 2002).

The chemistry and grade of metamictization of the dated zircons are not precisely known, allowing large room for speculation on their thermal properties. According to Rahn et al. (2004) young or U-poor zircons still retain their provenance age at a certain temperature, while old or U-rich grains start annealing their fission tracks under the same conditions. To assess the influence of metamictization on the data presented in this paper, the correlation between zircon fission track age and uranium content is illustrated in Figure 3.5. The

samples show a wide range of U contents which is very common in mixed suites of sedimentary zircons. The uranium contents over all the samples vary between 15 and 170ppm. According to Figure 3.5, high uranium contents generally correlate with younger grain ages. This is especially clear for the Jurassic samples YS 10 and Br 636 having experienced none or only a very slight thermal overprint. The trend is less clear and the slope of the correlation line less steep in the Carboniferous samples, having been subject to some post-Carboniferous annealing. The only exception is the sample YS 18 with very similar single grain ages for different uranium contents, indicating a complete resetting of fission tracks inherited from the source area (Garver 2005).

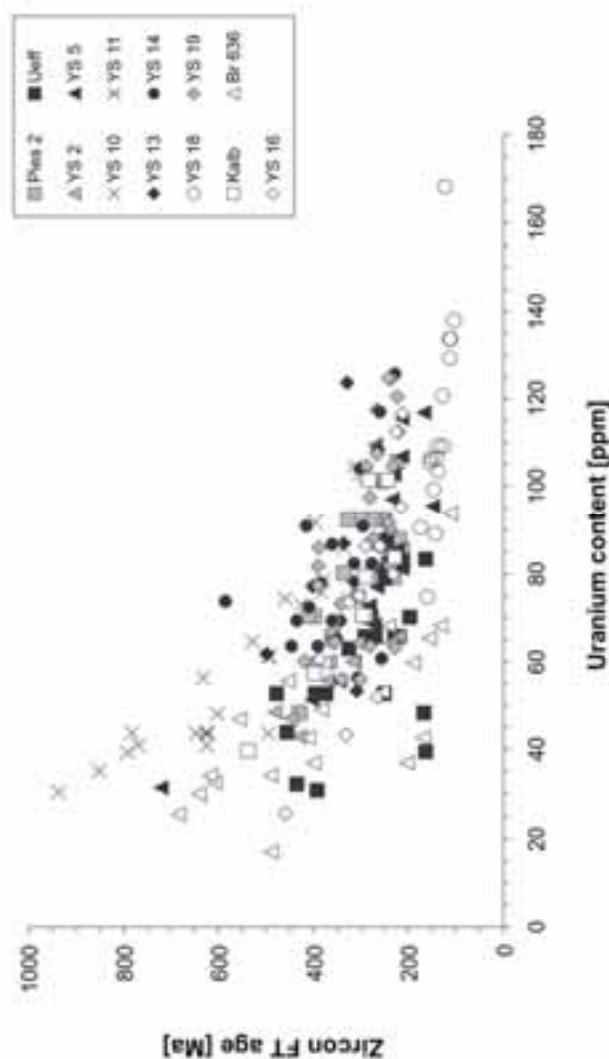


Figure 3.5: Zircon grain ages vs. Uranium content.

The integration of the stability data of fission tracks in zircon with the observed age patterns may help to evaluate the scenarios which are debated concerning the origin of the thermal anomaly in the southwestern part of the LSB. With this

objective, stratigraphic and sedimentological data as well as information from other thermal indicators will be compared to the new data presented in this publication. Special attention will be given to the early part of the history in order to explain the widespread annealing of fission tracks in zircons from Upper Carboniferous rocks. Four main theories are discussed: 1) burial during the Variscan orogeny, 2) Permian volcanism, 3) Permian extension and crustal thinning, and 4) hydrothermal activity.

During Carboniferous times, the LSB formed the northern foredeep basin of the Variscan orogen. Sedimentation contained debris accumulations from the south resulting in thicknesses of more than 3000m (Westphalian 316-305Ma). In Stephanian times (305-300Ma), the approaching Variscan front led to flysch sedimentation which reached thicknesses of approximately 600m in the Ruhr Basin (Büker et al. 1995). This was accompanied by heat flows of up to 85mW/m² (Büker et al. 1995). The calculated Late Carboniferous heat flows in the Ruhr Basin increase northwards towards the LSB. Assuming that these thicknesses and heat flows also occurred in the LSB, numerically calculated temperatures for the Upper Carboniferous samples between 47°C (Westphalian D) and 78°C (Westphalian C) may have been reached.

Based on the assumption that coalification of the Ruhr Basin occurred during the Late Carboniferous (Büker et al. 1995), calculated rank gradients of the Palaeozoic sequences from the Münsterland 1 and Senden 11 wells result in a palaeo-temperature gradient of 40±2°C/km (T_{peak} after Barker and Pawlewicz 1994). Extrapolating these values towards the LSB, a thickness of almost 6000m would be necessary to reach the zircon partial annealing zone (230°C for average zircons). Assuming that the dated zircons are highly metamict, a thickness of approximately 4000m would still be required to enter the ZPAZ (150°C). However, the Westphalian D strata in the basin reached only an overall thickness of about 700 to 800m. Therefore, it has to be considered that either a significant amount of Stephanian or Early Permian sediments was eroded to account for the missing thickness or that the average palaeo-temperature gradient was much higher than 40±2°C/km at that time. No evidence for these both cases has ever been documented.

The Upper Carboniferous samples with mixed zircon FT ages probably reflect partial fission track annealing during a Post-Carboniferous heating phase in the basin. In the Variscan foredeep, the lithosphere probably underwent E-W extension during Stephanian times (Plein 1993). According to Bachmann and Hoffmann (1995), widespread volcanism in the region occurred as a consequence of magmatic underplating. In the Emsland, Südoldenburg and Bremen regions, andesitic volcanism occurred between 296-290Ma. Residual volcanic thicknesses range from 80 to 230m. In the northern part of the LSB, one well drilled Rotliegend volcanic sediments with a thickness of 130m. In the

adjacent Netherlands, olivine gabbros were intersected by the wells Dwingelo 2 and Hardenberg 2 as well as by other boreholes in the vicinity of De Wijk and Wanneperveen (Marx et al. 1995, NITG-TNO 2000). Two dates of these plutons constrain ages of intrusion between 322 ± 15 and 290 ± 16 Ma (NITG-TNO 2000). All these information might support the idea of an Early Permian magmatic intrusion having caused zircon annealing. Similar results were found by Jacobs and Breitzkreuz (2003) for the NE German Basin. Younger single grain ages of the mixed zircon fission track ages in the basin however postdate this magmatic episode by up to 70Ma. Therefore, a local magmatic source that formed at about 290Ma cannot explain the observed partial resetting of the zircon fission tracks. To test whether a part of the partially annealed zircons in the area of the LSB and the neighbouring Münsterland Block may have resulted from the thermal influence of a pluton, also a numerical simulation was performed. Thermal plumes reaching the sedimentary basin fill can be responsible for heat flow values of 100 to 220mW/m² (Poelchau et al. 1997). A simple numerical simulation of the thermal history of the basin was performed in this study, assuming that magmatic activity caused the higher heat flows in the LSB. Considering a temperature of 150°C - the low temperature boundary for the zircon partial annealing zone in α -damaged zircons (Garver and Bartholomew 2001, Riley 2002) - and an additional accumulation of Stephanian sediments of 600m, a heat flow of 270mW/m² at the time of 296Ma would be required to fit the model. These values far exceeded those determined by Poelchau et al. (1997) and are not supported by the vitrinite reflectance measurements in the area (Table 3.2).

Nevertheless, any influence of a magmatic intrusion affecting the thermal history of the basin is not supported by this study. Büker et al. (1985) assumed heat flows of about 85mW/m² for the Late Carboniferous/Early Permian on the adjacent Münsterland Block. After Bodri and Bodri (1985) heat flows of 85mW/m² are in accordance with a thinning of the crust from 40 to 25km. Crustal extension and thinning accompanied with a narrower alignment of isotherms may have resulted in the upwelling of the asthenosphere (Neugebauer 1989, Bachmann and Grosse 1989). During this time of extension volcanism was favoured along NNE-SSW trending structures (Bachmann and Hoffmann 1995). The same fault pattern was noted in the LSB by Betz et al. (1987), and could be responsible for the upstream of hydrothermal fluids along deep reaching faults.

Perhaps the most probable origin for the partially reset zircons could be due to subsurface hydrothermal fluid circulation within the Westphalian layers during the Early Permian and before deposition of the Zechstein. During the latest stage of the Westphalian, widespread sandstones derived from braided river systems were deposited in the area of Osnabrück/Ibbenbüren providing pathways for hydrothermal fluids (Füchtbauer et al. 1991). Most probable is a combination of

hydrothermal fluid flow from aforementioned deep reaching fracture zones during this time accompanied with a widespread fluid circulation based on the high porosity of the Westphalian. Vitrinite reflectance data did not show any pronounced increase in reflectance, i.e. a “coalification jump” between the Mesozoic and Upper Carboniferous sections. This observation supports the view that vitrinite bearing, fine grained, less permeable rocks were not influenced by Permo-Triassic heating events, whereas the zircon bearing coarse grained sandstones hold this imprint. Such a situation is consistent with transient heating by fluids distal from a site of magmatic heating (Duddy et al. 1994). Widespread evidence of stratabound mineralization of siderite, lead-zinc-sulphides, and barite within the LSB may indicate such hydrothermal activity. The feeding channels for the ore forming solutions appear to be emplaced along marginal faults bounding the Carboniferous blocks in the LSB. The timing of mineralization is poorly constrained, but it may have occurred during extension at the time of the updoming in the Early Cretaceous (see Betz et al. 1987).

Another explanation has to be found for the exceptional zircon data from sample YS 18.

During the Latest Malm and Berriasian rifting set in (Dulce et al. 1993). Thereby subsidence of the LSB occurred due to divergent wrenching. During this time episode deep burial occurred in the centre of the LSB at elevated heat flows resulting in temperatures exceeding 320°C. This may be reflected by the partial annealing of zircons from the Upper Jurassic sample Br 636 as well as by the total annealing of zircons of Carboniferous sample YS 18. In that sample, however, the possibility of annealing inherited from an earlier Permian event must also be considered.

3.5.2.2. Apatite fission track results

- Apatite fission track lengths

While most of the Carboniferous surface samples provided good apatite yields and track length data, often less than 100 track lengths could be measured in the Mesozoic samples. The track length distributions are illustrated in Figure 3.2 and Table 3.3. Due to the young (Neogene) FT ages of the borehole samples, only three out of the seven samples yielded 90 or more horizontal confined track lengths. These may be used as an additional tool to interpret the cooling history. The data of outcropping Carboniferous rocks in the south of the Wiehengebirge Flexure Zone as well as Triassic samples from the centre of the basin show a high degree of similarities of mean track lengths (MTL) ranging from $14.0 \pm 0.2 \mu\text{m}$ to $13.1 \pm 0.2 \mu\text{m}$ with negative skewnesses and standard deviations from 1.1 to $2.0 \mu\text{m}$. According to Gleadow et al. (1986), this type of length distribution results from an accelerated cooling. Mean track lengths towards the

northern basin margin are much shorter and range from $11.8 \pm 0.5 \mu\text{m}$ to $10.0 \pm 0.4 \mu\text{m}$ with a standard deviation of $1.9 \mu\text{m}$ indicating a moderate to slow passage through the APAZ.

- Apatite fission track ages

Ten apatite fission track (FT) central ages and six confined track-length distributions were obtained from rocks of the LSB and from the Münsterland block at different depths and are displayed in Figures 3.2 and 3.6.

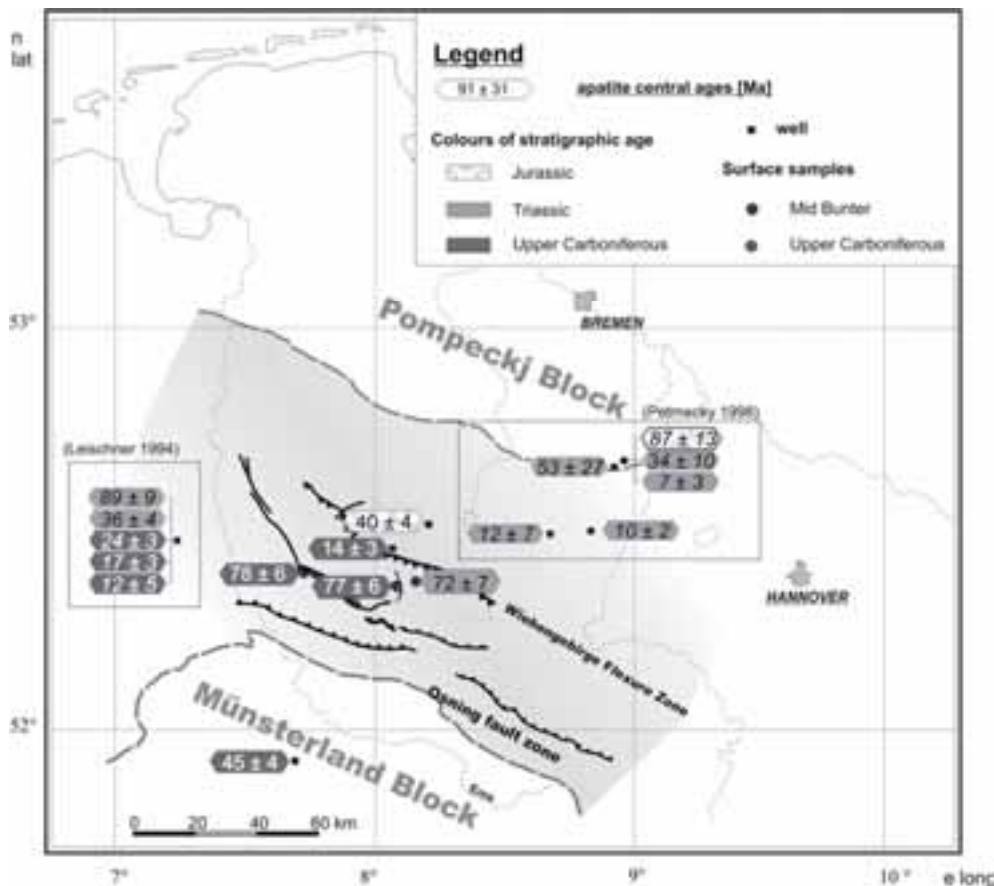


Figure 3.6: Map showing apatite ages.

a) Samples from Boreholes in the LSB

Samples YS 14, YS 15, and YS 16 from the northern part of the basin and YS 18 from the centre of the basin were collected from Carboniferous rocks at depths of 3500 to 3900m, corresponding to present-day temperatures of 125°-135°C.

The apatites yielded FT central ages of 19 ± 7 , 16 ± 5 , and 12 ± 3 Ma in the northern margin of the LSB and 14 ± 3 Ma near at the basin centre. These cooling ages

overlap on the 1σ error level. Single grains with no spontaneous tracks intersecting their polished surfaces (so called zero-track grains) were observed in all of the Carboniferous samples, but were not included in the calculation of the FT age. Thus, the central ages should be regarded as maximum ages of cooling to temperatures cooler than the apatite partial annealing zone. Furthermore, the central ages were obtained in most cases as an average of a few single grain ages. With the exception of sample YS 18, these were characterized by low age dispersions and passed the χ^2 -test. The distributions of the apatite FT single grain ages for the Carboniferous samples of the LSB are illustrated with radial plots (Galbraith 1990) and single grain-age frequency diagrams (Dunkl 2002) in Figure 3.7.

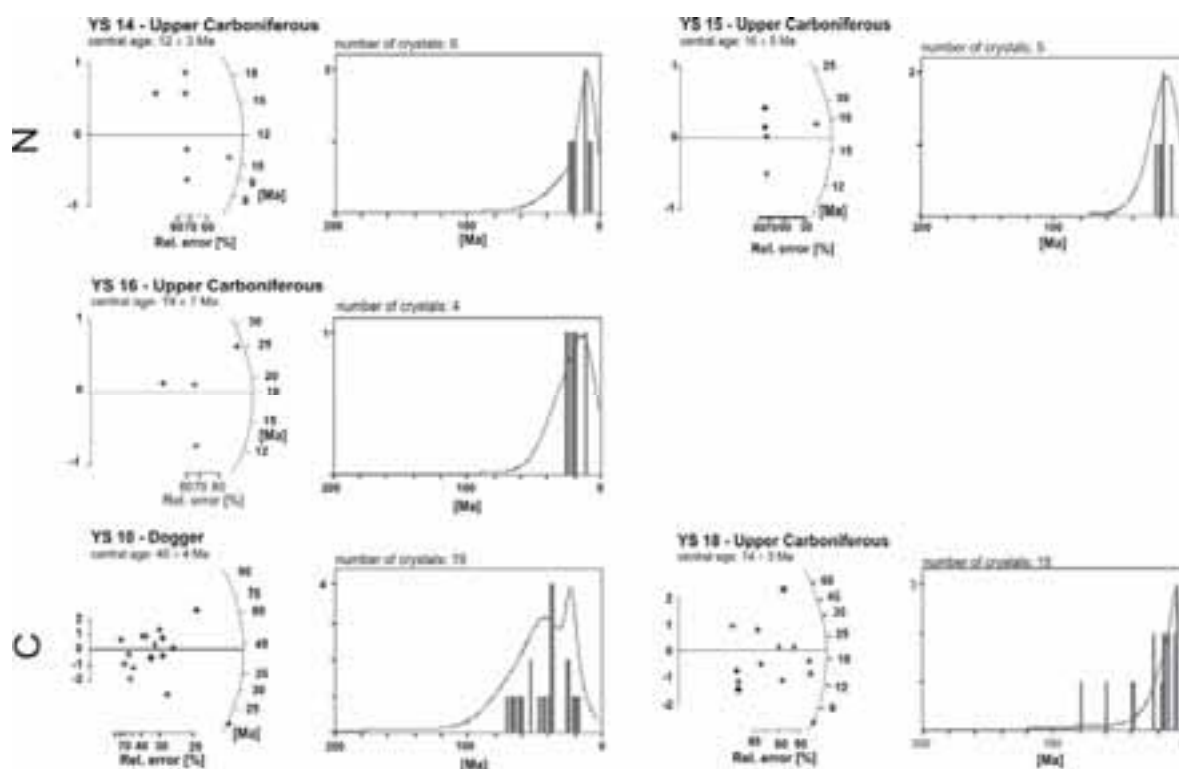


Figure 3.7: Radial plot diagrams and age spectra of apatite fission track ages. The horizontal line represents the central age and the shaded areas the stratigraphic age of each sample. Abbreviations: N= northern part of the basin, C= centre of the basin, S= southern part of the Wiehengebirge Flexure Zone, MB= Münsterland Block. For estimation components in a mixed distribution of apatite fission-track ages Trackkey 4.2 (Dunkl 2002) is used to express the analytical results.

The apatite FT single grain age spectra for the samples at the northern margin of the LSB are constrained to the Tertiary (between 27 ± 14 and 8 ± 6 Ma). For sample YS 18 from the basin centre, the single grain age spectrum ranges from Cretaceous to Late Miocene (from 79 ± 46 Ma to 5 ± 5 Ma).

Due to the low spontaneous track density counted in samples YS 14, YS 15, and YS 16, the interpretation of their cooling ages should be handled with care. No confined track length measurements were obtained in these samples.

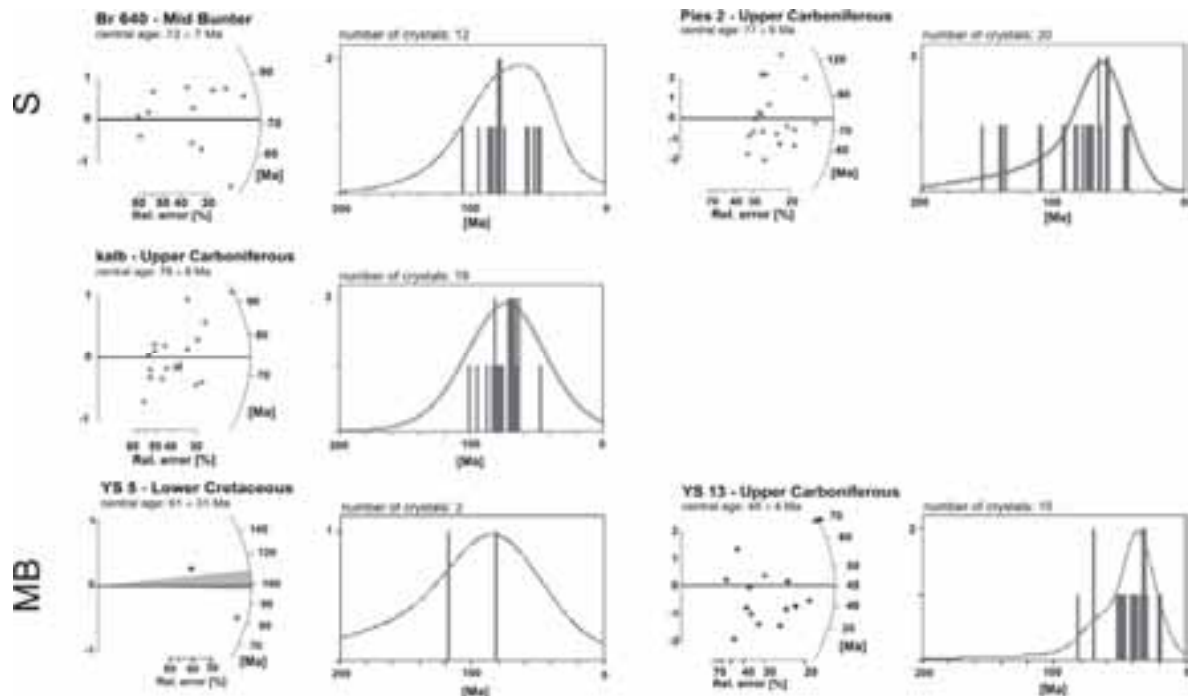


Figure 3.7 (cont.).

Sample YS 10 represents a Mid Jurassic sandstone from the centre of the basin at a depth of 2065m and a present-day temperature of $\sim 72^{\circ}\text{C}$. It shows an apatite FT central age of $40 \pm 4\text{Ma}$ which failed the χ^2 -test at the 5% level. Its single grain age spectrum varies between $71 \pm 14\text{Ma}$ and $16 \pm 9\text{Ma}$ (Figure 3.7). Although only 17 confined tracks could be measured in this sample, the large standard deviation ($1.9\mu\text{m}$) of the track-length distribution suggests a slow cooling rate through the apatite partial annealing zone (Figure 3.2, Gleadow et al. 1986).

b) Samples from Outcrops in the LSB

Samples Kalb and Pies 2 of Carboniferous depositional age and sample Br 640 of Bunter age were obtained from outcrops at the southern side of the Wiehengebirge Flexure Zone in the LSB. These yielded on the 1σ level identical apatite FT central ages of 78 ± 6 , 77 ± 6 , and $72 \pm 7\text{Ma}$. Samples Kalb and Br 640 had low age dispersion and passed the χ^2 -test, whereas Pies 2 carried large age dispersion and failed the χ^2 -test. Their single grain age spectra and radial plots are displayed in Figure 3.7. These show individual cooling ages ranging from

155±34Ma (Pies 2), 107±63Ma (Br 640), and 103±34Ma (Kalb) to 49±12Ma (Br 640), 48±30Ma (Kalb), and 44±15Ma (Pies 2). Confined track-length distributions for these samples display relatively long mean track lengths (between 13.1 and 13.9µm) and relatively small standard deviations (between 1.5µm and 2.0µm), suggesting rapid cooling rates through the apatite partial annealing zone (Figure 3.2, Gleadow et al. 1986).

c) Samples from the Münsterland Block

Sample YS 13 was obtained from a Carboniferous sandstone of the Münsterland Block at a depth of 1427m and a current temperature of ~57°C. The apatite FT central age of 45±4Ma carried a high age dispersion of 22% and failed the χ^2 -test. Its single grain age spectrum varies between 81±35 and 19±9Ma. Its confined FT track-length distribution displays short mean track length (12.2±.2µm) and a relatively narrow standard deviation (1.4µm) (Figure 3.2).

Sample YS 5 was taken from an Early Cretaceous sandstone at a depth of 280m and a recent temperature of ~25°C. The sample yielded only two ages of 116±72 and 82±34Ma which are identical on the 1 σ error level. Due to the low spontaneous track density and few grains in the sample, these data should be interpreted with caution.

- Interpretation and discussion of the apatite fission track ages

The samples YS 14, YS 15 and YS 16 from boreholes in the northern part of the LSB with central apatite ages between 19±7 and 12±3Ma indicate a cooling episode in the Miocene. Despite the fact that the apatites were located at depths corresponding to present-day temperatures of 125-135°C where total annealing should occur, these also reveal older age components of up to Cretaceous age. This points out that they must have experienced these elevated temperatures relatively recently. For temperatures of 120°C, total annealing of fission tracks in apatites is indicated to occur at a timescale of 10Ma (Laslett et al. 1987, Duddy et al. 1988, Brandon et al. 1998). Therefore a thermal perturbation at depth must appear to cause a down-bending and spreading of the isotherms in the basin. Numerical modelling was performed to test the temperature evolution of the LSB during this time. It indicates that a very low heat flow of ~45mW/m² was required during the Tertiary to keep the sediments at a temperature level between 120 and 60°C. Similar low heat flow values of 40 to 50mW/m² during the Tertiary have been required to satisfy the numerical models of the thermal evolution of the Glückstadt-Graben (Rodon and Littke; 2005). Moreover, present-day heat flows for the northern part of Germany and the North Sea calculated by Haenel (1986), range between 40-60mW/m². A low average thermal gradient for the uppermost crust of 29°C/km for the Miocene can be calculated based on the high temperature boundary of the apatite partial

annealing zone at 120°C contrasted to a surface temperature of 16°C (after Wygrala 1989). In comparison to the recently measured gradient of 33°C/km, this indicates a tendency towards increased heat flows during the last few hundred thousand/million years. This may be explained by a decoupled model of lithospheric shortening, including a regional uplift without inversion assuming a thickening of the mantle lithosphere without thickening of the overlying crust (Hillis 1992). Thus, the recent temperature increase might be as well a combination of upwards-dragged isotherms after exhumation accompanied by hot fluid circulation from the further east of the basin (Petmecky et al. 1999). The apatite fission track data also indicate that the system of hot hydrothermal fluids in the southern LSB might be a young geological phenomenon.

The Mesozoic sample YS 10 from the centre of the basin may also have been affected by the Miocene cooling. The sample was previous to the late cooling episode probably located at temperatures just cooler than the partial annealing zone. In the last million years, it reached a temperature of about 70°C just above the low temperature boundary of the partial annealing zone (60°C), enabling incipient annealing of tracks in the apatites.

Surface samples Pies 2, Kalb, Br 640, and the borehole sample YS 5 from the southern part of the Wiehengebirge Flexure Zone display central apatite FT ages ranging from 91±31Ma to 72±7Ma (Turonian–Campanian/Upper Cretaceous). These ages reflect the time of inversion in the LSB. According to AFTSolve modelling (Ketcham et al. 2000), their cooling paths illustrated in Figure 3.8 indicate an entrance into the APAZ during Campanian times. Samples closer to the Wiehengebirge Flexure Zone (Pies 2, Br 640) cooled below the APAZ at faster rates than the remote sample Kalb. Therefore, higher cooling rates (1.5-4°C/Myr) can be estimated for this period. The rocks were at temperatures below ~60°C already in Paleocene/Eocene times. Therefore, an additional deposition of 200-300m of Tertiary sediments followed by a Miocene uplift should not have affected them. In earlier studies from the eastern and western basin margins similar results were found by Leischner (1994) and Petmecky (1998) (Figure 3.6).

The apatite FT age from the Carboniferous sample YS 13 from the Münsterland Block also indicates a cooling episode during the Early Tertiary, despite the fact that it includes young single grain ages affecting its central age. The Carboniferous sample experiences today a temperature of 57°C suggesting that the Münsterland Block was already uplifted and denuded during the Early Tertiary.

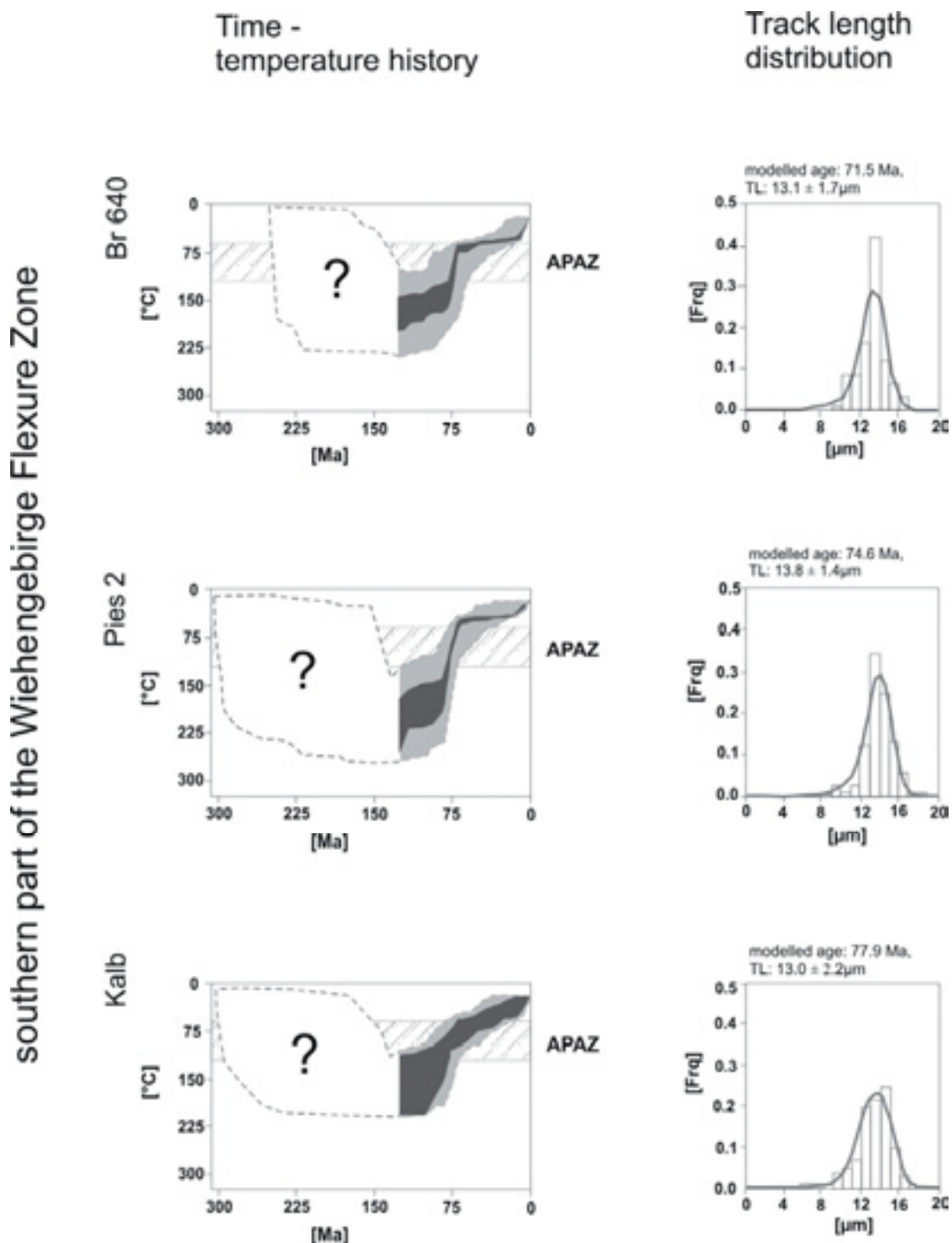


Figure 3.8: Time-Temperature histories modelled with AFTSolve (AFTSolve1.3.1 © 2003; Ketcham and Donelick 2000). Acceptable fits are light grey and good fits are dark grey. Track lengths distributions are displayed in bars and curves represent those estimated by forward modelling.

3.5.3. Regional Cooling and Denudation Pattern

The regional pattern of FT ages is dominated by a northwards decrease in zircon FT ages reflecting depositional ages in the south up to reset Permian ages in the north. One exception represents the sample of the basin centre with a cooling age of Lower Cretaceous after a complete resetting. Apatite FT ages reflect a south to north decrease within the basin. A south-north cross-section demonstrates that this decrease is not gradual (Figure 3.9). Instead, an abrupt change occurs which coincides with the position of the Wiehengebirge Flexure Zone. In deeply buried Carboniferous sandstones, young apatite FT ages are observed between the Wiehengebirge Flexure Zone and the northern margin of the basin. In contrast, much older apatite FT ages are observed in surface-near Carboniferous sandstones just south of the Wiehengebirge Flexure Zone (Figure 3.9d). This implies that the rocks on the southern side of the flexure zone have experienced clearly more uplift and erosion relative to rocks north of the flexure zone. Thus, the flexure represents a structure with significant influence on temperature history and coalification pattern. In a similar way, Petmecky et al. (1999) found that coalification in the vicinity of the so-called Uchte anomaly further east is bound to major tectonic elements.

3.6. Summary

In summary, the zircon fission track data provide evidence for widespread (hydro)thermal activity during i) the Permian, probably related to the rifting and crustal thinning of the Southern Permian Basin and ii) the Upper Jurassic and Lower Cretaceous respectively, related to more local extension in the LSB itself. Most, but not all observations can be explained by these heating/cooling events. The apatite fission track ages indicate one major cooling event in the Mid Cretaceous (~89-72Ma) reflecting the time of inversion of the LSB. The track-length data, together with ages, provide strong evidence for more or less rapid cooling of the basin centre and moderate cooling towards the basin margins during the Cretaceous. Apatite fission track ages from borehole samples which recently entered the upper part of the APAZ indicate that a continuous cooling during the Tertiary must be taken into account, followed by a young heating of the sedimentary sequences until present day.

The track length distributions of the Carboniferous and Bunter rocks close to the Wiehengebirge Flexure Zone indicate fast to slow cooling histories below ~120°C. Apatites from the Carboniferous rocks of the southern part of the basin suggest a moderate cooling history. Finally, apatite fission track ages from borehole samples which recently entered the upper part of the APAZ indicate a young heating of the sedimentary sequences until present day.

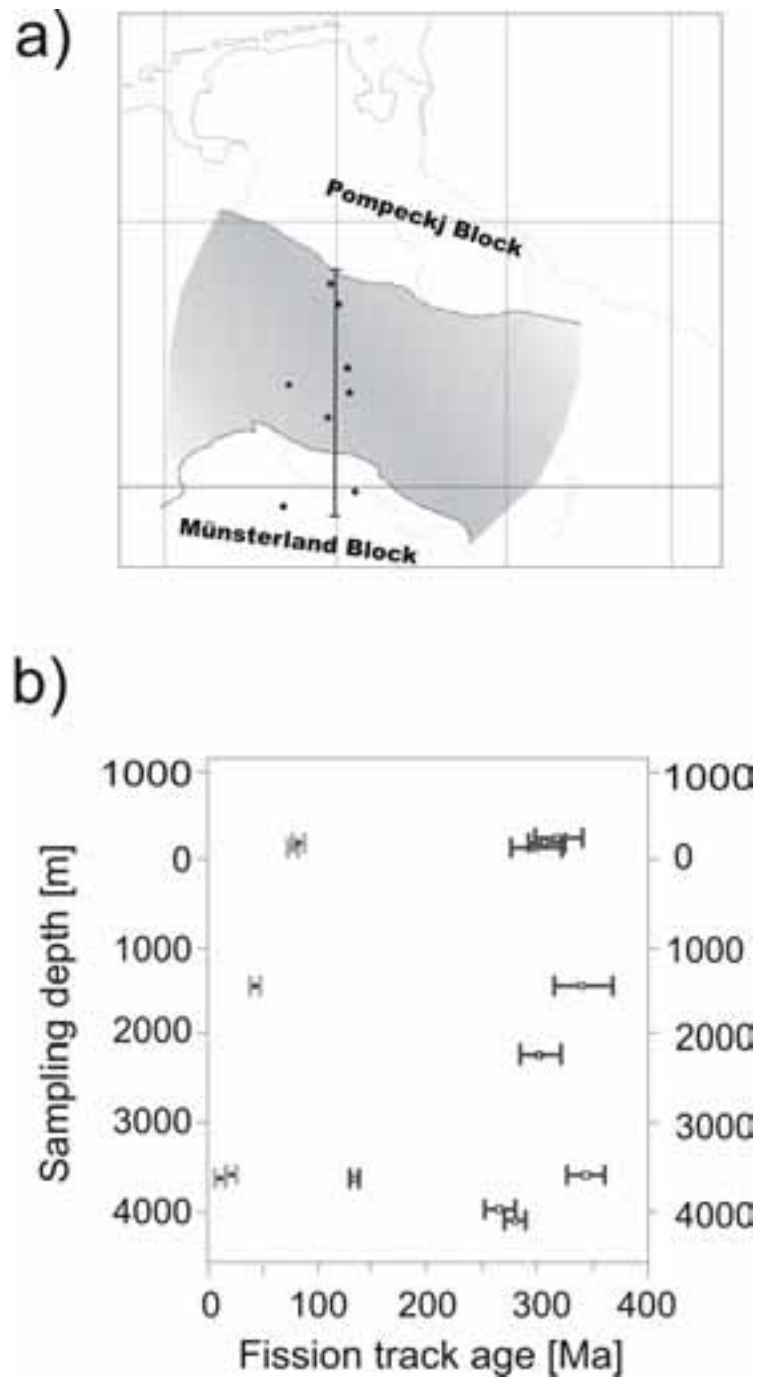


Figure 3.9: Thermochronological overview of the Upper Carboniferous in the LSB. a) South-North section through the LSB. Upper Carboniferous sample locations were projected on this line. b) Age-depth relationship for central apatites - and zircon FT ages of the Upper Carboniferous samples with the standard deviation of $\pm 1 \sigma$.

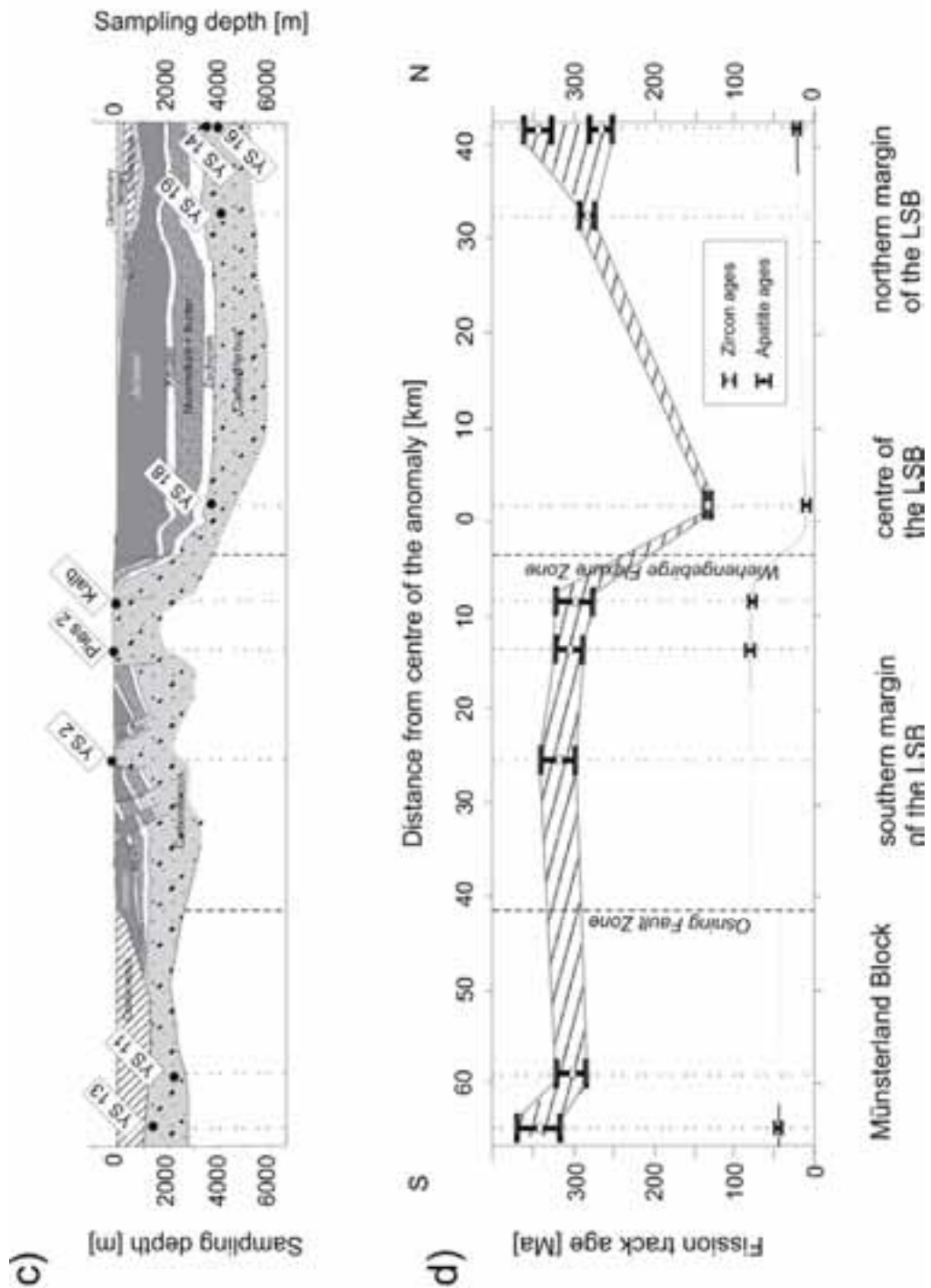


Figure 3.9 (cont.): Thermochronological overview of the Upper Carboniferous in the LSB. c) Schematic cross section of the sample locations and the present depth of the Upper Carboniferous. d) Apatite and zircon age distance profile across the two major faults demonstrates well marked age change. The position of the profile is given in a) and c).

4. Fluid systems and basin evolution of the western Lower Saxony Basin, Germany

Keywords fluid inclusions, vitrinite reflectance, structural modelling, basin modelling, Lower Saxony Basin

4.1. Abstract

The western Lower Saxony Basin is characterized by magnetic and gravity anomalies and an unusually strong coalification of surface-near sedimentary rocks, indicating that high temperatures were reached in the past. The temperature history of the basin has been disputed for many years leading basically to two different hypotheses: one proposes igneous intrusion during Mid Cretaceous time, causing the high maturity in this area, whereas the other theory explained the coalification as a result of deep burial during late Jurassic and early Cretaceous times.

Petrographical data are summarized which show the maturity distribution within the basin, reflecting maximum palaeotemperature conditions. This maturity distribution is visualized along three cross sections of up to 50km length, as well as the palaeotemperature distribution for six time steps. Furthermore, geochemical data on petroleum source rocks are presented which indicate early mature/immature type I/II kerogen in Wealden and Posidonia Shales and mature/overmature type III kerogen in the coal-bearing Upper Carboniferous. Fluid inclusion compositions in quartz crystals are highly variable ranging from liquid to gaseous, and gas compositions are also variable. These data were interpreted in the context of burial history.

This study provides new data and numerical models with the intention to clarify the cause of the high coalification in the basin. 2D structural and basin modelling along three cross sections, combined with new fluid inclusion measurements and results of previous coalification studies, 1D modelling, and fission track dating demonstrate high heat flow during the Late Jurassic extension stage followed by a deep burial of the basin during the Early Cretaceous, associated with only moderate heat flows. The presence of an igneous intrusion of Cretaceous age is not supported. Furthermore, timing of hydrocarbon generation from the three major source rocks is discussed.

4.2. Introduction

The Lower Saxony Basin (LSB) is one of several sedimentary basins within the Central European Basin system. The evolution of the LSB started during the

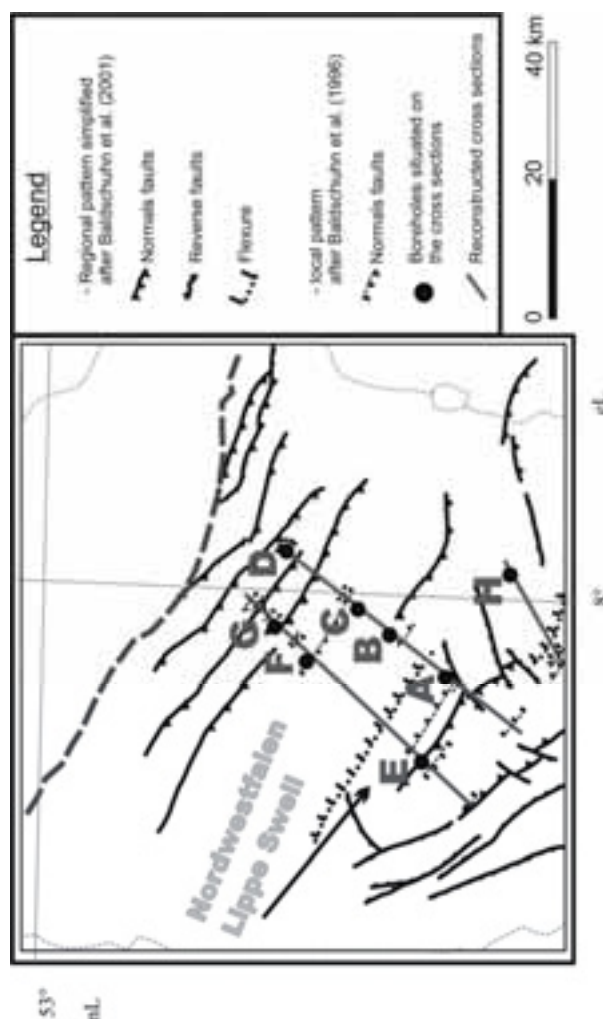


Figure 4.1: Locations of the reconstructed cross sections in relation to the main tectonic features within the Lower Saxony Basin. The Figure shows the simplified regional pattern (thick lines) after Baldschuhn et al. (2001) plus the local pattern (dotted lines) used for the structural reconstructions according to Baldschuhn et al. (1996).

Late Permian with extension and moderate subsidence, followed by down-warp of the northern part of the basin in Triassic times. Pre-existing NW-SE trending Variscan structural elements (Figure 4.1) were used during the following accelerated subsidence period. Already during Liassic times, basin differentiation set in. The climax of basin subdivision during the Late Jurassic led to the exposure of the Nordwestfalen-Lippe Swell and the resulting evolution of various sub-basins. Maximum subsidence rates in the NW-SE trending sub-basins were reached in Late Jurassic to Early Cretaceous times. During Late Cretaceous times, basin inversion and therefore uplift and erosion occurred based on compressional effects related to the Alpine orogeny. In

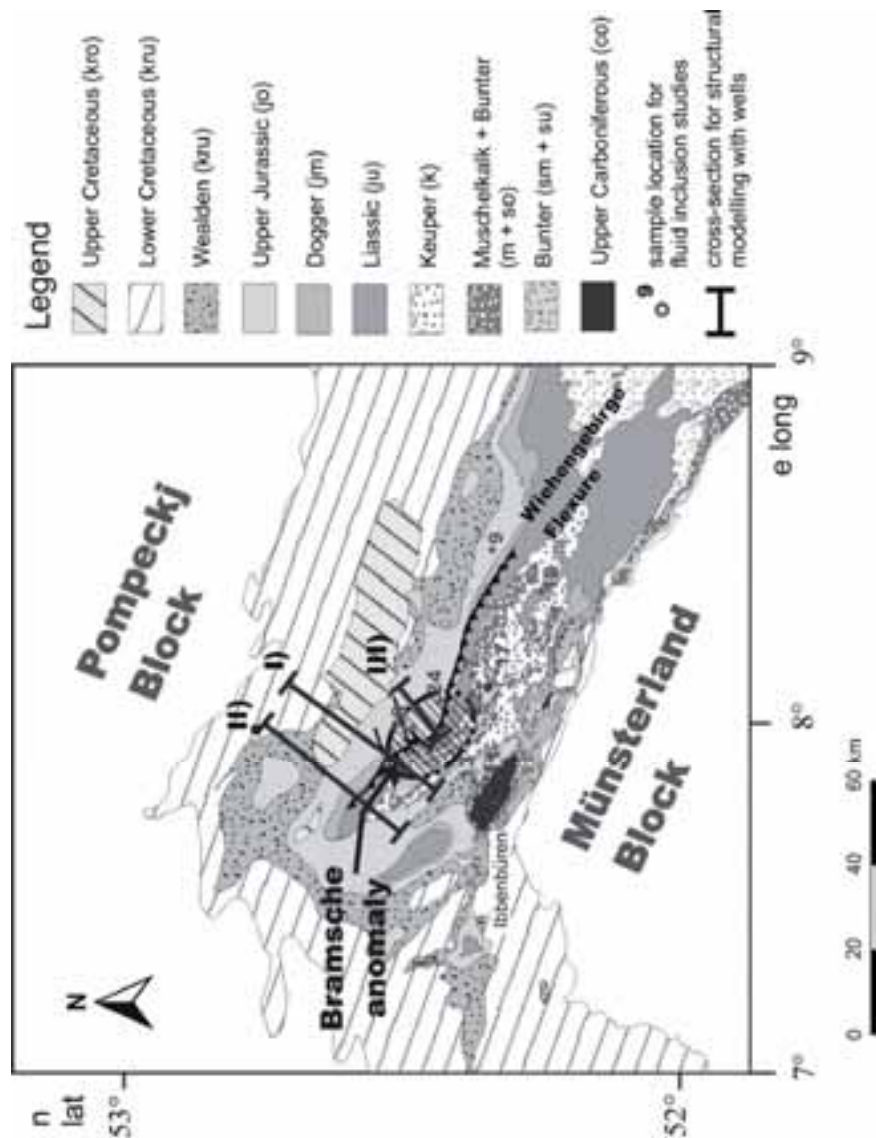


Figure 4.2: Geological overview of the study area in the western part of the LSB with the fluid inclusion sample locations as well as the position of the cross sections for the 2D modelling.

Tertiary times, a renewed almost imperceptible subsidence set in, continuing until recent times.

Important gas and oil source rocks include Upper Carboniferous coal-bearing strata as well as Jurassic (Toarcian/Posidonia Shale) and Cretaceous (Berriasian/Wealden) organic rich shales which are outcropping on the basin margins and on swells within the basin. Based on the geological settings, the LSB provides a region with proven high hydrocarbon potential (Figure 4.2). Petroleum exploration in this basin started already in 1864 and since then more than 100 oil fields have been discovered, more than 10,000 wells have been drilled, and more than 100,000km of seismic data have been shot. Thus, the LSB

can be regarded as a well-known example of a sedimentary basin that was partly inverted.

In the south western part of the LSB, anomalously high maturity of organic matter has been observed which reaches 3.0-4.5%VRr in Upper Jurassic and Lower Cretaceous sedimentary rocks (Bartenstein et al. 1971, Teichmüller et al. 1984, Koch and Arnemann 1975) and has been a matter of debate for many years. The area of high coalification coincides with a magnetic and a positive gravimetric anomaly (Breyer 1971, Hahn and Kind 1971). In early publications, these anomalies were interpreted as the effect of a deep-seated igneous intrusion, the so-called Bramsche Massif (Mundry 1971, Thyssen et al. 1971, Buntebarth and Teichmüller 1979, Giebeler-Degro 1986). In accordance with the lignite/sub-bituminous coal stage of Upper Campanian rocks overlying the Lower Cretaceous units, it was concluded that the intrusion was emplaced either in late Early Cretaceous or in early Late Cretaceous times (Stadler and Teichmüller 1971).

In recent years, numerical models of several wells east and west of the Bramsche Massif suggested a different interpretation, involving deep burial during Early Cretaceous times followed by Late Cretaceous/Tertiary uplift. This was probably related to inversion of specific local, fault-limited sub basins (Leischner et al. 1993, Petmecky et al. 1999). Estimations of maximum burial depths and thicknesses of now eroded sedimentary rocks range from about 3500 to 8000m (Füchtbauer and Müller 1970, Nodop 1971, Thiermann 1980, Drozdowski 1988, Baldschuhn and Kockel 1999, Brink 2002, Senglaub et al. 2006).

Additionally, information on structural evolution, subsidence rates, and igneous activity in the adjacent areas (Sissingh 2004), K/Ar-dating of illites (Gaupp et al. 1993), and fission track ages (Senglaub et al. 2005, Karg et al. 2005) provide some constraints with respect to the early temperature evolution. K/Ar ages of illite indicate an illite formation between 200 and 180Ma (Late Triassic-Early Jurassic). Zircon fission track data provide evidence for widespread (hydro-) thermal activity during the Permian and the Late Jurassic, respectively Early Cretaceous. Furthermore, apatite fission track ages indicate one major cooling event in the Mid Cretaceous (~89-72Ma), reflecting the time of inversion of the LSB (Senglaub et al. 2005). Assuming deep burial instead of a magmatic intrusion would result in a completely different maturity development of the main source rocks (Upper Carboniferous coals, Toarcian and Wealden organic matter rich shales) and thus would affect timing of hydrocarbon expulsion as well as migration and accumulation within the basin.

Therefore, a comprehensive, multi-disciplinary study, involving organic geochemistry, structural geology, and basin modelling has been carried out in

order to obtain information on the coalification evolution within this part of the basin.

Subsidence and erosion history of a basin combined with complementary structural information may provide insight into changes in basin dynamics with time, leading to conclusions on the basin type and possible mechanisms of basin formation. With this objective, back-stripping calculations based on three 2D structural models along transects through the “Bramsche anomaly” were performed with the 2DMoveV4 software (Midland Valley 2003). The results were implemented in the 2D basin modelling software PetroMod (IES). Numerical simulations were performed, taking into account the newly gained temperature information by Senglaub et al. (2005). Thus achieved quantitative 2D basin models should be consistent with maturity, fission track, and structural information.

Furthermore, new fluid inclusion data are presented and discussed as primary fluid inclusions hosted in diagenetically formed minerals record fundamental information for the reconstruction of the thermal history through time within a sedimentary basin. The analyses of the trapped fluids within the inclusions can provide specific information about the physico-chemical conditions at the time the host mineral was precipitated, if the inclusions have not been modified or re-equilibrated subsequent to their entrapment (van den Kerkhof and Hein 2001, Goldstein and Reynolds 1994).

4.3. Methods

4.3.1. Geochemical investigations (TOC and Rock-Eval data)

Total organic carbon content (TOC) of 272 samples was measured on pulverized aliquots of 100-200mg using a LECO RC-412 carbon combustion device combined with a programmable temperature controller. Temperature fractionation allows the performance of two measurement phases. During the first phase, organic carbon is burnt between temperatures of 300°-500°C, whereas in the second phase, at temperature up to 1050°C inorganic carbon is released.

Rock-Eval pyrolysis is a rapid method used to evaluate the oil and gas potential as well as the maturity of source rocks and other sedimentary rocks (Espitalie et al. 1977). The Rock-Eval 2 device used here consists of a micropyrolysis oven with thermocouple to monitor the temperature of the sample and a programmed system to raise the temperature to 530°C in oxygen-free nitrogen gas. The sample weights of 210 sediment samples varied from 10-120mg due to different TOC-contents (>0.5%).

Hydrocarbons released below 300°C are a measure of hydrocarbons present in the rock in a free or adsorbed state. The yield of volatile material generated by thermal cracking at 300-500°C provides information on the potential of the rock to yield oil. During pyrolysis, the temperature recorded at the maximum rate of volatiles released (T_{max}) is used to evaluate thermal maturity of the source rock. Thus, type and maturity of organic matter in petroleum source rocks can be characterized from Rock Eval pyrolysis data as shown in Figure 4.3.

4.3.2. Fluid inclusions

Nine selected samples of authigenic quartz crystals were provided by H. Klassen from the Naturkunde-Museum Osnabrück and originated from Carboniferous, Triassic, and Jurassic sandstone host rocks from the southern margin and centre of the LSB (Figure 4.2).

Microthermometric measurements were conducted using a Fluid Inc. USGS heating–freezing system mounted on a BX50 Olympus microscope and performed according to outlines in Roedder (1984) and Burruss (1987). The heating–freezing stage was calibrated with synthetic fluid inclusions supplied by Synflinc. Gas-bearing inclusions were analysed with a Jobin-Yvon Raman spectrometer combined with a 532nm Nd/YAG laser.

4.3.3. 2D moveV4 (Structural investigations)

The geological interpretations of depth converted 2D seismic profiles (Baldschuhn et al. 1996) are the basis for the structural balancing. The profiles were imported as images and digitised. The applied workflow consisted of back-stripping techniques based on *Move On Fault Restorations* and *Flexural Slip Unfolding/ Restore* as well as *Decompaction* (see also 2D moveV4 Manual, Midland Valley 2003).

During extensional movements, the hanging wall collapse is controlled by the shear vector, which specifies the path the hanging wall elements take during the collapse. The shear vector may be oriented vertically or synthetic or antithetic to the fault plane. *Move On Fault Restoration* uses the inclined shear algorithm, which maintains the area between bedding surfaces. It is most applicable to extensional tectonic regimes, where anticlinal rollover structures have developed on non-planar normal faults. Furthermore, this algorithm can be applied to the restoration or forward modelling of inverted basins and growth faults, where the thickness of beds may vary.

The Inclined Shear algorithm is also effective for restoring listric faults, which are defined as faults of decreasing dip with depth. The curvature or change in dip of a fault is responsible for deformation that occurs in the hanging wall. Inclined shear assumes that deformation occurs within the hanging wall along a

series of parallel ‘shear pins’ that translate along the fault plane by the horizontal distance specified by the heave.

The *Flexural Slip Unfolding* tool unfolds the rocks and then translates the unfolded components to their pre-deformation positions. The *Flexural Slip Unfolding* algorithm can best be applied to concentric folds made up of parallel layers. The algorithm works by first rotating the limbs of a fold, e.g. to a horizontal datum or an assumed regional unconformity. The effects of the flexural slip component of folding are removed by allowing the layers to slide relative to each other in the rotated fold limbs. The *Flexural Slip Unfolding* tool can in appropriate cases also be used to validate complex thrust deformations and the cover rocks surrounding intrusive salt structures.

The *Fault Parallel Flow* algorithm is designed to kinematically model geological structures in the hanging wall where deformation is accommodated by fault-parallel shear. The sections were restored to the sea level before the decompaction tool was applied. The created databases for the *Decompaction* algorithm comprise lithological standard values according to Sclater and Christie (1980) and to the program STRATAGEM by Shell (see also Burgess et al. 2006). As the layers are composed of different lithologies (see also Senglaub et al. 2006), an average surface porosity and depth coefficient have been calculated.

In order to determine the surface porosity and depth coefficient for a specific rock unit, porosity (as a % of total rock volume) is required for each rock unit at different depths (see also Poelchau et al. 1997). Porosity decay is assumed to be exponential, so that a best-fit exponential curve is fitted through the data points. The value of porosity at zero depth can then be predicted (surface porosity) and the gradient of the exponential curve is the depth coefficient. Based on the inhomogeneity of the Zechstein layer and the assumption that pure salt is incompressible, the applied depth coefficient for salt was chosen to be 0.05.

In the case that units got partially lost or a hiatus occurred, the information about the thickness of eroded sedimentary sequences was obtained from 1D basin modelling studies described by Senglaub et al. (2006). The results of the structural restorations were imported into the PetroMod basin modelling software.

4.3.4. Numerical Basin Modelling

Numerical basin modelling provides an integrated approach to understand and reconstruct major geological processes taking place during the evolution of sedimentary basins (Welte and Yalcin 1988, Poelchau et al. 1997).

To reveal the temperature and burial history of the western part of the LSB, the 2D finite element simulation program PetroMod (version 9.1) was used.

Balanced structural profiles created in 2DMove were imported as palaeo-steps. *Paleo Stepping* provides the possibility to simulate petroleum migration in complex tectonic environments. The *Paleo Sections* and their duration time (timescale according to the German Stratigraphic Commission 2002) are the basis of a forward modelling, beginning with the oldest layer in the section. In order to reflect the adequate initial geometry of the sedimentary sequence within the profiles, the segments of each horizon/fault had to be collected and put on the model grid.

For the grid-cells, lithologies (see Senglaub et al. 2006) and facies (source rock properties/characteristics, kinetic algorithms for calculation of hydrocarbon generation rates) had to be created and assigned. This could be done uniformly for one layer but the model may also contain multiple facies and lithologies, which can be interpolated between different cells, respectively.

During basin history the temperature field - crossed by a given stratigraphic layer - is controlled by variations of the heat flow, temperatures at the sediment/water interface, and thermal rock properties, such as thermal conductivity and heat capacity. These in turn are influenced by lithology, compaction, overpressuring and subsidence rates (see Yalcin et al. 1997 for details). Therefore, finally, boundary conditions i.e. sediment-water interface temperature, and heat flow have to be defined and assigned. A detailed description of the theoretical background of the applied modelling software is given in the PetroMod Reference Manual 9.0 (e.g. Hantschel et al. 2000).

After each simulation run, the calculated results have to be compared with measured values, in order to calibrate the model and check its geological reliability. The calibration is achieved mainly by variation of heat flow history or original thickness of now eroded sedimentary units within geologically reasonable limits (Wygrala 1989, Leischner et al. 1993, Yalcin et al. 1997). Calibration data used in the study presented here include measured maturity values such as vitrinite reflectance as well as information about the temperature history gained by fission track dating (Senglaub et al. 2005) and recent temperatures (Haenel 1980). The kinetic EASY%Ro-algorithm (Sweeney and Burnham 1990) was applied for the calculation of vitrinite reflectance. This algorithm is based on an Arrhenius first-order parallel reaction approach with a distribution of activation energies and one frequency factor. It has to be noted that the EASY%Ro-algorithm allows only the calculation of vitrinite reflectance values from 0.3 to 4.5% and therefore does not cover the whole maturity range observed in some wells.

4.4. Results

4.4.1. *Geochemical investigations*

Three stratigraphic units in the study area show source rock potentials.

The first unit is a thick succession of Westphalian sediments, which contains humic source rocks (Type III kerogen) in coals and shales. The average coal content of the Westphalian succession is about 5.5% (Scheidt and Littke 1989). The TOC of the coals and shaly coals differs between 20 and 80%. The second important source rock is the marine Lower Jurassic Posidonia Shale (Toarcian; 2-12% TOC). The third source rock is the bituminous marine Wealden shale of Lower Cretaceous age (Berriasian), in which TOC reach up to 8%.

Further source rocks are Upper Jurassic coals (Oxfordian) that show TOC values of up to 43%, but occur only in a small area west of Bramsche. Other stratigraphic units have TOC values below 3% and are generally considered to be of minor importance as source rocks.

The Posidonia and the Wealden shales show a moderate to high petroleum generation potential along the northern and southern margin of the basin (Figure 4.3). The organic matter of these Jurassic and Cretaceous source rocks still resides within the oil window. This is evident from Rock-Eval (Table 4.1) and vitrinite reflectance data (Table 4.2). Towards the basin centre, these sequences either reach the wet gas zone or are overmature so that the hydrocarbon generation capacity has been exhausted. The same trend is obvious for the Carboniferous sedimentary units. Gas generating Carboniferous coals are only located at the margins of the basin and on the Münsterland Block. The low OI values of the coals reported here are partly due to high maturity; however, low OI values of coals have also been reported from other places (Amijaya and Littke 2006 and references therein).

4.4.2. *Fluid Inclusions*

The final ice melting temperatures (T_m ice) in aqueous inclusions in quartz samples from fissures (veins) in the Ibbenbüren and Piesberg area are generally between -2.1 and -27.8°C (Table 4.3). This observation points to high salinities (with CaCl_2 and NaCl components). With decreasing depositional ages, the samples show lower final ice melting temperatures and therefore also lower salinities between 9-17wt.% NaCl equivalent. An exception is the easternmost sample 9, which contains a wide spectrum of salinities in the fluid inclusions. Remarkably low salinities (4-5wt.% NaCl equivalent) have been found in authigenic quartz crystals hosted by Upper Jurassic sediments (samples 20, 24) from the basin centre. Similar inclusions were related to a deep reaching

Table 4.1: Rock Eval results; Abbreviations: TOC (total organic carbon), T_{max} (temperature of maximum pyrolysis yield), HI (Hydrogen Index) and OI (Oxygen Index).

stratigraphy	lithostratigraphy	depth below NN [m]	coordinates		TOC [%]	T _{max} [°C]	HI [mgHC/ gC _{org}]	OI [mgCO ₂ / gC _{org}]
			Gauss-Krüger-System eastings	northings				
Wealden	shale	425	34 33 400	58 39 020	8	434	690	6
Wealden	shale	797	34 47 930	58 32 630	8	443	716	6
Wealden	shale	627	34 47 930	58 32 630	5	438	568	13
Wealden	shale	368	34 32 960	58 38 120	5	435	467	38
Wealden	shale	346	34 32 960	58 38 120	4	433	483	28
Wealden	shale	659	34 33 400	58 39 020	4	436	602	12
Wealden	shale	527	34 33 400	58 39 020	4	436	546	11
Wealden	shale	960	34 25 360	58 44 870	2	426	50	50
Wealden	shale	125	25 93 500	57 99 740	2	445	584	6
Wealden	shale	945	34 26 360	58 49 680	2	438	462	77
Toarcian	shale	563	34 08 150	58 00 060	12	435	487	4
Toarcian	shale	surface	34 42 975	58 02 075	11	482	0	51
Toarcian	shale	1,976	34 56 290	58 35 750	10	435	366	11
Toarcian	shale	480	34 08 150	58 00 060	9	434	502	8
Toarcian	shale	592	34 08 150	58 00 060	8	429	371	11
Toarcian	shale	1,630	34 26 360	58 49 680	7	428	506	23
Toarcian	shale	1,947	34 47 930	58 32 630	3	447	17	31
Toarcian	shale	surface	34 42 975	58 02 075	3	462	3	11
Toarcian	shale	475	25 93 500	57 99 740	3	444	90	7
Toarcian	shale	844	34 32 960	58 38 120	2	434	142	54

Table 4.1 (cont.).

stratigraphy	lithostratigraphy	depth below NN [m]	coordinates		TOC [%]	T _{max} [°C]	HI [mgHC/ gC _{org}]	OI [mgCO ₂ / gC _{org}]
			easting	northing				
Westphalian	coal	surface	34 10 482	57 97 917	81	465	62	4
Westphalian	coal	surface	34 32 675	57 98 775	77	545	0	1
Westphalian	coal	surface	34 33 775	57 98 725	68	540	1	2
Westphalian	coal	surface	34 10 482	57 97 917	68	487	44	9
Westphalian	coal	surface	34 33 775	57 98 725	67	538	0	2
Westphalian	coal	surface	34 33 775	57 98 725	56	543	1	1
Westphalian	coal	surface	33 33 775	56 98 725	42	542	2	2
Westphalian	coal	surface	34 33 075	57 98 800	41	550	1	4
Westphalian	shale	surface	35 08 700	59 01 750	1	533	3	70
Westphalian	shale	3,586	34 32 270	58 13 430	1	368	5	67
Westphalian	shale	3,467	34 32 270	58 13 430	1	360	8	35
Westphalian	shale	surface	34 08 700	58 01 750	1	447	3	71
Westphalian	shale	surface	36 08 700	60 01 750	1	397	8	69

circulation of meteoric fluids during the time of inversion in Upper Cretaceous times by Wolfgramm (2002).

Since the homogenization of a two-phase inclusion occurs along the liquid–vapour curve and then develops along the isochore slope which is defined by density and salinity of the inclusion, there can be a large difference between the measured homogenization temperatures (T_h) and the true trapping temperature (Roedder 1984). In the present case, the difference between minimum and maximum homogenization temperatures of the samples scatters by approximately 30 to 60°C for individual samples (Table 4.3).

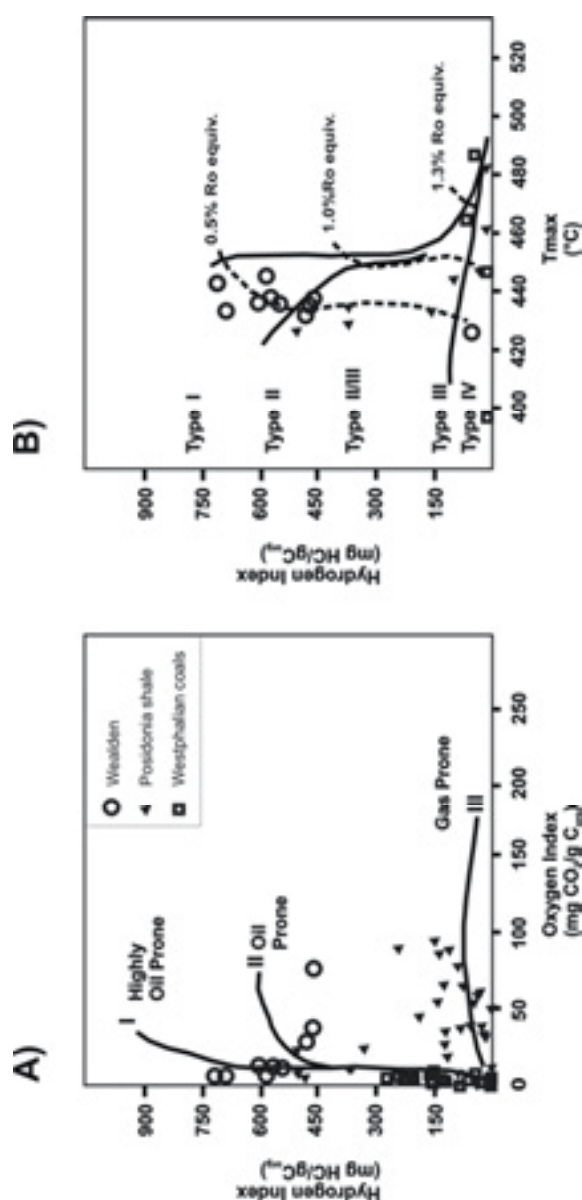


Figure 4.3: Plot of Rock-Eval pyrolysis data: A) van Krevelen–type diagram with Hydrogen Index and Oxygen Index values; B) Hydrogen Index and T_{max} values. T_{max} is temperature of maximum pyrolysis yield. Dashed lines indicate maturities equivalent to 0.5, 1.0 and 1.3% vitrinite reflectance.

Table 4.2: Vitrinite reflectance data used for the calibration for the 2D numerical models.

well	depth [m] below NN	stratigraphy	lithology	VRr %	standard dev.	number of meas.	provenance of data
Well A	150	Mid Keuper	shale	3.9	-	-	Bartenstein et al. (1971)
Well A	1,470	Westphalian D	coal	4.76	-	-	Bartenstein et al. (1971)
Well B	1,792	Upper Jurassic	shale	3.19	-	-	Bartenstein et al. (1971)
Well C	1,630	Upper Jurassic	shale	1.96	-	-	Bartenstein et al. (1971)
Well C	1,957	Dogger	shale	2.54	-	-	Bartenstein et al. (1971)
Well D	730	Upper Jurassic	shale	0.85	-	-	Bartenstein et al. (1971)
Well D	954	Dogger	shale	1.1	0.08	50	
Well D	1,054	Lias	shale	0.73	0.07	50	
Well D	1,155	Lias	shale	0.74	0.07	50	
Well D	1,558	Mid Keuper	shale	1.2	0.08	50	
Well D	2,465	Zechstein	dolomite	2.05	-	-	industrial data
Well D	2,572	Zechstein	dolomite	2.14	-	-	industrial data
Well D	2,573	Zechstein	dolomite	2.1	-	-	industrial data
Well D	2,574	Zechstein	dolomite	2.18	-	-	industrial data
Well D	2,669	Zechstein	dolomite	2.36	-	-	industrial data
Well D	2,811	Zechstein	shale	2.04	0.24	3	
Well D	2,814	Westphalian D	coal	2.05	-	-	Teichmüller et al. (1979)
Well D	2,921	Westphalian C	coal	2.14	-	-	industrial data
Well D	2,922	Westphalian C	coal	2.11	-	-	industrial data
Well D	2,923	Westphalian C	coal	2.18	-	-	industrial data
Well D	2,923	Westphalian C	coal	2.18	-	-	Teichmüller et al. (1979)
Well D	3,018	Westphalian C	coal	2.36	-	-	industrial data
Well E	145	Miocene	shale	0.24	-	-	industrial data
Well E	175	Oligocene	shale	0.35	-	-	industrial data
Well E	210	Eocene	shale	0.31	-	-	industrial data
Well E	295	Eocene	shale	0.33	-	-	industrial data
Well E	305	Liassic	shale	4.8	-	-	industrial data
Well E	400	Liassic	shale	4.5	-	-	industrial data
Well E	500	Liassic	shale	4.9	-	-	industrial data
Well E	550	Liassic	shale	4.6	-	-	industrial data
Well E	560	Upper Keuper	shale	5	-	-	industrial data
Well E	600	Upper Keuper	shale	4.8	-	-	industrial data
Well E	640	Mid Keuper	shale	4.7	-	-	industrial data
Well E	685	Mid Keuper	shale	5.7	-	-	industrial data
Well E	700	Mid Keuper	shale	5.2	-	-	industrial data
Well E	800	Mid Keuper	shale	5.5	-	-	industrial data
Well E	850	Lower Keuper	shale	5	-	-	industrial data
Well E	890	Upper Muschelkalk	shale	4	-	-	industrial data
Well E	1,020	Lower Muschelkalk	shale	4.4	-	-	industrial data
Well E	1,126	Upper Bunter	shale	4.4	-	-	industrial data
Well E	1,222	Upper Bunter	shale	5.1	-	-	industrial data
Well E	1,298	Mid Bunter	shale	5.6	-	-	industrial data

Table 4.2 (cont.).

well	depth [m] below NN	stratigraphy	lithology	VRr %	standard dev.	number of meas.	provenance of data
Well E	1,302	Mid Bunter	shale	6.9	-	-	industrial data
Well E	1,330	Mid Bunter	shale	4.9	-	-	industrial data
Well E	1,400	Mid Bunter	shale	6.4	-	-	industrial data
Well E	1,492	Mid Bunter	shale	8.1	-	-	industrial data
Well E	1,586	Lower Bunter	shale	6.8	-	-	industrial data
Well E	1,700	Lower Bunter	shale	6.4	-	-	industrial data
Well E	1,805	Zechstein	shale	7	-	-	industrial data
Well E	1,900	Zechstein	shale	6	-	-	industrial data
Well E	2,000	Zechstein	shale	4.3	-	-	industrial data
Well E	2,027	Zechstein	dolomite	4.3	-	-	industrial data
Well E	2,107	Zechstein	carbonate	4.5	-	-	industrial data
Well E	2,125	Zechstein	carbonate	4.3	-	-	industrial data
Well E	2,128	Zechstein	shale	3.7	-	-	industrial data
Well E	2,128	Zechstein	shale	4.5	-	-	industrial data
Well E	2,146	Westphalian D	coal	6	-	-	industrial data
Well E	2,156	Westphalian D	coal	5.7	-	-	industrial data
Well F	1,072	Upper Jurassic	shale	0.95	-	-	Bartenstein et al. (1971)
Well G	655	Lower Cretaceous	shale	1.02	0.24	18	
Well G	800	Wealden	shale	0.6	-	-	Bartenstein et al. (1971)
Well G	3,770	Zechstein	shale	3.7	-	-	industrial data
Well H	80	Upper Jurassic	shale	2.65	0.32	48	
Well H	205	Upper Jurassic	shale	3.03	0.31	14	
Well H	295	Upper Jurassic	shale	3.07	0.29	22	
Well H	490	Upper Jurassic	shale	3.13	0.21	10	
Well H	620	Dogger	shale	3.06	0.26	13	
Well H	770	Dogger	shale	3.39	0.20	12	
Well H	930	Dogger	shale	3.28	0.29	25	
Well H	1,755	Lias	shale	3.99	0.36	35	
Well H	1,872	Upper Keuper	shale	4.26	0.29	50	
Well H	1,930	Mid Keuper	shale	4.47	0.27	35	
Well H	2,222	Upper Muschelkalk	shale	4.51	0.21	50	
Well H	2,587	Mid Bunter	siltstone	4.65	0.17	41	
Well H	3,466	Westphalian D/C	coal	5.1	-	-	Teichmüller et al. (1979)
Well H	3,467	Westphalian D/C	shale	4.5	0.24	30	
Well H	3,486	Westphalian D/C	sandstone	4.64	0.14	50	
Well H	3,513	Westphalian D/C	sandstone	4.44	2	3	
Well H	3,514	Westphalian D/C	sandstone	4.39	3	2	
Well H	3,586	Westphalian D/C	coal	5.4	-	-	Teichmüller et al. (1979)
Well H	3,605	Westphalian D/C	coal	5.8	-	-	Teichmüller et al. (1979)
Well H	3,641	Westphalian D/C	coal	5.1	-	-	Teichmüller et al. (1979)
Well H	3,884	Westphalian D/C	siltstone	5.28	5	5	

Table 4.3: Results of fluid inclusion measurements. The ice melting temperature is an indicator for the salinity of the fluids. Minimal entrapment temperatures can be derived from the homogenization temperatures for each sample.

sample		stratigraphy	coordinates		depth [m]	ice melting temperature [°C]	salinities [wt %]	homogenization temperature [°C]	N
			easting [Gauss-Krüger-System]	northing					
FI - 7	Muschelkalk / Keuper	34 36 450	57 98 400	surface	-13.9 to -12.4	16 - 19	169.4-198.2	21	
FI - 9	Oxfordian (Malm)	34 64 680	57 96 400	surface	-27.8 to -10.7	15 - 27*	145.2-209.2	20	
FI - 11	Upper Carboniferous	34 16 275	57 96 942	1,470	-24.6 to -20.8	23 - 25*	163.7-190.6	20	
FI - 13	Oxfordian (Malm)	34 13 940	57 93 240	surface	-21.9 to -16.8	20 - 23	157.7-203.3	23	
FI - 17	Keuper	34 40 850	57 93 570	surface	-6.2 to -5.3	8-9	146.7-184.7	20	
FI - 18	Mid Keuper	34 56 390	57 88 030	surface	-13.7 to -9.9	16-17	128.4-194.9	20	
FI - 20	Oxfordian (Malm)	34 24 930	58 12 080	surface	-3 to -2.1	4-5	158.2-190.2	21	
FI - 22	Upper Carboniferous	34 33 775	57 98 725	surface	-20.6 to -12.9	17-23	178.9-202.4	20	
FI - 24	Oxfordian (Malm)	34 31 530	58 06 000	surface	-4.1 to -2.5	4-6	161.5-204.9	21	

salinity (wt %) according to Bodnar (1993)

* salinity (wt %) higher than 23 % according to the equation of Dubois & Marignac

Table 4.4: Composition of the gaseous inclusions in sample 9 and 11.

<u>Gaseous Inclusions</u>		gaseous inclusions		molar volume		CO ₂		CH ₄		N ₂		eutectic		melting	
sample				[cm ³ /mol]		[%]	[%]	[%]	[%]	[%]	temperature	temperature	[°C]	temperature	[°C]
FI - 9	A1		68		50	44	6				-67.7		0.8		
	B1		51		61.5	32	6.5				-63.5		-19.8		
	D1		47		62.5	29	8.5				-66.4		-46.0		
	E		55		54	37.5	8.5				-64.8		-25.2		
	F1		53		41	51.5	7.5				-66.0		-41.2		
FI - 11	A1		83		18	82					-81.5		-68.9		
	A3		83		12	88					-81.3		-69.0		
	B1		63		15	85					-88.6		-70.7		
	B3		68		14	86					-87.4		-68.9		
	C1		69		13.5	86.5					-83.1		-67.7		

Highest homogenization temperatures (>200°C) were measured in the Upper Carboniferous samples (Piesberg, Ibbenbüren) as well as in the Upper Jurassic samples from the central part of the basin. This regional distribution is in accordance with the general coalification pattern in the area (Senglaub et al. 2006).

The occurrence of gas-bearing inclusions is restricted to samples with high salinities. In two samples there is evidence of contemporaneous trapping of

aqueous and gas inclusions as indicated by the occurrence of both types of inclusions in the same clusters and/or growth zones. Raman spectroscopic analysis demonstrates that the gaseous inclusions are always CH₄-rich with variable contents of CO₂ and N₂ (Table 4.4). The sources of these gases have been intensively discussed in the past (Stahl 1971, Hoefs 1973, Fricke 1979, Leischner 1994, Krooss et al. 1995 and Petmecky 1998).

4.4.3. *Structural overview and geological setting*

Different time steps in the evolution of the basin are shown in Figure 4.4, based on 2DMove reconstructions imported into PetroMod thermal history modelling software.

The *Zechstein* deposits within the cross sections vary in thickness between 230m in the area of the later Mesozoic depocentres and up to 1740m on the northern basin margin.

In Triassic times, the central parts of the LSB subsided only at a moderate rate (Betz et al. 1987). In the northern part of the study area, increasing *Bunter* thicknesses from 340 up to 670m towards north and west are recognized. In the southern and northernmost parts, however, sedimentary sequences tail off culminating in a total disappearance of *Bunter* deposits on the northern high (Figure 4.4a).

The *Muschelkalk* deposits show - equal to the *Bunter* - increasing thicknesses west- and northwards, ranging between 370 up to 590m, as well as thicknesses of at least 100m on the northern swell.

In *Keuper* times, a slow shift of the depocentre towards the east is recognizable due to variation in thickness, which slightly increases from 250-360m in the westernmost cross section (profile II, Figure 4.1, 4.4) to 380-550m in the central cross section (profile I, Figure 4.4). In direction towards the northern margin, the sedimentary sequence tails off (210m). A change in basin configuration becomes evident in the thickness variation of the *Lower Jurassic* sediments. Greatest thicknesses (880m in profile I and 760m in profile II) were observed on the northern side of syn-sedimentary faults and decrease towards the northern margin to 210-180m.

In the northern sub-basin, *Mid Jurassic* thicknesses of up to 700m accumulated in the north of syn-sedimentary faults resulting from the evolving Wiehengebirge Flexure Zone. Towards the north, the number of syn-sedimentary faults is reduced and their dips point towards the basin centre. On the northern swell, a thickness of *Mid Jurassic* sediments of only 150-230m was recognized. The top of the *Mid Jurassic* sequence is erosive on a regional scale (Figure 4.4b).

Maximum Upper Jurassic values were reached in the northern parts of the cross sections with thicknesses up to 1580m. Due to the erosive contact with the overlying Late Cretaceous and Tertiary rocks, the true thickness of Upper Jurassic to Lower Cretaceous deposits is unknown. Thus, assumptions of several authors and 1D modelling results (Senglaub et al. 2006) were taken as a guideline for the reconstruction of the layer.

According to Gramann et al. (1997), an accumulation of up to 3000m for the rapidly subsiding graben centre in this area (Figure 4.4c) was assumed in the structural balancing. The thickness decreases (<250m) towards the northern basin margin and the intra-basin swells.

Lower Cretaceous deposits appear in an isolated way in the study area. Whereas small islands of Berriasian (Wealden) deposits were observed in the whole area, the later stages are more or less limited to the northern basin margin. The contact to younger sedimentary sequences within the basin is erosive. Based on the observations described by Klassen (1984), Betz et al. (1987) and Mutterlose and Böckel (1998), a former overburden between 800-1000m for Wealden sequences (Figure 4.4d) as well as 1500-1650m for post Berriasian sediments was applied in the structural reconstruction.

The sequence of *Upper Cretaceous* sedimentary rocks is incomplete in the LSB, with the greatest thicknesses of Cenomanian to Santonian sedimentary rocks in the north (up to 525m).

The structural layer reconstructions for the time of inversion resulted in a deduced erosion of 5500 (Liassic to Upper Cretaceous sequences/profile II) - 5900m (Bunter to Upper Cretaceous sequences/profile I) on the Nordwestfalen-Lippe Swell. The amount of erosion is reduced to less than 1300m (Senglaub et al. 2006; Figure 4.4e) towards the northern basin margin.

Before the LSB was affected by a second inversion pulse during the *Early Tertiary*, a marine ingressión enabled the accumulation of a few hundred metres of Upper Campanian deposits especially in the area of Dammer Oberkreidemulde (Kennedy and Kaplan 1997; only relicts of Campanian deposits are still preserved).

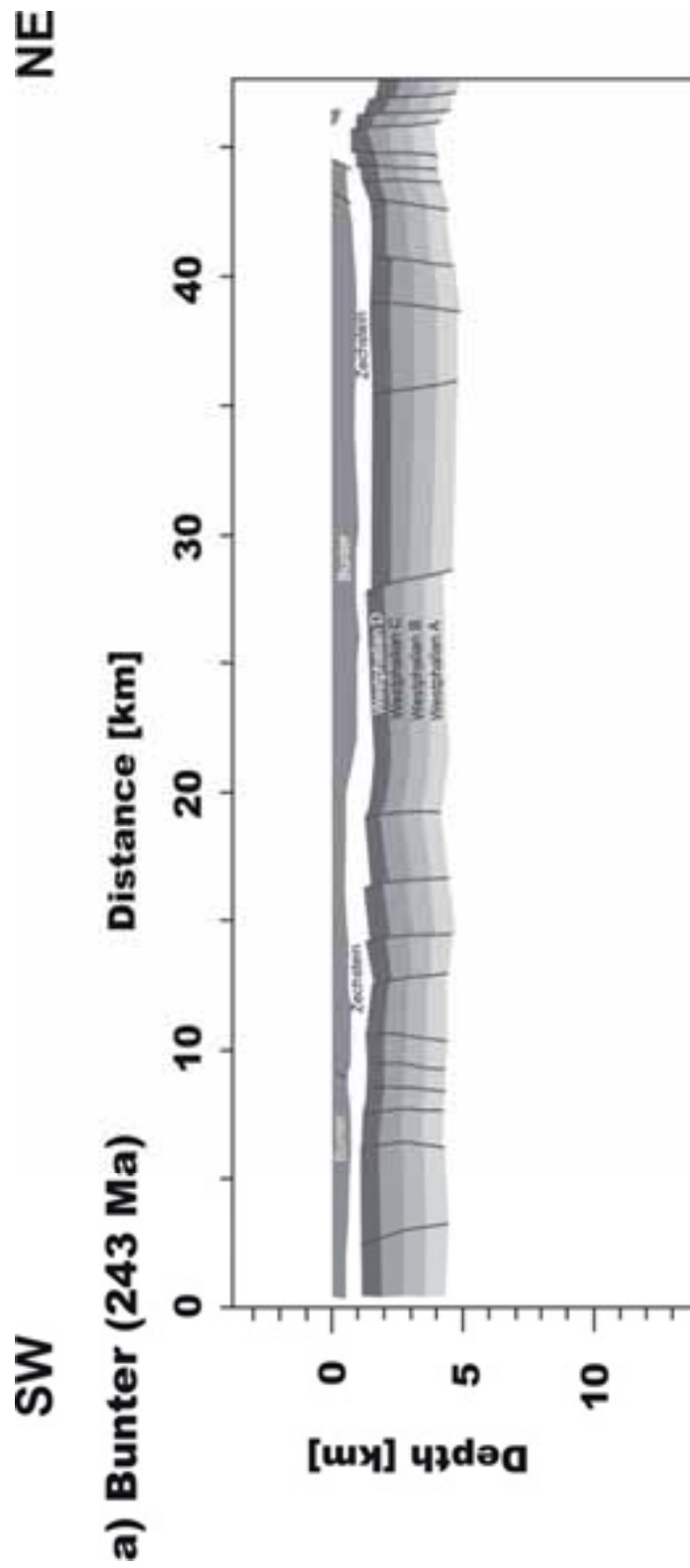


Figure 4.4: Structural reconstruction of profile I made in 2DMove for a) the Bunter (243Ma).

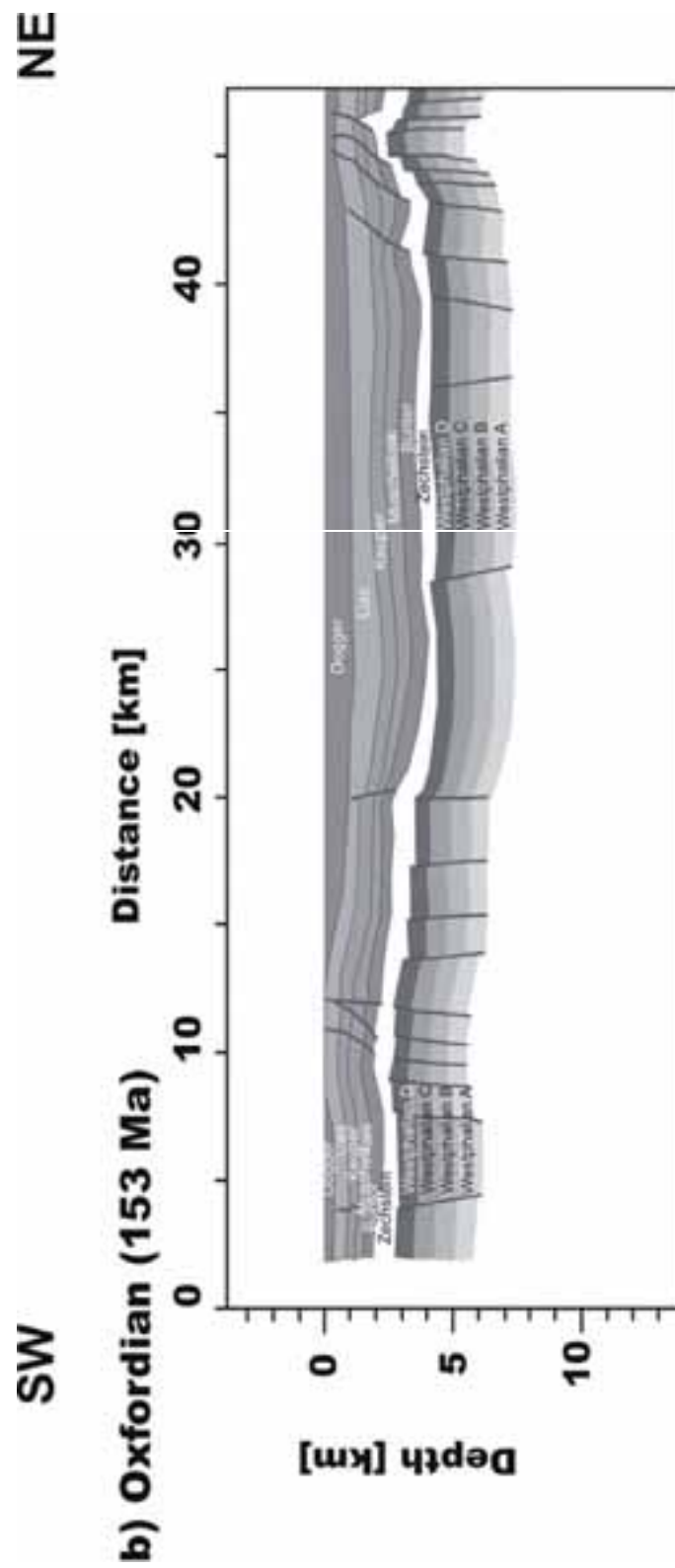


Figure 4.4 (cont.): Structural reconstruction of profile I made in 2DMove for b) the Oxfordian (153Ma).

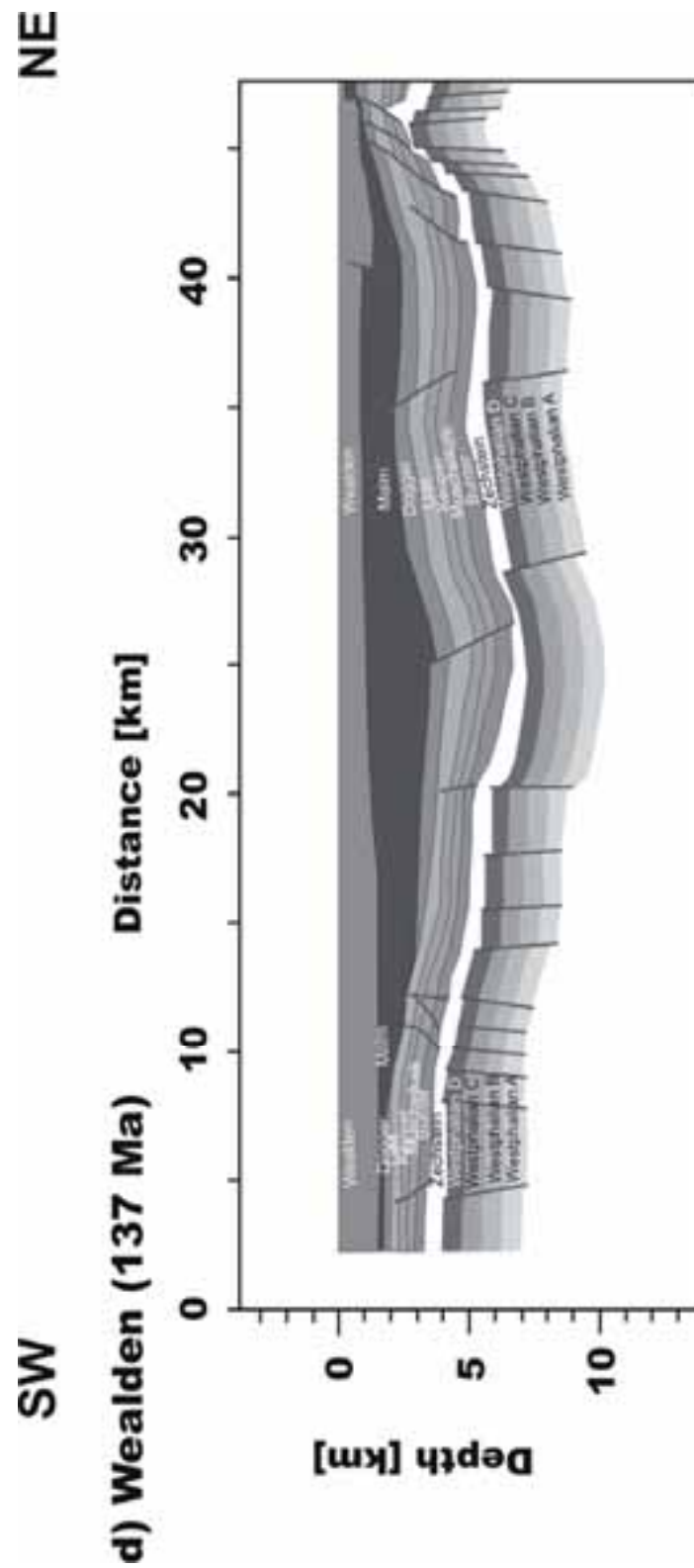


Figure 4.4 (cont.): Structural reconstruction of profile I made in 2DMove for d) the Early Cretaceous (137Ma).

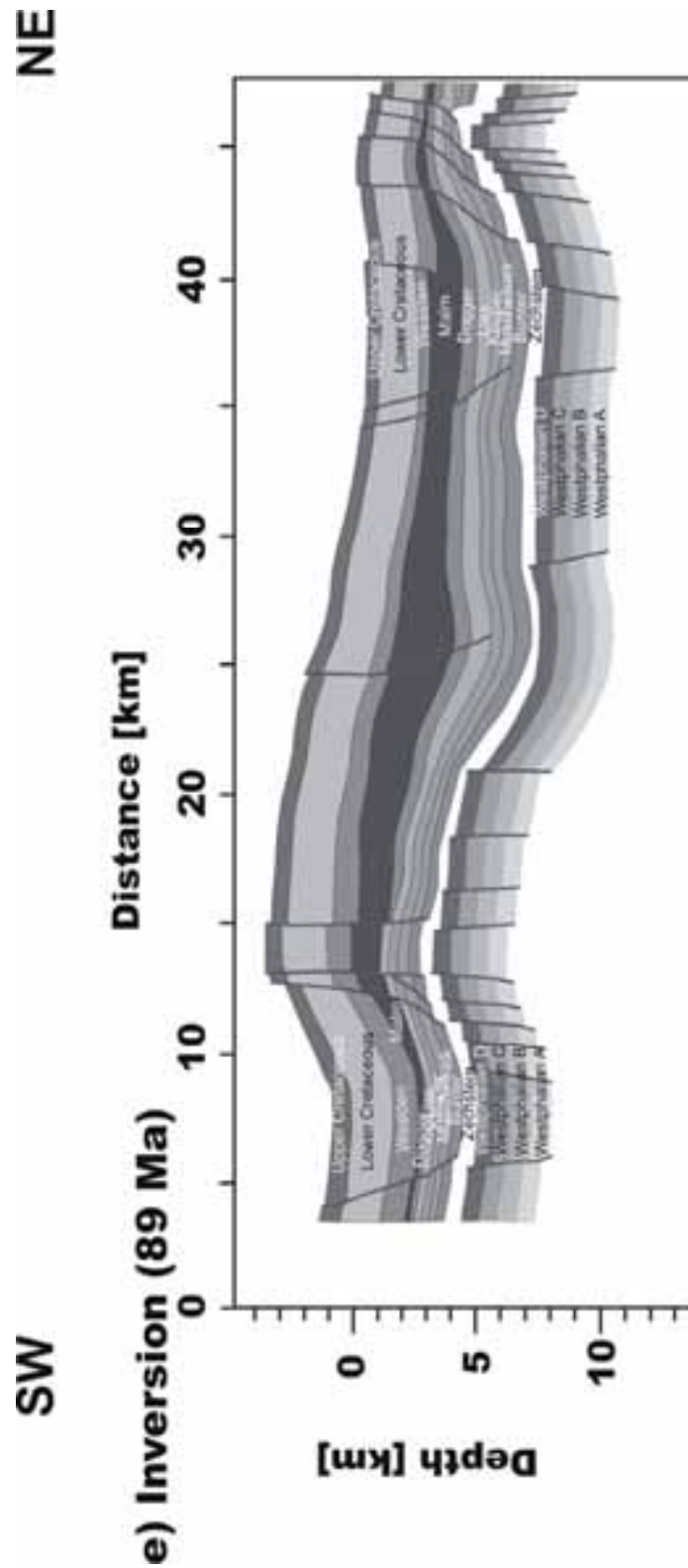


Figure 4.4 (cont.): Structural reconstruction of profile I made in 2DMove for e) the inversion (89Ma).

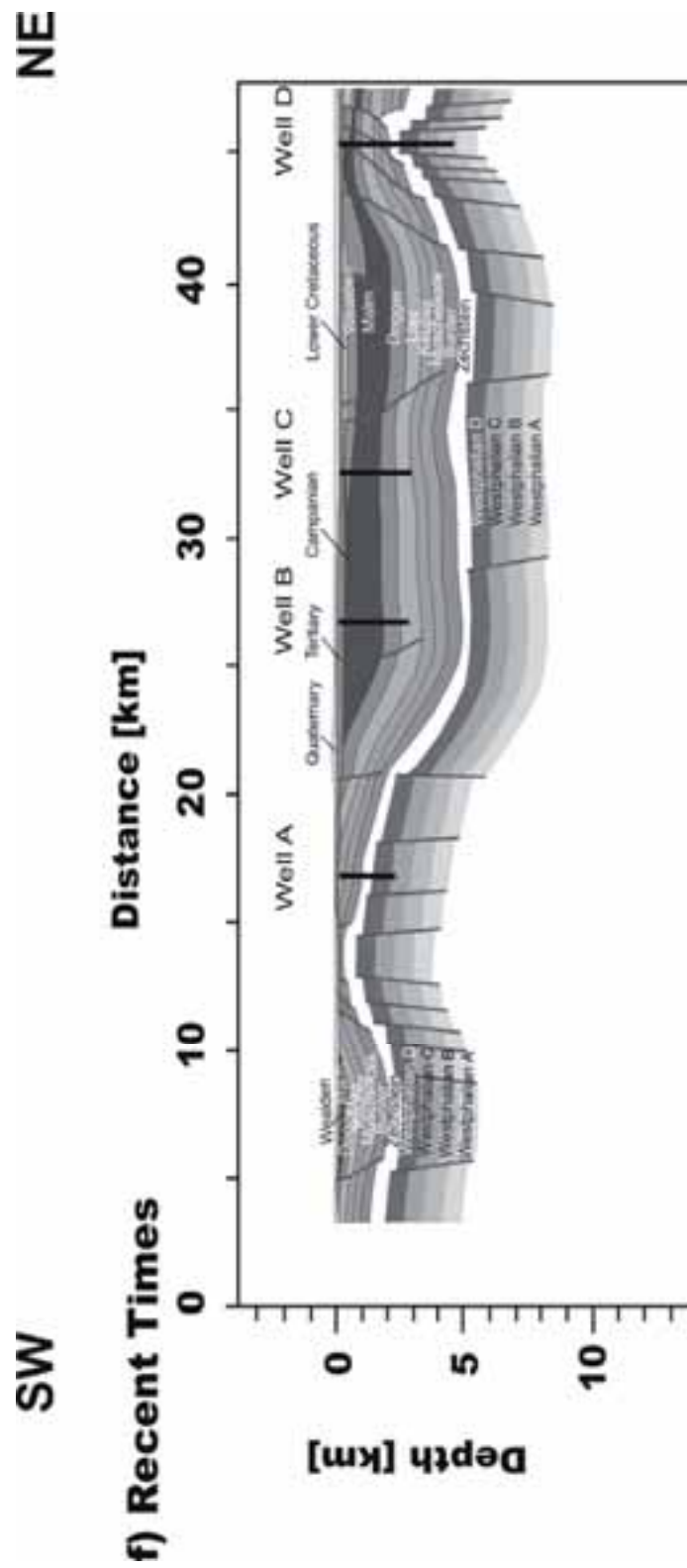


Figure 4.4 (cont.): Structural reconstruction of profile I made in 2DMove for f) recent situation.

Relatively thin Tertiary deposits (160-230m) and a successive layer thickening in the northern part of the study area form the top of the sedimentary sequence in the basin (Figure 4.4f).

4.4.4. Basin Modelling

The thermal and burial history was calibrated by comparing measured and calculated temperature sensitive parameters, e.g. vitrinite reflectance and fission track data.

Basal heat flow for times of maximum burial/maximum temperatures is a result of this calibration. In contrast, assumptions on basal heat flow variations for earlier times (Permian to Jurassic) are based mainly on palaeo-tectonic regimes and not well constrained.

In the first scenario, heat flows of 70-80mW/m² for the time of extension in Late Jurassic times were assumed, followed by a short cooling period, and renewed increasing heat flows in a range between 45-95mW/m² during the inversion in Late Cretaceous times (Leischner 1994, Petmecky et al. 1999). Thereafter, the heat flow in the model decreased to 45mW/m² until the Miocene, before an increase to the present heat flow of 60mW/m² occurred.

The calculated trends of organic matter maturation based on this heat flow scenario show a good fit with the measured vitrinite values for the basin margin and the Nordwestfalen-Lippe Swell. However, the calibration for the wells situated in the centre of the northern sub-basin does not provide a good fit. Based on this heat flow scenario, highest temperatures in the basin centre at the top Upper Carboniferous (Westphalian D - 360°C) and also the maximum coalification of the organic matter were reached during the time of maximum burial in Turonian times (~88Ma).

In the second and favourite scenario, higher heat flows during the time of extension (Upper Jurassic) in the Lower Saxony Basin are assumed which vary between 80 and 100mW/m² (Figure 4.5, wells A-F, H) with the exception of 140mW/m² for one well (Figure 4.5, Well G) at the western margin of the basin. It should be noted, however, that calibration data for well G are poor, whereas excellent data are available for some of the other wells. Afterwards, a slow cooling of the lithosphere set in until Tertiary times.

The heat flow in the models increases from the Miocene until in present times values of 60mW/m² are reached. This heat flow history provides the best match with the measured vitrinite reflectance (Figure 4.6).

4.4.5. Hydrocarbon generation

In the current study, the hydrocarbon potential along the three profiles has been considered for rocks from 3 stratigraphic intervals: Carboniferous, Liassic, and

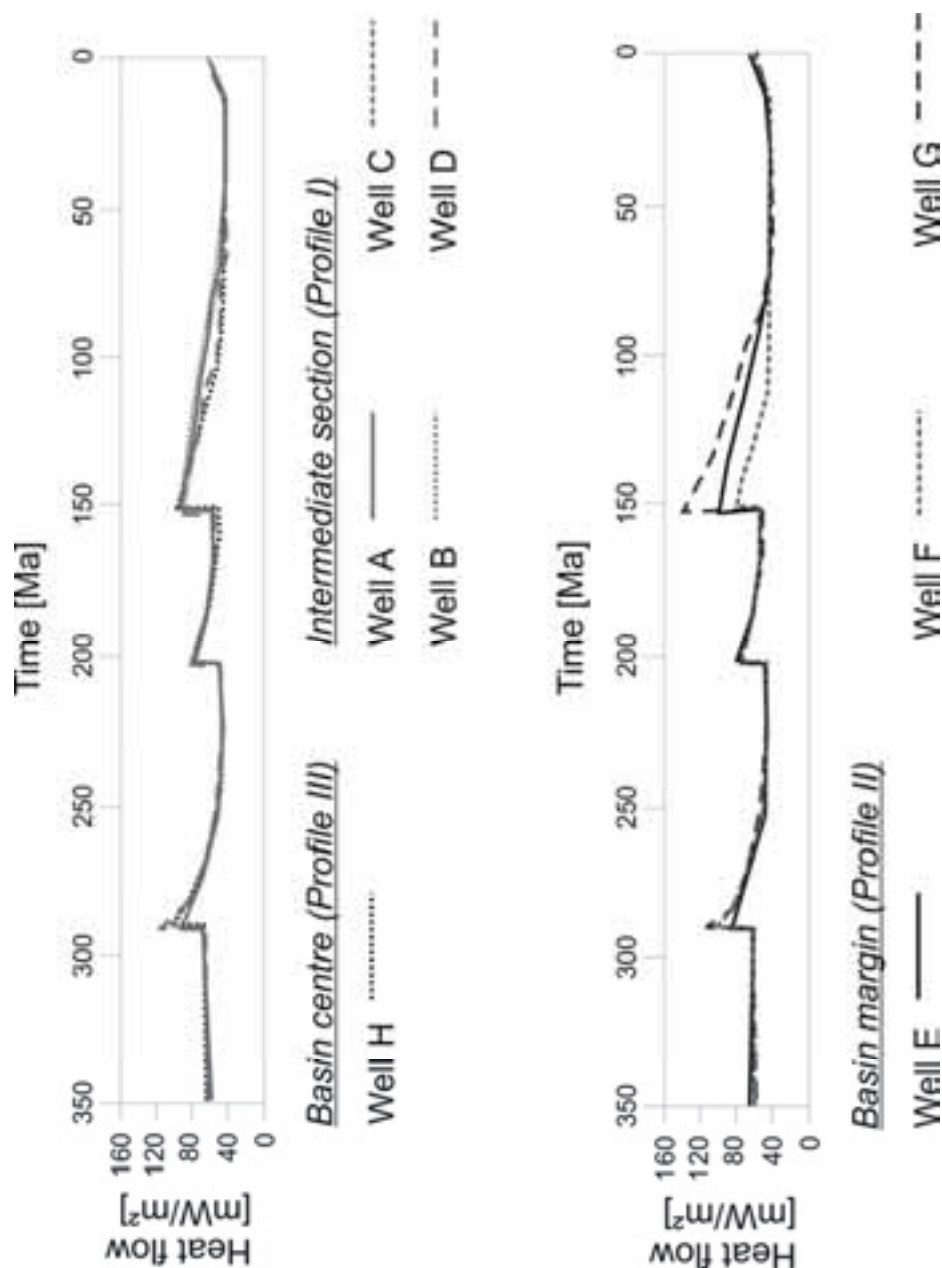


Figure 4.5: Applied heat flows for the maturity calibration of the different wells in the numerical basin modelling.

Wealden. As there is no or little hydrocarbon potential left in the centre, Figure 4.8 only illustrates the northern more marginal part of the LSB.

For the calculation of hydrocarbon generation from Carboniferous coals, the kinetic data set of Pepper and Corvi (1995) for a type III kerogen was applied. The organic matter of the Upper Carboniferous of the basin margins is situated in the condensate and wet gas window and transits slightly to the main dry gas window towards the basin centre. Based on 2D modelling results along the three

cross-sections (Figure 4.1), first hydrocarbon expulsion from Westphalian A (Langsettium) gas source rocks within the basin took place in the Late Carboniferous (309-298Ma). Afterwards the generation stopped. A renewed generation and expulsion from all Westphalian rocks started within the basin at the end of the Mid Triassic-Muschelkalk sedimentation (235Ma). According to the transformation potential of the Westphalian source rocks, the hydrocarbon generation within the basin was exhausted in Upper Jurassic times (157-140Ma). In the area of the northern basin margin, the hydrocarbon potentials for Westphalian A and B (Langsettium and Duckmantium) were exhausted in Tithonian times (142Ma, Figure 4.7a), whereas a hydrocarbon release from Westphalian C (Westphalian C) and Westphalian D took place until inversion times (87Ma, Figure 4.7a). These Westphalian sequences still have a small remaining hydrocarbon potential of 7% (Westphalian C) and 38% (Westphalian D). Towards the west, this hydrocarbon potential decreases to 1% (Westphalian C) and 28% (Westphalian D).

Hydrocarbon generation from the Liassic source rocks was calculated based on the kinetics of Dieckmann et al. (1998) for an immature type II kerogen from exactly this source rock. With a maturity of 0.7 to 1.0%VRr the organic matter of the basin margins entered the oil window. Towards the basin centre, the maturity of the source rock increased to a post mature stage (more than 4%VRr in the Bramsche area) and the organic matter reached the main dry gas window. In the centre of the basin, hydrocarbon generation started in Oxfordian times (153Ma) and was exhausted in Tithonian times (142Ma). The most prominent outcrop for the Liassic shale in this area is the “Schwarze Kreide” of Vehrte, where the Posidonia shale reached values of more than 2%VRr.

On the northern basin margin, the Posidonia shale generated hydrocarbons in the time interval between the Tithonian (142Ma) and the inversion (87Ma, Figure 4.7b). Only 45% of the hydrocarbon potential was released there.

For the Wealden, the same kinetic data set for kerogen type II was applied, because no specific kinetic data set was available. Application of kinetics for type I kerogen would have resulted in an even less pronounced hydrocarbon generation for this shallow source rock. It can be inferred that the organic matter of the basin margin hardly reached the oil window. Within the basin, only sparse areas with Wealden deposits can be found based on the huge removal during the inversion. In the eastern part of the LSB, however, the coalification of the Wealden increased up to more than 3%VRr. This fact indicates that the organic matter has reached the main dry gas zone. Due to the high sedimentation rates during the sag-phase, the Wealden source rock in the basin centre started to generate hydrocarbons shortly after deposition. The generation was interrupted because of the removal of the sediments during the inversion.

The Wealden source rocks (Figure 4.7c) on the basin margin began to generate hydrocarbons at the end of the Lower Cretaceous and stopped its release with the beginning of the inversion (87Ma). Based on the transformation ratio the remaining hydrocarbon potential lies in a range between 80 and 90%. During the inversion most of the hydrocarbons were lost along deep reaching faults (Binot et al. 1989, Leischner et al. 1993), but there is a significant potential for preserved accumulations, especially where inversion was less intense and where permeable faults are missing.

4.5. Interpretation and Discussion

The presented models are the result of the chosen burial and temperature history scenario for the western part of the Lower Saxony Basin taking into account the results from vitrinite reflectance measurements and fission track analysis. The selected burial history is based on existing thicknesses and their projections (mainly of the Triassic and Lower to Mid Jurassic sequences) over eroded regions as well as on thickness assumptions for the Upper Jurassic, Lower and Upper Cretaceous units published by several authors (see above).

The evolution of the LSB started during the Late Permian with extension and moderate subsidence, followed by down-warp of the northern part of the basin in Triassic times (see also van Wees et al. 2000).

The LSB was apparently affected by extensional stresses during the Triassic, which is indicated by the forming of horst and graben structures based on the reactivation of Variscan tectonic elements (Röhling 1986, 1988, Kockel 1991) already during Bunter times. Varying sediment thicknesses within the study area reflect the new stress regime, developed contemporaneously to the evolution of the North Sea rift system (Betz et al. 1987, van Wees et al. 2000).

Dilatation movements along the northern basin margin were strong enough so that raft tectonics (Jackson and Talbot 1991) could occur, which is evident by the rupture of Lower and Mid Bunter sequence blocks. They drifted apart (rafts), and Zechstein appeared on the surface (Figure 4.4a, Mohr et al. 2005).

Tectonic movements continued during the Muschelkalk (Wolburg 1969, Gaertner 1993, Frisch and Kockel 2003) and are reflected by a similar sedimentation pattern within the basin. It resulted in increasing syn-raft deposition on the northern basin margin, where the removed sequences of the raft-blocks were re-accumulated between the rafts.

Syn-sedimentary movements on NW-SE and W-E trending faults in the study area along with varying sediment thicknesses indicate a differentiation in sub-basins within the Lower Saxony Basin already during Early Jurassic times. In particular, comparison of thicknesses of sedimentary units points to the

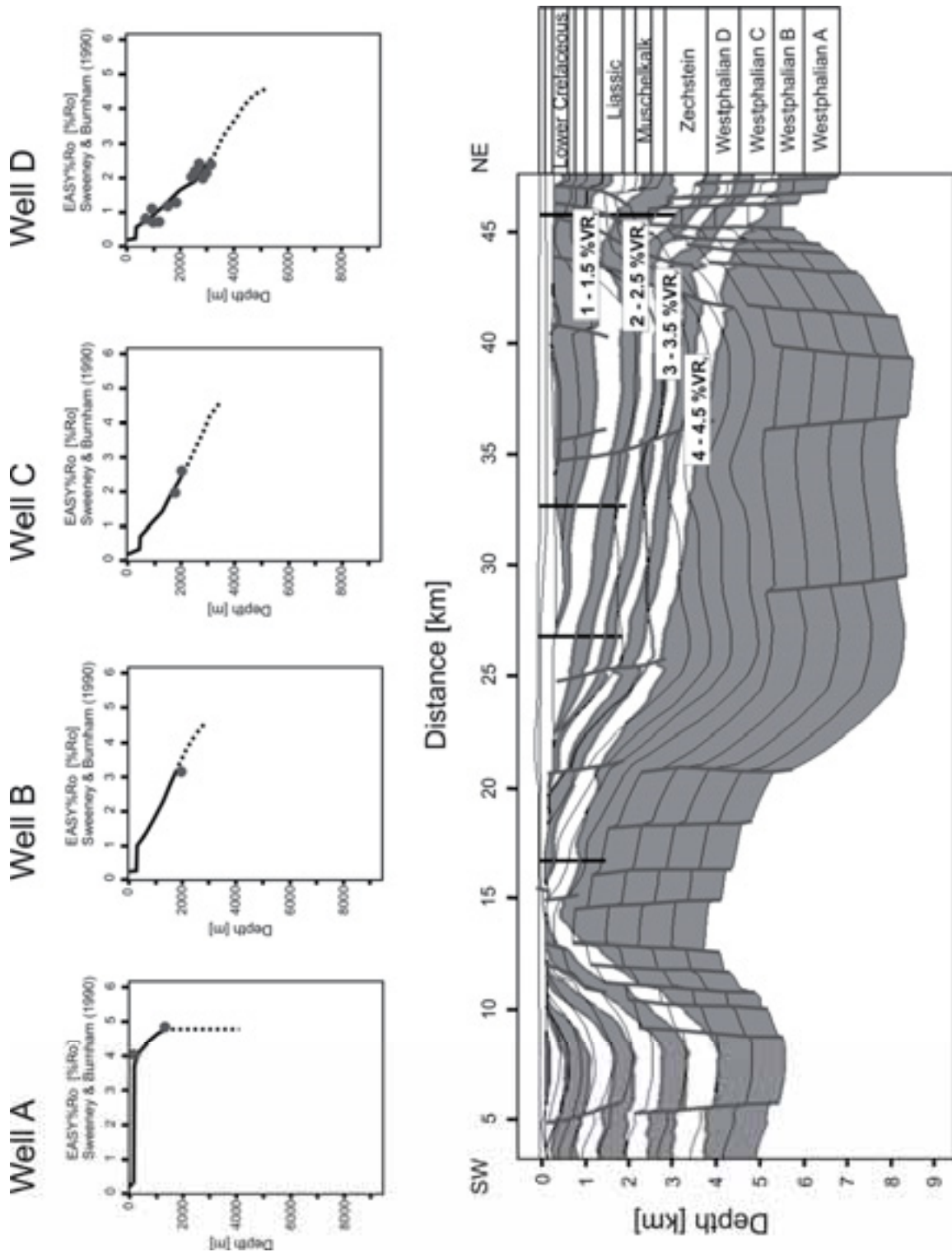


Figure 4.6a): Resulting maturity calibration for the wells as well as for the cross sections after using the heat flows shown in Figure 4.5 (profile I).

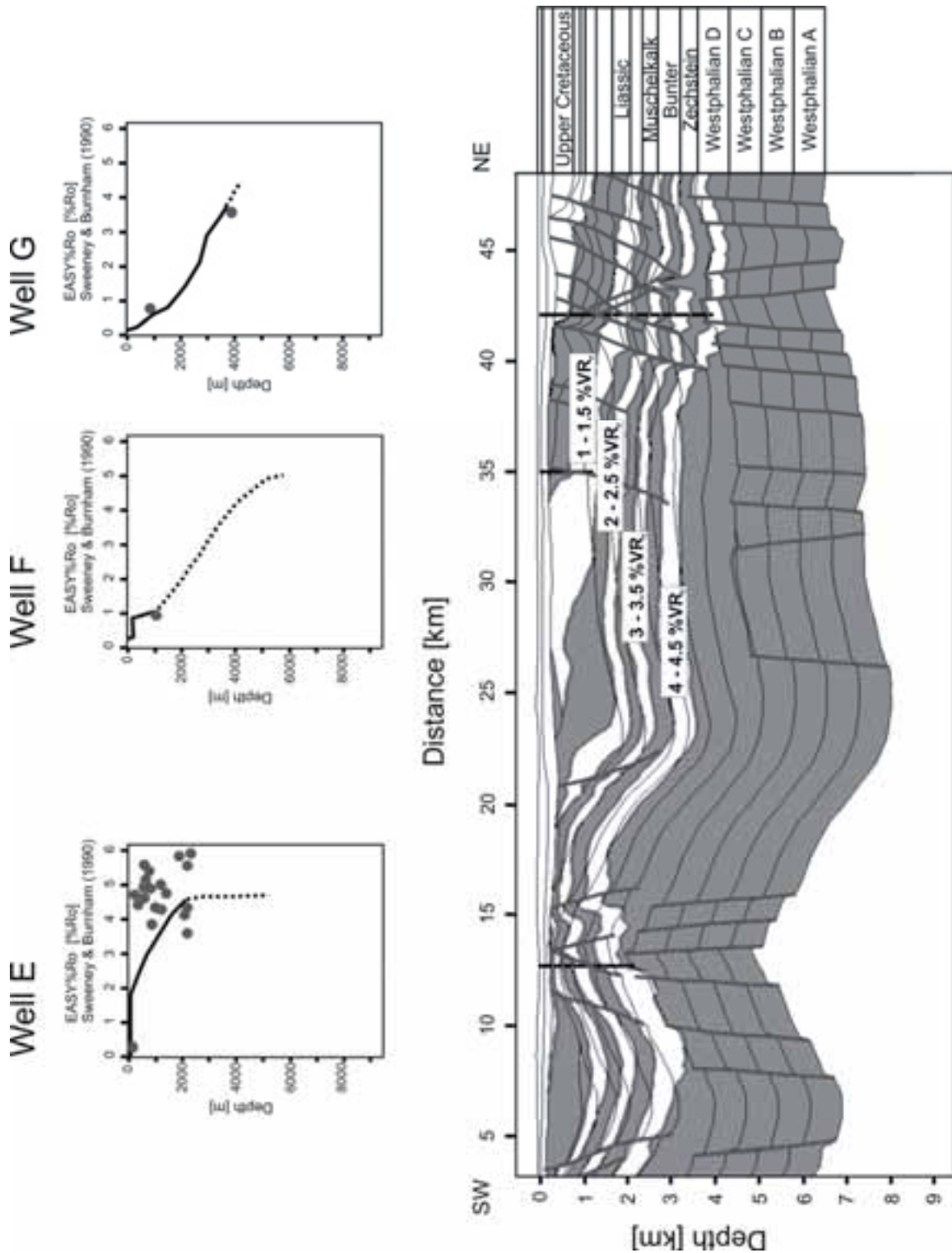


Figure 4.6b): Resulting maturity calibration for the wells as well as for the cross sections after using the heat flows shown in Figure 4.5 (profile II).

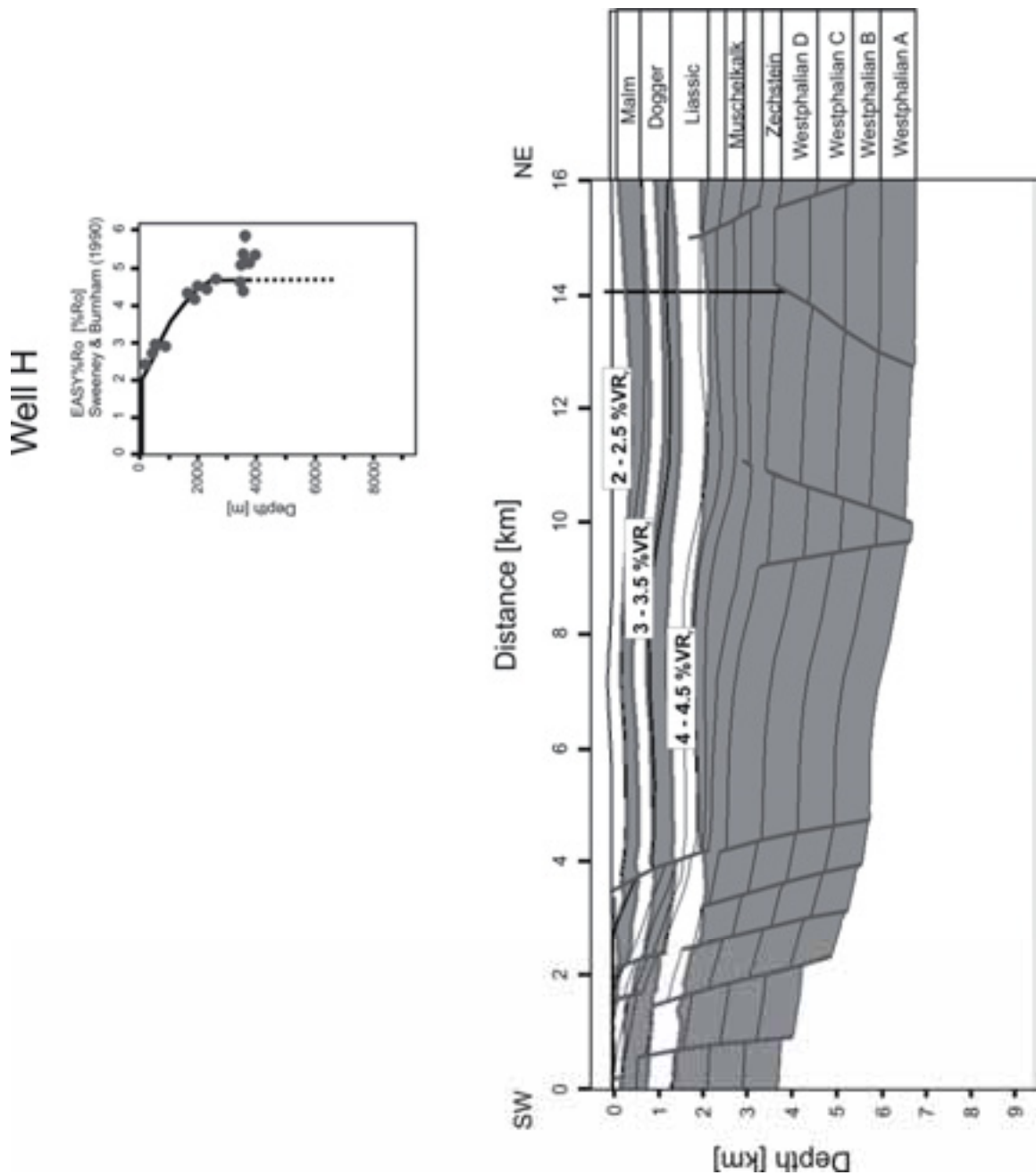


Figure 4.6c): Resulting maturity calibration for the wells as well as for the cross sections after using the heat flows shown in Figure 4.5 (profile III).

evolution of a new sub-basin between the Wiehengebirge Flexure Zone and the Ibbenbüren area during Dogger times (see also Baldschuhn et al. 2001).

The Mid Jurassic discordance mirrors a major tectonic pulse during this time, which affected the area of the LSB (see also Betz et al. 1987). The greatest amounts of erosion in the study area were reached on the southern flank of the rising Nordwestfalen-Lippe Swell, where the denudation transgressed onto Liassic deposits. Increasing thicknesses in the sub-basins might be the result of removed sequences from the swells (Figure 4.4b).

Major North Sea Rifting offshoots are recognizable within the LSB, affecting Late Jurassic and Early Cretaceous rocks. During this period, a large SW dipping half graben developed within the northern part of the basin. Rapid subsidence along with fast sedimentation resulted in thick sediment accumulations with thick saline intercalations (Münder Marl Formation).

The Early Cretaceous shift of the depocentre towards the Nordwestfalen-Lippe Swell (Binot et al. 1989, Dulce et al. 1993) was considered in the structural balancing with increasing thicknesses of Wealden and Lower Cretaceous sediments in this area. However, sedimentation was continuous in the actively subsiding parts of the LSB.

With the decrease in the rate of crustal extension across the North Sea rift during early Late Cretaceous, subsidence ceased.

During the Turonian, tectonic activity in the LSB resumed and became more intense, as indicated by turbidites and slump deposits along its southern margin (Voigt and Koch 1977). During the subsequent inversion of the LSB (Coniacian - Campanian), the fault system along its northern margin became reactivated and the sedimentary fill was uplifted with respect to the adjacent stable Pompeckj Block located north of the study area.

The former most deeply buried part within the half graben became the most uplifted part of the basin and approximately 6000m of sediment were removed until Tertiary times there.

The thin Tertiary deposits indicate a slight subsidence for the period of Eocene to early Miocene. A successive layer thickening in the northern part of the study area is evidence for an ongoing northward tilting throughout this time (Frisch and Kockel 2003; Figure 4.4f).

Using lesser thicknesses than those assumed here would lead to worse fits between measured and calculated calibration data, even if higher heat flows were applied for the time of extension in the Late Jurassic/Early Cretaceous. One argument in favour of higher heat flows during this time could be the occurrence of some igneous intrusions in the neighbouring Netherlands (Sissingh 2004). However, in the area of the LSB such intrusions were either not reported or have a Permian rather than Cretaceous age. Therefore, the simple rift scenario was preferred followed by a sag-phase and the development of syn-sedimentary half grabens where rapid sedimentation occurred.

The first heat flow scenario was chosen in accordance with Sandiford (1999), assuming a slight increase in heat flows during the inversion phase. This concept has been successfully applied in other parts of the LSB before (Petmecky et al. 1999). However, in our study area the resulting temperature history derived from this scenario is not in accordance with zircon fission track results in the basin centre that indicate an earlier maturation in this area (Senglaub et al. 2005).

The second heat flow scenario is in accordance with thermo-kinematic considerations of e.g. Ziegler et al. (1995), Negrodo et al. (1995) and Hansen and Nielsen (2002, 2003), which imply that the crustal zones of reduced strength thicken under compression and consequently the basin inverts.

The resultant heat flow history is characterized by increased heat flows during the Early Permian initiation of the Central European Basin system, elevated heat flows in Late Triassic/Early Jurassic times during first basin differentiation (see also van Wees et al. 2000) as well as high heat flows due to crustal extension and initiation of the Lower Saxony Basin during the Late Jurassic/Early Cretaceous (Figure 4.5).

According to the second heat flow scenario, temperatures in the basin rose from the initiation of the LSB in Lower Jurassic times until the crustal extension event during Upper Jurassic/Lower Cretaceous (Figure 4.8a, b, and c) times. During the following basin sag-phase a lithospheric cooling took place, combined with rapid subsidence and fast sediment accumulation. As burial was faster than cooling, a temperature upward dragging towards younger sediments occurred. Therefore, Upper Carboniferous sediments in the northern basin centre experienced their highest temperatures of 420°C during this time (Figure 4.8d) before inversion (Figure 4.8e).

Post-inversion the heat flows further decreased in the basin. Recent subsurface temperatures (Haenel 1980) in correlation with new fission track results (Senglaub et al. 2005) give evidence that from the Miocene onward, a renewed increase in temperatures must have taken place (Figure 4.8f).

According to the preferred temperature history, highest coalification was reached on the northern flank of the Wiehengebirge Flexure Zone close to the basin centre in the area of Bramsche. Towards the northern basin margin and the southern flank of the Nordwestfalen-Lippe Swell, the maturity of the organic matter is diminished. The same trend of decreasing coalification is recognizable in direction of the western basin margin (profiles I and II in comparison with profile III).

The resulting calibration for the wells implies rising rank gradients from the northern part of the basin to the Wiehengebirge Flexure Zone. The observed

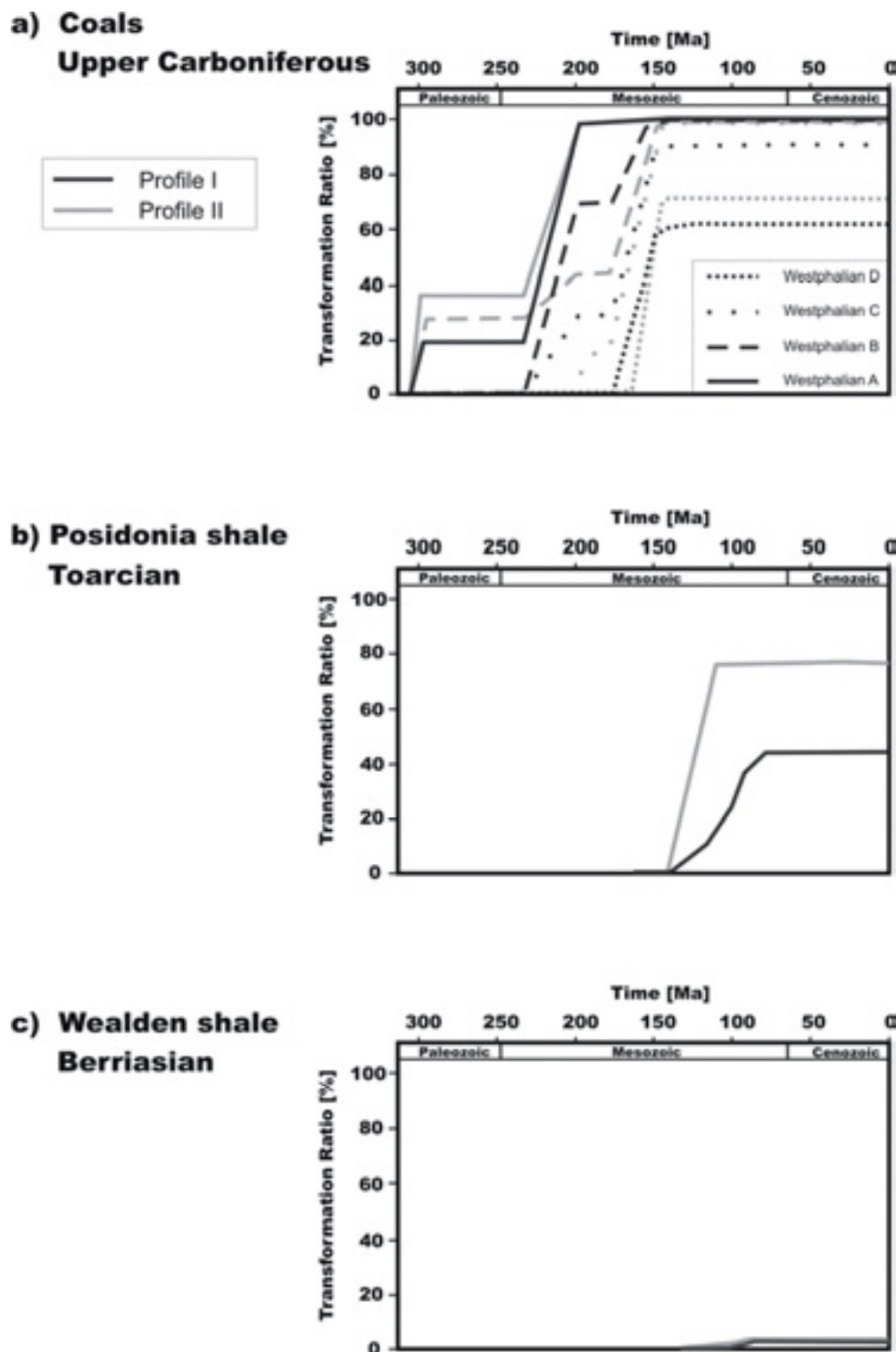


Figure 4.7: Hydrocarbon release of the three main source rocks in the study area. Because the hydrocarbon potential of two of the source rocks is already exhausted in the basin centre, the figure is only focused on the northern margin.

rank gradients are low to moderate and do not show any evidence for an igneous intrusion (Figure 4.6).

The favoured temperature history is more or less similar for all the wells in the centre of the northern sub-basin and a great number of calibration data was used to calibrate these models. Correlation of the applied heat flow with crustal thickness after Bodri and Bodri (1985) led to the conclusion that during the crustal extension event the lithosphere was about 26km thick. Towards the western margin of the LSB, however, reliable calibration data are very limited.

Higher heat flows of up to 140mW/m² during the extension phase were required to obtain the maturity of 3.7%VRr at the base of the Zechstein in a depth of 3770m (Well G). One reason for the elevated heat flow is the high conductivity of about 1000m thick-wedged Zechstein evaporates in this area. In case of a different salt thickness during the Late Jurassic extension phase, different heat flows might result.

The maturity of the Upper Carboniferous in wells of the northern and southern margin area of the Lower Saxony Basin ranges between 1.8 and 2.5%VRr. Only in the vicinity of the Appeldoorn Gas field further west, high vitrinite reflectance values (3.2-3.5%VRr; Kus et al. 2005) have been found for the top Carboniferous which are similar to the values reported for well G. For this area a Cretaceous magmatic body - similar to the Bramsche Massif- is favoured by some authors (e.g. Brückner-Röhling et al. 1994), although the supporting maturity data are very limited.

Another explanation for high coalification on top of the Carboniferous could be the influence of Permian volcanic activity. In the Emsland, Südoldenburg, and Bremen regions, andesitic volcanism took place between 296-290Ma (Bachmann and Hoffmann 1995, Marx et al. 1995). In the northern part of the LSB, some wells drilled residual Rotliegend volcanic sediments. In the western prolongation of the LSB in the Netherlands, olivine gabbros were intersected by wells (Marx et al. 1995, NITG-TNO 2000). According to K/Ar age determinations performed by Sissingh (2004), most of these igneous intrusions are of Permo-Carboniferous age. Additionally, zircon fission track data from the northern part of the basin support a Permian (hydro-)thermal event (Senglaub et al. 2005). However, these intrusions will have influenced only Pre-Permian sediments and not the Zechstein and Post-Zechstein deposits.

The average homogenization temperature of 170°C for the authigenically formed primary fluid inclusion samples indicates an entrapment during the deep burial stage of the basin. In principle, the variation in homogenization temperatures might be a result of re-equilibration/stretching of the inclusions during further burial. In this case, the higher temperatures would not represent the diagenetic mineral formation temperatures (Goldstein 1986, Burruss 1987, Muchez et al. 1991). The term re-equilibration has been used to describe fluid

inclusions that have changed volume, or have lost or gained components, or both and can occur during continued burial or uplift of the rock to the surface. Thus, deeply buried samples showed a wide range in homogenization temperatures and salinities, reflecting continued re-equilibration during burial and exposure to fluids of different salinities as burial progressed (Goldstein 1986) as presented in the samples. Reasons for this evolution could be an increasing departure of the confining pressure where the largest inclusions begin to re-equilibrate as fractures are generated at sharp corners of the inclusion and extend into the surrounding host (Vityk et al. 1996). Some of the fluid that escapes along these fractures might have been trapped in the surrounding quartz to produce a halo of very small fluid inclusions adjacent to the fracture. Hall and Sterner (1993) conducted experimental studies of water loss from aqueous fluid inclusions. As a result of water loss, the salinity of the remaining inclusions would have increased.

However, a range in liquid-to-vapour ratios is not always indicative of re-equilibration. If the inclusions were trapped in a boiling (or immiscible fluid) system, a bimodal distribution of phase ratios can result as well, with a complete range between the end-member ratios from trapping mixtures of the two phases present (Bodnar 2003).

Following trapping, fluid inclusions might have followed a P-T path that maintained an internal pressure in the inclusion equal to the confining (or lithostatic) pressure, or might have followed paths such that the internal pressure was greater than or less than the confining pressure. If the inclusion followed an isochoric path such that the confining pressure and the internal pressure were always equal, re-equilibration was unlikely to occur. In most natural systems the rocks do not follow a PT path that approximates the inclusion isochore (Bodnar 2003). Rather, the confining (geologic) pressure is either greater than, or less than, the internal pressure in the inclusions. In these cases the inclusion is not in equilibrium with the surrounding rock and re-equilibration may occur (see Diamond 2003).

If the inclusion followed a P-T path that resulted in internal overpressure, the first modification that inclusions might have experienced was a change in shape. Inclusions tend to become more regularly shaped (see also Bodnar et al. 1985) which was observed in most of the samples.

Another possible reason for the different homogenization temperatures and variable salinities within the sample might be stretching, which can occur as a result of volume increase without fluid loss. When a group of inclusions with initially uniform homogenization temperatures is overheated to a certain amount, the amount of stretching (percent volume increase) of the inclusions is highly variable, resulting in a wide range of homogenization temperatures (Bodnar 2003).

Vityk et al. (2000) noted that stretching of fluid inclusions in quartz requires the diffusive loss of fluid from the inclusion into the surrounding quartz host, to initiate the stretching process. However, normal petrographic observations would not reveal the presence of water-bearing dislocations, and one might assume that the change in homogenization temperature was due solely to volume change. According to observations made by Bodnar (2003), both volume change and fluid loss (or gain) occurs in all, or certainly in most of the cases.

However, based on these observations, the homogenization temperatures might be a result of different stages of burial in combination with variable pressure and temperature regimes, which caused stretching and re-equilibration within the fluid inclusions over the geological time. Nevertheless, at least two different fluid circulation phases can be extracted based on the different salinity inventory.

Based on numerical models, suitable temperature conditions for the fluid entrapment predominantly occurred after the basin initiation in Early Jurassic times (200Ma) followed by the rapid burial of the basin in Late Jurassic/Early Cretaceous (150-90Ma) times. Similar observations were made by Nollet et al. (2005) for the Buntsandstein (Lower Triassic) of the southern part of the LSB. The age range roughly correlates with K/Ar ages of 135 and 92Ma, which were determined by Hagedorn and Lippolt (1993) for the western part of the Harz Mountains. In contrast, authigenic illites in Rotliegend volcanics and sedimentary rocks of the Northeast German Basin are older (206 to 156Ma, Brecht and Wolfgramm 1998). According to Gaupp et al. (1993), the illite formation in Rotliegend sandstones of the North German Basin took place between 200 and 180Ma (Late Triassic - Early Jurassic). Samples from different stratigraphic intervals contained fluids of variable salinities, which indicate more than one fluid circulation event. Possibly, the mineral-forming fluids originated directly from Zechstein units or contain altered evaporites (i.e. anhydrite or gypsum; Lüders et al. 2005, Rieken 1988). Probable saline sources for the high NaCl content in the fluid inclusions could be the Zechstein salt, but also evaporitic layers within the Upper Bunter, Muschelkalk and Keuper, and the Münders Marl salt of the Upper Jurassic. The deeply circulating water in evaporite-bearing sedimentary basins is mainly comprised of subsidence and infiltration solutions as well as saline residual water (Rieken 1988). In recent times, this phenomenon has been quantified on the basis of water analysis from brines within the North German Basin (Magri et al. 2005). According to these data, the salinity of aquifer water strongly depends on the proximity to the Zechstein evaporite formation.

More than one fluid circulation phase within the basin might be an explanation for the different gas content within the gaseous inclusion samples. The high CH₄

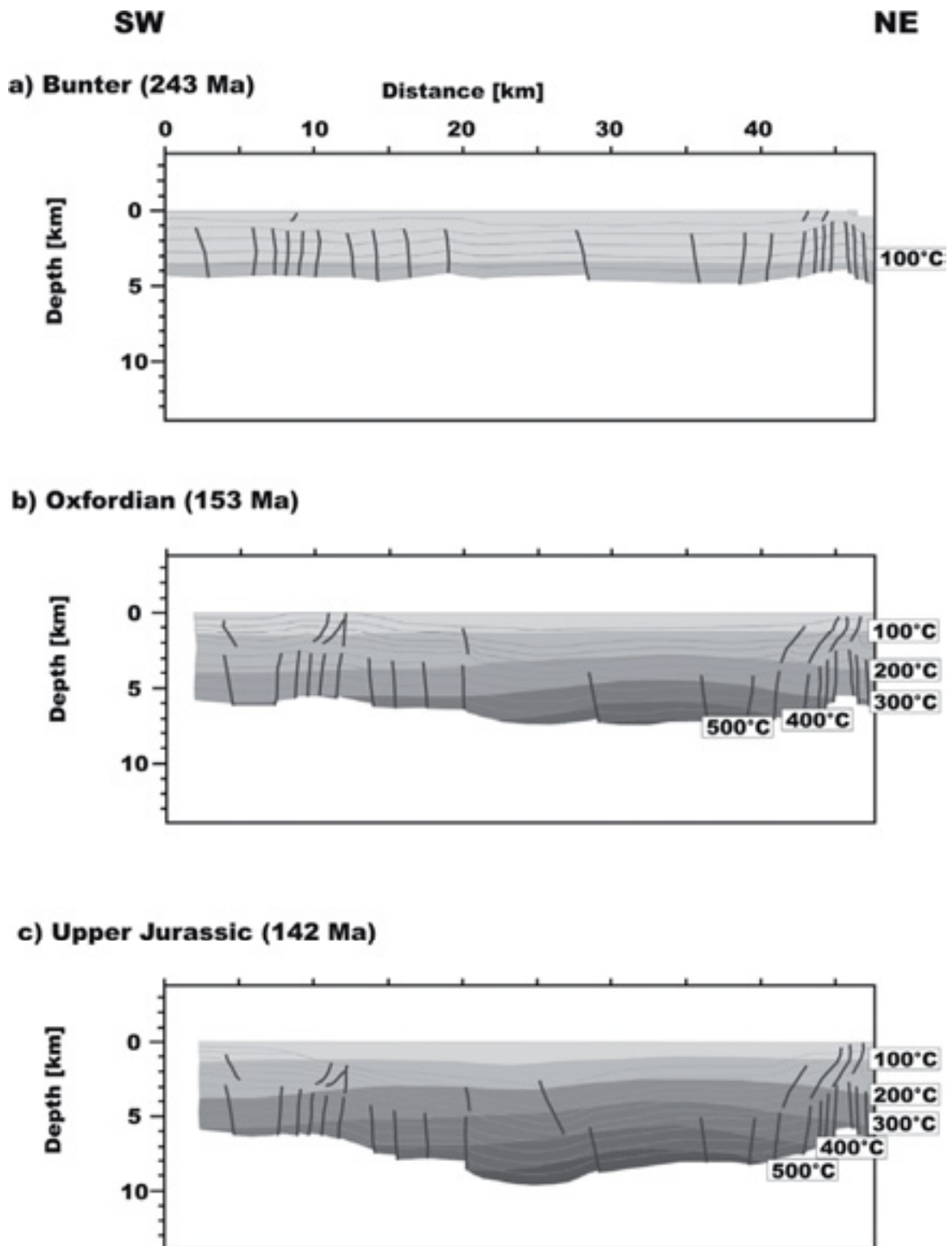


Figure 4.8: Resulting temperature history model for cross section I after the calibration of the wells with the heat flow scenario described in the text. The Figures show different temperature regimes during the time of a) the Bunter (243 Ma), b) the Oxfordian (153 Ma), c) the Late Jurassic (142 Ma).

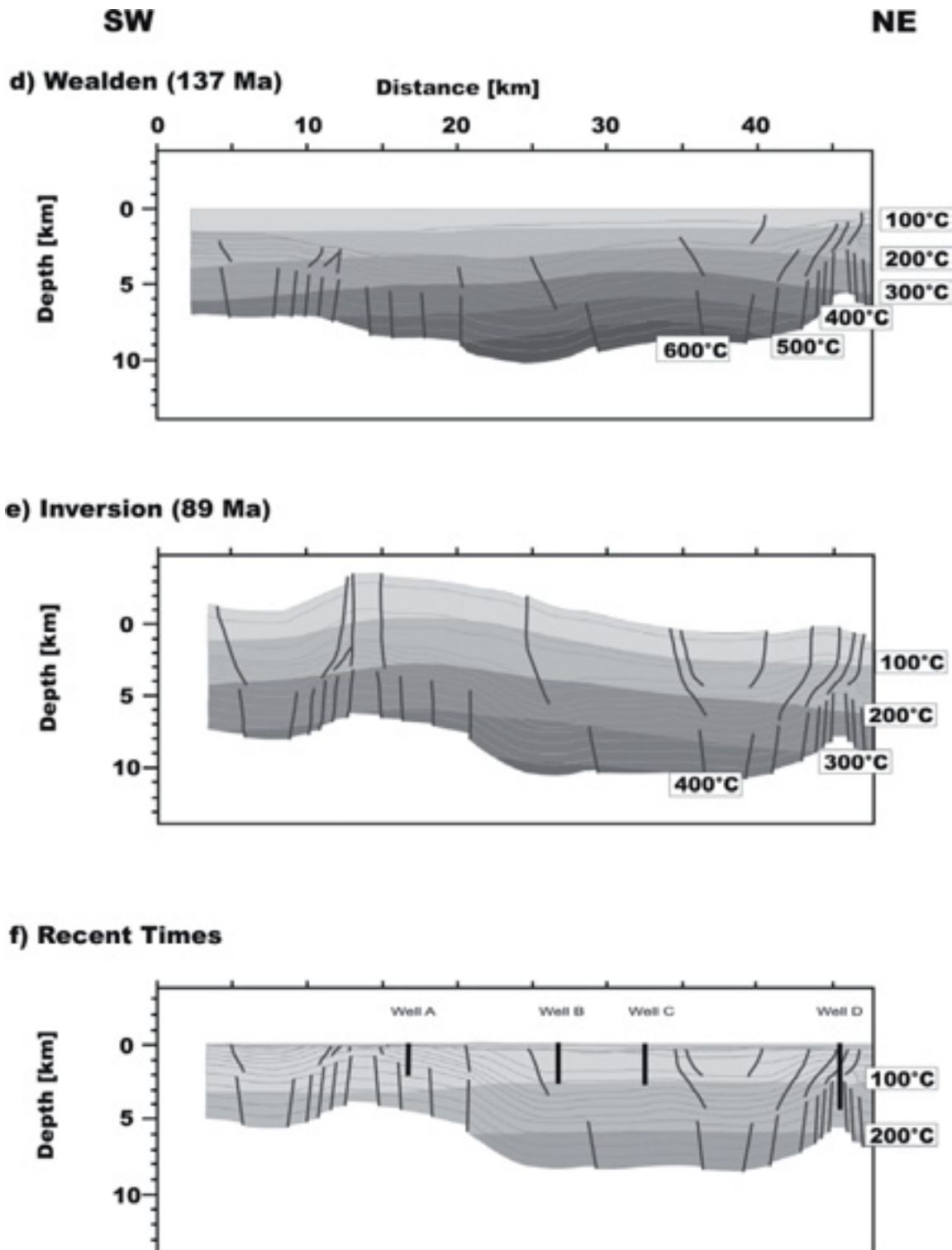


Figure 4.8 (cont.): Resulting temperature history model for cross section I after the calibration of the wells with the heat flow scenario described in the text. The Figures show different temperature regimes during the time of d) the Early Cretaceous (137 Ma), e) the inversion (89 Ma), and f) recent times.

values observed in the fluid inclusions might be a product of gas generated and expelled from Carboniferous coals, which are known to be the principal gas source rocks in northern Germany (Littke et al. 1995, Littke and Leythaeuser 1993). In general, CH₄ is produced from organic matter. During early diagenetic burial, methane originates from bacteria; with increasing depths and temperatures, huge amounts of methane will be provided by the thermal cracking of kerogen and oil (Schoell 1980).

The source of natural CO₂ can either be organic or inorganic. Organic sources include the thermal breakdown of oxygen-rich organic matter (type III kerogen or coal), biogenic sulphate reduction (BSR), as well as thermochemical sulphate reduction (TSR). Inorganic sources include contact metamorphism or (thermo) decomposition of carbonates, reactions between clay and carbonates at temperatures >100°C, or the release of volatiles from a cooling magma. Carbon dioxide (CO₂) is known to occur in variable, but partly high concentration in Upper Permian (Zechstein) reservoirs in the Lower Saxony Basin. Not only the CO₂/CH₄ ratio is highly variable there, but also the carbon isotope composition of CO₂ (Petmecky 1998). Accordingly, there seem to be several sources of CO₂ (Fischer et al. 2006).

Free N₂ may essentially originate from sedimentary sources by the decomposition of organic and/or inorganic sedimentary matter during late diagenesis and early metamorphism. Alternatively, “deep sources”, e.g. mantle gas, have been invoked. A sedimentary nitrogen source, i.e. shales and/or coals has been favoured in a number of previous studies for the European Basin System (e.g. Krooss et al. 1995, Littke et al. 1995, Gerling et al. 1998, Mingram et al. 2005). These sedimentary nitrogen sources tend to release nitrogen at very high stages of maturation, i.e. in the anthracite stage corresponding to temperatures higher than 200°C (Littke et al. 1995, Krooss et al. 1995, 2005).

Lüders et al. (1999) and Wolfgramm (2002) showed that CH₄ and CO₂ are predominant in inclusions of the Permo-Carboniferous Rotliegend units as well as in early diagenetic minerals, while N₂ rich fluids are more prominent in later stage hydrothermal veins.

As the source for the gaseous inclusions of the Upper Carboniferous sample 11 (311Ma), the host rock itself is considered. Based on the almost uniform 80%CH₄ and 20%CO₂ composition, a burial entrapment at the beginning of the gas release could be assumed. Numerical models show that the average homogenization temperatures of 172°C and therefore the entrapment should have occurred between 180Ma and the inversion event. This is in accordance with the hydrocarbon expulsion time of the Upper Carboniferous (Westphalian) source rocks.

Compared with the observations described above, the gaseous inclusions of the Upper Jurassic (host rock Oxfordian, 153Ma) sample 9 from the eastern part of

the study area show an average composition of 54%CO₂, 39%CH₄ and 7%N₂. The high amount of nitrogen in the inclusion is probably related to generation from coals of high levels of maturity, because nitrogen release takes place at high temperatures corresponding to the anthracite stage of coals (Krooss et al. 2005). This is also applicable to other parts of the North German Basin, where the natural gas is sourced from coal-bearing strata and marine shales of Carboniferous age. The gas composition ranges from predominantly hydrocarbons to predominantly nitrogen (up to 90%) or carbon dioxide (up to 90%) in most of the areas of north Germany (Littke et al. 1995, Mingram et al. 2005, Fischer et al. 2006).

According to the gas composition of the fluid inclusions of sample 9 -which points to a Carboniferous origin- and due to numerical models for the area where sample 9 (Table 4.4) is situated, the fluid entrapment must have taken place during the rapid burial of the basin. At this time the coals reached their maximum maturity. The gas generation in the Upper Carboniferous coals was exhausted between 157-140Ma.

4.6. Conclusions

The new fluid inclusion data support a detailed temperature history for the Lower Saxony Basin based on recently gained vitrinite reflectance and fission track data. It accounts for the hydrothermal influence on the basin during the Lower Permian as well as elevated heat flows during the Liassic basin differentiation and during the extension event in Late Jurassic/Early Cretaceous times.

Based on the aforementioned data, the theory of an igneous intrusion during the time of Early to Late Cretaceous can be discarded. Instead, a new burial and heat flow history (Figure 4.5) is preferred. The high maturity of the basin is mostly explained by elevated heat flows during the rift phase in Late Jurassic/Early Cretaceous times followed by a rapid burial based on the cooling lithosphere during the sag-phase of the basin in Early Cretaceous times.

The new burial and heat flow history bears consequences on the hydrocarbon generation from the three main source rocks in the basin (Upper Carboniferous coals, Posidonia and Wealden shales). Hydrocarbon release from both, the Upper Carboniferous coal sequence as well as the Posidonia shale in the basin centre, was already exhausted during Late Jurassic/Early Cretaceous times. Towards the basin margin, the maturity decreases and therefore the remaining hydrocarbon potential of the different source rocks is distinctly higher.

Concurrent with the hydrocarbon release, fluid circulation took place. At least two different fluid circulation events could be distinguished based on homogenization temperatures and gaseous inclusion compositions. High

methane values in the gaseous inclusions indicate a fluid circulation event, which occurred during an early stage of hydrocarbon release from the Westphalian coals, shortly after the basin initiation during Early Jurassic times. A second fluid circulation event was recognized based on high nitrogen contents in the gaseous inclusions, which suggest to a high level of maturity of the Westphalian coals. These fluids were probably released during the rapid burial of the basin in Early Cretaceous times.

5. Final conclusions

Based on the findings represented in the previous chapters two major influences on the thermal evolution during the evolution of the Lower Saxony Basin are identified. These will be discussed in this chapter in relation to the depositional development and petroleum systems of the basin (see also Figure 5.1).

5.1. Sedimentary basin evolution

- Prerift - phase

The Lower Permian is characterized by a continental and arid environment. Succeeding strike slip movements led to the evolution of a pull-apart basin in the area of Northern Germany accompanied with magmatic activities (Bachmann and Grosse 1989, Ziegler 1988). This led to the intrusion of igneous rocks in the area of the Netherlands (Marx et al. 1995, NITG-TNO 2000) and Northwestern Germany.

The only volcanic remainders of this time in the LSB are Rotliegend spilites which were found in wells in the NE of the basin, probably conserved in a NW-SE striking graben system which was peneplained again before the Zechstein epoch. Zircon fission track ages, discussed in chapter 3, give evidence that at least the underlying Upper Carboniferous sandstones experienced a hydrothermal influence during this time.

With Triassic regression renewed continental conditions led to the sedimentation of primarily sand- and siltstones, intercalated with mudstones and salt. Continuous extension provoked rafting on the northern flank of the LSB (represented in chapter 4).

- Rift – phase

In the Lower Jurassic first offshoots of a subsequent rifting in combination with extensional basin evolution occurred followed by returning marine conditions and accumulation of shales and marls. Contemporaneous echeloned syn-sedimentary faulting towards the basin centre occurred (see also Drozdowski 1985 and authors therein) leading to highest sedimentation rates in the middle of the basin (see chapter 4).

During Middle to Upper Jurassic times an intensive rifting period set in. Based on non uniform basin differentiation, the Nordwestfalen-Lippe Swell was exposed and gave way for erosion. On its northern and southern flanks half grabens developed which were filled with sediments sourced by the erosion of

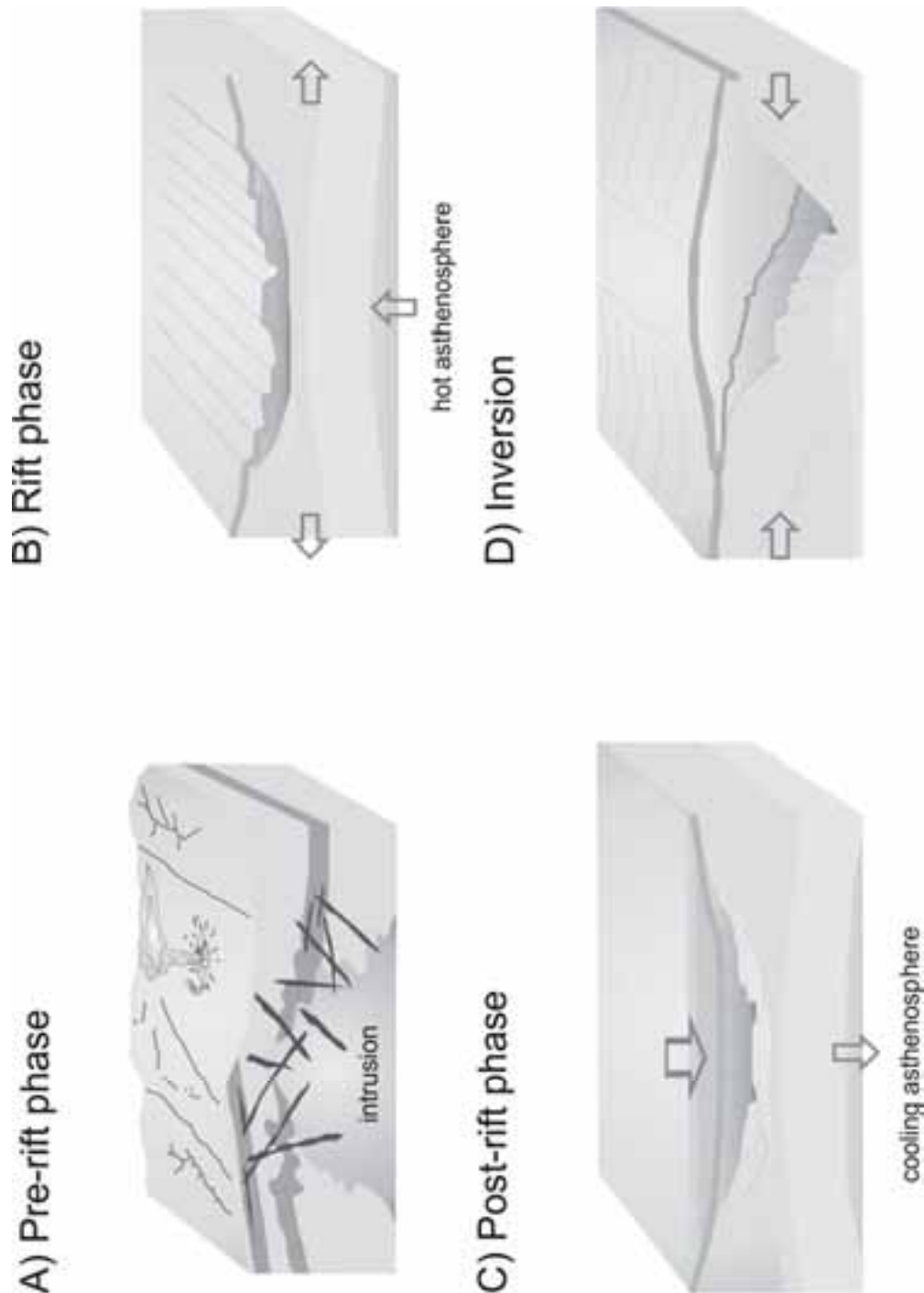


Figure 5.1: Schematic diagram of the structural evolution of the Lower Saxony Basin starting with 5.1.A) the pre-rift phase during the Rotliegend with magmatism in the surrounding areas and hydrothermal influence within the basin, 5.1.B) the rift phase with an upwelling asthenosphere and therefore increasing heatflows, 5.1.C) the syn-rift-phase when based on the cooling of the asthenosphere thermal contraction led to the subsidence of the basin, 5.1.D) inversion and uplift of the former rift basin based on compressional processes.

the basin margins and surrounding highs (e.g. the Münsterland or Pompeckj Block).

During the main phase of rifting the centre of the LSB was considered to develop fast growing half grabens, separated by the arising Nordwestfalen-Lippe Swell (Gramann et al. 1997). The graben systems captured large amounts of sediments. Fast sedimentation rates in the basin centre compensated the sea level rise and therefore lagoonal conditions were predominating with accumulation of evaporites.

In modelling (chapters 2 and 4) highest layer thicknesses were applied for the period of the Munder Marl sequence of the Upper Jurassic section decreasing from 3000m in the Bramsche area to 200m on the northern margin. This idea is supported by a current Tithonian borehole thickness of 1800m in a well located in the northern part of the basin. Additional evidence for this theory gives Munder Marl rock salt appearing in the western part of the Ibbenbueren area. According to Schott (1951), Dulce et al. (1993) and Baldschuhn and Kockel (1999) the rule of thumb is that huge accumulation of rock salt only occurs when the thickness of the Upper Jurassic Munder Marl formation exceeds 1000m.

However, only slightly increasing Upper Jurassic thicknesses are observed for the northern and southern basin margin. The same findings are valid for Lower Cretaceous sequences.

These observations are in conflict with supposed sediment thicknesses estimated by Leischner (1994) and Petmecky (1998) which were working in adjacent areas of the basin and presumed highest thicknesses for Lower Cretaceous times. However, an explanation for the different subsidence patterns could be that during the rifting in the LSB the extension pushed forward outwards from a central region.

- Post rift - phase

During the Lower Cretaceous the basin centre still captured the main deposits with slightly decreasing thicknesses towards the basin rift shoulders.

Between Barrêmian and Aptian times first erosion must have taken place on the northern rift shoulder which is evident from sediment thicknesses of the northern margin.

The latest stage of the Lower Cretaceous was characterized by ceasing thermal subsidence and the entire North German Basin including adjacent highs (Münsterland and Pompeckj Block) was affected by the Albian transgression. This led to a uniform sedimentation of Upper Cretaceous sediments in the LSB.

- Inversion phase

Reasons for the inversion as well as compression and dextral lateral movement must be seen in the progressing opening of the northern Atlantic in Upper Cretaceous times in combination with the European and African continent-continent collision known as the Alpine Orogeny (Ziegler 1987, 1989).

First inversion tectonic offshoots for the LSB were dated for the Lower Coniacian based on phacoidal slide masses in the area of Halle/Westfalen (Voigt and Koch 1977). Intensive inversion tectonics took place in the time span between Coniacian and Santonian. With it the LSB developed to the Lower Saxony Tectogene. During this inversion, the basin fill was uplifted and overthrust on the Münsterland Block to the south as well as on the Pompeckj Block to the north (Drozdowski 2003). Former graben boundary faults reversed thrust the graben rocks partly onto the former shoulders and were deeply eroded (e.g. Binot et al. 1993).

- Post inversion

After the final inversion phase during the Early Tertiary the LSB began to subside slightly during Late Tertiary times followed by a northward tilting throughout this time until present (Frisch and Kockel 2003).

5.2. High maturity based on deep burial or an igneous intrusion?

For the inversion period thickness of eroded sedimentary rocks reached values up to 6000m in the centre of the basin (Figure 5.2). This is in coincidence with an assumed uplift of 6000m for the centre of the LSB corresponding to seismic velocity measurements on Carboniferous sedimentary rocks in the vicinity of the Bramsche anomaly (Brink 2002). The amounts of missing or eroded thicknesses, respectively (presented in chapter 2), are a result of punctual models covering a broad area within the southwestern Lower Saxony Basin.

The amount of erosion for the Piesberg area (7270m) as well as the Ibbenbüren area (4400m) must be considered from another point of view. These Carboniferous horsts probably evolved during the dextral lateral movements on the Osning lineament in Upper Cretaceous times, where many horsts in the area of the Osning fault zone have been uplifted as en-echelon anticlines (Kenkmann and Hambach 1994). The structures of the Ibbenbüren fault block indicate a compression and uplift of the Ibbenbüren fault block by strike-slip movements at the en echelon Osning lineament (Drozdowski 1988). Drozdowski assumed the cause for the different tectonical behaviour as missing Permian Zechstein salt in the underground. Additionally, missing Zechstein salt -normally intercepting or moderating tectonics- induced the unbuffered continuation of the movements up to the surface (Ziegler 1990).

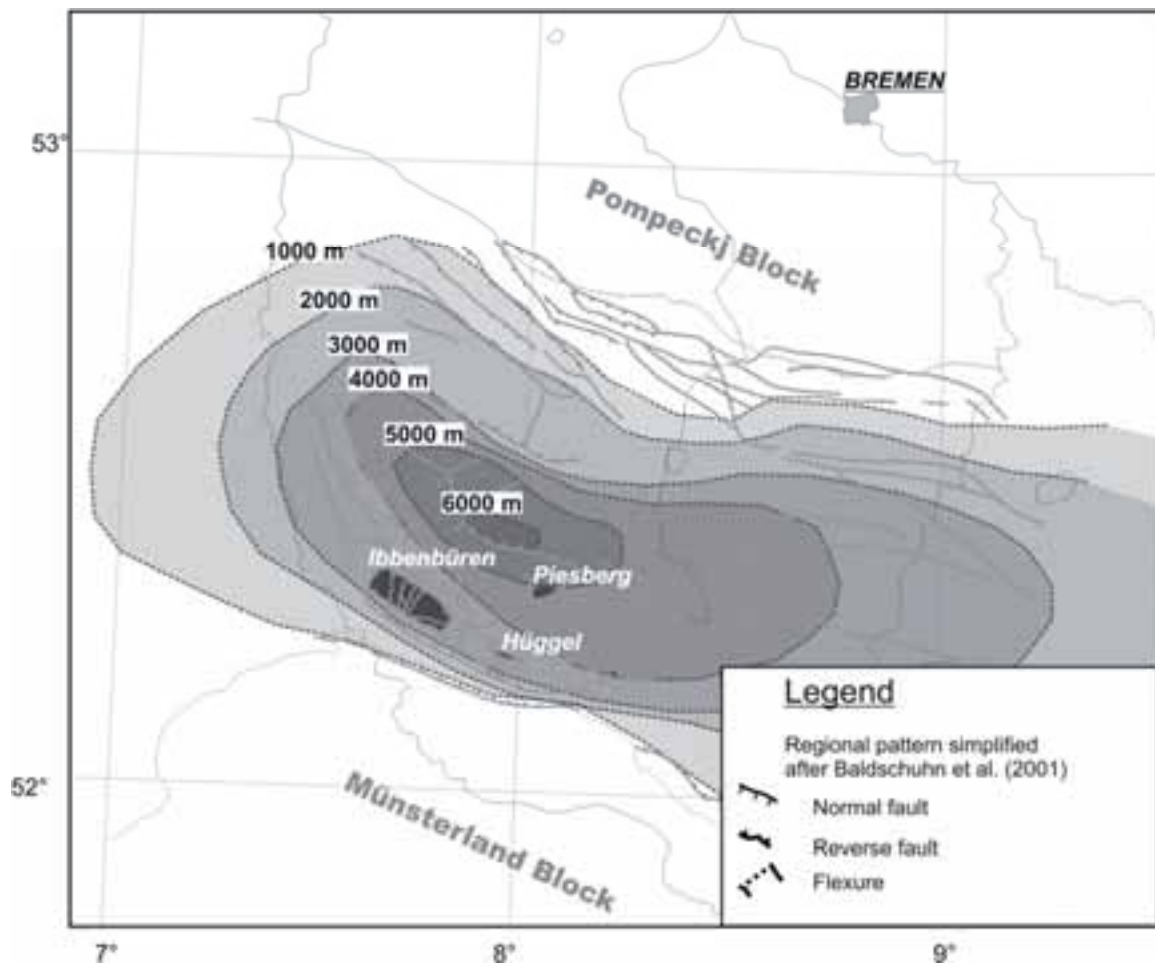


Figure 5.2: Illustrates the erosion isolines distributed over the area of the western Lower Saxony Basin. The main uplift and erosion took place in the former deepest buried centre of the basin which coincides with the coalification anomaly found by several authors.

However, the amount of erosion for the Piesberg area confirms the assumed erosion thickness of 8000m for the outcropping Upper Carboniferous sandstones in the Piesberg area (Füchtbauer and Müller 1970).

The estimated erosion is in conflict with authors such as Nodop (1971) and Buntebarth (1985), who proposed maximum erosion for the LSB and the Ibbenbüren area of up to 4000m. Though, both esteemed reasons for the high maturity of the organic matter in the Lower Saxony Basin as being caused by the igneous intrusion of the “Bramsche Massif”.

However, the observed rank gradient in the LSB is very low which indicates burial rather than an igneous intrusion.

5.3. Heat flow

Heat flows are often difficult to interpret because of complications due to convective heat transport, shallow magmatic intrusions, groundwater convection, and the variability of conductive sediments and rocks.

Evident from Lower Cretaceous zircon cooling ages of the basin centre (chapter 3) elevated heat flows between 80 and 100mW/m² must have occurred before 130Ma and are assumed for the rifting period in the basin. This complies with a lithospheric thinning between 27–20km (Bodri and Bodri 1985). Assuming that the continental crust had a thickness of 30km before thinning this would lead to a crustal stretching factor of approximately 1.4 (Allen and Allen, 2005). In coincidence with the stretching factor the basin might have experienced subsidence due to rifting of a scale less than 6km (Sclater and Christie 1980, Figure 5.3a). This is in coincidence with modelling results which suggest the highest amounts of rift sedimentation (average 5km) are deposited in the basin centre.

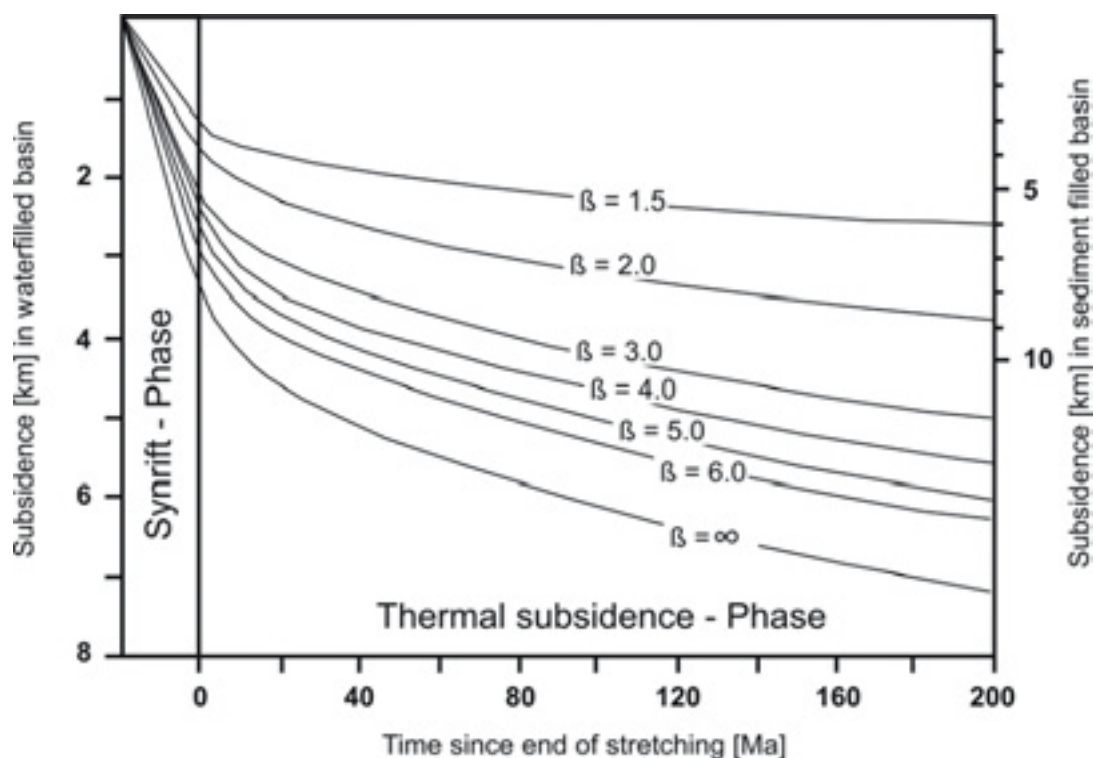


Figure 5.3a: Diagram shows the relation of stretching factors within the lithosphere and their influence of the subsidence of a basin after rifting (after Sclater and Christie 1980).

Based on cooling of the upwelling asthenosphere thermal contraction followed (McKenzie 1978) and therefore the chosen heat flows for the time of the subsequent subsidence decreased (see chapter 4).

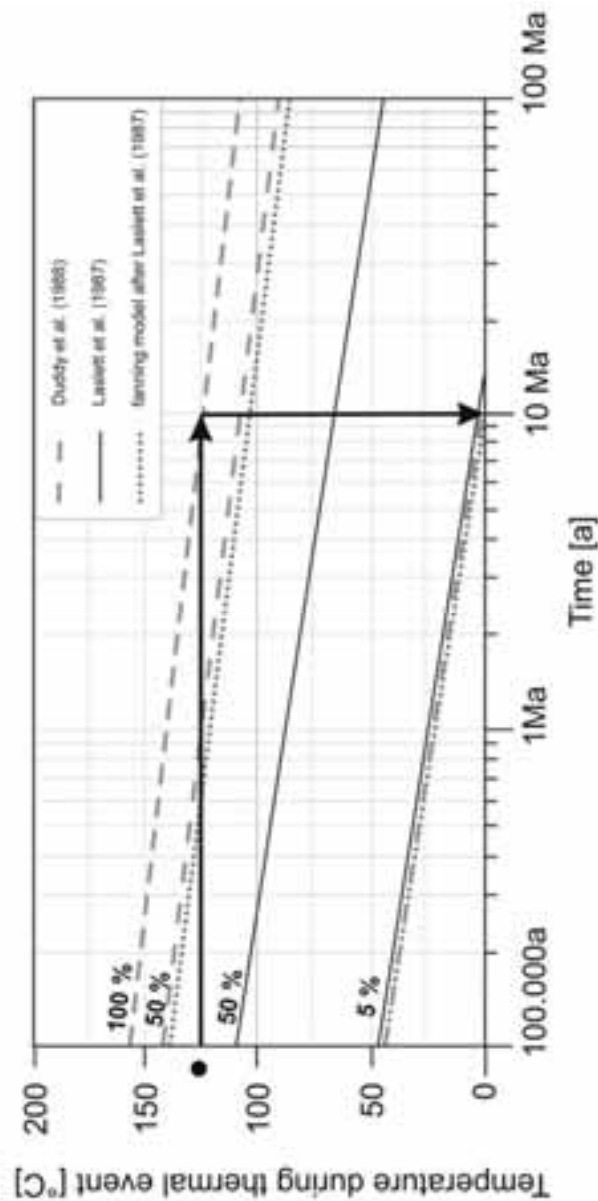


Figure 5.3b: Annealing behaviour of apatites over time. The black dot on the isotherm of 125° illustrates the recent temperatures of samples found on the northern basin margin which still contain apatite fission tracks. According to the annealing behaviour of apatite all fission tracks should be annealed after 10Ma. The reason why the samples still contain fission tracks might be a lowering of the geothermal gradient during Tertiary times.

As discussed in chapter 3 apatite fission track data from boreholes of the northern part of the LSB as well as apatite fission track data of Leischner (1993) and high geothermal gradients at present time in the eastern part of the basin (Petmecky, 1999) indicate a cooling episode in the Miocene followed by heat flows increasing during the last few hundred thousand/million years (Figure 5.3b).

This might have reanimated the hydrocarbon generation in the basin during the latest Tertiary.

5.4. Petroleum systems

Three working petroleum systems were identified for the LSB (Figure 5.4).

- Carboniferous coals

The first major source rock for the main gas generation in Northwestern Germany includes coaly layers with average TOC's of 5% and was deposited in the Upper Carboniferous. During the subsequent Lower Permian period wide spread extrusion of igneous rocks occurred, intercalated with sedimentary rocks over the entire North German Basin. These volcanoclastic sediments provide the main reservoir rocks for the underlying Carboniferous in recent times. Contemporaneous occurring strike slip movements led to the rotation of fault blocks and provided structural traps for later vertical migrating hydrocarbons. During the following Zechstein period a transition to shallow marine conditions occurred and rock salts as a regional seal were accumulated.

The Westphalian coals in the basin centre lost their generation potential entirely at the end of Middle Jurassic times, but they are still in the gas window at the margins of the basin.

- Posidonia shale (Toarcian)

In the Lower Jurassic a second important source rock, the oil prone Posidonia shale with TOC's range between 2-12%, was deposited. During Middle and Upper Jurassic times the depositional environment changed and deltaic marine conditions led to the accumulation of possible reservoir rocks for the hydrocarbons expelled from the underlying source rock.

Thereby fault blocks were rotated and subsided differently which gave way for the evolution of structural traps. Thus, the generated hydrocarbons during the synrift interval may have migrated updip along the half graben and should be preserved on the crest of the structures at the basin margins. Intercalations of salt

within the Upper Jurassic shales provided a basin wide seal for the underlying Posidonia shale.

However, high accumulation rates in Upper Jurassic times in the middle of the basin provoked an early expulsion of hydrocarbon from the Posidonia shale in this area, where further hydrocarbon potential is available. Oil that is preserved from the generation prior to inversion must have experienced long migration and is therefore far away from the kitchen area (Binot et al. 1993). At the basin margins the Posidonia shale is located in the peak oil window and still offers hydrocarbon potential. This is important because based on increasing temperatures during the last 10Ma years the Posidonia shale might have restarted hydrocarbon generation.

- Wealden shale (Berriasian)

With the transition to postrift subsidence the third main source rock known as the Wealden Shale with TOC contents up to 8% was deposited at the beginning of the Lower Cretaceous. Prograding deltaic sandstones were deposited during the Valangian at the margin of the LSB, which constitute reservoir rocks.

Upper Cretaceous shales act as a regional seal for hydrocarbons generated from the Wealden source rock. Due to the basin geometry at the time of the main hydrocarbon generation during the sag phase long distance migration might have occurred. The Wealden in the centre of the basin should have entered the oil generation window in Lower Cretaceous times.

During the inversion Wealden deposits covering the centre of the basin were eroded. However, according to recent maturity of outcropping Wealden of the basin centre, the Wealden had already entered the gas window or the potential for generating hydrocarbons should have been almost exhausted prior to inversion (see also Bartenstein et al. 1971).

On the basin margins the Wealden entered the early oil generation stage. It becomes more mature in the direction towards the basin centre. This is only valid for areas where the Wealden remains preserved.

- Migration

Paleo-kitchens for the above mentioned petroleum systems were limited to the centre of the basin. Based on the inversion all Pre-Turonian traps in the basin centre might have breached which gave ways for vertical hydrocarbon migration into shallower reservoirs or were destroyed and former accumulated hydrocarbons were lost. Traps existing in the basin at present times were formed during the inversion.

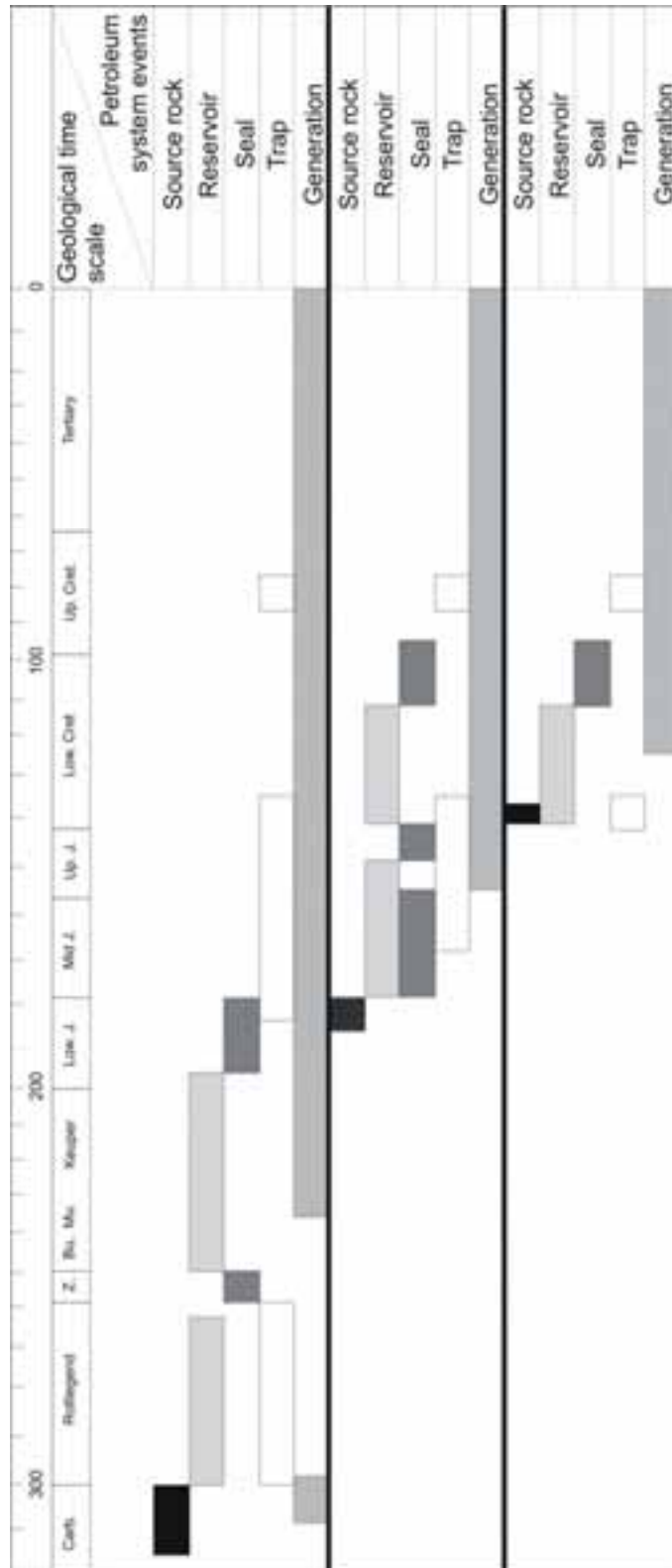


Figure 5.4: Timing of hydrocarbon generation and preservation of the three different petroleum systems found in the basin in relation to the seal and trap formation.

According to Binot et al. (1993) the recent occurrence of oil from the Turonian and Berriasian source rocks shows a clear connection with the regional distribution. For example, oil from the Posidonia shale was found in the western part of the basin where the reservoir rocks of the Wealden petroleum system are lacking. Pure “Wealden” oil occurs on the western margin of the basin, where the Posidonia shale was eroded during the Middle Jurassic or where the Posidonia shale is already overmature. In some areas there exist mixtures of both petroleum systems based on the breaching of the Jurassic reservoirs.

However, inversion of the faults could have resulted in an uplift and thrust of the graben structures over the top of existing reservoirs and might have created new-stacked structural traps. This type of potential trap could be important with significant shortening and inversion. Large amounts of horizontal shortening may place Triassic sedimentary rocks containing salts and evaporites above Jurassic source and reservoir rocks in the footwall, providing an effective seal. This seal formed by the thrusting of the Triassic sequence could help to maintain traps formed during rifting in the Jurassic and help to form a new trap that can collect hydrocarbons remigrated by subsequent inversion.

5.5. Conclusions

Based on the findings discussed in the previous chapters a revised thermal evolution of the Lower Saxony Basin was developed, disproving the influence of a magmatic intrusion on the maturity of the organic matter in the Lower Saxony Basin. Elevated heat flows during the rifting in Upper Jurassic times followed by a deep burial of the basin centre are more likely to have caused the high coalification of the organic material.

However, the existence of an igneous intrusion beneath the Lower Saxony Basin can not be denied based on gravity and magmatic data, but either the magmatic intrusion is positioned at greater depth or -more probably- the intrusion had already occurred in earlier stages of the basin evolution, for instance in Permian times.

These new allegations might have a great impact on the timing of hydrocarbon generation and migration within the basin, because it contradicts the previous opinion that the coalification of the source rocks in the Lower Saxony Basin was caused by the igneous intrusion of Upper Cretaceous time.

Based on the deep burial of the basin during Upper Jurassic and Lower Cretaceous times the source rocks generated hydrocarbons at an earlier stage which might have migrated updip towards the basin margins. This would create a possibility to find preserved hydrocarbons below thrust sections on the basin margins. Additionally, based on the overthrust there is a possibility that early mature source rocks on the basin margins were overridden by the thrust and

moved into the peak oil window on the base of the thrust. Finally, there is a possibility for all source rocks that based on the low geothermal gradient during Tertiary times the hydrocarbon generation was decelerated or stopped and restarted 10Ma years ago.

6. References

- Altebäumer FJ (1982): Untersuchungen Zur Kohlenwasserstoff-Genese an Tonsteinen Des Lias Delta (Pliensbachium) Im Nordwestdeutschen Becken Unter Besonderer Berücksichtigung Des Einflusses Der Intrusion Der Massive Von Bramsche Und Vlotho.
- Altebäumer FJ, Leythaeuser D, Schaefer RG (1983): Effect of Geological Rapid Heating on Maturation and Hydrocarbon Generation in Lower Jurassic Shales from NW-Germany. In: Bjoroy MC, Cornford C, de Groot K, Ellington G, Galimov E, Leythaeuser D, Pelet R, Rullkötter J, Speers G (eds), *Advanced Organic Geochemistry 1981. Organic Geochemistry*, pp 80-86.
- Allen PA, Allen JR (1990) *Basin Analysis: Principles and Applications*. Blackwell, Oxford, 451 pp.
- Allen PA, Allen JR (2005) *Basin analysis: principles and applications*, 2nd edition Blackwell Scientific Publications, Oxford.
- Amijaya H, Littke R (2006) Properties of thermally metamorphosed coal from Tanjung Enim Area, South Sumatra Basin, Indonesia with special reference to the coalification path of macerals. *International Journal of Coal Geology*, 66(4), pp 271-295.
- Bachmann GH, Grosse S (1989) Struktur und Entstehung des Norddeutschen Beckens - Geologische und geophysikalische Interpretation einer verbesserten Bouguer-Schwerekarte. Das Norddeutsche Becken. Niedersächsische Akademie Geowissenschaften Hannover, Veröffentlichung 2, pp 23-47.
- Bachmann GH, Hoffmann N (1995) Entstehung des Mitteleuropäischen Rotliegend-Beckens. *Terra Nostra* 95/7 - 11th Meeting on Geodynamics of the European Variscides - 2nd Symposium on Permocarboneous Igneous Rocks 27. - 29. Oktober 1995, GFZ Potsdam, extended abstracts, pp 12-15.
- Baldschuhn R, Best G, Kockel F (1991) Inversion Tectonics in the North-West German Basin. In: Spencer AM (ed) *Generation, Accumulation and Production of Europe's Hydrocarbons*. EAPG, Special Publication, pp 149-159.
- Baldschuhn R, Frisch U, Kockel F (1996) *Geotektonischer Atlas von NW-Deutschland 1:300 000, Teil 1-17*. Bundesanstalt für Geowissenschaften und Rohstoffe, Hannover.

- Baldschuhn R, Kockel F (1999) Das Osning-Lineament am Südrand des Niedersachsen-Beckens. *Zeitschrift der Deutschen Geologischen Gesellschaft*, 150(4), pp 673-695.
- Baldschuhn R, Binot F, Fleig S, Kockel F (2001) Geotektonischer Atlas von Nordwest-Deutschland und dem deutschen Nordsee-Sektor -- Strukturen, Strukturentwicklung, Paläogeographie. *Geologisches Jahrbuch*, A 153, pp 3-95, 3 CD-ROMs.
- Barker CE (1989) Temperature and time in the thermal maturation of sedimentary organic matter. In: Naeser ND, McCulloh TH (eds) *Thermal history of Sedimentary Basins*. Springer, New York, pp 75-98.
- Barker CE, Goldstein RH (1990) Fluid-inclusion technique for determining maximum temperature in calcite and its comparison to the vitrinite reflectance geothermometer. *Geology*, 18, pp 1003-1006.
- Barker CE, Pawlewicz MJ (1994) Calculation of Vitrinite Reflectance from Thermal Histories and Peak Temperatures. A Comparison of Methods. In: Mukhopadhyay PK, Dow WG (eds) *Vitrinite Reflectance as a Maturity Parameter: Applications and Limitations*. ACS Symposium Series, pp 216-229.
- Bartenstein R, Teichmüller R, Teichmüller M (1971) Die Umwandlung der organischen Substanz im Dach des Bramscher Massivs. *Fortschritte in der Geologie von Rheinland und Westfalen*, 18, pp 501-538.
- Bernet M, Brandon, MT, Garver JI, Molitor B (2004) Fundamentals of detrital zircon fission-track analysis for provenance and exhumation studies with examples from the European Alps. In Bernet M, Spiegel C (eds) *Detrital Thermochronology: Provenance Analysis, Exhumation, and Landscape Evolution of Mountain Belts*. Geological Society America Special Publication 378, pp 126.
- Betz D, Führer F, Greiner G, Plein E (1987) Evolution of the Lower Saxony Basin. *Compressional Intra-Plate Deformations in the Alpine Foreland*. *Tectonophysics*, 137, pp 127-170.
- Binot F, Gerling P, Hiltmann W, Kockel F, Wehner H (1989) *Genese und Migration von Erdölen im Niedersächsischen Becken. Entwicklung einer integrierten geologisch-geochemischen Explorationsmethode auf Kohlenwasserstoffe. Abschlussbericht über das westliche niedersächsische Becken, Fördervorhaben BMFT 032 6450 A. Bundesanstalt für Geowissenschaften und Rohstoffe, Archiv-Nr. 106255, Hannover, 54 pp.*
- Binot F, Gerling P, Hiltmann W, Kockel F, Wehner H (1993) The Petroleum System in the Lower Saxony Basin. In AM Spencer (ed.) *Generation*,

- Accumulation and Production of Europe's Hydrocarbons III, Special Publication of the European Association of Petroleum Geoscientists, No. 3.
- Bodnar RJ (1993) Revised equation and table for determining the freezing point depression of H₂O–NaCl solutions. *Geochimica Cosmochimica Acta*, 57, pp 683–684.
- Bodnar RJ (2003) Reequilibration of fluid inclusions. In: Samson I, Anderson A, Marshall D (eds) *Fluid Inclusions: Analysis and Interpretation*. Mineralogical Association Canada, Short Course 32, pp 213-230.
- Bodnar RJ, Reynolds TJ, Kuehn CA (1985) Fluid inclusion systematics in epithermal systems. In: Berger BR, Bethke PM (eds) *Society of Economic Geologists, Reviews in Economic Geology*, 2, *Geology and Geochemistry of Epithermal Systems*, pp 73-98.
- Bodri L, Bodri B (1985) On the correlation between heat flow and crustal thickness. *Tectonophysics*, 120, pp 69-81.
- Brandon MT, Roden-Tice MK, Garver JI (1998) Late Cenozoic exhumation of the Cascadia accretionary wedge in the Olympic Mountains, northwest Washington State. *GSA Bulletin*, 110/8, pp 985-1009.
- Brauckmann FJ (1984) Hochdiagenese Im Muschelkalk Der Massive Von Bramsche Und Vlotho. *Bochumer geologische und geotechnische Arbeiten*, 14, pp 1-195.
- Brecht GA, Wolfgramm M (1998) Mesozoic thermal activity in the NE-German Basin recorded in authigenic phyllosilicates of Permocarboiferous SiO₂-rich volcanic rocks. *Book of Abstracts, 15th conference of Clay Mineralogy and Petrology*, pp 30-31.
- Breyer F (1971) Geophysikalische und geologische Beiträge zur oberflächen-nahen Tektonik im Dach des Bramscher Massivs. *Fortschritte in der Geologie von Rheinland und Westfalen*, 18, pp 353-386.
- Brink HJ (2002) Die Anomalie von Bramsche - Wieder eine offene Frage. *Erdöl, Erdgas, Kohle*, 118(1), pp 18-22.
- Brink HJ, Franke D, Hoffmann N, Horst W, Onken O (1990) Structure and evolution of the North German Basin. In: Freeman R, Giese P, Mueller S (eds) *The European Geotraverse. Integrative Studies*, European Science Foundation, Strasbourg, pp 195–212.
- Brix MR, Stöckhert B, Seidel E, Theye T, Thomson SN, Küster M (2002) Thermobarometric data from a fossil partial annealing zone in high pressure – low temperature rocks of eastern and central Crete, Greece. *Tectonophysics*, 349, pp 309-326.

- Brückner-Röhling S, Hoffmann N, Koch J, Kockel F, Krull P, Stumm M (1994) Tiefengas, Die Struktur-, Mächtigkeits- und Inkohlungskarten des Norddeutschen Oberkarbon- und Permbeckens und seiner Ränder, 1:500 000. Bundesanstalt für Geowissenschaften und Rohstoffe, Archiv-Nr. 111 531, Hannover, pp 1–77.
- Büchner M (1986) Geothermisch bedingte Veränderungen in Rhät- und Jura-Gesteinen des Unteren Weserberglandes als Folge des Vlothoer Glutflußmassivs. *Berichte Naturwissenschaftl. Verein Bielefeld und Umgebung*, 28, pp 109-138.
- Büker C (1996): Absenkungs-, Erosions- Und Wärmeflussgeschichte Des Ruhr-Beckens Und Des Nordöstlichen Rechtsrheinischen Schiefergebirges. *Berichte des Forschungszentrums Jülich*, 3319, pp 1-212.
- Büker C, Littke R, Welte DH (1995) 2d-Modelling of the Thermal Evolution of Carboniferous and Devonian Rocks of the Eastern Ruhr Basin and Northern Rhenish Massif, Germany. *Zeitschrift Deutsche Geologische Gesellschaft* 146(2), pp 321-339.
- Buntebarth G (1985) Das Temperaturgefälle im Dach des Bramscher Massivs aufgrund von Inkohlungsuntersuchungen im Karbon von Ibbenbüren. *Fortschritte in der Geologie von Rheinland und Westfalen*, 33, pp 255-264.
- Buntebarth G, Teichmüller R (1979) Zur Ermittlung der Paläotemperaturen im Dach des Bramscher Intrusivs aufgrund von Inkohlungsdaten. *Fortschritte in der Geologie von Rheinland und Westfalen*, 27, pp 171-182.
- Burgess PM, Lammers H, van Oosterhout C, Granjeon D (2006) Multivariate sequence stratigraphy: Tackling complexity and uncertainty with stratigraphic forward modeling, multiple scenarios, and conditional frequency maps. *American Association of Petroleum Geologists Bulletin*, 90/12, pp 1883-1901.
- Burnham AK, Sweeney JJ (1989) A chemical kinetic model of vitrinite reflectance maturation. *Geochimica et Cosmochim Acta* 53, pp 2649-2657.
- Burruss RC (1987) Diagenetic palaeotemperatures from aqueous fluid inclusions: re-equilibration of inclusions in carbonate cements by burial heating. *Mineralogical Magazine*, 51, pp 477–481.
- Deutloff O, Teichmüller M, Teichmüller R, Wolf M (1980) Inkohlungsuntersuchungen Im Mesozoikum Von Vlotho (Niedersächsisches Tektogen). *Neues Jahrbuch für Geologie und Paläontologie, Monatshefte*, 6, pp 321-341.
- Diamond LW (2003) Systematics of H₂ O inclusions. In Samson I, Anderson A, Marshall D (eds) *Fluid Inclusions: Analysis and Interpretation*. Mineralogical Association Canada, Short Course Ser. 32, pp 55-79.

- Dieckmann V, Horsfield B, Schenk HJ, Welte DH (1998) Kinetics of petroleum generation and cracking by programmed-temperature closed-system pyrolysis of Posidonia Shale. *Fuel*, 77, pp 23-31.
- Diegel FA, Karlo JF, Schuster DC, Shoup RD, Tauvers PR (1995) Cenozoic structural evolution and tectono-stratigraphic framework of the northern Gulf Coast continental margin. In: Jackson MPA, Roberts DG, Snelson S (eds) Salt tectonics; a global perspective. American Association of Petroleum Geologists Memoir 65, pp 109-151.
- Dodson MH (1973) Closure temperature in cooling geochronological and petrological systems. *Contribution Mineralogical Petrology*, 40, pp 259-274.
- Drozdowski G (1985) Tiefentektonik der Ibbenbürener Karbonscholle. In Drozdowski G, Engel Wolf R, Wrede V (eds) Beiträge zur Tiefentektonik westdeutscher Steinkohlenlagerstätten. Geologisches Landesamt Nordrhein-Westfalen, Krefeld 1985.
- Drozdowski G (1988) Die Wurzel der Osning-Überschiebung und der Mechanismus herzynischer Inversionsbewegungen in Mitteleuropa. *Geologische Rundschau*, 77, pp 127-141.
- Drozdowski G (2003) Geologische Entwicklung und tektonischer Bau. In: Geologischer Dienst NRW (ed) Geologie im Weser- und Osnabrücker Bergland. Krefeld, pp 16-30.
- Drozdowski G, Wrede V (1994) Faltung und Bruchtektonik – Analyse der Tektonik im Subvariscikum. *Fortschritte in der Geologie von Rheinland und Westfalen*, 38, pp 7-187.
- Dubois M, Marignac C (1997) The H₂O-NaCl-MgCl₂ ternary phase diagram with special application to fluid inclusion studies. *Economic Geology*, 92, pp 14-119.
- Duddy IR, Green PF, Bray RJ, Hegarty KA (1994) Recognition of the thermal effects of fluid flow in sedimentary basins. In Parnell J (ed) *Geofluids: Origin, Migration and Evolution of Fluids in Sedimentary Basins*. Geological Society London Special Publication, 78, pp 325-345.
- Duddy IR, Green PF, Laslett GM (1988) Thermal annealing of fission tracks in apatite-3. Variable temperature behaviour. *Chemical Geology*, 73, pp 25-38.
- Dulce G, Harms F, Katschorek T, Kockel F (1993) Paläogeographie und syn-sedimentäre Tektonik im Oberjura des Niedersachsen-Beckens. Bundesanstalt für Geowissenschaften und Rohstoffe, Archiv-Nr. 110 820, Hannover, 112 pp.

- Dunkl I (2002) Trackkey: A Windows program for calculation and graphical presentation of fission track data. *Computers and Geosciences* 28(1), pp 3-12.
- Espitalie J, Laporte JL, Madec M, Marquis F, Leplat P, Paulet J, Boutefeu A (1977) Méthode rapide de caractérisation des roches mères, de leur potentiel pétrolier et de leur degré d'évolution. *Revue de l'Institut Français du Pétrole*, 32, pp 23-42.
- Fischer M, Botz R, Schmidt M, Rockenbauch K, Garbe-Schönberg D, Glodny J, Gerling P, Littke R (2006) Origins of CO₂ in Permian carbonate reservoir rocks (Zechstein, Ca2) of the NW-German Basin (Lower Saxony). *Chemical Geology*, 227/3-4, pp 184-213.
- Flotow A v, Berroth A, Schmehl H (1931) Relative Bestimmungen der Schwerkraft auf 115 Stationen in Norddeutschland. *Veröffentlichung preußisch geodätisches Institut* 106, pp 1-88.
- Fricke K (1979) C¹³/C¹²-Untersuchungen des CO₂-Gases einer Mofette in Ostwestfalen sowie Vergleiche mit anderen C¹³/C¹²-Daten in Europa. *Der Mineralbrunnen*, 29, pp 5-7.
- Frisch U, Kockel F (2003) Der Bremen-Knoten im Strukturnetz Nordwest Deutschlands: Stratigraphie, Paläogeographie, Strukturgeologie. *Berichte des Fachbereichs Geowissenschaften Bremen*, 223, pp 1-379.
- Füchtbauer H, Müller G (1970) Sedimente und Sedimentgesteine. *Sediment-Petrologie T II*. Schweizerbart, Stuttgart, 726 pp.
- Füchtbauer H, Jankowski B, David E, David F, Frank F, Kraft T, Sedat B, Selter V, Strehlau K (1991) Sedimentologie des Nordwestdeutschen Oberkarbons. *DGMK-Forschungsbericht*, Hamburg, 468, pp 75-115.
- Gaertner H (1993) Zur Gliederung des Muschelkalks in Nordwestdeutschland in Tiefbohrungen anhand von Bohrlochmessungen. In Hagdorn H, Seilacher A (eds) *Muschelkalk, Schöntaler Symposium 1991*, Goldschneck, Stuttgart, pp 57-64.
- Galbraith RF, Laslett GM (1993) Statistical models for mixed fission track ages. *Nuclear Tracks* 21, pp 459-470.
- Gallagher K (1995) Evolving temperature histories from apatite fission-track data. *Earth Planetary Science Letter* 126, pp 421-435.
- Gallagher K, Brown R, Johnson C (1998) Fission Track Analysis and its applications to geologic problems. *Annual Review Earth Planetary Sciences* 26, pp 519-572.

- Galy A, France-Lanord C (2000) Higher Erosion Rates in the Himalaya: Geochemical Constraints on Riverine Fluxes. Cambridge Publications, Oxford, Conference Abstracts 5(2), pp 423.
- Garver JI (2005) Stability of Fission Tracks in radiation-damaged zircon from the Cordillera Huayhuash, Northern Peru. GSA abstracts, 37/1, pp 76.
- Garver JI, Bartholomew A (2001) Partial resetting of fission tracks in detrital zircon: dating low temperature events in the Hudson Valley (NY). GSA Special Paper, 33, pp 83.
- Gaupp R, Matter A, Platt J, Ramseyer K, Walzebuck J (1993) Diagenesis and fluid evolution of deeply buried Permian (Rotliegendes) gas reservoirs, Northwest Germany. American Association of Petroleum Geologists, Bulletin 77, pp 1111–1128.
- Geologischer Dienst NRW (2003) Geologie im Weser- und Osnabrücker Bergland. Krefeld, 219 pp.
- Gerling P, Lokhorst A, Nicholson RA, Kotarba M (1998) Natural gas from Pre-Westphalian sources in Northwest Europe – a new exploration target. International Gas Research Conference, Proceedings, San Diego, pp 219–229.
- German Stratigraphic Commission (2002) A Geological Time Scale 2002. In: G S Commission (ed) Stratigraphic Table of Germany 2002, Potsdam.
- Giebeler-Degro M (1986) Zur Tiefenerkundung des Niedersächsischen Tektogens durch dreidimensionale Simulationsrechnung. Thesis, TU Clausthal, 202 pp.
- Gleadow AJW (1981) Fission track dating methods: what are the real alternatives? Nuclear Tracks 5, pp 3-14.
- Gleadow AJW, Duddy IR, Green PF, Lovering JF (1986) Confined fission track lengths in apatite: a diagnostic for thermal analysis. Contribution Mineralogical Petrology, 94, pp 405-415.
- Glennie KW (2001) Exploration Activities in the Netherlands and North-West Europe since Groningen. Geologie en Mijnbouw / Netherlands Journal of Geosciences, 80(1), pp 33-52.
- Goldstein RH (1986) Reequilibration of fluid inclusions in low-temperature calcium-carbonate cement. Geology, 14, pp 792–795.
- Goldstein RH, Reynolds TJ (1994) Systematics of fluid inclusions in diagenetic minerals. SEPM (Society for Sedimentary Geology) Short Course, 31, 199 pp.

- Gramann F, Heunisch C, Klassen H, Kockel F, Dulce G, Harms F-J, Katschorek T, Mönnig E, Schudack M, Schudack U, Thies D, Weiss M (1997) Das Niedersächsische Oberjura-Becken - Ergebnisse interdisziplinärer Zusammenarbeit. *Zeitschrift der Deutschen Geologischen Gesellschaft*, 148, pp 165-236.
- Green PF, Duddy IR, Gleadow AJW, Tingate PR, Laslett GM (1986) Thermal annealing of fission tracks in apatite: 1. a qualitative description. *Chemical Geology* 59, pp 237-253.
- Green PF, Duddy IR, Laslett GM, Hegarthy KA, Gleadow AJW, Lovering JF (1989) Thermal annealing of fission tracks in apatite 4. Quantitative modelling techniques and extension to geological time scales. *Chemical Geology* 79, pp 155-182.
- Gretener PE, Curtis CD (1982) Role of temperature and time on organic metamorphism. *American Association of Petroleum Geologists Bulletin*, 66, pp 1124-1149.
- Günther K, Drozdowski G, Hiss M (1998) Neue Erkenntnisse zum geologischen Bau des „Kleinen Berges“ zwischen Bad Laer und Bad Rothenfelde (südwestliches Niedersachsen) aufgrund der Ergebnisse der Tiefbohrung 'Bad Laer Z 1'(1993). *Mitteilungen Geologisches Institut Universität Hannover* 38, pp 87-113.
- Haenel R (1980) Atlas of Subsurface Temperatures in the European Community. Commission European Community, 43 maps Brussels.
- Hagedorn B, Lippolt HJ (1993) Isotopic age constraints for epigenetic mineralizations in the Harz Mts (Germany) from K-Ar, $^{40}\text{Ar}/^{39}\text{Ar}$ and Rb/Sr data of authigenic K-feldspars. In Möller P, Lüders V (eds) *Formation of Hydrothermal Vein Deposits. Monograph Series on Mineral Deposits*, 30, pp 87-102.
- Hahn A, Kind EG (1971) Eine Interpretation der magnetischen Anomalie von Bramsche. *Fortschritte in der Geologie von Rheinland und Westfalen*, 18, pp 423-428.
- Hahn A, Kind EG, Mishra DC (1976) Depth Estimation of Magnetic Sources by Means of Fourier Amplitude Spectra. *Geophysical Prospecting*, 24, pp 287-308.
- Hall DL, Sterner SM (1993) Preferential water loss from synthetic fluid inclusions. *Contribution to Mineralogy and Petrology*, 114, pp 489-500.
- Hansen DL, Nielsen SB (2002) Does thermal weakening explain basin inversion? *Earth Planetary Science Letters*, 198, pp 113-127.

- Hansen DL, Nielsen SB (2003) Why rifts invert in compression. *Tectonophysics*, 373, pp 5-24.
- Hantschel T, Kauerauf AI, Wygrala B (2000) Finite element analysis and ray tracing modeling of petroleum migration. *Marine and Petroleum Geology*, 17, pp 815-820.
- Hasebe N, Mori S, Tagami T, Matsui R (2003) Geological partial annealing zone of zircon fission-track system: additional constrains from the deep drilling MITI-Nishikubiki and MITI Mishima. *Chemical Geology*, 199, pp 45-52.
- Hertle M, Littke R (2000) Coalification Pattern and Thermal Modelling of the Permo-Carboniferous Saar Basin (SW-Germany). *International Journal Coal Geology*, 42, pp 273-296.
- Hillis RR (1992) A two-layer lithospheric compressional model for the Tertiary uplift of the southern United Kingdom. *Geophysical Research Letter*, 19, pp 573-576.
- Hoefs J (1973) Ein Beitrag zur Isotopengeochemie des Kohlenstoffs in magmatischen Gesteinen. *Contributions to Mineralogy and Petrology*, 41, pp 277-300.
- Hurford AJ (1990) Standardization of fission track dating calibration: recommendation by the Fission Track Working Group of the I.U.G.S Subcommission on Geochronology. *Chemical Geology (Isot Geosci)* 80, pp 171-178.
- Hurford AJ, Carter A (1991) The role of fission track dating in discrimination of provenance. In: Moreton AC, Todd SP, Haughton PDW (eds) *Developments in sedimentary provenance studies*. Geological Society London, Special Publication, 57, pp 67-78.
- Hurford AJ, Green PF (1983) The zeta age calibration of fission track dating. *Chemical Geology* 1, pp 285-317.
- Jackson MPA, Talbot CJ (1991) A Glossary of Salt Tectonics. *Geological Circular*, 91/4, pp 1-44.
- Jacobs J, Breitzkreuz C (2003) Zircon and apatite fission-track thermochronology of Late Carboniferous volcanic rocks of the NE German Basin. *International Journal Earth Science*, 92, pp 165-172.
- Jendrzewski L (1995) Organische Geochemie der höheren Unterkreide Nordwestdeutschlands: Ablagerungsmilieu und Zyklus. *Berichte Forschungszentrum Jülich* 3134, pp 1-211.
- Jochum J, Friedrich G, Leythaeuser D, Littke R (1995a) Intraformational Redistribution of Selected Trace Elements in the Posidonia Shale (Hils

- Syncline, Nw Germany) Caused by the Thermal Influence of the Vlotho Massif. *Geochemistry of Black Shales in Central Europe*. - *Ore Geological Review*, 9, pp 353-362.
- Jochum J, Friedrich G, Leythaeuser D, Littke R, Ropertz B (1995b) Hydrocarbon-Bearing Fluid Inclusions in Calcite-Filled Horizontal Fractures from Mature Posidonia Shale (Hils Syncline, Nw Germany). *Geochemistry of Black Shales in Central Europe*. - *Ore Geological Review*, 9, pp 363-370.
- Karg H, Carter A, Brix MR, Littke R (2005) Late – and post – Variscan cooling and exhumation history of the northern Rhenish massif and the southern Ruhr Basin: new constraints from fission track analysis. *International Journal of Earth Science*, 94/2, pp 180-192.
- Karweil J (1969) Aktuelle Probleme der Geochemie der Kohle. In: Schenk PA, Havernaar I (eds) *Advances in organic geochemistry, 1968*, Pergamon Press, Oxford, pp 59-84.
- Kasuya HG, Naeser CW (1988) The effect of α -damage of fission track annealing in zircon. *Nuclear Tracks Radiat Measure*, 14, pp 477–480.
- Kenkmann T, Hambach U (1994) Paläospannungsanalyse und strukturgeologische Untersuchungen des Waldhügels bei Rheine (Westf.) und des Osnings. *Göttinger Arbeiten Geologie Paläontologie*, Sb 1, 5. Symposium TSK, pp 197-199.
- Kennedy WJ, Kaplan U (1997) Ammoniten aus dem Campan des Stewweder Berges, Dammer Oberkreidemulde, NW-Deutschland. *Geologie und Paläontologie von Westfalen*, 50, pp 31–245.
- Kerkhof AM vd, Hein UF (2001) Fluid inclusion petrography. Special volume in honour of Jacques Touret. In: Andersen T, Frezzotti M-L, Burke EAJ (eds) *Fluid inclusions: Phase relationships methods - applications*. *Lithos*, 55, pp 27-47.
- Ketcham RA, Donelick RA, Donelick MB (2000) AFTSolve: A program for multikinetic modeling of apatite fission-track data. *Geological Mathematical Research*, 2/1 (electronic).
- Ketcham RA, Donelick RA, Carlson WD (1999) Variability of apatite fission-track annealing kinetics: III Extrapolation to geological time scales. *American Mineralogists*, 84, pp 1235-1255.
- Klassen H (1984) *Geologie des Osnabrücker Berglandes*. Naturwissenschaftliches Museum Osnabrück, 672 pp.
- Klassen H (1991) Der obere Dogger und tiefe Malm im westlichen Niedersächsischen Becken. In: *Der tiefere Untergrund des nordwestdeutschen Beckens: Sedimentologie-Tektonik-Kohlenwasserstoffe*. Beiträge der DGG-

- DGMK-Gemeinschaftstagung Braunschweig 1989, DGMK-Bericht 468, pp 259-295.
- Koch J, Arnemann H (1975) Die Inkohlung in Gesteinen des Rhät und Lias im südlichen Nordwestdeutschland. *Geologisches Jahrbuch*, A 29, pp 33-43.
- Kockel F (1991) Die Strukturen im Untergrund des Braunschweiger Landes. *Geologisches Jahrbuch*, A 127, pp 391-404.
- Kockel F (1998) Die kaledonische Ära, die variszische Ära, das Rotliegend. In: *Geotektonischer Atlas von NW-Deutschland 1:300 000, Die paläogeographische und strukturelle Entwicklung NW-Deutschlands; Band 2*, Hannover.
- Kockel F, Wehner H, Gerling P (1994) Petroleum Systems of the Lower Saxony Basin, Germany. In: Magoon LBD, Dow WG (eds) *The Petroleum System from Source to Trap*. American Association Petroleum Geology Memoir, Tulsa, pp 573-586.
- Krooss BM, Friberg L, Gensterblum Y, Hollenstein J, Prinz D, Littke R (2005) Investigation of the pyrolytic liberation of molecular nitrogen from Palaeozoic sedimentary rocks. *International Journal of Earth Sciences*, 94, pp 1023-1038.
- Krooss BM, Littke R, Müller B, Frielingsdorf J, Schwochau K, Idiz EF (1995) Generation of nitrogen and methane from sedimentary organic matter: implications on the dynamics of natural gas accumulations. *Chemical Geology*, 126, pp 291-318.
- Kus J, Cramer B, Kockel F (2005) Effects of a Cretaceous structural inversion and a postulated high heat flow event on petroleum system of the western Lower Saxony Basin and the charge history of the Appeldorn gas field. *Netherlands Journal of Geosciences/Geologie en Mijnbouw*, 84, pp 3-24.
- Laslett GM, Kendall WS, Gleadow AJW, Duddy IR (1982) Bias in measurement of fission track length distributions. *Nuclear Tracks* 6, pp 79-85.
- Laslett GM, Green PF, Duddy IR, Gleadow AJW (1987) Thermal annealing of fission tracks in apatite: 2. A quantitative analysis. *Chemical Geology* 65, pp 1-13.
- Leischner K (1994) Kalibration simulierter Temperaturgeschichten von Sedimentgesteinen. *Berichte des Forschungszentrums Jülich*, 2909, pp 1-309.
- Leischner K, Welte DH, Littke R (1993) Fluid Inclusions and Organic Maturity Parameters as Calibration Tools in Basin Modelling. In: Doré AG, Augustson JH, Hermanrud C, Stewart DJ, Sylta O (eds) *Basin Modelling: Advances and Applications*. Norwegian Petroleum Society, Special Publication, Elsevier, Amsterdam, pp 161-172.

- Leythaeuser D, Hagemann HW, Hollerbach A, Schaefer RG (1980) Hydrocarbon Generation in Source Beds as a Function of Type and Maturation of Their Organic Matter: A Mass Balance Approach. Proceedings of the World Petroleum Congress, 2, pp 31-41.
- Leythaeuser D, Littke R, Radke M, Schaefer RG (1988) Geochemical Effects of Petroleum Migration and Expulsion from Toarcian Source Rocks in the Hills Syncline Area, Nw-Germany. In: Mattavelli L (ed) Adv. Org. Geochem. 1987. Org. Geochem. Pergamon, Oxford, pp 489-502.
- Littke R, Rullkötter J (1987) Mikroskopische and makroskopische Unterschiede zwischen Profilen unreifen und reifen Posidonienschiefers aus der Hilsmulde. Facies, 17, pp 171-180.
- Littke R, Baker DR, Leythaeuser D (1988) Microscopic and Sedimentologic Evidence for the Generation and Migration of Hydrocarbons in Toarcian Source Rocks of Different Maturities.- In: Mattavelli L (ed), Adv. Org. Geochem. 1987. Org. Geochem. Pergamon, Oxford, pp 549-559.
- Littke R, Leythaeuser D (1993) Migration of oil and gas in coals. In: Law BE, Rice DD (eds) Hydrocarbons from Coal. American Association Petroleum Geology, Studies in Geology, 38, pp 219-236.
- Littke R, Krooss B, Idiz E, Frielingsdorf J (1995) Molecular Nitrogen in Natural Gas Accumulations: Generation from Sedimentary Organic Matter at High Temperatures. American Association Petroleum Geologists Bulletin, 79/3, pp 410-430.
- Littke R, Cramer C, Hertle M, Karg H, Stroetmann-Heinen V, Oncken O (2000) Heat Flow Evolution, Subsidence, and Erosion in the Rhenohercynian Orogenic Wedge of Central Europe. Geological Society London Special Publication, 179, pp 231-255.
- Lommerzheim A (1988) Die Genese und Migration von Kohlenwasserstoffen im Münsterländer Becken. Dissertation, Univ Münster, 260 pp.
- Lopatin NV (1971) Temperature and geologic time as factors in coalification. Izv.Akad Nauk SSSR, Ser Geol 3, pp 95-106.
- Lüders V, Hoth P, Reutel C (1999) Fluid- and Gasmigration in the eastern part of the North German Basin, In: Lüders V, Schmidt-Mumm A, Thomas R (eds) European Current Research On Fluid Inclusions. GeoForschungs-Zentrum Publications, Germany, pp 71-72.
- Lüders V, Reutel C, Hoth P, Banks DA, Mingram B, Pettke T (2005) Fluid and gas migration in the North German Basin: fluid inclusion and stable isotope constraints. International Journal of Earth Sciences, 94, pp 990-1009.

- Mackenzie AS, Leythaeuser D, Altebäumler FJ, Disko U, Rullkötter J (1988) Molecular measurements of maturity for Lias delta shales in N.W. Germany. *Geochemica Cosmochimica Acta*, 52, pp 1145-1154.
- Magri F, Bayer U, Jahnke C, Clausnitzer V, Diersch HJ, Fuhrman J, Möller P, Pekdeger A, Tesmer M, Voigt HJ (2005) Fluid-dynamics driving saline water in the North East German Basin. *International Journal of Earth Sciences*, 94, pp 1056-1069.
- Marx J, Huebscher H-D, Hoth K, Korich D, Kramer W (1995) Vulkanostratigraphie und Geochemie der Eruptivkomplexe. In Plein E (ed) *Norddeutsches Rotliegend-Becken. Rotliegend-Monographie, Teil II.* Courier Forschungsinstitut Senckenberg, Frankfurt a.M, 183, pp 54-83.
- McClay KR (1995) The Geometries and Kinematics of Inverted Fault Systems: A Review of Analogue Model Studies. In: Buchanan JG, Buchanan PG (eds) *Basin Inversion.* Geological Society London Special Publication, 88, pp 97-118.
- McKenzie DP (1978) Some remarks on the development of sedimentary basins. *Earth and Planetary Science Letters*, 40, pp 25-32.
- Midland Valley (2003) *2DMoveV4 Manual 2003.* Midland Valley, 434 pp.
- Mingram B, Hoth P, Lüders V, Harlov DE (2005) The significance of fixed ammonium in Palaeozoic sediments for the generation of nitrogen-rich natural gases in the North German Basin. *International Journal of Earth Sciences*, 94, pp 1010-1022.
- Mohr M, Kukla PA, Urai JL, Bresser G (2005) Multiphase salt tectonic evolution in NW Germany: seismic interpretation and retro-deformation. *International Journal of Earth Sciences*, 94, pp 917-940.
- Muchez P, Viaene W, Marshall JD (1991) Origin of shallow burial cements in the Late Viséan of the Campine Basin, Belgium. *Sedimentary Geology*, 73, pp 257-271.
- Mukhopadhyay PK, Dow WG (1994) Vitrinite reflectance as a maturity parameter. *AGS Symp Ser 570*, American Chemical Society, pp 216-229.
- Mundry E (1971) Der Temperaturverlauf im Dach des Bramscher Massivs nach der Wärmeleitungstheorie. *Fortschritte in der Geologie von Rheinland und Westfalen*, 18, pp 539-546.
- Mutterlose J (1992) Migration and Evolution Patterns of Floras and Faunas in Marine Early Cretaceous Sediments of NW Europe. *Palaeogeography Palaeoclimatology Palaeoecology* 94, pp 261-282.
- Mutterlose J, Böckel B (1998) The Barrêmian-Aptian interval in NW Germany: a review. *Cretaceous Research*, 19, pp 539-568.

- Mutterlose J, Bornemann A (2000) Distribution and facies patterns of the Lower Cretaceous sediments in northern Germany: a review. *Cretaceous Research* 21, pp 733-759.
- Naeser CW (1976) Fission track dating. Open-File Rep. – U.S. Geological Survey, pp 76-190.
- Negredo AM, Fernandez M, Zeyen H (1995) Thermo-mechanical constraints on kinematic models of lithospheric extension. *Earth Planetary Science Letters*, 134, pp 87-98.
- Neugebauer HJ (1989) Dynamisch-thermische Aspekte der Beckenentwicklung. *Mintrop-Seminar*, 9, pp 287-302, Bochum.
- Neunzert GH, Gaupp R, Littke R (1996) Absenkungs- und Temperaturgeschichte paläozoischer und mesozoischer Formationen im Nordwestdeutschen Becken. *Zeitschrift Deutsche Geologische Gesellschaft* 147(2), pp 183-208.
- NITG-TNO (2000) Geological Atlas of the Subsurface of the Netherlands, Explanations to Map Sheet VI Veendam-Hoogeveen. Netherlands Institute of Applied Geoscience TNO, Harlem, 152 pp.
- Nodop J (1971) Tiefenrefraktionsseismischer Befund im Profil Vermold-Lübbecke-Nienburg. *Fortschritte in der Geologie von Rheinland und Westfalen*, 18, pp 411-422.
- Noeth S (1991) Die Conodontendiagenese Als Inkohlungsparameter Und Ein Vergleich Unterschiedlich Sensitiver Diageneseindikatoren Am Beispiel Von Triassedimenten Nord- Und Mitteldeutschlands. *Bochumer geologische und geotechnische Arbeiten*, 37, pp 1-169.
- Noeth S, Karg H, Littke R (2001) Reconstruction of Late Palaeozoic Heat Flows and Burial Histories at the Rhenohercynian-Subvariscan Boundary, Germany. *International Journal Earth Science (Geologische Rundschau)* 90, pp 234-256.
- Nollet S, Hilgers C, Urai JL (2005) Sealing of fluid pathways in overpressure cells: a case study from the Buntsandstein in the Lower Saxony Basin (NW Germany). *International Journal of Earth Sciences*, 94, pp 1039-1055.
- Pepper AS, Corvi PJ (1995) Simple kinetic models of petroleum formation. Part I: oil and gas generation from kerogen. *Marine and Petroleum Geology*, 12/3, pp 291-319.
- Petmecky SP (1998) Numerische Simulation der Entwicklungsgeschichte des zentralen Niedersächsischen Beckens unter besonderer Berücksichtigung der Erdgaslagerstätten-Bildung. *Berichte des Forschungszentrums Jülich*, 3567.

-
- Petmecky SP, Meier L, Reiser H, Littke R (1999) High Thermal Maturity in the Lower Saxony Basin: Intrusion or Deep Burial? *Tectonophysics*, 304, pp 317-344.
- Plein E (1978) Rotliegend-Ablagerungen im Norddeutschen Becken. *Zeitschrift Deutsche Geologische Gesellschaft* 129/(1), pp 71-97.
- Plein E (1993) Bemerkungen zum Ablauf der paläogeographischen Entwicklung im Stefan und Rotliegend des Norddeutschen Beckens. *Geologisches Jahrbuch*, A 131, pp 99-116.
- Poelchau HS, Baker DR, Hantschel T, Horsfield B, Wygrala B (1997) Basin Simulation and the Design of the Conceptual Basin Model. In Welte DH, Horsfield B, Baker DR (eds) *Petroleum and basin evolution*. Springer, Heidelberg, pp 3-70.
- Radke M, Horsfield B, Littke R, Rullkötter J (1997) Maturation Effects and Parameters. In: Welte DH, Horsfield B, Baker DR (eds) *Petroleum and Basin Evolution*. Springer-Verlag, Berlin, Heidelberg, pp 169-229.
- Rahn MK (2001) The metamorphic and exhumation history of the Helvetic Alps, Switzerland, as revealed by apatite and zircon fission tracks. PhD Thesis, Universität Freiburg, Freiburg, 140 pp.
- Rahn MK, Brandon MT, Batt GE, Garver GI (2000) Fission-track annealing in 'zero-damage' zircons: field constraints and an empirical model. 9th International Conference of Fission Track Dating Thermochronology, Lorne, Australia, Abstract, 271 pp.
- Rahn MK, Brandon MT, Batt GE, Garver GI (2004) A zero damage model for fission track annealing in zircon. *American Mineralogist*, 89, pp 473-484.
- Reich H (1948) Geophysikalische Karte Von Nordwestdeutschland 1:500000, Bl. 1: Magnetik, Bl. 2: Gravimetrik. Reichsamt für Bodenforschung, Hannover.
- Reich H (1949) Die Geophysikalische Erforschung Nordwestdeutschlands 1932-1947, Ein Überblick. *Erdöl und Tektonik in Nordwestdeutschland*, pp 21-28.
- Rieken R (1988) Lösungs-Zusammensetzung und Migrationsprozesse von Paläo-Fluidsystemen in Sedimentgesteinen des Nordwestdeutschen Beckens. *Göttinger Arbeiten für Geologie und Paläontologie*, 37, pp 1-116.
- Riley BCD (2002) Preferential thermal resetting of fission tracks in radiation-damaged detrital zircon grains: case study from the Laramide of Arizona. *GSA Paper*, 212-12, GSA, Boulder, Colorado.
- Ritter U (1986) Heat flow during the Carboniferous and Mesozoic of the Northwest German Basin. *Geologische Rundschau*, 75, pp 293-300.

- Rodon S, Littke R (2005) Thermal maturity in the Central European Basin system (Schleswig-Holstein area): Results of 1D basin modelling and new maturity maps. *International Journal Earth Science Special Publication*, pp 815-833.
- Roedder E (1984) Fluid inclusions. *Reviews in Mineralogy*, 12. Mineralogical Society of America.
- Röhling HG (1986) Die Gliederung des Unteren und Mittleren Buntsandsteins nach Bohrlochmessungen (Gamma-Ray und Sonic-Log) im Nordwestdeutschen Becken. – BMFT-Förderungsvorhaben Nr. 03E 6336 A. Bundesanstalt für Geowissenschaften und Rohstoffe, Archiv-Nr. 100 003, Hannover.
- Röhling HG (1988): Paläogeographie des Unteren und Mittleren Buntsandsteins im Nordwestdeutschen Becken. – BMFT-Förderungsvorhaben Nr. 03E 6336 A, Bundesanstalt für Geowissenschaften und Rohstoffe, Archiv-Nr. 104 107, Hannover.
- Rullkötter J, Leythaeuser D, Littke R, Mann U, Müller PJ, Radke M, Schaefer RG, Schenk HJ, Schwochau K, Witte EG, Welte DH (1988) Organic Matter Maturation under the Influence of a Deep Intrusive Heat Source: A Natural Experiment for Quantification of Hydrocarbon Generation and Expulsion from a Petroleum Source Rock (Toarcian Shale, Northern Germany). In: Mattavelli L (ed), *Adv. Org. Geochem. 1987. Org. Geochem.* Pergamon, Oxford, pp 847-856.
- Sandiford M (1999) Mechanics of basin inversion. *Tectonophysics*, 305, pp 109-120.
- Scheidt G, Littke R (1989) Comparative Organic Petrology of Interlayered Sandstones, Siltstones, Mudstones and Coals in the Upper Carboniferous Ruhr Basin, Northwest-Germany, and Their Thermal History and Methane Generation. *Geologische Rundschau* 78(1), pp 375-390.
- Schmidt A (1914) Die magnetische Vermessung I. Ordnung des Königreichs Preußen, 1898 bis 1903, nach den Beobachtungen von M Eschenhagen und J Edler. Veröffentlichung Preußisches Meteorologisches Institut, Berlin: 7 Kt.
- Schmitz U, Wenzlow B (1990) Maturity Anomalies of the Western Lower Saxony Basin in Their Regional Context. *Zentralblatt für Geologie und Paläontologie*, Teil 1(8), pp 1091-1103.
- Schoell M (1980) The hydrogen and carbon isotopic composition of methane from natural gases of various origins. *Geochimica et Cosmochimica Acta*, 44, pp 649-661.

- Schott W (1951) Der obere weiße Jura und die tiefste Unterkreide im deutsch-holländischen Grenzgebiet. *Geologisches Jahrbuch* 65, pp 213-270.
- Slater JG, Christie PAF (1980) Continental stretching: an explanation of the post-mid-Cretaceous subsidence of the Central North Sea Basin. *Journal of Geophysical Research*, 85, pp 3711-3739.
- Senglaub Y, Brix MR, Adriasola A, Littke R (2005) New information on the thermal history of the southwestern Lower Saxony Basin, northern Germany, based on fission track analysis. – *International Journal of Earth Sciences*, 94, pp 876-896.
- Senglaub Y, Littke R, Brix MR (2006) Numerical modelling of burial and temperature history as an approach for an alternative interpretation of the Bramsche anomaly, Lower Saxony Basin. *International Journal of Earth Sciences*, 95, pp 204-224.
- Sissingh W (2004) Paleozoic and Mesozoic igneous activity in the Netherlands: a tectonic review. *Netherlands Journal of Geosciences/Geologie en Mijnbouw*, 83/2, pp 113-134.
- Skupin K (2003) Kreide. In: *Geologischer Dienst NRW (ed) Geologie im Weser- und Osnabrücker Bergland*. Krefeld, pp 65-70.
- Slater JP, Jaupart C, Garson D (1980) The heat flow through oceanic and continental crust and the heat loss of the Earth. *Reviews Geophysics and Space Physics*, 18, pp 269-311.
- Stadler G (1971) Die Vererzungen im Bereich des Bramscher Massivs und seiner Umgebung. *Fortschritte in der Geologie von Rheinland und Westfalen* 18, pp 439-500.
- Stadler G, Teichmüller M (1971) Die Umwandlung der Kohlen und die Diagenese der Ton- und Sandsteine in der Untertagebohrung 150 der Steinkohlenbergwerke Ibbenbüren. *Fortschritte in der Geologie von Rheinland und Westfalen*, 18, pp 125-146.
- Stadler G, Teichmüller R (1971) Zusammenfassender Überblick über die Entwicklung des Bramscher Massivs und des Niedersächsischen Tektogens. *Fortschritte in der Geologie von Rheinland und Westfalen*, 18, pp 547-564.
- Stahl W (1971) Isotopen-Analysen an Carbonaten und Kohlendioxid-Proben aus dem Einflussbereich und der weiteren Umgebung des Bramscher Intrusivs und hydrothermalen Carbonaten aus dem Siegerland. *Fortschritte in der Geologie von Rheinland und Westfalen*, 18, pp 429-438.
- Süss MP (1996) *Sedimentologie und Tektonik des Ruhr-Beckens: Sequenzstratigraphische Interpretation und Modellierung eines*

- Vorlandbeckens der Varisciden. Bonner Geowissenschaftliche Schriften, 20, 148 pp.
- Sweeney JJ, Burnham AK (1990) Evaluation of a Simple Model of Vitrinite Reflectance Based on Chemical Kinetics. American Association of Petroleum Geologists Bulletin, 74, pp 1559-1570.
- Tagami T, Galbraith RF, Yamanda R, Laslett GM (1998) Revised annealing kinetics of fission tracks in zircon and geological implications. In: Van den haute P, De Corte F, (eds) Advances in fission-track geochronology. Kluwer, Dordrecht, pp 99–112.
- Tagami T, Shimada C (1996) Natural long-term annealing of zircon fission track system around a granitic pluton. Journal Geophysical Research 101(B), pp 11353–11364.
- Taylor GH, Teichmüller M, Davis A, Diessel CFK, Littke R, Robert P (1998) Organic Petrology.- Gebrüder Borntraeger, Berlin, 704 pp.
- Teichmüller M (1963) Die Kohlenflöze der Bohrung Münsterland 1 (Inkohlung, Petrographie, Verkohlungsverhalten). Fortschritte in der Geologie von Rheinland und Westfalen 1, pp 129-178.
- Teichmüller M, Teichmüller R (1951) Inkohlungsfragen im Osnabrücker Raum. Neues Jahrbuch Geologie Paläontologie, Monatshefte 1951, pp 69-85.
- Teichmüller M, Teichmüller R (1958) Inkohlungsuntersuchungen und ihre Nutzenanwendung. Geologie en Mijnbouw, 20, pp 41-66.
- Teichmüller M, Teichmüller R, Bartenstein H (1979) Inkohlung und Erdgas in Nordwestdeutschland - Eine Inkohlungskarte der Oberfläche des Oberkarbons.- Fortschritte in der Geologie von Rheinland und Westfalen, 27, pp 137-170.
- Teichmüller M, Teichmüller R, Lorenz V (1983) Inkohlung und Inkohlungsgradienten im Permokarbon der Saar-Nahe-Senke. Zeitschrift Deutsche Geologische Gesellschaft 134, pp 153-210.
- Teichmüller M, Teichmüller R, Bartenstein H (1984) Inkohlung und Erdgas - Eine neue Inkohlungskarte der Karbon-Oberfläche in Nordwest-Deutschland. Fortschritte in der Geologie von Rheinland und Westfalen, 32, pp 11-34.
- Teichmüller M, Teichmüller R (1985) Inkohlungsgradienten in der Anthrazitfolge des Ibbenbürener Karbons. Fortschritte in der Geologie von Rheinland und Westfalen, 33, pp 231-253.
- Thiermann A (1970) Erläuterungen zu Blatt 3712 Tecklenburg. Geologische Karte Nordrhein Westfalen, 1:25000, Erläuterungen Blatt 3712 Tecklenburg. Krefeld, 243 pp.

- Thiermann A (1980) Erläuterungen zu Blatt 3612 Mettingen. Geologische Karte von Nordrhein-Westfalen, 1:25000, Erläuterungen Blatt 3612 Mettingen. Krefeld, 200 pp.
- Thyssen F, Allnoch HG, Lütkebohmert G (1971) Einige Ergebnisse geophysikalischer Arbeiten im Bereich der Bramscher Anomalie. Fortschritte in der Geologie von Rheinland und Westfalen, 18, pp 395-410.
- Trusheim F (1961) Über radioaktive Leithorizonte im Buntsandstein Norddeutschlands zwischen Ems und Weser. Erdöl und Kohle 14, pp 797-802.
- Vityk MO, Bodnar RJ, Dudok IV (1996) Fluid inclusions in "Marmarosh Diamonds": Evidence for tectonic history of the Folded Carpathian Mountains, Ukraine. *Tectonophysics*, 255, pp 163-174.
- Vityk MO, Bodnar RJ, Doukhan J-C (2000): Synthetic fluid inclusions: XV. TEM investigation of plastic flow associated with reequilibration of synthetic fluid inclusions in natural quartz. *Contributions Mineralogy and Petrology*, 139, pp 285-297.
- Voigt E, Koch W (1977) Neue Daten über die submarine Großgleitung turoner Gesteine im Teutoburger Wald bei Halle/Westf. *Zeitschrift der Deutschen Geologischen Gesellschaft*, 128, pp 57-79.
- Voigt T, Eynatten H v, Franzke HJ, Gaupp R (2002) Fazies, Mächtigkeiten und Herkunft der Kreidesedimente im Harzvorland – ein Schlüssel zum Verständnis der Harzhebung. In: Hüssner H, Hinderer M, Götz AE, Petschik R (eds) *Schriftenreihe Deutsche Geologische Gesellschaft, Kurzfassungen und Programm „Sediment 2002“*, pp 211-212.
- Wagner GA, Van den haute P (1992) *Fission track dating*, Enke-Verlag, Stuttgart, 285 pp.
- Wagner GA (1968) Fission-track dating of apatites. *Earth Planetary Science Letter*, 4, pp 411-414.
- Waples DW (1980) Time and temperature in petroleum formation: application of Lopatin's method to petroleum exploration. *American Association Petroleum Geology Bulletin*, 64, pp 916-926.
- Waples DW, Suizu M, Kamata H (1992) The art of maturity modeling, Part 2. Alternative models and sensitivity analysis. *American Association Petroleum Geology Bulletin*, 76, pp 47-66.
- Wees v J-D, Stephenson RA, Ziegler PA, Bayer U, McCann T, Dadlez R, Gaupp R, Narkiewicz M, Bitzer F, Scheck M (2000) On the Origin of the Southern Permian Basin, Central Europe. *Marine Petroleum Geology*, 17, pp 43-59.

- Welte DH, Yalcin MN (1988) Basin modelling – a new comprehensive method in petroleum geology. *Organic Geochemistry*, 13, pp 141-151.
- Welte DH, Yüklér MA (1981) Petroleum origin and accumulation in basin evolution. *American Association Petroleum Geology Bulletin*, 65, pp 1387-1396
- Wolburg J (1969) Die epirogenetischen Phasen der Muschelkalk- und Keuperentwicklung Nordwestdeutschlands, mit einem Rückblick auf den Buntsandstein. *Geotektonische Forschungen*, 32, pp 1-65.
- Wolfgramm M (2002) Fluidentwicklung und Diagenese im Nordostdeutschen Becken – Petrographie, Mikrothermometrie und Geochemie stabiler Isotope. PhD Thesis, Martin Luther Universität Halle-Wittenberg, 170 pp.
- Wygrala B (1989) Integrated study of an oil field in the southern Po-basin, Northern Italy. Dissertation Universität Köln, Berichte Forschungszentrum Jülich, 2313, 217 pp.
- Yalcin MN, Littke R, Sachsenhofer RF (1997) Thermal history of sedimentary basins. In: Welte DH, Horsfield B, Baker DR (eds) *Petroleum and basin evolution; insights from petroleum geochemistry, geology and basin modelling*, Springer, Berlin, pp 71-167.
- Yamada R, Tagami T, Nishimura S, Ito H (1995) Annealing kinetics of fission tracks in zircon: an experimental study. *Chemical Geology*, 122, pp 249-258.
- Yamaji A (1986) Analysis of vitrinite reflectance-burial depth relations in dynamical geological settings by direct integration method. *Japanese Association Petroleum Technology* 5(1/3), pp 1-8.
- Ziegler PA (1982) Triassic Rifts and Facies Patterns in Western and Central Europe. *International Journal Earth Science (Geologische Rundschau)* 71(3), pp 747-772.
- Ziegler PA (1987) Late Cretaceous and Cenozoic intra-plate compressional deformations in the Alpine foreland – a geodynamic model. *Tectonophysics*, 137, pp 389-420.
- Ziegler PA (1988) Evolution of the Arctic-North Atlantic and the Western Tethys - The American Association of Petroleum Geologists, Tulsa, Oklahoma, *American Association Petroleum Geology Memoir* 43, pp 1-197.
- Ziegler PA (1989) Evolution of Laurussia. A study in Late Palaeozoic plate tectonics, Kluwer Academic Publishers, 102 pp.
- Ziegler PA (1990) Geological Atlas of Western and Central Europe. The Hague (Shell International) 2nd Edition, 239 pp.

Ziegler PA, Cloething S, van Wees JD (1995) Dynamics of intra-plate compressional deformation: the alpine foreland and other examples. *Tectonophysics*, 252, pp 7-59.

CV

Yvonne Adriasola Muñoz	DATE OF BIRTH	02.03.1972
	PLACE OF BIRTH	Räckelwitz

▪ **PROFESSIONAL EXPERIENCE**

- | | |
|------------------------|---|
| Nov. 2005 – Present | Petroleum Geologist, Exploration & Reservoir Consultancy, Fugro Robertson Limited, North Wales, UK.
Member of the Exploration Opportunity Screening Team undertaking prospect evaluation studies in frontier basins. Responsibilities include the compilation of geological and geochemical information, maturity mapping for special source rock intervals and basin modelling. |
| Sept. 2001 – Nov. 2005 | Scientific Assistant, Institute of Geology & Geochemistry of Petroleum & Coal, RWTH Aachen University, Germany.
Petrophysical investigations of the anisotropic behaviour of vitrinites. Responsible for TOC device LECO RC-412, supervision of Master students and planning of field trips. |
| Sept. 2001 – May 2002 | Software Tester for basin analysis modelling software PetroMod®, IES, Aachen. |
| March – May 2001 | Scientific Worker, German Federal Institute for Geosciences and Natural Resources (BGR), Hannover.
Compilation, evaluation and interpretation of hydrocarbon data |
| June – Aug. 1999 | Practical work in organic-geochemistry at the sedimentary laboratory GCA, Lehrte, Germany. |
| Sept. – Dec. 1998 | Field mapping of ore deposits in the northern part of Mexico for the Mexican Federal Authority “Consejo de Recursos Minerales”. |

▪ **EDUCATION**

- | | |
|------------------------|---|
| April 2002 – Dec. 2006 | PhD, RWTH Aachen University.
Research on the thermal history of the Lower Saxony Basin (western Germany) using geochemical and petrophysical investigation methods (TOC, RockEval, vitrinite reflectance and fluid inclusion measurements), apatite and zircon fission track dating as well as structural balancing (2DMove) and basin modelling (2D PetroMod). |
| Sept. 1994 - May 2001 | Study of Geology at the Institute of Geology and Palaeontology of the University of Hannover.
- Jan. 1997 Pre-diploma in Geology.
- May 2001 Diploma in Geology. Topic “Investigations into the influence of salt-dynamic on the hydrocarbon generation in the Staßfurt Carbonates (Z2) of the well Gorleben Z1 (northern Germany), using geochemical analysis and 1D basin modelling (PDI). Structural observations regarding salt movement/piercing and resulting volumetric changes within the salt layer. |
| Dec. 1989 – May 1993 | Abitur, Ratsgymnasium of Stadthagen, Germany. |